EF3 COL 2.0-27-A

## 2.5.2 Vibratory Ground Motion

This subsection provides a detailed description of vibratory ground motion assessments that were carried out for the Fermi 3 site. The subsection begins with a review of the approaches outlined in U.S. Nuclear Regulatory Commission (NRC) Regulatory Guides 1.165 and 1.208 for conducting the vibratory ground motion studies. Following this review of the regulatory framework used for the project, results of the seismic hazard evaluation are documented and the site-specific ground motion response spectra (GMRS) for horizontal and vertical motions are developed.

Regulatory Guide 1.165 provides guidance on methods acceptable to the NRC to satisfy the requirements of the seismic and geologic regulation, 10 CFR 100.23, "Reactor Site Criteria," for assessing the appropriate safe shutdown earthquake (SSE) ground motion levels for new nuclear power plants. Regulatory Guide 1.165 states that an acceptable starting point for this assessment at sites in the central and eastern United States (CEUS) is the probabilistic seismic hazard analysis (PSHA) conducted by the Electric Power Research Institute and Seismic Owners Group (EPRI-SOG) in the 1980s (Reference 2.5.2-201, Reference 2.5.2-202). The EPRI-SOG study involved a comprehensive compilation of geological, geophysical, and seismological data; evaluations of the scientific knowledge concerning earthquake sources, maximum earthquakes, and earthquake rates in the CEUS by six multidisciplinary teams of experts in geology, seismology, and geophysics; and, separately, development of state-of-knowledge earthquake ground motion modeling, including epistemic and aleatory uncertainties.[1] The uncertainty in characterizing the frequency and maximum magnitude of potential future earthquakes associated with these sources and the ground motion that may be produced was assessed and explicitly incorporated into the seismic hazard model.

Regulatory Guide 1.165 further specifies that the adequacy of the EPRI-SOG hazard results must be evaluated in light of new data and

1. Epistemic uncertainty is uncertainty attributable to incomplete knowledge about a phenomenon that affects the ability to model it. Epistemic uncertainty is reflected in a range of viable models, model parameters, multiple expert interpretations, and statistical confidence. In principle, epistemic uncertainty can be reduced by the accumulation of additional information. Aleatory uncertainty (often called aleatory variability or randomness) is uncertainty inherent in a nondeterministic (stochastic, random) phenomenon. Aleatory uncertainty is accounted for by modeling the phenomenon in terms of a probability model. In principle, aleatory uncertainty cannot be reduced by the accumulation of more data or additional information.

interpretations and evolving knowledge pertaining to seismic hazard evaluation in the CEUS. Appendix E, Section E.3, of Regulatory Guide 1.165 outlines a three-step process for this evaluation, as follows:

1. Evaluate whether recent information suggests significant differences from the previous seismic hazard characterization.
2. If potentially significant differences are identified, perform sensitivity analyses to assess whether those differences have a significant effect on site hazard.
3. If Step 2 indicates that there are significant differences in site hazard, then the PSHA for the site is revised by either updating the previous calculations or, if necessary, performing a new PSHA. If not, the previous EPRI-SOG results may be used to assess the appropriate SSE ground motions.

Regulatory Guide 1.165 calls for the SSE ground motions to be based on the site PSHA results for a reference probability of the median $10^{-5}$ hazard level. The basis for the selected reference probability is described in Appendix B of Regulatory Guide 1.165.

Regulatory Guide 1.208 provides additional guidance on performance goal-based methods acceptable to the NRC to satisfy the requirements of 10 CFR 100.23 for assessing the appropriate site-specific performance goal-based ground motions for new nuclear power plants. Specifically, the performance-based approach described in American Society of Civil Engineers/Structural Engineering Institute Standard 43-05, “Seismic Design Criteria for Structures, Systems, and Components in Nuclear Facilities,” may be used to define site-specific performance goal–based GMRS at the ground surface based on mean hazard results (Reference 2.5.2-203). The development of mean seismic hazard results is to be based on a site-specific PSHA combined with site-specific site amplification analyses. The procedures to be used to perform the PSHA and site amplification studies are similar to those described in Regulatory Guide 1.165, but additional detailed guidance is provided in Regulatory Guide 1.208. Regulatory Guide 1.208 also provides guidance on an alternative approach for addressing the lower-bound magnitude used in the PSHA based on the likelihood that earthquakes of various sizes can produce potentially damaging ground motions. The ground motion measure used to correlate with the threshold of potential damage is

cumulative absolute velocity (CAV). The alternative approach using the CAV filter is used to develop the final GMRS for the Fermi 3 site.

This subsection discusses the following aspects of vibratory ground motion:

- Seismicity (Subsection 2.5.2.1)
- Geologic structures and seismic source models (Subsection 2.5.2.2)
- Correlation of earthquake activity with seismic sources (Subsection 2.5.2.3)
- Probabilistic seismic hazard analysis and controlling earthquake (Subsection 2.5.2.4)
- Seismic wave transmission characteristics of the site (Subsection 2.5.2.5)
- Ground motion response spectra (Subsection 2.5.2.6)

### 2.5.2.1 Seismicity

An important component in developing a seismic hazard model for the Fermi 3 site is the seismic history of the region. The selected starting point for developing the site-specific PSHA for the Fermi 3 site is the EPRI-SOG (Reference 2.5.2-201) seismic hazard model for the CEUS. The data used to assess earthquake occurrence rates for the seismic sources in the EPRI-SOG model were those in the earthquake catalog.

The first step in the three-step process for evaluating the adequacy of this model for the assessment of seismic hazards at the Fermi 3 site involved an assessment of the effect of recent information on the characterization of the seismicity of the central United States. The development of an updated earthquake catalog for the project region and surrounding areas is described in Subsection 2.5.2.1.1. Information on significant earthquakes in the site region is provided in Subsection 2.5.2.1.2. Discussion of large-magnitude historical and prehistoric earthquakes that are significant to the seismic hazard at the Fermi 3 site that have occurred beyond the site region is provided in Subsection 2.5.2.3 and Subsection 2.5.2.4.1.

The Fermi 3 Seismic Category I structures are founded on bedrock or on lean concrete fill above bedrock and are not subject to liquefaction potential as discussed in Subsection 2.5.4.8. No reports or studies exist on liquefaction and paleoliquefaction in the site vicinity (40 km [25 mi] radius) as presented in Subsection 2.5.1.2.6.6. Subsection 2.5.1.2.5

evaluates the site geologic hazard. The site is also relatively flat and the slopes are considered stable as discussed in Subsection 2.5.5.

#### 2.5.2.1.1 Earthquake Catalog

Earthquake occurrence rates for the seismic sources developed in the EPRI-SOG study were based on the EPRI-SOG CEUS earthquake catalog that was developed for the time period of 1627 through February 1985. The EPRI-SOG catalog has gone through two significant revisions. Seeber and Armbruster (Reference 2.5.2-204) conducted a thorough review of the catalog, revising the magnitude estimates and locations of many events, removing some events as non-earthquakes and adding others. The revised earthquake catalog is denoted as the National Center for Earthquake Engineering Research (NCEER)-91 catalog (Reference 2.5.2-205). The NCEER-91 catalog forms the basis for the project catalog and events within it are considered to be EPRI events. Subsequently, Mueller et al. reviewed the NCEER-91 catalog along with additional information and developed a catalog of independent[2] earthquakes for use in the 2002 U.S. Geological Survey's National Seismic Hazard Mapping Program (Reference 2.5.2-206). The version of this catalog, which is referred to as the U.S. Geological Survey (USGS) 2002 CEUS catalog, is obtainable from the USGS National Seismic Hazard Mapping Project website (Reference 2.5.2-207). The Geological Survey of Canada developed the Seismic Hazard Earthquake Epicenter File (SHEEF) for use in the Fourth Generation Seismic Hazard Maps of Canada (Reference 2.5.2-209). These catalogs were combined with the Catalog of Ohio Earthquakes (Reference 2.5.2-210) and newly identified historical earthquakes from studies by Metzger (Reference 2.5.2-211, Reference 2.5.2-212) and Fujita (Reference 2.5.2-213). Fujita and Sleep (Reference 2.5.2-214) and Seeber and Armbruster (Reference 2.5.2-215) reviewed the seismicity of Michigan and western Lake Ontario, respectively, and removed events associated with mine collapse or blasting and weather events. Events occurring before 1985 that were not included in EPRI are labeled as "added historical" on Figure 2.5.2-201 through Figure 2.5.2-209.

2. The PSHA formulation used in this study assumes that the temporal occurrence of earthquakes conforms to a Poisson process, implying independence between the times of occurrence of earthquakes. Thus it is necessary to remove dependent events (such as foreshocks and aftershocks) from the earthquake catalog before estimating earthquake frequency rates.

The catalog for the Fermi 3 site consists of the previously discussed catalogs between 35 and 50°N and 70 to 95°W and recent earthquakes (post-EPRI) through April 2008 obtained from the following sources:

- Advanced National Seismic System (ANSS) website (Reference 2.5.2-216).
- USGS National Earthquake Information Center website (Reference 2.5.2-217).
- Ohio Seismic Network website operated by the Ohio Geological Survey (Reference 2.5.2-210).
- National Earthquake Database operated by the Geological Survey of Canada (Reference 2.5.2-218).

Upon deletion of duplicate entries and removal of aftershocks, the locations for some events were revised based on literature reviews (Reference 2.5.2-215, Reference 2.5.2-219, Reference 2.5.2-221, Reference 2.5.2-222).

Figure 2.5.2-201 shows the spatial distribution of earthquakes in the project earthquake catalog. The window covered by the project catalog (between 35 and 50°N and 70 to 95°W) incorporates the 320-km (200-mi.) radius site region and all seismic sources contributing significantly to the Fermi 3 site earthquake hazard. Figure 2.5.2-202 shows the locations of earthquakes within 320-km (200-mi.) of the Fermi 3 site. The earthquakes are color coded on Figure 2.5.2-201 and Figure 2.5.2-202 to indicate those events included in the EPRI-SOG earthquake catalog for the time period of 1758 to 1985, historical events added to the EPRI-SOG catalog, and those events that occurred after the EPRI-SOG catalog (1985 to 2006). The added historical earthquakes and the earthquakes occurring since the EPRI-SOG study have similar spatial distributions as the earthquakes contained in the EPRI-SOG catalog, and no new concentrations of seismicity are apparent in the updated catalog.

Appendix 2.5AA lists the earthquakes in the updated catalog that have occurred within 320-km (200-mi.) of the Fermi 3 site. The list consists of 123 events of body-wave magnitude ($m_b$) ≥ 3 that occurred between 1776 and April 2, 2008.

Focal depths are either not determined (set equal to 0) or fixed (set to 5, 10, 15, or 33 km) for most of the earthquakes. Only one event has listed depths greater than 10 km (6 mi.). The earthquakes do not show any correlation between depth and magnitude.

The body-wave magnitude scale, $m_b$, was used as the uniform magnitude scale in the original EPRI-SOG earthquake catalog and is the magnitude scale used in the catalog developed for the Fermi 3 study. Estimated seismic moments are provided for the 320-km (200-mi.) radius catalog in Appendix 2.5AA. The values listed were determined by first estimating the moment magnitude (**M**) using the three relationships described in Subsection 2.5.2.4. The seismic moment from each moment magnitude estimate was further evaluated by using the Hanks and Kanamori relationship and then averaging the results (Reference 2.5.2-225).

#### 2.5.2.1.2 Significant Earthquakes in the Site Region (320-km [200-mi] radius)

Seismicity in Michigan is sparse and many of the historical events in Michigan were determined to be atmospheric shock waves, explosions, cryoseisms, or erroneous reports (Reference 2.5.2-214). Faust et al. (Reference 2.5.2-219) determined a focal depth for an earthquake recorded in central Michigan between 10 and 15 km (6 and 9 mi.) and postulated that the earthquake may be associated with a northwest-southeast reactived basement fault. Ruff et al. (Reference 2.5.2-220) monitored the seismicity in western Ohio and Indiana and correlated seismicity of the Anna region with the Anna-Champaign, Logan, and Auglaize faults. Where the data is interpretable, events in the Anna region occur in the upper 10 km (6 mi.) of the crust. Hansen (Reference 2.5.2-226) summarized the seismicity in Ohio as shallow events occurring along faults or pre-existing zones of weakness in Precambrian rocks. Seismicity near eastern Lake Erie and western Lake Ontario is associated with the Akron Magnetic Boundary (Reference 2.5.2-215). Mereu et al. (Reference 2.5.2-227) related the patterns of seismicity to fluid flow along basement structures. Earthquake magnitudes do not exceed $m_b$ 5.2 within the site region. The locations of the earthquakes listed in the project catalog are shown on Figure 2.5.2-202. Subsection 2.5.1.1.4.4.1 discusses significant earthquakes associated with the New Madrid seismic zone. Significant earthquakes associated with the Wabash Valley seismic zone are discussed in Subsection 2.5.1.1.4.4.2. Significant earthquakes occurring in the site region are described as follows:

**January 31, 1986**

As discussed in Subsection 2.5.1.1.4.3.3.1, the largest historic event in the northeastern Ohio seismic zone was the January 31, 1986, magnitude ($m_b$) 5.0 event located about 40 km (24.4 mi.) east of Cleveland in southern Lake County, Ohio, and about 17 km (10.4 mi.) south of the Perry Nuclear Power Plant (Reference 2.5.2-224). This earthquake was located 175 km (108 mi.) from the site. The earthquake produced Modified Mercalli intensity (MMI) VI to VII at distances of 15 km (9 mi.) from the epicenter and short-duration high accelerations of 0.18 g at the Perry plant (Reference 2.5.2-224). The Fermi 3 site experienced Modified Mercalli Intensity (MMI) IV–V during this event (Reference 2.5.2-228). Thirteen aftershocks were detected by April 15, 1986, with magnitudes ranging from 0.5 to 2.5 and focal depths ranging from 2 to 6 km (1.2 to 3.7 mi.) (Reference 2.5.2-224). Although these events were within 12 km (7.4 mi.) of a deep waste disposal injection well, Nicholson et al. (Reference 2.5.2-224) argue a natural origin for the earthquakes.

**July 12, 1986**

The July 12, 1986, event near the town of St. Marys in Auglaize County was the largest earthquake to occur in the Anna seismic zone since 1937 (Reference 2.5.2-226). This earthquake was located 184 km (114.3 mi.) from the site. Schwartz and Christensen (Reference 2.5.2-223) determined a hypocenter of 5 km (3 mi.) for the magnitude ($m_b$) 4.5 event and a focal mechanism (strike = 25°, dip = 90°, rake = 175°) representing mostly strike-slip with a small oblique component approximately parallel to the Anna-Champaign fault and a nearly horizontal *P* axis oriented east-northeast. The earthquake produced an MMI V1 event (Reference 2.5.2-226). The Fermi 3 site experienced approximately MMI III during this event (Reference 2.5.2-229).

**September 25, 1998**

A moderate earthquake centered near Jamestown, Pennsylvania, at the southern end of the Pymatuning Reservoir, had a magnitude ($m_b$) 5.0 ($m_b$Lg = 5.2) event that occurred on September 25, 1998. This earthquake was located 184 km (114.3 mi.) from the site. Harvard University interpreted the fault-plane solution as a northwest-southeast-oriented fault (strike, 303°). Movement on the fault, according to Michigan State University, was thrust with a small left-lateral

component. The maximum peak MMI was VI. Shaking was greatest in Ohio, Pennsylvania, Michigan, New York, and Ontario; however, an isoseismal map was not generated. (Reference 2.5.2-230)

**January 26, 2001**

A magnitude 2.6 foreshock on January 19, 2001, preceded the magnitude 4.5 event at 10:03 pm January 25, 2001 (3:03 am January 26, 2001 UTC), which had a MMI of VI, followed by a magnitude 3.2 event on June 3, 2001, and a magnitude 2.3 event on June 5, 2001 (Reference 2.5.2-231). These earthquakes were located 208 km (129.2 mi.) from the site. The Ohio Seismic Network was installed in 1999 and precisely recorded the 2001 earthquakes (Reference 2.5.2-231). Modified Mercalli intensities reached a maximum of VI. Similar to the 1998 Pymatuning event, waveforms exhibit north-south asymmetry with abrupt southward termination. The isoseismal map for this event indicates that the Fermi 3 site did not experience significant ground motions.

**April 18, 2008**

The April 18, 2008 Mw 5.2 event occurred outside of Mount Carmel, Illinois (Reference 2.5.2-232) and was located approximately 550 km (342 mi.) from Fermi 3. Shaking reached MMI VI near the epicenter (Reference 2.5.2-233). This event was felt widely throughout the central United States, including Alabama, Arkansas, Georgia, Illinois, Indiana, Iowa, Kansas, Kentucky, Michigan, Minnesota, Mississippi, Missouri, Nebraska, North Carolina, Ohio, Tennessee, West Virginia, Wisconsin, and southern Ontario, Canada (Reference 2.5.2-232). Centoid-moment-tensor analysis indicates movement along this rupture is mostly strike slip (Reference 2.5.2-232). The depth of the earthquake varies, ranging from 11.6 km (7.2 mi.) (USGS) to 15 km (9.3 mi.) (Global CMT and SLU Regional Moment Tensor Solution) to 18 km (11 mi.) (USGS body-wave moment tensor solution). The April 18, 2008 event was the largest earthquake in the Illinois basin since the magnitude 5.4 event in November 1968 and the magnitude 5.2 event in June 1987. (Reference 2.5.2-232) As discussed below in Subsection 2.5.2.4.1.2, the maximum magnitude distribution for the Wabash Valley source zone is controlled by large-magnitude paleoearthquakes.

### 2.5.2.2 Geologic Structures and Seismic Source Models

As outlined previously, Appendix E, Section E.3, of Regulatory Guide 1.165, Step 1, specifies that recent information should be reviewed to evaluate if this information indicates significant differences from the previous seismic hazard. Subsection 2.5.1 presents a summary of available geological, seismological, and geophysical data for the site region and adjoining areas that provides the basis for evaluating seismic sources that contribute to the seismic hazard to the Fermi 3 site. This subsection presents a description of the seismic source characterizations from the EPRI-SOG evaluation (Reference 2.5.2-201) (Subsection 2.5.2.2.1), followed by a summary of general approaches and interpretations of seismic sources used in more recent seismic hazard studies (Subsection 2.5.2.2.2. Subsection 2.5.2.3 and Subsection 2.5.2.4 present evaluations of the new information relative to the EPRI-SOG seismic source evaluations (Reference 2.5.2-201).

#### 2.5.2.2.1 EPRI-SOG Source Evaluations

During the 1980s, the Seismic Owners Group (SOG) conducted a comprehensive seismic hazard methodology development program at EPRI (Reference 2.5.2-201). The SOG program emphasized earth science assessments of alternative explanations of earthquakes in the CEUS, with a particular emphasis on a systematic understanding and expression of uncertainties (Reference 2.5.2-201). Seismic sources and associated interpretations necessary for hazard calculations at any nuclear power plant site in the CEUS were developed (Reference 2.5.2-201). Six earth science teams (EST) provided input interpretations: Bechtel Group, Dames & Moore, Law Engineering, Rondout Associates, Weston Geophysical, and Woodward-Clyde Consultants (Reference 2.5.2-201). Each team produced a report (Volumes 5 through 10 of the EPRI-SOG study [Reference 2.5.2-201]) that provided descriptions of how the seismic sources were identified and defined.

The seismic source characterizations developed by the EPRI-SOG expert teams were used to conduct PSHAs for nuclear power plant sites in the CEUS that were reported in EPRI (Reference 2.5.2-202). The calculations performed for each site excluded the seismic sources defined by each EPRI-SOG expert team that in combination contributed less than one percent to the total hazard computed from all sources defined by that expert team. The EPRI identification of seismic sources that are significant to assessing the seismic hazard at the Fermi site was

based on calculations made with the ground motion models presented in EPRI-SOG (Reference 2.5.2-201, Reference 2.5.2-202). Since that time, there have been advances in the characterization of earthquake ground motions for CEUS earthquakes. These advances are described in Subsection 2.5.2.4.2. Because the potential contribution of a seismic source to the hazard at a site is dependent in part on the ground motion model used to compute the hazard, the identification of the significant EPRI-SOG seismic sources was re-examined using updated ground motion models. This examination is presented in Subsection 2.5.2.4.3.1. Table 2.5.2-201 through Table 2.5.2-206 list the seismic sources for each of the six EPRI-SOG ESTs that are included in the updated PSHA for the Fermi 3 site. These seismic sources are shown on Figure 2.5.2-204 through Figure 2.5.2-209 and are described in Subsections 2.5.2.2.1.1, 2.5.2.2.1.2, 2.5.2.2.1.3, 2.5.2.2.1.4, 2.5.2.2.1.5, and 2.5.2.2.1.6.

#### 2.5.2.2.1.1 Bechtel (BEC) Team

The EPRI (Reference 2.5.2-202) calculations for the Fermi 3 site included six seismic sources defined by the BEC team (Reference 2.5.2-234; Figure 2.5.2-204). These sources are listed in Table 2.5.2-201 and are described below.

- **New Madrid Region (Source BEC-BZ0).** This background zone surrounds, but does not contain, the New Madrid source (source 30) defined by the BEC team. This background zone includes the following tectonic feature source zones: Reelfoot Rift (source 31), Rough Creek-Shawneetown fault zone (source 33), Wabash Valley fault zone (source 34), Cottage Grove faults (source 35), and Saint Genevieve fault (source 36) and secondary seismic zones Ozarks (source J) and Southern Illinois (source K). A moderate to large earthquake could occur within this zone. (Reference 2.5.2-234)
- **Northern Great Plains Region (Source BEC-BZ3).** This background source zone covers an extensive area in the central United States. The background zone contains ten individual seismic source zones, many of which are located more than 320 km (200 mi.) from the site. The individual seismic sources within the background zone are the Ouachita fold belt (source 38), Oklahoma aulacogen (source 39), Meers fault (source 40), Nemaha ridge (source 41), Tennessee-Montana geopotential trend (source 42), Midcontinent gravity high (source 43), Colorado lineament (source 44), and the southeast Oklahoma (source L), El Reno area (source M), and

northern Illinois faults (Plum River/Sandwich faults) (source N2). Some of these individual sources have no associated seismicity in the moderate-to-large range and others are the sites of historic earthquakes of moderate magnitude. (Reference 2.5.2-234)

- **Southern Eastern Craton Region (Source BEC-BZ6).** This background zone is located in the eastern United States and is adjacent to the Northern Great Plains Region (source BZ3). The zone contains five seismic sources: Clarendon-Linden fault (source 11), Frankfort-Bucyrus rift (source 27), Kentucky River faults (source 45), Niagara peninsula (source D), and the Anna, Ohio, area (source N1). All five sources have been the sites of moderate-to-large earthquakes. (Reference 2.5.2-234)
- **Frankfort-Bucyrus (Source BEC-27).** This seismic source is defined by a zone of high-frequency magnetic and gravity highs. It extends from Ohio to Tennessee and is composed of two subfeatures: an unnamed Precambrian rift structure in western Ohio and a gravity high in Kentucky. (Reference 2.5.2-234)
- **Southern Illinois Region (Source BEC-K).** This source encompasses an area of recognized seismicity in southern Illinois. Tectonic features that could explain this seismicity are not recognized, thus the boundaries of the source zone were defined exclusively on the basis of the historic seismicity pattern. (Reference 2.5.2-234)
- **Anna, Ohio, area (Source BEC-N1).** This seismic source encompasses Paleozoic faults near Anna, Ohio. These faults have been inferred on the basis of local geopotential data interpretation and drillhole data. The faults trend E-W and N-S and are presumed to have steep dips. Ordovician rocks appear to be affected by these faults but the overlying Pleistocene glacial deposits are not offset. (Reference 2.5.2-234)

#### 2.5.2.2.1.2 Dames & Moore (DAM) Team

The EPRI (Reference 2.5.2-202) calculations for the Fermi 3 site included seven seismic sources defined by the DAM team (Reference 2.5.2-235; Figure 2.5.2-205). These sources are listed in Table 2.5.2-202 and are described below.

- **Eastern Marginal Basin (Source DAM-8).** This source zone occupies much of a marginal basin that developed during the Paleozoic (early Cambrian through the Carboniferous). Seismicity is

diffuse throughout the zone and includes several moderate-sized earthquakes, including the 1980 Sharpsburg, Kentucky, event. This seismic source is a background or default zone for three other seismic sources: Dunkard basin (source 5), Rome Trough (source 6), and East Continent Gravity High (source 7). (Reference 2.5.2-235)

- **Anna, Ohio (Source DAM-12).** An area of intense crustal disturbance, interpreted to indicate high stress conditions, is encompassed by this source zone. The zone incorporates the juncture of the Paleozoic Bowling Green and Champaign faults, plus the intersections of the Findlay, Kankakee, and Cincinnati arches. Strong geophysical anomalies are present that may define the strong lithologic contrasts in basement rocks indicated by drilling. (Reference 2.5.2-235)
- **Findlay Arch/Algonquin Axis (Sources DAM-14 and 14-B).** These seismic sources are defined as a positive basement feature that separates the Michigan and Appalachian basins. It is not associated with high levels of seismicity. (Reference 2.5.2-235) The Findlay arch parallels the subsurface trace of the Grenville Front that extends from Canada into the United States, separating older from younger basement rocks. The arch developed primarily during the Paleozoic (early Ordovician, Late Mississippian, and post-Pennsylvanian). The Findlay arch is a zone of little or no geophysical response. (Reference 2.5.2-235)
- **Michigan Basin (Source DAM-15).** The Michigan basin is a Paleozoic basin that apparently subsided over a late Precambrian rift (Reference 2.5.2-235). This seismic source incorporates the structural Michigan basin, the Mid-Michigan Geophysical anomaly, and the edge of the exposed Canadian Shield. Seismicity roughly parallels the edges of Paleozoic strata and is concentrated along the southern, southeastern, and northeastern boundaries of the source zone. (Reference 2.5.2-235)
- **Southern Illinois/Southern Indiana/Fairfield Basin (Source DAM-18).** This zone defines an area of moderately high seismicity from adjoining areas of lower seismicity (Reference 2.5.2-235). The Illinois and Fairfield basin developed in the Paleozoic and have moderate historic seismicity. (Reference 2.5.2-235)
- **Wisconsin-Michigan Block (Source DAM-70).** This zone encircles the Wisconsin dome and includes the Midcontinent rift that trends

north through Iowa and Minnesota to join the Lake Superior syncline (Reference 2.5.2-235). This large regional seismic source lacks tectonic structures that could generate future moderate-to-large earthquakes. As there is no tectonic basis for this source zone, the pattern of historical seismicity defines the potential future activity. (Reference 2.5.2-235)

- **Southern Canada Province (Source DAM-73).** This zone flanks both sides of the Findlay-Algonquin axis (source 14) and extends from western Ohio northward into Ontario, separating the Michigan basin (source 15) from the Greater Appalachian basin (Reference 2.5.2-235). There is no tectonic basis for this source zone, which is considered a regional seismic source (similar to the Wisconsin-Michigan block (source 70), thus the pattern of historical seismicity defines the potential future activity. (Reference 2.5.2-235)

#### 2.5.2.2.1.3 Law Engineering (LAW) Team

The EPRI (Reference 2.5.2-202) calculations for the Fermi 3 site included six seismic sources defined by the LAW team (Reference 2.5.2-236; Figure 2.5.2-206). These seismic sources are listed in Table 2.5.2-203 and are described briefly below.

Four of the seismic sources defined by the LAW team within a 320-km (200-mi.) radius of the Fermi site are seismotectonic regions delineated as background seismic source zones. These are defined by a similar expression of several geophysical and geologic parameters, which suggest consistency of basement and upper crustal structure. (Reference 2.5.2-236)

- **Wabash Valley Arm (Source LAW-07).** This seismic source is based on a Paleozoic Reelfoot Rift that is considered to be part of the New Madrid rift complex. (Reference 2.5.2-236)
- **Laurentian (Source LAW-111).** The boundaries of this source zone are interpreted from magnetic and gravity data. The western boundary is the Grenville Front and the eastern boundary is along the St. Lawrence Lowlands. (Reference 2.5.2-236)
- **Ohio-Pennsylvania Block (Source LAW-112).** This source zone is characterized by a north-northeast-trending magnetic pattern that delineates the zone from the adjacent Laurentian block (source 111) to the north. The western boundary corresponds to the Grenville Front

and the southeastern boundary is the New York–Alabama lineament. (Reference 2.5.2-236)

- **Wisconsin Block (Source LAW-114).** This seismic source is defined by magnetic and gravity trends that are approximately concentric around the north end of the large gravity high that defines the Mississippi Embayment. (Reference 2.5.2-236)
- **Indiana Block (Source LAW-115).** This seismic source is characterized by north and northwest magnetic trends with high-frequency magnetic highs. Similar to the Ohio-Pennsylvania block to northeast, the eastern boundary has been interpreted as the Grenville Front; the southeastern boundary is the New York–Alabama lineament. (Reference 2.5.2-236)
- **Illinois Block (Source LAW-116).** The Illinois block is characterized by long-wavelength, low-frequency magnetic anomalies located northwest of the Mississippi Embayment province (source BSZ 117). (Reference 2.5.2-236)

#### 2.5.2.2.1.4 Rondout Associates (RND) Team

The EPRI (Reference 2.5.2-202) calculations for the Fermi 3 site included seven seismic sources defined by the RND team (Reference 2.5.2-237; Figure 2.5.2-207). These sources are listed in Table 2.5.2-204 and are described briefly below.

- **New Madrid Rift Complex (Source RND-02).** This seismic source encompasses multiple structural features that are associated on the basis of geological, geophysical, and seismic information. The features are extensions of the Reelfoot Rift, which is interpreted to break into three arms near the confluence of the Mississippi and Ohio rivers. Two of these arms, the St. Louis Arm and the Southern Indiana Arm, are included in this source zone and are considered to be possible sources of future earthquakes. (Reference 2.5.2-237)
- **Southern Illinois and Indiana (Source RND-04)**. This seismic source zone contains seismicity that is not related to a known tectonic feature. The source zone lies north of the Southern Indiana and St. Louis Arms of the New Madrid Rift Complex (source 2) and therefore may be associated with the seismicity associated with that source zone. (Reference 2.5.2-237)
- **Anna, Ohio (Source RND-08).** This seismic source encompasses a region in which several moderate-intensity earthquakes have

occurred in historic time. The seismicity occurs at the intersection of the Fort Wayne Geophysical anomaly, interpreted as a late Precambrian rift zone, and the interpreted extension of the Grenville Front, a feature that is a fault and/or metamorphic contact that separates basement rock of different ages. Another possible origin of the seismicity in the Anna, Ohio, region may be a pronounced change in the basement rock strength characteristics. (Reference 2.5.2-237)

- **Southeast Michigan (Source RND-10).** This region was defined as a seismic source on the basis of analogy and proximity with the Anna, Ohio, region (source 8). Within the Southeast Michigan seismic source, the Mid-Michigan Geophysical anomaly, an expression of the segment of the Midcontinent Rift System, intersects and extends into the Grenville basement province (A rift intersecting the Grenville Front is analogous to the subsurface conditions in the Anna, Ohio, region). Mafic rift-related rocks are juxtaposed with the low gravity granite intrusive to the North. (Reference 2.5.2-237)
- **Northwestern Ohio (Source RND-11).** This seismic source zone is defined on the basis of two major basement inhomogeneities, which may serve as stress concentrators and thus localize the observed seismic activity in the zone. A gravity minimum is recognized in the western part of the source zone, and a positive gravity and magnetic anomaly, known as the Sandusky anomaly, is present in the northeastern part. (Reference 2.5.2-237)
- **Cleveland, Ohio (Source RND-12).** This seismic source zone defines a region that has a high level of low-intensity earthquakes. Regional geophysical data can be interpreted to indicate two major basement features: a north-northeast-striking vertical basement discontinuity (possibly a fault) and a northwest-striking lineament (the Pittsburgh-Washington lineament). These structural features tectonic features may be associated with the historic seismicity. (Reference 2.5.2-237)
- **Pre-Grenville Precambrian Craton (Source RND-52).** This background seismic source consists of PreCambrian crust that predates the Grenville orogeny not already included in a seismic source zone. (Reference 2.5.2-237)

#### 2.5.2.2.1.5 Weston Geophysical (WGC) Team

The EPRI (Reference 2.5.2-202) calculations for the Fermi 3 site included five seismic sources defined by the WGC team (Reference 2.5.2-238; Figure 2.5.2-208). These sources are listed in Table 2.5.2-205 and are described briefly below.

- **Anna, Ohio (Source WGC-29).** This seismic source is part of the Southern Ontario–Ohio-Indiana background source (source 101). The Anna, Ohio, region had repeated moderate-magnitude seismicity in 1875 and in the 1930s. Faults, including the Bowling Green and Champaign faults, are located in the region. Three basement arches, the Cincinnati, Kankakee, and Findlay arches, also intersect in the region. The combination of these geologic features, the seismicity, and strong geophysical anomalies are the basis for the WGC team to assess a high probability of activity for this source. (Reference 2.5.2-238)
- **Indiana Arm (Source WGC-33).** This seismic source zone is defined by the Indiana Arm, a part of the New Madrid Rift. (Reference 2.5.2-238)
- **Northern Interior (Source WGC-100).** This background seismic source covers a large region of the north-central United States and adjacent parts of Canada. No identified active seismic sources occur within the zone. (Reference 2.5.2-238)
- **Southern Ontario–Ohio-Indiana (Source WGC-101).** This background seismic source includes three seismic source zones: the Niagara Peninsula (source 7), the Clarendon-Linden structure (source 8), and the Anna, Ohio, tectonic feature (source 29). In addition, the Rome Trough–Kentucky River fault zone feature is contained within the zone (no seismic source has been modeled for this feature). Within this zone, an earthquake having a magnitude of about 5 occurred in northeastern Ohio in 1986. (Reference 2.5.2-238)
- **North-Central (Source WGC-105).** This background seismic source was delineated because it is more seismically active than the adjoining Northern Interior (source 100) zone to the north. Included in this seismic source is the Sandwich–Plum River fault source area in northern Illinois. This region has experienced scattered seismicity ranging from small to moderate magnitudes, and although faults have

been identified, there is not a strong correlation of seismicity with the faults. (Reference 2.5.2-238)

#### 2.5.2.2.1.6 Woodward-Clyde Consultants (WCC) Team

The EPRI (Reference 2.5.2-202) calculations for the Fermi 3 site included nine seismic sources defined by the WCC team (Reference 2.5.2-239; Figure 2.5.2-209). These sources are listed in Table 2.5.2-206 and are described briefly below.

- **Attica, NY Intersection (Source WCC-34).** This seismic source consists of the intersection of the Clarendon-Linden Fault (source 32) and the Western New York–Southern Ontario Trend (source 33). This seismic source also corresponds spatially with a circular gravity anomaly. The seismic potential along the portion of the Clarendon-Linden fault system may be high within this source; however the seismic potential for the rest of the system may be low. Recurrent seismicity within this zone may be due to stress concentrated in the region. (Reference 2.5.2-239)
- **Northeastern Ohio Gravity Source (Source WCC-35).** This seismic zone is associated with a circular positive gravity anomaly and a poorly defined negative magnetic anomaly. The WCC team did not identify a structure. Instead they attribute these anomalies to a deep crustal expression, possibly due to thinner crust. Seismicity occurs on the flanks of the anomaly. One earthquake with magnitude near 5 occurred in this region in 1986 (Reference 2.5.2-239)
- **Michigan-Ohio Geophysical Anomaly (Source WCC-36).** This seismic source is defined by a northwest-trending alignment of gravity and magnetic anomalies that have been interpreted as an ancient rift structure. The isostatic gravity anomaly highs are expressed as localized, generally circular, positive anomalies, and these plus the magnetic anomalies extend from Michigan to central Ohio and possibly into northern Kentucky. With the exception of the seismicity that is localized in the vicinity of Anna, Ohio, the level of seismicity along the feature is relatively quiet. (Reference 2.5.2-239)
- Bowling Green–Auglaize Fault System (Source WCC-37). This seismic zone is a narrow linear zone that encompasses the Bowling Green–Auglaize fault system. The possible fault is inferred from monoclinal structure and geophysical anomalies. The structure corresponds to a north-south-trending negative gravity anomaly and a

north-northwest-trending negative anomaly on the vertical gradient, which may be associated with the Grenville Front. Seismicity within the zone is not localized along the fault and occurs in the region of the northern and central portions. The southern portion of the zone includes earthquakes associated with Anna, Ohio, to the west. (Reference 2.5.2-239)

- **Champaign-Anna Fault System (Source WCC-38).** The basis for this seismic source is the Champaign-Anna fault system, which trends west-northwest within the Michigan-Ohio Geophysical anomaly (source 36). The fault system is identified primarily on the basis of geophysical data. Seismicity is not strongly co-located with the Champaign-Anna fault as earthquakes occur north of the fault. Several historic earthquakes with magnitudes near the lower bound of moderate-to-large earthquakes have occurred in the Anna, Ohio, region. (Reference 2.5.2-239)
- **Anna, Ohio, Geophysical Intersection (Source WCC-39).** This source zone is defined to include a region in which a number of geological and geophysical structures intersect. These include the Cincinnati, Findlay, and Kankakee arches; the Bowling Green–Auglaize and Champaign-Anna fault systems (sources 37 and 38, respectively); geophysical anomalies; and, possibly the Grenville Front. The interaction of these features may be producing a concentration of stress and thus an increased potential for earthquake occurrence. Recurring seismicity in the region of Anna, Ohio, is located in the general vicinity of these intersections. (Reference 2.5.2-239)
- **Southern Indiana Arm (Source WCC-43).** This source zone is defined by the Southern Indiana Arm, which extends to the northeast from the northeastern end of the Reelfoot Rift, and the Wabash River fault system. (Reference 2.5.2-239)
- **New Madrid Loading Volume (Source WCC-44).** This source zone includes those areas surrounding the Reelfoot Rift. This zone encompasses a zone that is thought to concentrate stress in the region of the 1811 and 1812 New Madrid region. (Reference 2.5.2-239)
- **Background Zone 67 (Source WCC-B67).** The Fermi 3 site lies within a large background zone defined as a rectangular area (2° by 2°) surrounding the Fermi 2 Nuclear Power Plant site. This zone is not

based on any geological, geophysical, or seismological features. (Reference 2.5.2-239)

#### 2.5.2.2.2 Post-EPRI Seismic Source Characterizations

Seismic hazard source characterization studies conducted since completion of the 1988 EPRI-SOG study that are pertinent to the Fermi 3 seismic hazard analysis are described in the following subsections. (Reference 2.5.2-201)

##### 2.5.2.2.2.1 USGS Earthquake Hazard Mapping Source Characterization Model

As part of the USGS National Seismic Hazard Mapping Program, updated seismic hazard maps for the conterminous United States were produced in 2002 and 2008 (Reference 2.5.2-240, Reference 2.5.2-241). Input for revising the source characterization used in the 1996 hazard maps (Reference 2.5.2-242) was provided by researchers through a series of regional workshops. Key issues that were addressed in the 2002 and 2008 updated source characterizations included new information regarding the location, size, and recurrence of repeated large-magnitude earthquakes in the New Madrid source region. Although the USGS program does not use formal expert elicitation and full uncertainty quantification, the resulting seismic hazard model provides information on the current understanding of the seismic potential of the study region and the catalog of recorded earthquakes.

The USGS source model and earthquake catalog (in body-wave magnitude [$m_b$]) developed by the USGS are shown on Figure 2.5.2-210. The updated earthquake catalog for the USGS 2008 model extends through 2006. The general approach used by the USGS for modeling distributed seismicity in the CEUS is based on gridded, spatially smoothed seismicity in large background zones. (Reference 2.5.2-206)

Two broad regions are defined with different maximum magnitudes in the USGS 2008 model: an extended margin zone (maximum magnitude [$M_{max}$] = **M** 7.5) and a craton zone ($M_{max}$ = **M** 7.0) where **M** is the moment magnitude. In addition, the USGS source model includes an East Tennessee regional source zone and alternative fault-line sources for repeated large-magnitude earthquakes in the New Madrid seismic zone (NMSZ) (Figure 2.5.2-210). The maximum magnitude probability distribution assigned to the northern section of the New Madrid fault source is **M** 7.1 (wt 0.15), **M** 7.3 (wt 0.2), **M** .5 (wt 0.5), and **M** 7.8

(wt 0.15), where the fraction in parenthesis is the weight (wt) assigned as defined by the relative contribution of the earthquakes. The maximum magnitude probability distribution assigned to the southern and central sections is **M** 7.3 (wt 0.15), **M** 7.5 (wt 0.2), **M** 7.7 (wt 0.5), and **M** 8.0 (wt 0.15). The USGS model uses a mean recurrence time of 500 years and 750 years for repeated large-magnitude earthquakes in the New Madrid region. These are weighted equally for the northern section. Additionally, a 1000-year branch was added to the 2008 recurrence model with an assigned weight of 0.1. The USGS 2008 model assumes a time-independent behavior and includes the potential for clustered occurrence of large earthquakes (Reference 2.5.2-206, Reference 2.5.2-241).

The 2008 update to the CEUS seismic source model includes the following components:

- An updated catalog through 2006 that accounts for magnitude uncertainty.
- A reduction in the magnitudes in the northern NMSZ by 0.2 units and an added logic tree branch for a recurrence rate of one event every 750 years.
- An added logic tree branch for a 1/1,000-year recurrence rate of earthquakes in the NMSZ with low weight (0.1).
- Implementation of a temporal cluster model for New Madrid earthquakes as one alternative.
- A modified model for the fault geometry for the NMSZ to include five hypothetical strands and increased weight on the central strand to 0.7.
- A revised dip of the Reelfoot fault to 38°.
- A maximum magnitude distribution for seismicity-derived hazard sources.
- A revised geometry of the large Charleston zone that extends it further offshore to include the Helena Banks fault zone.
- Inclusion of an alternative set of earthquake occurrence rates that incorporate the effects of magnitude uncertainty.

#### 2.5.2.2.2.2 Exelon Generation Company, LLC, Early Site Permit for the Clinton Site

Exelon Generation Company, LLC (EGC), updated the EPRI-SOG seismic source parameters for selected sources as part of an Early Site

Permit (ESP) application for the Clinton site in central Illinois. (Reference 2.5.2-243) Updates for the PSHA consisted of the following:

- Addition of fault sources for repeated large-magnitude earthquakes in the NMSZ.
- Revised maximum magnitude distribution for the Wabash Valley – Southern Illinois source zone(s).
- Revised maximum magnitude distribution for the central Illinois basin/background source.
- Updated ground motion attenuation models.

#### 2.5.2.2.2.3 TVA Bellefonte Nuclear Site, Units 3 and 4, COLA

The model for repeated large-magnitude earthquakes in the NMSZ developed for the EGC ESP study was adopted with some modifications in the updated PSHA completed for the TVA Bellefonte Nuclear Site, Units 3 and 4, COLA. (Reference 2.5.2-244)

### 2.5.2.3 Correlation of Earthquake Activity with Seismic Sources

Regulatory Guides 1.165 and 1.208 indicate that earthquake activity should be correlated with seismic sources. The principal database for assessing earthquake recurrence is the historical and instrumental earthquake record. To satisfy this requirement, an updated catalog of independent historical and instrumental earthquakes covering the Fermi 3 site region was developed (see discussion in Subsection 2.5.2.1.1).

The distribution of earthquake epicenters from the EPRI (pre-1985) catalog, the more recent (post-1985) instrumental events, and updated historical earthquakes for the site region with respect to the EPRI-SOG sources are shown on Figure 2.5.2-204 through Figure 2.5.2-209. Comparison of the updated earthquake catalog to the EPRI-SOG earthquake catalog and EPRI-SOG sources yields the following conclusions:

- The updated earthquake catalog does not show a pattern of seismicity within the site region different from that exhibited by earthquakes in the EPRI-SOG catalog that would suggest a new seismic source, i.e., one in addition to those included in the EPRI-SOG characterizations.
- The updated earthquake catalog shows similar spatial distribution of earthquakes to that shown by the EPRI-SOG catalog, suggesting that no significant revisions to the geometry of seismic sources defined in

the EPRI-SOG characterization are required based on seismicity patterns.

- Relocated EPRI events in the Anna, Ohio, seismic zone (Reference 2.5.2-220) show a better correlation with Fort Wayne rift structures (subsurface Anna-Champaign, Logan, and Auglaize faults) than was recognized by the ESTs.
- Seismicity in the Northeastern Ohio seismic zone, including several post-EPRI events, has been associated with the Akron Magnetic Boundary (Reference 2.5.2-215).
- Added historical events in the Wabash Valley seismic zone by Metzger et al. (Reference 2.5.2-212) have increased seismicity rates in source zones in southern Illinois and Indiana.
- The updated catalog does not show any earthquakes within the site region that can be associated with a known geologic structure, with the exception of the Anna and Northeastern Ohio seismic zones discussed in the bulleted items listed above.
- The closest principal sources of seismic activity are in the vicinity of Anna, Ohio, and Cleveland, Ohio. These areas lie at a distance of greater than 150 km (90 mi.) from the Fermi 3 site. Concentrations of seismicity in these areas were recognized and considered by the EPRI-SOG teams, as discussed in Subsection 2.5.2.2.1.

### 2.5.2.4 Probabilistic Seismic Hazard Analysis and Controlling Earthquake

This subsection describes the PSHA conducted for the Fermi 3 site. Following the procedures outlined in Appendix E, Section E.3, of Regulatory Guide 1.165, Subsection 2.5.2.4.1 and Subsection 2.5.2.4.2 discuss new information on seismic source characterization and ground motion characterization, respectively, that is potentially significant relative to the EPRI-SOG seismic hazard model (Reference 2.5.2-201). Subsection 2.5.2.4.3 presents the results of PSHA sensitivity analyses used to test the effect of the new information on the seismic hazard. Using these results, an updated PSHA was performed, as described in Subsection 2.5.2.4.4. The results of that analysis are used for the development of uniform hazard response spectra and identification of the controlling earthquakes (Subsection 2.5.2.4.4.2).

#### 2.5.2.4.1 New Information Relative to Seismic Sources

This section describes potential updates to the EPRI-SOG seismic source model. Seismic source characterization data and information that could affect the predicted level of seismic hazard include the following:

- Identification of possible additional seismic sources in the site region.
- Changes in the characterization of the rate of earthquake occurrence for one or more seismic sources.
- Changes in the characterization of the maximum magnitude for other EST seismic sources.

Based on the review of new geological, geophysical, and seismological information that is summarized in Subsection 2.5.1, the review of seismic source characterization models developed for post-EPRI-SOG seismic hazard analyses (Subsection 2.5.2.2.2), and a comparison of the updated earthquake catalog to the EPRI-SOG evaluation (Subsection 2.5.2.3), the EPRI-SOG source models have been modified for the Fermi 3 COLA as follows:

- Fault sources are added for repeated large-magnitude earthquakes in the New Madrid Seismic Zone
- The maximum magnitude distribution for the Wabash Valley – Southern Illinois source zone(s) is revised
- The maximum magnitude distribution for selected EPRI-SOG team sources are updated based on updated earthquake catalog events.

##### 2.5.2.4.1.1 Updated Characterization of Large-Magnitude New Madrid Seismic Zone Earthquakes

The NMSZ extends from southeastern Missouri to southwestern Tennessee and is located more than 700 km (435 mi.) southwest of the Fermi 3 site (Figure 2.5.1-207). The NMSZ produced a series of large-magnitude earthquakes between December 1811 and February 1812 (Reference 2.5.2-245 through Reference 2.5.2-248). A detailed discussion of recent information about the location, size, and frequency of repeated large-magnitude events that have occurred in the NMSZ is provided in Subsection 2.5.1.1.4.4.1.

The updated characterization of fault sources that are judged to be the sources for the 1811-1812 New Madrid earthquake sequence and similar paleoearthquake sequences in the NMSZ follows the characterization initially developed in the EGC ESP application (Reference 2.5.2-243) and

subsequently implemented, with only one exception in the Bellefonte Units 3 & 4 COLA (Reference 2.5.2-244). The Bellefonte model uses a time period of interest of 50 years rather than the longer period of 60 years used in the EGC ESP application. The summary of the updated characterization model outlined below is based on the more complete discussion from the Bellefonte FSAR (Reference 2.5.2-244), which is excerpted in Appendix 2.5BB.

The locations of the faults that make up the New Madrid central fault system sources relative to the Fermi 3 site are shown on Figure 2.5.1-207, inset C. The logic tree used to represent the uncertainty in the seismic source characterization model for the NMSZ central fault system is shown on Figure 2.5.2-211.

**NMSZ Central Faults Source Geometry**

Three fault sources are included in the updated characterization of the central fault system of the NMSZ: (1) the New Madrid South (NS) fault; (2) the New Madrid North (NN); and (3) the Reelfoot fault (RF). The first three levels of the logic tree for these sources address the uncertainty regarding the location and extent of the causative faults that ruptured during the 1811 and 1812 earthquake sequence. This uncertainty is represented by alternative geometries and fault behavior for the NN, NS, and RF faults, which have been reported in the published literature. (Figure 2.5.2-212 and Figure 2.5.2-213). These alternative geometries affect the distance from earthquake ruptures on these fault sources to the Fermi 3 site.

**NMSZ Central Faults Maximum Earthquake Magnitude**

The next level of the logic tree addresses the maximum magnitude for earthquakes on the three New Madrid fault sources. As discussed in Subsection 2.5.1.1.4.4.1 researchers have suggested that the sizes of prehistoric earthquakes associated with these sources are similar to the 1811 and 1812 earthquakes. Using the concept of characteristic earthquakes, seismic source characterizations of the New Madrid seismic source zone typically consider the 1811 and 1812 earthquakes to represent the maximum earthquake for this source. As illustrated in Figure 2.5.2-214 the frequency of repeated large earthquakes interpreted from paleoliquefaction data is greater than obtained by extrapolating a Gutenburg-Richter recurrence relationship fit to the observed seismicity rate for smaller-magnitude earthquakes. A characteristic earthquake

recurrence curve better fits the more frequent repeated large magnitude events observed in the paleoliquefaction record. Table 2.5.2-207 summarizes recent estimates of the magnitude of the New Madrid 1811 and 1812 main shocks. Table 2.5.2-208 presents the resulting characteristic magnitude distribution for each of the three faults based on weights assigned to the various magnitude estimates, as discussed in Appendix 2.5BB. The alternative sets of ruptures allow for sequences of multiple large-magnitude earthquakes in which the arguments for the high versus low magnitude assessments for the individual faults are considered to be highly correlated as shown in the logic tree on Figure 2.5.2-211 and given in Table 2.5.2-208.

The magnitudes listed in Table 2.5.2-208 are considered to represent the size of the expected maximum earthquake rupture for each fault within the NMSZ. Following the development of the characteristic earthquake recurrence model by Youngs and Coppersmith (Reference 2.5.2-249), as modified by Youngs et al. (Reference 2.5.2-250), the size of the next characteristic earthquake is assumed to vary randomly about the expected value following a uniform distribution over the range of ±¼ magnitude units. This range represents the aleatory variability in the size 2.5BBof individual characteristic earthquakes.

**NMSZ Central Faults Earthquake Recurrence**

The paleoseismic record of the New Madrid seismic zone includes evidence from paleoliquefaction, sediment rupture and deformation, fluvial response, and biotic response.

Estimates of the recurrence interval for New Madrid characteristic earthquakes include a Poisson (memoryless) and a renewal model. The Brownian Passage Time (BPT) model developed by Ellsworth et al. (Reference 2.5.2-251) and Matthews et al. (Reference 2.5.2-252) was used by EGC to represent the distribution of the time between earthquake sequences in the renewal model.

Figure 2.5.2-215 shows the uncertainty distributions for the mean repeat time between New Madrid earthquake sequences obtained by EGC (Reference 2.5.2-253). The occurrence rates for New Madrid large-magnitude earthquake sequences were estimated using the distributions for mean repeat time shown on Figure 2.5.2-215. Table 2.5.2-209 lists the discrete distributions for mean repeat time and the

equivalent Poisson rates. The Poisson and renewal recurrence models are given equal weight (Figure 2.5.2-211).

The paleoliquefaction data gathered in the New Madrid region indicate that the prehistoric earthquakes have occurred in sequences closely spaced in time relative to the time period between sequences, similar to the 1811 and 1812 sequence. Figure 2.5.2-216 shows the estimated earthquake sizes and event locations for the 1811 to 1812 sequence and the two previous sequences. These data indicate that the RF has ruptured in all three sequences, but the NN and NS sources may have produced earthquakes on the order of one magnitude unit smaller than the 1811 and 1812 earthquakes in some previous sequences. As discussed in Appendix 2.5BB, the revised EGC model for New Madrid sequences to consist of two alternative models of rupture or earthquake sequences. In Model A, all ruptures are similar in size to the 1811 and 1812 earthquakes. In Model B, one-third of the sequences are the same as Model A, one-third of sequences contain a smaller rupture of the NN, and one-third of sequences contain a smaller rupture of the NS. The difference in magnitude from the 1811 and 1812 ruptures was set to be no more that one-half magnitude unit, and no ruptures are allowed to be less than **M** 7. All three earthquakes were included in the hazard calculation in all rupture sequences.

#### 2.5.2.4.1.2 Updated Maximum Magnitude Distribution for Wabash Valley Seismic Zone Sources

The updated characterization of the maximum magnitude distribution for the Wabash Valley–Southern Illinois and Indiana source zone used in the updated Fermi 3 PSHA follows the characterization developed for the EGC ESP site without modification, as described in the EGC ESP application, i.e., SSAR, Section 2.1.5.2.2 of Appendix B. (Reference 2.5.2-254). This section of the EGC ESP SSAR, which is excerpted in Appendix 2.5CC, is summarized as follows.

The updated maximum magnitude distribution for the Wabash Valley–Southern Illinois source zone is based on recent analysis of paleoliquefaction features in the vicinity of the lower Wabash Valley of southern Illinois

Based on interpretations of the size of the prehistoric earthquakes recorded by these paleoliquifaction features, the following maximum magnitude probability distribution is used in the updated PSHA to capture

the range in uncertainty in the magnitude of the largest prehistoric earthquakes in the lower Wabash Valley region: **M** 7.0 (wt 0.1), **M** 7.3 (wt 0.4); **M** 7.5 (wt 0.4); **M** 7.8 (wt 0.1). The highest weight is given to the range from M 7.3 to 7.5 where most of the magnitude estimates lie. This updated maximum magnitude distribution is assigned to the EPRI-SOG seismic sources defined by the ESTs to represent the Wabash Valley region, as indicated in Table 2.5.2-201 through Table 2.5.2-206.

#### 2.5.2.4.1.3 Updated Maximum Magnitude Distribution for Other Source Zones

The updated earthquake catalog was used to obtain the largest earthquake observed in each of the EPRI-SOG seismic sources. This review suggested modification of the maximum magnitude distributions for a few sources. The $m_b$ 5.0 1986 and the $m_b$ 5.2 1998 earthquakes in Ohio are larger than the minimum maximum magnitude assigned by the Law Engineering team to their source 112 and by the Woodward-Clyde team to their background source for the Fermi site. Accordingly, the maximum magnitude distributions for these two sources were modified to account for these post-EPRI-SOG earthquakes using the approach applied by each EST for assessing maximum magnitude. In addition, the Law Engineering team's source 111 contains the 1935 $m_b$ 6.2 Charlevoix earthquake. The maximum magnitude distribution for this source was also updated to account for this earthquake following the procedure outlined by the Law Engineering team. The updated maximum distributions for these sources are listed in Table 2.5.2-203 and Table 2.5.2-206.

EGC (Reference 2.5.2-254) updated a number of the EPRI-SOG regional background source zones to account for the occurrence of a prehistoric earthquake near Springfield, Illinois, with an estimated magnitude of approximately **M** 6.5. Several of these sources (Bechtel's source BZ3, Law Engineering's source 116, Rondout's source 52, and Weston Geophysical's source 105) are included in the set of sources used for the updated PSHA for the Fermi 3 site. The maximum magnitude distributions for these sources were updated to the EGC (Reference 2.5.2-254) assessment. The updated maximum distributions for these sources are listed in Table 2.5.2-201, Table 2.5.2-203, Table 2.5.2-204 and Table 2.5.2-205.

#### 2.5.2.4.1.4 Earthquake Occurrence Rates within EPRI-SOG Completeness Regions

Subsection 2.5.2.1.1 describes the development of an updated earthquake catalog for the Fermi 3 site region. This updated catalog includes modifications to the EPRI-SOG catalog by subsequent researchers, the addition of earthquakes that have occurred after completion of the EPRI-SOG seismic source characterization studies (post-March 1985), and the identification of additional earthquakes in the time period covered by the EPRI-SOG evaluation for the project region (1758 to March 1985). The effect of the new catalog information was assessed by evaluating the effect of the new data on earthquake magnitude estimates and on earthquake recurrence estimates within the 320-km (200-mi.) region around the Fermi 3 site.

The earthquake recurrence rates computed in the EPRI-SOG evaluation included a correction to remove bias introduced by uncertainty in the magnitude estimates for individual earthquakes (Reference 2.5.2-201). The bias adjustment was implemented by defining an adjusted magnitude estimate for each earthquake, $m_b$*, and then computing the earthquake recurrence parameters by maximum likelihood using earthquake counts in terms of $m_b$*. The adjusted magnitude is defined by the relationship

$$m_b^* = m_b - \beta\sigma^2_{m_b|m_b\ instrumental}/2 \qquad \text{[Eq. 1]}$$

when *mb* is based on instrumentally recorded $m_b$ magnitudes and by the relationship

$$m_b^* = m_b + \beta\sigma^2_{m_b|X}/2 \qquad \text{[Eq. 2]}$$

when $m_b$ is based on other size measures *X*, such as maximum intensity, $I_0$, or felt area (Reference 2.5.2-201). The change in sign in the correction term from negative in Equation 1 to positive in Equation 2 reflects the effects of the uncertainty in the conversion from size measure X to $m_b$. Parameter β is the Gutenberg-Richter *b*-value in natural log units. Values of the adjusted magnitude $m_b$* were computed for the earthquakes in the updated catalog using the assessed uncertainties in the magnitude estimates and a value of $\beta$ equal to 0.95 × ln(10) based on the global *b*-value of 0.95 assigned to the CEUS by Frankel et al. (Reference

2.5.2-240) and Petersen et al. (Reference 2.5.2-241). Values of $\sigma_{m_b|X}$ range from 0.55 for $m_b$ estimated from maximum intensity, to 0.3 to 0.5 for $m_b$ estimated from various other magnitude scales or felt area (Reference 2.5.2-201). The value of $\sigma_{m_b|m_b instrumental}$ is typically set at 0.1.

The EPRI-SOG procedure for computing earthquake recurrence rates was based on a methodology that incorporated data from both the period of complete catalog reporting and the period of incomplete catalog reporting (Reference 2.5.2-201). For the period of incomplete reporting, a probability of detection, $P^D$, was defined that represented the probability that the occurrence of an earthquake would ultimately be recorded in the earthquake catalog for the region. The CEUS was subdivided into 13 completeness regions that represented different histories of earthquake recording (Reference 2.5.2-201). Figure 2.5.2-217 these completeness regions.

The total time span of the EPRI-SOG catalog was then divided into six time intervals. Then using the observed seismicity and information on population density and the history of earthquake reporting across the CEUS, the probability of detection was estimated for each time interval within each completeness region for six magnitude intervals. Earthquake recurrence estimates were then made using the "equivalent period of completeness," TE, for each completeness region and all of the recorded earthquakes within the usable portion of the catalog. The equivalent period of completeness is computed by the expression

$$T_{ij}^{E} = \sum_{k} T_k \times P_{ijk}^{D} \qquad \text{[Eq. 3]}$$

where $P_{ijk}^{D}$ is the probability of detection for completeness region *i*, magnitude interval *j*, and time period *k* of length $T_k$ (Reference 2.5.2-201). The estimated values of the probability of detection for all of the completeness regions are given in EPRI-SOG (Reference 2.5.2-201).

The updated earthquake catalog includes newly identified earthquakes for the time period covered by the EPRI-SOG catalog, reassessment of the sizes of previously identified events, and earthquakes that have occurred after completion of the EPRI-SOG evaluation. The addition of more earthquakes to the time period covered by the EPRI-SOG catalog would suggest an increase in computed occurrence rate. However, may of these events occur in time periods where the probability of detection is less than 1.0. Thus, adding these events to the catalog would also affect

the assessment of the probability of detection for these time periods, and increase the resulting assessment of *TE*.

Because the EPRI-SOG assessment of the probability of detection was obtained from a single assessment over the entire CEUS, a proper update would require an update of the earthquake catalog for the entire region. As this has not been done, an approximate effect of the additional earthquakes identified for the time period 1660 to 1985 was made by assessing the probability of detection for those completeness regions most affected by the catalog update while holding the values in the other regions fixed at the EPRI-SOG values. This assessment was performed using the EPRI-SOG program EQPARAM (Reference 2.5.2-201). Table 2.5.2-210 lists the probability of detection obtained for completeness regions 4 and 5 in the EPRI-SOG study and obtained based on the updated catalog. In making the updated assessment, it was assumed that the probability of detection is 1.0 for the time period of March 1985 through April 2008 for all magnitude intervals. The analysis results indicate that the additional historical earthquakes added to the updated catalog have increased the probability of detection for the earlier time periods.

The effect of the updated earthquake catalog and probability of detection estimates on earthquake occurrence rates was assessed by computing earthquake recurrence rates for EPRI-SOG completeness regions 4 and 5. Figure 2.5.2-218 shows the cumulative annual frequency of earthquakes for the entire area covered by completeness region 4 and for that portion that lies within 320 km (200 mi.) of the Fermi 3 site. Somewhat higher rates are computed from the updated catalog for the entire completeness region 4. However, there is little difference in the occurrence rate for the region within 320 km (200 mi.) of the Fermi 3 site. Figure 2.5.2-219 shows similar results for completeness region 5, with a similar conclusion. The impact of the revised rates on the site hazard is not clear from these results and will be assessed in PSHA sensitivity analyses.

#### 2.5.2.4.2 New Information Relative to Earthquake Ground Motions

##### 2.5.2.4.2.1 Models for Median Ground Motions

The EPRI (Reference 2.5.2-202) calculation of seismic hazard characterized epistemic uncertainty in median (mean log) earthquake

ground motions by using three strong-motion attenuation relationships: McGuire et al. (Reference 2.5.2-255), Boore and Atkinson (Reference 2.5.2-256), and Nuttli (Reference 2.5.2-257) combined with the response spectral relationships of Newmark and Hall (Reference 2.5.2-258). These relationships were based to a large extent on modeling earthquake ground motions using simplified physical models of earthquake sources and wave propagation.

Estimating earthquake ground motions in the CEUS has been the focus of considerable research since completion of the EPRI-SOG studies. The research has produced a number of ground motion attenuation relationships. EPRI completed a study in 2006 to update methods used to characterize the estimation of strong ground motion in the CEUS for application in PSHA for nuclear facilities (Reference 2.5.2-259). This study was conducted following the Senior Seismic Hazard Analysis Committee (SSHAC) guidelines for a Level III analysis (Reference 2.5.2-260). The SSHAC provided guidance on the appropriate methods to use for quantifying uncertainty in evaluations of seismic hazard (Reference 2.5.2-260).

In a SSHAC Level III analysis, the responsibility for developing the quantitative description of the uncertainty distribution for the quantity of interest lies with an individual or team designated the Technical Integrator. The Technical Integrator is guided by a panel of experts whose role is to provide information, advice, and review. In the EPRI study, a panel of six ground motion experts was assembled (Reference 2.5.2-259). During a series of workshops, the experts provided advice on the available CEUS ground motion attenuation relationships that were considered appropriate for estimating strong ground motion in the CEUS. The experts also provided information on the appropriate criteria for evaluating the available ground motion models. The Technical Integrator then used this information to develop a composite representation of the current scientific understanding of ground motion attenuation in the CEUS.

The EPRI study recommended four alternative sets of median ground motion models (termed model clusters) to represent alternative modeling approaches for defining the median ground motions as a function of earthquake magnitude and source-to-site distance (Reference 2.5.2-259). Three of these ground motion clusters are appropriate for use in assessing the hazard from moderate-sized local earthquakes

occurring randomly in source zones, and all four are to be used for assessing the hazard from sources whose hazard contribution is from large-magnitude earthquakes.

EPRI (Reference 2.5.2-259) proposed the logic tree structure to be used with these models that is shown on the left-hand side of Figure 2.5.2-220. The first (leftmost) level of the logic tree shown in the figure provides the weights assigned to the three median cluster models appropriate for local sources. The second level addresses the appropriate ground motion cluster median model to use for large-magnitude distant earthquake sources. For the Fermi 3 site, these sources are associated with the Wabash Valley sources and the source of repeating large earthquakes at New Madrid. Two alternatives are provided: to use the cluster model used for the local sources or to use the cluster 4 model. The effect of this logic structure on the PSHA is that by following the branch for cluster 1 at the first node, two options are available: (1) using the cluster 1 model for the large-magnitude sources, and (2) using cluster 4 for the large-magnitude sources and cluster 1 for all other sources. This same logic is repeated for the branches for clusters 2 and 3.

EPRI provided estimates of the epistemic uncertainty in the median ground motion model for each cluster (Reference 2.5.2-259). As shown by the third level of the logic tree (Figure 2.5.2-220), the uncertainty in each cluster median model is modeled by a three-point discrete distribution with ground motion relationships for the 5th, 50th, and 95th percentiles of the epistemic uncertainty in the median attenuation relationship for each ground motion cluster.

The EPRI (Reference 2.5.2-259) ground motion median models for clusters 1, 2, and 3 were based in large part on the CEUS ground motion models developed by Silva et al. (Reference 2.5.2-261), Atkinson and Boore (Reference 2.5.2-262), and Campbell (Reference 2.5.2-263), respectively. Silva et al. (Reference 2.5.2-264) and Atkinson and Boore (Reference 2.5.2-265) have since developed updated versions of their models. In addition, Tavakoli and Pezeshk (Reference 2.5.2-266) present a hybrid ground motion model for the CEUS based on the approach developed by Campbell (Reference 2.5.2-263). These newer models are compared to the EPRI (Reference 2.5.2-259) models on Figure 2.5.2-221.

The two plots on the left of Figure 2.5.2-221 compare the EPRI (Reference 2.5.2-259) 5th , 50th , and 95th percentile 10-Hertz (Hz) and

1 Hz median models for ground motion cluster 1 with the three single-corner stochastic models developed by Silva et al. (Reference 2.5.2-264). The updated models all fall well within the range of the EPRI (Reference 2.5.2-259) models.

The two plots in the center of Figure 2.5.2-220 compare the EPRI (Reference 2.5.2-259) 5th , 50th , and 95th percentile 10 Hz and 1 Hz median models for ground motion cluster 2 with the model developed by Atkinson and Boore (Reference 2.5.2-265). The Atkinson and Boore (Reference 2.5.2-265) model uses rupture distance as the distance measure, while the EPRI (Reference 2.5.2-259) cluster 2 models use Joyner-Boore distance. The comparisons shown on Figure 2.5.2-221 were made assuming that the top of rupture for the M 5 earthquake is at a depth of 4 km (2.5 mi.), based on a mean point-source depth of 6 km (3.7 mi.) (Reference 2.5.2-261). The median ground motions produced by the updated Atkinson and Boore (Reference 2.5.2-265) model fall within the range of the EPRI (Reference 2.5.2-259) cluster 2 medians except for distances less than about 7 km (4.3 mi.) for large-magnitude earthquakes.

The two plots on the right of Figure 2.5.2-221 compare the EPRI (Reference 2.5.2-259) 5th , 50th , and 95th percentile 10 Hz and 1 Hz median models for ground motion cluster 3 with the model developed by Tavakoli and Pezeshk (Reference 2.5.2-266). The Tavakoli and Pezeshk (Reference 2.5.2-266) model predictions generally fall within the range of the EPRI (Reference 2.5.2-259) cluster 3 medians except for small magnitudes at short rupture distances.

As presented in Subsection 2.5.2.4.4, large-magnitude earthquakes at very small distances are not a significant contributor to the hazard. Also, small-magnitude earthquakes have only a small contribution to the low-frequency hazard. On the basis of the comparisons shown on Figure 2.5.2-221, it is concluded that the EPRI (Reference 2.5.2-259) median ground motion models are appropriate for use in computing the hazard for the Fermi 3 site.

#### 2.5.2.4.2.2 Models for Ground Motion Aleatory Variability

The EPRI (Reference 2.5.2-259) study also provided a characterization of the aleatory variability in CEUS ground motions based on an assessment of information available at the time. More recently, EPRI conducted a study focused in part on evaluating the appropriate aleatory

variability for CEUS ground motions (Reference 2.5.2-267). The thrust of the study was to identify reasons why the aleatory variability for CEUS motions may be different than that observed for the large empirical database of strong ground motion in the western United States (WUS) and other tectonically active regions, and then evaluate the extent to which these reasons are supported by empirical data. The result of the EPRI study was a recommended model for aleatory variability for CEUS ground motions (Reference 2.5.2-267).

The EPRI (Reference 2.5.2-267) model for aleatory variability in CEUS ground motions is represented by the fourth and fifth levels of the ground motion logic tree shown on Figure 2.5.2-220. The fourth level of the logic tree addresses the overall aleatory model. Two alternatives were defined: (1) model 1A is based on WUS aleatory variability with an additional component of intra-event variability for CEUS earthquakes and (2) Model 1B is unmodified WUS aleatory variability. Model 1A was favored based on the available data.

The EPRI included an additional component of aleatory variability to account for variability in source depth at small source-to-site distances when the Joyner-Boore distance measure is used for ground motion models based on point-source numerical simulations (Reference 2.5.2-259). EPRI (Reference 2.5.2-267) evaluated the empirical evidence for additional aleatory variability at small Joyner-Boore distances and concluded that the adjustments proposed by EPRI (Reference 2.5.2-259) were not supported by empirical data. Instead, three alternatives were recommended:

1. Model 2A — no adjustment.
2. Model 2B — an additional 0.12 standard error in the natural log of ground motion amplitude.
3. Model 2C — an additional 0.23 standard error.

The additional standard error is to be combined with model 1A or 1B as the sum of variances to produce the final standard error for Joyner-Boore distances less than or equal to 10 km (6.2 mi.). A log-linear decrease in the additional standard error is to be applied over the distance range of 10 to 20 km (6.2 to 12.4 mi.), with no additional adjustment for distances greater than 20 km (12.4 mi.). These alternative models define the fifth level of the logic tree shown on Figure 2.5.2-220. These additional standard error models are applied to the EPRI median models that use

the Joyner-Boore distance measure (clusters 1, 2, and 4) (Reference 2.5.2-259).

#### 2.5.2.4.2.3 Conversion from Body Wave to Moment Magnitude

The last level of the ground motion logic tree shown on Figure 2.5.2-220 addresses the relationship between body wave magnitude, $m_b$, and moment magnitude, **M**. This conversion is required because the EPRI (Reference 2.5.2-259, Reference 2.5.2-267) ground motion models are defined in terms of **M**, whereas the EPRI-SOG recurrence rates are defined in terms of $m_b$. The epistemic uncertainty in the conversion between $m_b$ and **M** was addressed by using the three $m_b$-**M** relationships.

1. Atkinson and Boore (Reference 2.5.2-262):

$$\mathbf{M} = -0.39 + 0.98 m_b \qquad \text{for } m_b \le 5.5$$

$$\mathbf{M} = 2.715 - 0.277 m_b + 0.127 m_b^2 \qquad \text{for } m_b > 5.5 \qquad \text{[Eq. 4]}$$

2. Johnston (Reference 2.5.2-268):

$$\mathbf{M} = 1.14 + 0.24 m_b + 0.0933 m_b^2 \qquad \text{[Eq. 5]}$$

3. EPRI (Reference 2.5.2-269):

$$m_b = -10.23 + 6.105\mathbf{M} - 0.7632\mathbf{M}^2 + 0.03436\mathbf{M}^3 \qquad \text{[Eq. 6]}$$

These three models are assigned equal weight, as the models are all credible.

#### 2.5.2.4.3 PSHA Sensitivity Analysis

This subsection describes the sensitivity studies that were carried out to address any need for changes in the EPRI-SOG PSHA model used in EPRI (Reference 2.5.2-202). Based on the assessments in Subsection 2.5.2.4, and consistent with the requirements of Regulatory Guide 1.165, Regulatory Position E.3, the following PSHA model adjustments were studied as part of PSHA sensitivity tests for the Fermi 3 site:

- Selection of appropriate set of seismic sources for each EPRI-SOG expert team.

- Sensitivity to new data relative to the occurrence of large earthquakes in the NMSZ.
- Sensitivity to the updated maximum magnitude distributions for Wabash Valley seismic zone sources.
- Sensitivity to adjustment of the minimum value of maximum magnitude for a few additional EPRI-SOG sources.
- Sensitivity to adjustment in earthquake occurrence rates based on the updated earthquake catalog.

Sensitivity analyses were not conducted to address the effect of the updated ground motions models developed by EPRI (Reference 2.5.2-259, Reference 2.5.2-267) because these have become the standard set of models for the assessment of seismic hazards for proposed new power plants.

As discussed above in Subsection 2.5.2.2.1, the specific subset of EPRI-SOG seismic sources to include for each EST was assessed using updated ground motion models. The selection of the appropriate set is based on the contribution of individual sources to the total hazard at the site. The assessment of the contribution of more distant sources will be affected by the level of hazard contributed by the local sources.

#### 2.5.2.4.3.1 Selection of EPRI-SOG Seismic Sources

As discussed above in Subsection 2.5.2.2.1, the specific subset of EPRI-SOG seismic sources to include for each EST was assessed using the updated EPRI ground motion models that will be used to compute the PSHA for the Fermi 3 site (Reference 2.5.2-259, Reference 2.5.2-267). The sources examined included those within 320 km (200 mi.) of the site and those at larger distances with somewhat higher rates of seismicity, such as sources in the vicinity of the Wabash Valley seismic zone and New Madrid seismic zone. These calculations were performed for each individual team. Seismic sources were added until additional sources produced less than a one percent increase in the frequency of exceedance in the $10^{-4}$ to $10^{-5}$ range. The source contributions were tested for 10 Hz and 1 Hz ground motions. The calculations were performed using the preferred set of ground motion models for each ground motion cluster (i.e., the highest weighted path through the logic tree for each ground motion cluster). This corresponds to use of the 50th percentile cluster median model and aleatory variability models 1A

and 2A. A single $m_b$-**M** conversion relationship was used (Reference 2.5.2-262).

EPRI (Reference 2.5.2-259) provided ground motion models for the mid-continent region that covered most of CEUS

#### 2.5.2.4.3.1.1 Bechtel Team Seismic Sources

Figure 2.5.2-222 shows the mean hazard curves computed for the Bechtel team's sources listed in Table 2.5.2-201 and shown on Figure 2.5.2-204. The EPRI (Reference 2.5.2-259) ground motion cluster 4 models are applied to the Wabash Valley related sources BZ0 and K.

#### 2.5.2.4.3.1.2 Dames & Moore Team Seismic Sources

Figure 2.5.2-223 shows the mean hazard curves computed for the Dames & Moore team's sources listed in Table 2.5.2-202 and shown on Figure 2.5.2-205. As indicated in Table 2.5.2-202, a modification was made to the value of P* for Dames & Moore source 8. The original value of P* assigned to this source was 0.08 as an alternative to smaller feature-specific sources within the boundary of source 8. However, two $m_b$ 5 earthquakes, 1/31/1986 and 9/25/1998, have occurred within source 8 post the EPRI-SOG catalog. These events occurred well away from the internal feature-specific sources. Therefore, the value of P* for the Dames & Moore source 8 was increased to 1.0. The EPRI (Reference 2.5.2-259) ground motion cluster 4 models are applied to the Wabash Valley related source 18.

#### 2.5.2.4.3.1.3 Law Engineering Team Seismic Sources

Figure 2.5.2-224 shows the mean hazard curves computed for the Law Engineering team's sources listed in Table 2.5.2-203 and shown on Figure 2.5.2-206. The EPRI (Reference 2.5.2-259) ground motion cluster 4 models are applied to the Wabash Valley related source 7.

#### 2.5.2.4.3.1.4 Rondout Associates Team Seismic Sources

Figure 2.5.2-225 shows the mean hazard curves computed for the Rondout Associates team sources listed in Table 2.5.2-204 and shown on Figure 2.5.2-207. The EPRI (Reference 2.5.2-259) ground motion cluster 4 models are applied to the Wabash Valley related sources 2 and 4.

#### 2.5.2.4.3.1.5 Weston Geophysical Team Seismic Sources

Figure 2.5.2-226 shows the mean hazard curves computed for the Weston Geophysical team's sources listed in Table 2.5.2-205 and shown on Figure 2.5.2-208. The EPRI (Reference 2.5.2-259) ground motion cluster 4 models are applied to the Wabash Valley related source 33.

#### 2.5.2.4.3.1.6 Woodward-Clyde Consultants Team Seismic Sources

Figure 2.5.2-227 shows the mean hazard curves computed for the Woodward-Clyde Consultants team's sources listed in Table 2.5.2-206 and shown on Figure 2.5.2-209. The EPRI (Reference 2.5.2-259) ground motion cluster 4 models are applied to the Wabash Valley related sources 43 and 44.

### 2.5.2.4.3.2 PSHA Sensitivity to Revisions of EPRI-SOG Sources and Additional Sources

Figure 2.5.2-228 shows the effect of possible revisions of the EPRI-SOG seismic sources and the inclusion of the source of repeated large earthquakes at New Madrid on the total hazard at the Fermi 3 Site. The inclusion of the source repeated large New Madrid earthquakes and the updating of the maximum magnitude distributions for the Wabash sources produce increases in the total mean hazard, particularly for 1 Hz spectral acceleration. Updating the maximum magnitude distributions for the local EPRI-SOG sources to account for recent or recently discovered earthquakes produces a slight increase in the hazard. The effect of the incorporation of the approximate estimate of the change in seismicity rates based on the updated catalog produces a decrease in the hazard at exceedance frequencies in the range of $10^{-4}$ to $10^{-5}$. This reduction is likely due to the fact that the added historical earthquakes are at large distances from the Fermi 3 site and are not affecting the seismicity rate locally. The increased recording period with limited additional seismicity thus produces a slight reduction in the local seismicity rate.

Based upon these results, the updated PSHA for the Fermi 3 site is conducted using the updates to the maximum magnitude distributions for the EPRI-SOG seismic sources described above and given in Table 2.5.2-201 through Table 2.5.2-206. The updated seismicity rates were not used as they were based on an approximate analysis of catalog completeness. This is a slight conservatism as the updated seismicity suggest slightly lower hazard.

#### 2.5.2.4.4 PSHA for the Fermi 3 Site

The PSHA for the Fermi 3 site was conducted using the updated seismic source model described in Subsection 2.5.2.4.3.2. Earthquake ground motions were modeled using the median ground motion models and the ground motion aleatory variability models developed by EPRI (Reference 2.5.2-259 and Reference 2.5.2-267). The logic tree defining the epistemic uncertainty in the ground motion characterization is shown on Figure 2.5.2-220.

The hazard analysis was conducted using the $m_b$ magnitude scale because the earthquake occurrence rates for the EPRI-SOG seismic sources are defined in terms of $m_b$ magnitudes. Epistemic uncertainty in the conversion from $m_b$ magnitudes to moment magnitudes (**M**) for ground motion estimation was modeled by using the three equally weighted conversion relationships listed on Figure 2.5.2-220. Conversion of the moment magnitude estimates for the size of the repeated earthquakes associated with New Madrid and for the updated maximum magnitude distributions for the Wabash Valley sources into $m_b$ magnitudes for summation of the hazard was done in a consistent manner such that the original value of **M** was recovered for ground motion estimation. For example, when the Boore and Atkinson (Reference 2.5.2-262) relationship was used to convert $m_b$ to **M** for ground motion estimation, its inverse was used to convert the **M** values for the New Madrid and Wabash Valley earthquakes into $m_b$ values.

Earthquakes occurring in the EPRI-SOG seismic sources were modeled as point sources, and the EPRI models for distance adjustment and additional aleatory variability resulting from the use of point sources (epicenter) to model earthquakes were applied (Reference 2.5.2-259). The models based on the assumption of a random rupture location with respect to the epicenter were used. Earthquakes occurring on the New Madrid source of repeated large earthquakes were modeled as extended ruptures, and the distance adjustment and additional aleatory variability models were not applied to these sources.

EPRI concluded that there was no basis for truncation of the lognormal distribution for ground motion amplitude other than the strength of the subsurface materials (Reference 2.5.2-267). Accordingly, untruncated lognormal distributions for earthquake ground motions were used in the PSHA.

The EPRI ground motion models represent the ground motions for a generic hard rock condition in the CEUS (Reference 2.5.2-259). Thus the site-specific PSHA results presented in this subsection represent the motions on outcropping rock with a shear-wave velocity in excess of about 2743 m/s (9000 fps). The effect of the sediments overlying this generic rock condition on defining the hazard at other locations is addressed in Subsection 2.5.2.5 and Subsection 2.5.2.6.

The initial generic CEUS hard rock hazard was computed using a fixed lower-bound magnitude of $m_b$ 5.0. These results were used to develop the appropriate response spectra and time histories for the site response analyses. Once the site amplification functions were developed, a second hazard assessment was performed incorporating the CAV approach to define the minimum magnitude truncation for the PSHA.

#### 2.5.2.4.4.1 PSHA Results for Generic Hard Rock Conditions

PSHA calculations were performed for response spectral accelerations at the seven structural frequencies provided in the EPRI ground motion model: 0.5, 1.0, 2.5, 5, 10, 25, and 100 Hz (peak ground acceleration [PGA]) (Reference 2.5.2-259). Figure 2.5.2-229 through Figure 2.5.2-235 show the resulting mean hazard curves and the 5th, 16th, 50th (median), 84th, and 95th fractile hazard curves for each ground motion measure. These values are listed in Table 2.5.2-211 through Table 2.5.2-217. At low spectral frequencies (≤1 Hz) the mean hazard approaches or exceeds the 84th percentile hazard due to the relatively large epistemic uncertainty in the ground motion models at these frequencies as compared to that for higher-frequency ground motions (e.g., see Figure 2.5.2-221).

Figure 2.5.2-236 shows the contribution of three groups of seismic sources to the mean hazard for 10 Hz and 1 Hz spectral acceleration. As was found in the sensitivity test described in Subsection 2.5.2.4.3.2, the repeating large-magnitude New Madrid (NM) fault dominates the hazard for 1 Hz spectral accelerations. The EPRI-SOG Wabash Valley sources with updated maximum magnitude distributions motions also have a significant contribution to the 1 Hz hazard.

Figure 2.5.2-237 shows the effect of the alternative ground motion cluster models on the median hazard. As described in Subsection 2.5.2.4.2.1, the cluster 4 model is only used for seismic sources where the hazard is dominated by large-magnitude earthquakes. Thus the results labeled

cluster 4 represent the median hazard computed assigning a weight of one to the use of cluster 4 for the large-magnitude sources (e.g., Wabash Valley sources and the repeated large earthquake source at New Madrid) combined with the weighted average of the hazard obtained from the other three cluster models for all other sources. In general, use of the cluster 3 ground motion model produces the highest hazard.

Figure 2.5.2-238 shows the effect of the epistemic uncertainty in the median ground motion models for each cluster on the mean hazard, respectively. The uncertainty in the hazard is somewhat greater for low-frequency motions than for high-frequency motions, reflecting greater uncertainty in the median low-frequency ground motion models. Examination of the hazard results indicated that the alternative aleatory variability models developed by EPRI (Reference 2.5.2-267) produced similar hazard.

Figure 2.5.2-239 shows the effect of using the alternative $m_b$-**M** conversion relationships on the computed mean hazard. Similar estimates of seismic hazard are obtained using each of the relationships. The effect of the alternative models on the hazard disappears at ground motion levels where the hazard is dominated by the repeated large earthquakes at New Madrid. As discussed previously, the alternative models were used in such a way that the moment magnitudes for the repeated large earthquakes specified on Figure 2.5.2-211 are always used for ground motion estimation.

Figure 2.5.2-240 shows the range in the computed hazard from just the updated EPRI-SOG sources and the mean hazard obtained from the seismic source models for the individual teams. The difference between the individual teams' results is similar for 10 Hz motion and for 1 Hz motions.

The other model uncertainties that were found to have a significant contribution to the uncertainty in the hazard were the uncertainty in the seismicity parameters for the 10 Hz motions and the uncertainty in the expected magnitude of the repeated large earthquakes occurring at New Madrid.

#### 2.5.2.4.4.2 Uniform Hazard Spectra for Generic CEUS Rock and Identification of Controlling Earthquakes

The mean hazard results listed in Table 2.5.2-211 through Table 2.5.2-217 were interpolated to obtain uniform hazard response spectra

(UHRS) for generic CEUS hard rock conditions. The spectra were computed for mean annual frequencies of exceedance of $10^{-3}$, $10^{-4}$, $10^{-5}$, and $10^{-6}$. These spectra are shown on Figure 2.5.2-241 and listed in Table 2.5.2-218.

Figure 2.5.2-242 through Figure 2.5.2-245 show the deaggregation of the mean hazard for the four values of exceedance frequency. Following the procedure outlined in Appendix D of Regulatory Guide 1.208, the deaggregation is conducted for two frequency bands: (1) the average of the 5 Hz and 10 Hz hazard results representing the high-frequency (HF) range and (2) the average of the 1 Hz and 2.5 Hz hazard results representing the low-frequency (LF) range. The results shown on the figures were obtained by first computing the percentage contribution of events in each magnitude-distance bin individually for the four spectral frequencies (1, 2.5, 5, and 10 Hz). The HF deaggregation was then obtained by averaging these values for 5 and 10 Hz and the LF deaggregation obtained by averaging the results for 1 and 2.5 Hz. The HF deaggregation shows a progression from domination of the hazard by large, distant earthquakes at a mean exceedance frequency of $10^{-3}$ to dominance by nearby small-magnitude earthquakes at a mean exceedance frequency of $10^{-6}$. This effect can be seen in the change in shapes of the UHRS, which become more sharply peaked at 25 Hz as the contributions from nearby smaller-magnitude earthquakes increase. The LF deaggregation indicates that the distant large-magnitude earthquakes dominate the hazard at all four levels of exceedance frequency.

Appendix C of Regulatory Guide 1.165 specifies how the deaggregation results are used to define what are called controlling earthquakes for the HF and LF motions. These earthquakes represent the weighted mean magnitude and weighted geometric mean distance, where the weights are defined by the relative contributions to the total hazard for each magnitude and distance interval. Table 2.5.2-219 lists the mean magnitudes and geometric mean distances computed for the HF and LF spectral frequency ranges for the four mean annual frequency of exceedance levels. The values for the LF hazard are listed considering all earthquakes and considering only those earthquakes occurring at distances greater than 100 km (62 mi.), consistent with the procedure outlined in Appendix C of Regulatory Guide 1.165.

The approach to be used to compute the effects of the Fermi 3 site sediments on the generic hard rock motions is Approach 2B for site response analyses described in NUREG/CR-6728 (Reference 2.5.2-270). This approach defines what are called reference earthquakes (RE). The REs are defined in the same manner as the controlling earthquakes defined in Appendix C of Regulatory Guide 1.165.

Comparison of the computed controlling or RE magnitudes and distances with the deaggregation results indicates that in many cases the mean magnitude and mean distance correspond to a magnitude-distance bin that has a relatively small contribution to the hazard, particularly for the HF hazard results. Site response Approach 2B addresses this problem by using a range of magnitude-distance pairs to reflect the distribution of earthquakes contributing to the HF and LF hazard. Typically, three deaggregation earthquakes (DE) at high frequency and three at low frequency are adequate to represent the distribution of earthquakes contributing to the hazard. These are designated DEL, DEM, and DEH for the low-magnitude, middle-magnitude, and high-magnitude DEs, respectively. The site response uses ground motions representative of the DEL, DEM, and DEH as input ground motions.

For the Fermi 3 site, the DEL, DEM, and DEH magnitude-distance values were defined to represent the modes in the magnitude-distance deaggregation. As shown by the red-blue-green color coding on Figure 2.5.2-242 through Figure 2.5.2-245, three magnitude-distance domains were identified that represent peaks in the deaggregated hazard and that, in combination, account for greater than 99 percent of the hazard. The DE magnitude and distances are computed as the weighted mean values over the defined domains. The resulting DEs are listed in Table 2.5.2-219. The weight assigned to each DE is defined by the relative contribution of the earthquakes in the magnitude-distance domain to the total hazard. The resulting weights are listed in the right-hand column of Table 2.5.2-219. The weighted combination of the DEs also produces a magnitude-distance pair that is very close to the RE.

#### 2.5.2.4.4.3 Response Spectra for Reference and Deaggregation Earthquakes

Smooth response spectra were developed to represent each of the reference and DEs listed in Table 2.5.2-219. These spectra were developed using the EPRI (Reference 2.5.2-259) median ground motions models, the EPRI (Reference 2.5.2-267) aleatory variability models, and

the spectral shape functions for CEUS ground motions presented in McGuire et al. (Reference 2.5.2-270).

The DEs are intended to represent the motions from earthquakes that are contributing to the hazard in a specific frequency range, either 1 to 2.5 Hz (LF) or 5 to 10 Hz (HF) for the purpose of computing site amplification functions. The development of the appropriate spectral shapes for the DEs uses the concept of the conditional mean spectrum developed by Baker and Cornell (Reference 2.5.2-271). The conditional mean spectrum is defined as the expected earthquake spectrum given that the spectral acceleration matches a specific value at a specific frequency. This spectrum is constructed taking into account the correlation between response spectral amplitudes at two different frequencies observed in strong ground motion. For example, the $10^{-4}$ UHRS amplitude at a frequency of 10 Hz may represent the 84th percentile ground 10 Hz spectral acceleration based on the DEL magnitude and distance and one of the EPRI ground motion models (Reference 2.5.2-259, Reference 2.5.2-267). Given that the spectral acceleration at 10 Hz represents a 1-epsilon ground motion, the expected value of epsilon at other frequencies is equal to the epsilon at 10 Hz multiplied by the correlation coefficient between the motions at 10 Hz and other frequencies. The resulting conditional mean spectrum represents the expected frequency content of earthquake motions that produce ground motions equal to the UHRS at the target frequency of 10 Hz.

Baker and Cornell developed a model for the correlation coefficient between spectral accelerations at any two frequencies (Reference 2.5.2-271). Their model covered the frequency range of 0.2 to 20 Hz. Baker and Jayaram (Reference 2.5.2-272) have extended the Baker and Cornell (Reference 2.5.2-273) model to cover the frequency range of 0.1 to 100 Hz.

This extended model was used to compute conditional mean spectra for the DEs. As an example, the $10^{-4}$ DEH for LF is listed in Table 2.5.2-219 as an $m_b$ 7.1 earthquake occurring at a distance of 500 km (310 mi.) from the site. A combination of a median ground motion model, aleatory variability model, and $m_b$-**M** conversion defined in the ground motion model logic tree (Figure 2.5.2-220) is used to compute number of standard deviations (denoted by $\varepsilon$) that the 1 Hz and 2.5 Hz $10^{-4}$ UHRS accelerations lies away from the median ground motion defined by the selected model. These two values of $\varepsilon$ are averaged and assigned to a

frequency equal to the geometric mean of 1 and 2.5 Hz. The expected value of $\varepsilon$ at other frequencies is then computed using the Baker and Jayaram model (Reference 2.5.2-272). The conditional mean spectral shape is then computed using the selected median and aleatory variability models. The spectral shape is smoothed between the seven frequencies defined in the EPRI ground motion model using the average of the single-corner and double corner spectral shape models developed in McGuire et al. (Reference 2.5.2-270).

The McGuire et al. (Reference 2.5.2-270) spectral shape models are also used to extrapolate the EPRI median ground motion model from a frequency of 0.5 Hz down to a frequency of 0.1 Hz (spectral period of 10 seconds) to extend the construct response spectra for the DEL and DEM events and the HF RE events from 0.5 Hz to 0.1 Hz. The magnitudes and distances for these events fall within the ranges of values considered by McGuire et al. (Reference 2.5.2-270) in developing their spectral shapes. The DEH events and the LF RE events represent large earthquakes occurring at large distances from the Fermi 3 site. The ability of the McGuire et al. (Reference 2.5.2-270) spectral shape models to represent the low-frequency portion of the spectrum for these events was examined by comparing the predicted spectral shape with spectral shapes of recent CEUS ground motion models that provide ground motion values at frequencies below 0.5 Hz.

Figure 2.5.2-250 presents response spectral shapes for a moment magnitude 7¾ earthquake at a distance of 750 km (466 mi.). This magnitude is the average moment magnitude converted from the $m_b$ value of 7.3 representing the LF REs, and the distance is the closest distance to the source of the repeated large earthquakes at New Madrid. The spectral shapes are presented in terms of pseudo-spectral velocity as this provides a clearer picture of the low-frequency spectral shape. The spectral shapes are normalized by the predicted amplitude at a frequency of 0.5 Hz as it is the extrapolation below 0.5 Hz that is of interest. Normalized spectral shapes are presented for the two McGuire et al. (Reference 2.5.2-270) CEUS spectral shape models and for a number of recently developed models. Also shown are normalized spectral shapes obtained using the models of Silva et al. (Reference 2.5.2-264), Atkinson and Boore (Reference 2.5.2-265), Campbell (Reference 2.5.2-263), Tavakoli and Pezeshk (Reference 2.5.2-266), and Somerville et al. (Reference 2.5.2-274). The recently developed ground

motion models suggest that the extrapolation of the response spectral shape below 0.5 Hz for this large, distant earthquake is closer to constant spectral velocity (1/T spectral acceleration scaling). Therefore, constant spectral velocity scaling was used to extend the DEH and LF RE spectra from 0.5 Hz to 0.1 Hz.

The extrapolation from 0.5 Hz to 0.1 Hz requires an assessment of the aleatory variability in spectral acceleration at frequencies less than 0.5 Hz. The EPRI (Reference 2.5.2-267) models are based on empirical ground motion models developed as part of the Pacific Earthquake Engineering Research (PEER) Center's Next Generation Attenuation (NGA) Project. The five NGA ground motion models available from PEER (Reference 2.5.2-275 through Reference 2.5.2-279) include estimates of aleatory variability for spectral frequencies between 0.1 and 100 Hz. These models indicate that the standard deviation of the natural log of spectral acceleration is, on average, 15 percent higher at a frequency of 0.1 Hz than it is at a frequency of 0.5 Hz. A linear increase in aleatory variability with decreasing log frequency from 0 percent at 0.5 Hz to 14 percent at 0.1 Hz was used to extend the EPRI (Reference 2.5.2-267) aleatory variability models down to a frequency of 0.1 Hz. The calculation is then repeated for each combination of median, aleatory variability, and $m_b$-**M** conversion defined in the ground motion model logic tree (Figure 2.5.2-220). A weighted average of these spectra is then computed using the weights defined on Figure 2.5.2-220. The resulting spectral shape is then smoothed and rescaled to match on average the UHRS at 1 and 2.5 Hz. The resulting DE response spectra are shown on Figure 2.5.2-246 through Figure 2.5.2-249.

The RE or controlling earthquake spectra are used to define a smooth spectral shape representative of the rock UHRS. Their primary use in Approach 2B is to produce a smooth surface spectrum consistent with the rock UHRS when multiplied by the site amplification function. As such, they represent the composite effects of a range of earthquake magnitude and distances, and it is desirable that their spectra lie close to the UHRS over a broad frequency range. Accordingly, the spectral shapes for the REs were developed using the above process with the modification that the correlation in $\varepsilon$ between spectral frequencies was set to 1.0. The resulting RE spectral shapes are also shown on Figure 2.5.2-246 through Figure 2.5.2-249.

As can be seen on Figure 2.5.2-246 through Figure 2.5.2-249, the rock UHRS at 0.5 Hz typically lies above the low-frequency (LF) RE spectra. Thus scaling the low-frequency RE spectrum by the low-frequency amplification function will underestimate the appropriate surface motions that are hazard consistent with the rock UHRS. To address this issue, the rock UHRS was extended from 0.5 Hz down to 0.1 Hz by computing a second low-frequency RE spectrum that matches the UHRS at 0.5 Hz. This additional spectrum is denoted by the "LF Extended" spectral shape shown on Figure 2.5.2-246 through Figure 2.5.2-249. This spectral shape was developed using constant spectral velocity scaling, as it primarily represents the hazard from a large, distant earthquake.

#### 2.5.2.5 Seismic Wave Transmission Characteristics of the Site

The uniform hazard response spectra shown on Figure 2.5.2-241 represent ground motions occurring on generic CEUS hard rock conditions. As described in Subsection 2.5.4.2.1, the materials underlying the Fermi 3 site consists of thin layers of fill, lacustrine deposits, and glacial till overlying dolomite of the Bass Islands and Salina groups. The velocities of the upper approximately 130 m (425 ft.) of these rocks are generally lower than the generic CEUS hard rock velocity, thus necessitating an assessment of site amplification to develop the site surface motions.

Site response analyses were conducted to evaluate the effect of the sedimentary bedrock on the generic CEUS hard rock ground motions. The intent of these analyses is to develop ground motions at the surface that are hazard-consistent with the hazard levels defined for the generic rock conditions. This hazard consistency is achieved through the use of the site response Approach 2B outlined in NUREG/CR-6728 (Reference 2.5.2-270). The following steps are involved in this approach:

1. Characterize the dynamic properties of the subsurface materials.
2. Randomize these properties to represent their uncertainty and variability across the site.
3. Based on the deaggregation of the rock hazard, define the distribution of magnitudes contributing to the controlling earthquakes for HF and LF ground motions (these are termed DEs in McGuire et al. (Reference 2.5.2-270), and define the response spectra appropriate for each of the DEs.

4. Obtain appropriate rock site time histories to match the response spectra for the DEs.
5. Compute the mean site amplification function for the HF and LF controlling earthquakes based on the weighted average of the amplification functions for the DEs.
6. Scale the response spectra for the controlling earthquakes by the mean amplification function to obtain surface motions.
7. Envelop these scaled spectra to obtain surface motions hazard-consistent with the generic CEUS hard rock hazard levels.

Step 3 of this process is described in Subsection 2.5.2.4.4.2. Steps 6 and 7 are described in Subsection 2.5.2.6. Steps 1, 2, 4, and 5 are presented in this subsection.

#### 2.5.2.5.1 Dynamic Properties of the Fermi 3 Site

The shear ($V_s$) and compression ($V_p$) wave velocity data obtained at the Fermi 3 site are described in Subsection 2.5.4.4.1.

The interval velocity data was used to construct travel time plots in terms of layered velocity models (Reference 2.5.2-280). These are shown by the lines labeled “PS Layered Model” on Figure 2.5.2-251, Figure 2.5.2-252, Figure 2.5.2-253, and Figure 2.5.2-254. These interpretations provide a useful basis for defining the appropriate velocity for depth intervals where the average velocity is relatively constant. The interval velocity data and the interpreted layered velocity models indicate three general velocity layers with the rock units. As presented in Subsection 2.5.4.4.1, the average interval shear wave velocities in Salina Group Unit B are generally greater than 9200 fps, and, therefore, elevation 48 m (156 ft.) is taken to be the point at which CEUS generic hard rock is encountered at the site.

The interval velocity data shown on Figure 2.5.2-251, Figure 2.5.2-252, Figure 2.5.2-253, and Figure 2.5.2-254 indicate that the transition from the Bass Islands Group to the Salina Group Unit F occurs over a transition zone rather than as an abrupt step. The thickness of this zone is in the range of 2 to 6 m (6 to 20 ft.). Similarly, there appears to be a transition in velocity at the boundary between Salina Group Units F and E. Velocities in this transition zone were assessed by computing the harmonic mean of the suspension interval velocities over specific depth ranges. These velocity values are indicated by curves labeled “Averaged

PS" on Figure 2.5.2-251, Figure 2.5.2-252, Figure 2.5.2-253, and Figure 2.5.2-254. The "Averaged PS" velocities are close to the PS Layered Model values where the averaging is done over the same depth range, indicating that the two approaches for estimating an average layer velocity produce consistent estimates.

Using the PS Layered Model and Averaged PS interpretations, velocity profiles were developed for each boring as shown on Figure 2.5.2-251, Figure 2.5.2-252, Figure 2.5.2-253, and Figure 2.5.2-254. Figure 2.5.2-255 compares these four velocity profiles. The four profiles have similar characteristics, indicating that a single velocity profile is appropriate for the Fermi 3 site. This profile is computed as the geometric mean of the velocity profiles developed for each boring and is shown on Figure 2.5.2-255.

Regulatory Guide 1.208 states that the site SSE (defined as the ground motion response spectrum (GMRS)) is to be defined at the ground surface or at the top of the first competent layer, nominally with a velocity of 1000 fps or greater. The materials overlying the Bass Islands Group rock consist of approximately 4 m (13 ft.) of fill, approximately 1.5 m (5 ft.) of low-velocity lacustrine deposits, and 3.4 m (11 ft.) of glacial till. The fill and lacustrine deposits are to be removed in the Fermi 3 area during construction (Subsection 2.5.4.2.1.1). The glacial till materials are proposed to remain except in the vicinity of seismic Category I structures. The measured shear-wave velocities in the till in the vicinity of the seismic Category I structures are in the range of 940 to 1150 fps, with a geometric mean velocity of 1000 fps; therefore, the GMRS location is taken to be at the top of the till with and average elevation of 172 m (563 ft.) NAVD 88.

In addition to the GMRS, foundation input response spectra (FIRS) are needed at the base of the Reactor/Fuel Building (R/FB), the Control Building (CB), and the Fire Water Service Complex (FWSC). Foundation elevation for these structures are approximately 160 m (524 ft.), 164 m (540 ft.), and 177 m (582 ft.) NAVD 88, respectively (Table 2.5.4-224). The R/FB and CB are founded within the Bass Islands Group and the FIRS analyses profiles for these facilities are constructed by removing material above the foundation elevation from the GMRS profile shown on Figure 2.5.2-255. The FWSC is to be founded on lean concrete fill extending to the bedrock with an estimated Young's modulus of 142,200 ksf and a bulk unit weight of 145 pcf (Subsection 2.5.4.10.2). Using a

Poisson's ratio of 0.2 for lean concrete, the assigned values of Young's modulus and bulk density translate into a shear wave velocity of approximately 3600 fps. The FIRS analysis profile for the FWSC was constructed by placing approximately 9 m (30 ft.) of lean concrete on the top of the Bass Islands Group rocks.

The velocities and average layer thickness of the GMRS and three FIRS analysis profiles are listed in Table 2.5.2-220.

#### 2.5.2.5.1.1 Density

Table 2.5.2-220 lists the average unit weight of the subsurface materials. These are taken from Table 2.5.4-202.

#### 2.5.2.5.1.2 Shear Modulus and Damping

The top layer of the GMRS analysis profile consists of glacial till. The average plasticity index (PI) of this material is 14. As discussed in Subsection 2.5.4.7.5, a representative set of modulus reduction and damping relationships for this material were selected to be those developed by Vucetic and Dobry (Reference 2.5.2-281) for clays with a PI of 15. These relationships are shown on Figure 2.5.2-256. The curves developed by Vucetic and Dobry (Reference 2.5.2-281) are based in large part on remolded samples. In order to account for possible aging effects producing more linear behavior in the till, a second set of modulus reduction and damping relationships were also used. These consist of the Vucetic and Dobry (Reference 2.5.2-281) relationships for clays with a PI of 50 and are shown on Figure 2.5.2-256. The laboratory test results presented in Subsection 2.5.4.7.5 fall within the range of these two published relationships and within the range of randomized modulus reduction and damping relationships used in the site response analyses.

The remaining portion of the GMRS profile consists of dolomites and claystones with shear wave velocities in excess of 3,000 fps. This material is expected to remain essentially linear at the levels of shaking defined by the rock hazard. The damping within these materials was established using the following procedure.

The site response analyses were conducted using an updated version of program SHAKE originally developed by Schnabel et al. (Reference 2.5.2-282). The energy lost in shear-wave propagation was measured by the shear-wave quality factor, $Q_S$, which can be equated to two other representations of energy loss in wave-propagation analysis. For the linear

viscoelastic wave-propagation modeling used in program SHAKE, the material damping, $\xi$, is obtained by the relationship:

$$\xi = \frac{1}{2Q_S} \quad \text{[Eq. 7]}$$

Parameter $Q_S$ is also related to the high-frequency attenuation parameter $K$ developed by Anderson and Hough (Reference 2.5.2-283) by the relationship:

$$\kappa = \frac{H}{Q_S V_S} \quad \text{[Eq. 8]}$$

where $H$ is the thickness of the crust over which the energy loss occurs, typically taken to be 1 to 2 km (0.6 to 1.2 mi.) (Reference 2.5.2-284). Silva and Darragh (Reference 2.5.2-284) find that $Q_S$ is proportional to shear-wave velocity:

$$Q_S = \gamma V_S \quad \text{[Eq. 9]}$$

where $\gamma$ is the constant of proportionality. Using this assumption, the amount of high-frequency attenuation in the $i^{th}$ layer of a velocity profile, $k_i$, is given by the relationship:

$$\kappa_i = \frac{H_i}{\gamma V_{Si}^2} \quad \text{[Eq. 10]}$$

where $H_i$ is the layer thickness and $V_{Si}$, is the layer shear-wave velocity. Given the total value of $k$ appropriate for the site, one can solve for the corresponding value of $\gamma$. Using the resulting value of $\gamma$ and Equations 7, 8, and 10, the appropriate damping values for each layer are then obtained.

The attenuation models for CEUS hard rock are developed assuming a shallow crustal $k$ of approximately 0.006 second (Reference 2.5.2-283). This point is placed at elevation 48 m (156 ft.). The material above this elevation will contribute additional damping and thus add to the total site $k$. EPRI (Reference 2.5.2-285) gives the following relationship between $k$ and site shear-wave velocity:

$$\log(\kappa) = 2.2189 - 1.0930 \log(V_S) \qquad \text{[Eq. 11]}$$

where $V_s$ is shear-wave velocity in fps and *k* is in seconds. The average shear-wave velocity of the rocks above elevation 48 m (156 ft.) is 5700 fps. Using this value in Equation 11 yields a *k* value of 0.013 seconds. Subtracting the hard rock value of 0.006 yields a remaining *k* of 0.007 seconds. If this value is attributed to the top 131 m (396 ft.) of dolomite, the damping values computed using the above equations will be in the range of 3 to 7 percent. This value appears to be large in comparison with the low strain damping values typically assigned to soft rock materials. Silva et al. (Reference 2.5.2-286), as modified by Silva (Reference 2.5.2-287), proposed modulus reduction and damping relationships for soft rock that have low-strain damping values on the order of 3 percent. These would be expected to apply to relatively low velocity rocks. The Salina Group Unit F layer at the Fermi site is perhaps in the upper range of soft rock velocities. A set of modulus reduction and damping relationships used by EPRI (Reference 2.5.2-285) to model the behavior of soft rock that has low-strain damping values on the order of 1 percent or less. Based on these values, it was assumed that the low-stain damping in the softest rock layer, Salina Group Unit F is in the range of 1 percent to 3 percent. Using Equations 7, 8, and 10, damping values were computed for the remaining rock layers assuming that $Q_S$ is proportional to $V_s$. The resulting values are listed in Table 2.5.2-221 along with the corresponding values of a *k* for each layer. The result is that the assigned values of damping add an additional *k* of 0.001 to 0.003 seconds.

The value of *k* assigned to a site profile is a measure of the total damping due to both material damping and scattering effects. To account for this in a one-dimensional (1-D) site response model, the conversion from *k* to material damping should account for the scattering (reflection) of waves off layer boundaries, particularly velocity reversals. In addition to those present in the initial velocity model, the process of profile randomization to account for site variability, discussed in Subsection 2.5.2.5.1.3, will introduce additional velocity reversals. The amount of *k* that is attributed to scattering in the site velocity profiles was assessed by comparing the median response of the randomized velocity profiles to a simple model with uniform velocity layers. The process used is shown on Figure 2.5.2-257. The randomized velocity profiles are used to compute the response of the site with the value of *k* set to zero in the rock layers under

a very low level of input motion. The randomized velocity profiles are then replaced by a simple model of a single layer with a velocity equal to the average velocity of the rock profile (5680 fps). The response computed using this model and zero *k* is higher at high frequencies. The response analysis for the single-layer model is repeated, gradually increasing the value of *k* until the high-frequency response is similar to that for the randomized site profiles. As shown on Figure 2.5.2-257, the resulting value of *k* is 0.001 seconds.

The range in total site *k* obtained by combing the generic CEUS hard rock value, the site scattering value and the values based on the damping assigned to the rock layers is 0.008 to 0.010 seconds.

The dynamic properties of the lean concrete backfill were assessed based on test data on the dynamic properties of low strength concrete mixtures in Hasek (Reference 2.5.2-288). The shear modulus of the materials tested was in the range of 25,000 to 59,000 psi (Reference 2.5.2-288). Using a bulk density of 145 pcf, this translates into a range in shear wave velocity of about 900 to 1400 fps. The low-strain damping ratios from these tests were in the range of 1.5 to 2.5 percent (Reference 2.5.2-288). The planned shear wave velocity for the lean concrete backfill is on the order of three to four times that of the test samples given in Hasek (Reference 2.5.2-288). The assumption above that $Q_S$ is proportional to velocity suggests that a fourfold increase in velocity should translate into a four fold decrease in damping. Therefore, the low-strain damping in the lean concrete backfill was assumed to be 0.5 percent. The lean concrete backfill was assumed to remain linear for shear strains less than 0.01 percent and then exhibit a mild degree of nonlinearity at higher strains. The assumed modulus reduction and damping relationships are shown on Figure 2.5.2-256.

#### 2.5.2.5.1.3 Randomization of Dynamic Properties

Site response analyses were conducted using randomized shear-wave velocity profiles to account for variations in shear-wave velocity. The randomized profiles were generated using the shear-wave velocity correlation model developed in Silva et al. (Reference 2.5.2-286). In this model, the shear-wave velocity in the sediment layers are modeled as correlated, lognormal distributed variables. The expression for the correlation coefficient between the velocities in two adjacent layers, $\rho$ is given by:

$$\rho(h,t) = (1-\rho_d(h))\rho_t(t) + \rho_d(h) \qquad \text{[Eq. 12]}$$

where $\rho_d(h)$ represents the depth-dependent correlation (generally increasing with increasing depth), and $\rho_t(t)$ is the thickness-dependent correlation (generally decreasing with increasing layer thickness). The factors $\rho_d(h)$ and $\rho_t(t)$ are obtained from the expressions:

$$\rho_d(h) = \begin{cases} \rho_{200}\left[\dfrac{h+h_0}{200+h_0}\right]^b & for \quad h \le 200\ m \\ \rho_{200} & for \quad h > 200\ m \end{cases} \qquad \text{[Eq. 13]}$$

and

$$\rho_t(t) = \rho_0 \exp\left[-\left(\frac{t}{\Delta}\right)^{\alpha}\right] \qquad \text{[Eq. 14]}$$

where *h* is the average of the midpoint depths of layers *i* and *i-1*, and *t* is the difference between those midpoint depths. Parameters $h_0$, $p_0$, $p_{200}$, $\Delta$, $\alpha$, and $\beta$ are parameters of the model. The correlation model parameters developed in Silva et al. for stiff soil sites were used in the simulations (Reference 2.5.2-286). Stiff soil site parameters were chosen because the site is underlain by a relatively flat-lying sedimentary rock sequence that is assumed to have velocity variability similar to a layered soil site.

The data from the Fermi site display low to moderate variability in velocity at shallow depth with a $\sigma_{ln(Vs)}$ of approximately 0.1, increasing to 0.2 in the Salina Group Unit F. These values are similar to those obtained from analyses of individual firm soil sites (Reference 2.5.2-286), and these values were used to develop randomized velocity profiles. The locations of velocity layer boundaries were randomized to vary uniformly within the range of layer thickness observed in the site borings.

Sixty randomized $V_s$ profiles were generated for the GMRS profile. Figure 2.5.2-258 and Figure 2.5.2-259 show the randomized velocity profiles. The statistics of the randomized profiles are compared to the input target values for median velocity and standard deviation (sigma) of $ln(V_s)$ on Figure 2.5.2-260.

The modulus reduction and damping relationships were also randomized, as shown on Figure 2.5.2-261, Figure 2.5.2-262, and Figure 2.5.2-263. The standard deviation in the modulus reduction and damping were set so that the randomized relationships fell within recommended bounds provided by Silva (Reference 2.5.2-287). The damping ratio curves were limited to a maximum of 15 percent damping as recommended in Appendix E of Regulatory Guide 1.208.

The damping in the sedimentary rocks beneath the soil profile was computed using the randomized sedimentary rock layer velocities and thicknesses and the selected values of $\kappa$.

#### 2.5.2.5.2 Acceleration Time Histories for Input Rock Motions

Response spectra were developed for each DE, as described in Subsection 2.5.2.4.4.3. Thirty time histories were developed for each DE from the time history sets given in McGuire et al. (Reference 2.5.2-270). Table 2.5.2-222 lists the time history sets used. The selected time histories were scaled to approximately match the target DE spectrum using a limited number of iterations of the program RASCALS (Reference 2.5.2-289). Figure 2.5.2-264 shows the response spectra for the 30 time histories scaled to match the HF and LF DEL and DEH spectra for mean $10^{-4}$ ground motions.

The purpose of randomization of the site properties is to account for natural variability in defining the site response. Part of the natural variability is variability in the ground motions of an individual earthquake. That is why only weak scaling of the time histories was performed. The weak scaling produces recordings that have, in general, the desired relative frequency content of the DE spectra while maintaining a degree of natural variability. The use of three DE for both HF and LF motions along with a large number of recordings provides adequate coverage of the frequency band of interest. The acceleration time histories represent free field outcropping motions for generic CEUS hard rock.

#### 2.5.2.5.3 Site Amplification Functions

Site amplification functions were developed for each DE. The 60 randomized velocity profiles were paired with the 60 sets of randomized modulus reduction and damping curves (one profile with one set of modulus reduction and damping curves). Each of the 30 scaled time histories was used to compute the response of two profile-soil property curves sets. For each analysis, the response spectrum for the computed

surface motion was divided by the response spectrum for the input motion to obtain a site amplification function. The arithmetic mean of the 60 individual response spectral ratios is then computed to define the amplification function.

Figure 2.5.2-265 shows an example of the statistics of the 60 individual site amplification functions for one analysis case. Shown are the median (mean log), 16th percentile (mean log – sigma log), 84th percentile (mean log + sigma log), and arithmetic mean amplification. The mean amplification function is used in Approach 2B.

For each DE, mean amplification functions were computed for the three sets of values of rock damping and for the two sets of modulus reduction and damping relationships for the till. The results from the three DEs are then combined to produce a weighted mean amplification function for the RE. Figure 2.5.2-266 shows the site response model logic tree used to compute the RE mean amplification function. The weights assigned to the DEs are given in Table 2.5.2-222.

The sensitivity of the mean amplification function to the value of rock damping is shown on Figure 2.5.2-267. The range in damping leads to approximately a 15 percent difference in mean amplification at 100 Hz, 20 percent difference near 40 Hz, decreasing to about less than 8 percent at 10 Hz. The effect of the assigned damping continues to decreases for frequencies below 10 Hz.

Figure 2.5.2-268 shows the effect of the alternative property curves assigned to the glacial till on the mean amplification for the GMRS profile. The difference in the high-frequency amplification computed using the two sets of modulus reduction and damping is generally in the range of 5 to 8 percent.

Figure 2.5.2-269 shows the DEL, DEM, and DEH amplification functions for $10^{-4}$ ground motions for the GMRS profile and the weighted mean amplification. The site amplification functions are insensitive to the differences in the DE.

Figure 2.5.2-270 shows the mean GMRS site amplification functions for the four levels of input motion. Because the non-linear behavior is limited to the thin glacial till layer, the site amplification is insensitive to the level of motion for frequencies less than about 8 Hz. The statistics for the level of effective strain computed in the analyses for the $10^{-4}$ and $10^{-5}$ input ground motions are show on Figure 2.5.2-271 and 2.5.2-272,

respectively. The effective strains are generally less than 0.01 percent, except in the glacial till.

The process described above for developing the GMRS profile amplification functions was repeated for the three FIRS profiles. For the R/FB and CB profiles, the analyses were performed with all material above the foundation elevation removed.

Figure 2.5.2-273, Figure 2.5.2-274, and Figure 2.5.2-275 show the mean site amplification functions for $10^{-4}$ and $10^{-5}$ input ground motions for the FIRS profiles for the R/FB, CB, and FWSC, respectively. These profiles show little sensitivity to the level of motion because the rock is assumed to behave linearly and the lean concrete backfill has very linear modulus reduction and damping relationships.

### 2.5.2.6 Ground Motion Response Spectra

#### 2.5.2.6.1 Hazard-Consistent Surface Spectra

Surface hazard spectra for the GMRS profile are obtained by scaling the rock RE and UHRS by the site amplification functions. The process used is illustrated on Figure 2.5.2-276 for the $10^{-4}$ level ground motions.

- The reference (controlling) spectra for LF and HF motions developed were scaled by the appropriate smoothed amplification function to produce ground surface spectra.
- The generic hard rock UHRS was also scaled using the appropriate LF and HF amplification values.
- A smooth envelope of the scaled spectra is constructed to define the surface $10^{-4}$ UHRS.

The rock UHRS exhibit a sharp peak at 25 Hz as shown on Figure 2.5.2-241. This peak is an artifact of the fact that the PSHA is computed for frequencies of 10, 25 and 100 Hz and that the RE spectra are defined for frequencies in the range of 5 to 10 Hz. The spectral shapes for CEUS earthquakes developed in McGuire et al. (Reference 2.5.2-270) show a broader peak in the spectrum in the frequency range of 10 to 100 Hz. Therefore, the approach described in Subsection 2.5.2.4.4.3 was used to smoothly interpolate the rock UHRS between 10 and 100 Hz. An additional HF RE spectral shape was constructed to match the rock UHRS at 25 Hz. This shape was then adjusted to match the UHRS at 10 and 100 Hz by applying adjustment factors that varied linearly with log frequency from 0 at 25 Hz to the appropriate value at 10 or 100 Hz. This

smoothed rock UHRS was then multiplied by the HF amplification function.

The amplification functions and the corresponding surface spectrum shows a dip in the frequency range of 6 to 12 Hz. This results from peaks in the response occurring near 20 Hz from the glacial till layer and near 4 Hz from the overall rock profile. The dip was conservatively removed in constructing the surface UHRS. As a result, the final spectra will be conservative in the frequency range of 6 to 12 Hz.

Similar operations were performed to develop surface spectra for the $10^{-5}$ and $10^{-6}$ exceedance level motions. These smooth envelope spectra represent the surface UHRS for the site defined as free field outcropping motions at elevation 172 m (563 ft.)

Figure 2.5.2-277 shows the development of the surface UHRS for the R/FB FIRS profile. The same process was used as described above for the GMRS profile, including smoothing through the dip in the spectrum between 6 and 12 Hz.

#### 2.5.2.6.2 Incorporation of Cumulative Absolute Velocity (CAV)

The PSHA results used above for developing the RE and DE spectra were computed using a fixed lower bound magnitude of $m_b$ 5. Regulatory Guide 1.208 indicates that an alternative method that is based on the probability that earthquakes of a given magnitude can produce damaging ground motions, defined as ground motions with a CAV greater than 0.16 g-second, may be used. EPRI developed an approach for conducting a PSHA incorporating the probability that ground motions produced by an earthquake with magnitude value *m* will have a value of CAV greater than 0.16 g-second (Reference 2.5.2-290).

The EPRI CAV model was implemented in a second set of PSHA calculations for the Fermi 3 site. These calculations include the contributions from all earthquakes above $m_b$ 4.0 weighted by the probability that they can produce a CAV greater than 0.16 g-second. The EPRI CAV model uses moment magnitude (**M**) as the magnitude scale. The model results indicate that earthquakes of magnitude less than **M** 4 have very little probability of producing a CAV greater than 0.16 g-second (Reference 2.5.2-290). The magnitude conversions used in the PSHA convert an $m_b$ magnitude of 4.0 into **M** magnitudes that are less than 4.0.

The EPRI CAV model is based on ground motions recorded at the surface (Reference 2.5.2-290). Therefore, computation of PSHA using

this model requires incorporation of site amplification into the PSHA calculation. The site amplification incorporated in the CAV PSHA is based on Approach 2B — the use of a mean amplification function that may be amplitude dependent. The dependence of the site amplification functions on the amplitude of the input rock motion exhibited in the results presented in Subsection 2.5.2.5.3 was incorporated into the computation of the surface hazard spectra incorporating CAV.

Two sets of PSHA calculations with site amplification were performed. The first set incorporated the CAV filter and site amplification, producing surface hazard curves. The second set was performed using site amplification and a fixed lower-bound magnitude of $m_b$ 5.0, producing surface hazard curves that are comparable to amplification of the rock hazard results by the site transfer functions. The purpose of performing these two sets of calculations is to provide ratios of CAV/non-CAV spectral values at the seven spectral frequencies used in the PSHA calculations. These spectral ratios are then used to adjust the smooth surface spectra discussed in Subsection 2.5.2.6.1 to produce the final hazard-consistent surface spectra.

Figure 2.5.2-278 through Figure 2.5.2-284 compare the surface mean hazard curves computed with and without CAV for the seven spectra frequencies of 0.5, 1, 2.5, 5, 10, 25, and 100 Hz, respectively. Also shown on these figures is the corresponding generic CEUS mean rock hazard curve from Subsection 2.5.2.4.4.

The surface mean hazard results shown on Figure 2.5.2-278 through Figure 2.5.2-284 are interpolated to obtain the spectral accelerations corresponding to mean annual frequencies of exceedance of $10^{-4}$, $10^{-5}$, and $10^{-6}$. The ratio of the surface spectra accelerations computed with CAV to those computed without CAV for the seven spectral frequencies are then used to scale the smooth surface spectra described in Subsection 2.5.2.6.1 to produce hazard-consistent mean surface UHRS that are based on the use of the CAV filter. The CAV/no-CAV spectral ratios at intermediate periods are obtained by log-log interpolation. Figure 2.5.2-285 shows the resulting mean $10^{-4}$, $10^{-5}$, and $10^{-6}$ surface UHRS for the GMRS profile.

#### 2.5.2.6.3 GMRS

##### 2.5.2.6.3.1 Horizontal GMRS

Regulatory Guide 1.208 defines the GMRS as a risk-consistent design response spectrum computed from the site-specific UHRS at a mean annual frequency of exceedance of $10^{-4}$ by the relationship:

$$GMRS = DF \times UHRS\ (10^{-4}) \qquad \text{[Eq. 15]}$$

Parameter *DF* is the design factor specified by the expression:

$$DF = \text{Maximum}\ (1.0,\ 0.6(A_R)^{0.8}) \qquad \text{[Eq. 16]}$$

in which *AR* is the ratio of the UHRS ground motions for annual exceedance frequencies of $10^{-4}$ and $10^{-5}$, specifically:

$$A_R = \frac{UHRS(10^{-5})}{UHRS(10^{-4})} \qquad \text{[Eq. 17]}$$

Regulatory Guide 1.208 also specifies that when the value of *AR* exceeds 4.2, value of the GMRS is to be no less than 0.45 × $SA(0.1H_D)$, that is, 45 percent of the $10^{-5}$ UHRS. Figure 2.5.2-286 shows the horizontal GMRS calculated using the two approaches. The final GMRS is taken as the envelope of the two, which for the Fermi 3 site is given by 0.45 × $SA(0.1H_D)$. These values are listed in Table 2.5.2-223 along with the horizontal mean $10^{-4}$ and $10^{-5}$ UHRS.

##### 2.5.2.6.3.2 Vertical GMRS

McGuire et al. (Reference 2.5.2-270) recommended vertical to horizontal (V/H) spectral ratios for generic CEUS hard rock. These are given as a function of frequency for three levels of horizontal peak acceleration, as shown on Figure 2.5.2-287. Because the shear-wave velocity of the site is relatively high, as the assessed value of site $\kappa$ is not much greater than the generic hard rock value, the vertical GMRS were developed from the horizontal GMRS using these V/H values for peak acceleration between 0.2 g and 0.5 g. A vertical GMRS was then computed by multiplying the horizontal GMRS by this V/H ratio. The resulting vertical GMRS is listed in Table 2.5.2-223 along with the values of V/H. The horizontal and vertical GMRS are shown on Figure 2.5.2-288.

#### 2.5.2.6.4 FIRS

The process described in Subsection 2.5.2.4 was used to develop FIRS for the three foundation elevations. These are shown on Figure 2.5.2-289, Figure 2.5.2-290, and Figure 2.5.2-291 for the R/FB, CB, and FWSC FIRS, respectively. These spectra are listed in Table 2.5.2-224, Table 2.5.2-225, and Table 2.5.2-226. Also shown on the three figures are the ESBWR Certified Seismic Design Response Spectra (CSDRS) (Reference 2.5.2-291). The FIRS are enveloped by the ESBWR CSDRS in all cases.

### 2.5.2.7 References

2.5.2-201 Electric Power Research Institute and Seismic Owners Group, *Seismic Hazard Methodology for the Central and Eastern United States*, Technical Report NP-4726-A, Vols. 1 – 10, 1988.

2.5.2-202 Electric Power Research Institute, *Probabilistic Seismic Hazard Evaluations at Nuclear Power Plant Sites in the Central and Eastern United States*, Technical Report NP-6395-D, 1989.

2.5.2-203 American Society of Civil Engineers/Structural Engineering Institute, *American Society of Civil Engineers, Seismic Design Criteria for Structures, Systems, and Components in Nuclear Facilities*, ASCE Standard ASCE/SEI 43-05, 2005.

2.5.2-204 Seeber, L., and J.G. Armbruster, “The NCEER-91 Earthquake Catalog: Improved Intensity-Based Magnitudes and Recurrence Relations for U.S. Earthquakes East of New Madrid,” National Center for Earthquake Engineering Research, NCEER-91-0021, 1991.

2.5.2-205 Seismic Data from the Center for Earthquake Research and Information, National Center for Earthquake Engineering Research, “NCEER Catalog Search,” http://folkworm.ceri.memphis.edu/catalogs/html/cat_nceer.html

2.5.2-206 Mueller, C., M. Hopper, and A. Frankel, *Preparation of Earthquake Catalogs for the National Seismic-Hazard Maps: Contiguous 48 States,* U.S. Geological Survey Open-File Report 97-464, 1997.

2.5.2-207 U.S. Geological Survey, Earthquake Hazards Program, Seismic Hazard Maps, "USGS National Seismic Hazard Map, Data, and Documentation" www.earthquake.usgs.gov/research/hazmaps/products_data/ , accessed 22 February 2007.

2.5.2-208 Environmental Systems Research Institute, ESRI ArcGIS 9.1, Data & Maps, Media Kit, 2006.

2.5.2-209 Adams, J., and S. Halchuk, "Fourth Generation Seismic Hazard Maps of Canada: Values for over 650 Canadian Localities Intended for the 2005 National Building Code of Canada," Geological Survey of Canada Open File 4459, 2003, http://earthquakescanada.nrcan.gc.ca/hazard/OF4459/index_e.php, accessed 25 April 2008.

2.5.2-210 Hansen, M.C., comp., "Catalog of Ohio Earthquakes," Ohion Department of Natural Resources, Ohio Geological Survey, OhioSeis: The Ohio Seismic Network, http://www.dnr.state.oh.us/geosurvey/html/eqcatabt/tabid/8299/Default.aspx, accessed 27 March 2008.

2.5.2-211 Metzger, A.G., "Documentation, Location and Size — Estimation of 'New' Historical Earthquakes in the Central United States," U.S. Geological Survey Contract No. 1434-95-G-2604, Program element II, objective 2, June 1997.

2.5.2-212 Metzger, A.G., J.G. Armbruster, and L. Seeber, "Documentation, Location and Size — Estimation of 'New' Historical Earthquakes in the Central United States: Continuation," U.S. Geological Survey Contract No. 1434-HQ-97-GR-03064, Final Technical Report Annual Summary, Vol. 37, March 2000.

2.5.2-213 Fujita, K. comp., "Tectonic Earthquake Felt or Occurring in Michigan," Department of Geological Sciences, Michigan State University, 29 August 2000, http://www.msu.edu/~fujita/earthquake/mieqlist.html, accessed 1 November 2007.

2.5.2-214 Fujita, K., and N.H. Sleep, "A Re-examination of the Seismicity of Michigan," *Tectonophysics*, Vol. 186, 1991.

2.5.2-215 Seeber, L., and J.G. Armbruster, “Natural and Induced Seismicity in the Lake Erie – Lake Ontario Region: Reactivation of Ancient Faults with Little Neotectonic Displacement,” *Géographie Physique et Quaternaire*, Vol. 47, No. 3, 1993.

2.5.2-216 Northern California Earthquake Data Center, Advanced National Seismic System Composite Earthquake Catalog, “ANSS Catalog Search,” http://www.ncedc.org/anss/catalog-search.html, accessed 27 October 2007.

2.5.2-217 U.S. Geological Survey, Earthquake Hazards Program, “Earthquake Rectangular Area Search,” http://neic.usgs.gov/neis/epic/epic_rect.html, accessed 28 March 2007.

2.5.2-218 Natural Resources Canada, “Earthquakes Canada,” http://earthquakescanada.nrcan.gc.ca/index_e.php , accessed 2 April 2008.

2.5.2-219 Faust, T.H., K. Fujita, K.G. Mackey, L.J. Ruff, and R.C. Ensign, “The September 2, 1994 Central Michigan Earthquake,” *Seismological Research Letters*, Vol. 68, No. 3, 1997.

2.5.2-220 U.S. Nuclear Regulatory Commission, *Geophysical Investigations of the Western Ohio – Indiana Region*, NUREG/CR-3145, Final Report 1986 – September 1992, Washington, DC, January 1994.

2.5.2-221 Dineva, S., D. Eaton, and R. Mereu, “Seismicity of the Southern Great Lakes: Revised Earthquake Hypocenters and Possible Tectonic Controls,” *Bulletin of the Seismological Society of America*, Vol. 94, No. 5, October 2004.

2.5.2-222 Tuttle, M.P., E.S. Schweig, J.D. Sims, R.H. Lafferty, L.W. Wolf, and M.L. Haynes, “The Earthquake Potential of the New Madrid Seismic Zone,” *Bulletin of the Seismological Society of America*, Vol. 92, No. 6, 2002.

2.5.2-223 Schwartz, S.Y., and D.H. Christensen, “The 12 July 1986 St. Marys, Ohio Earthquake and Recent Seismicity in the Anna, Ohio Seismogenic Zone,” *Seismological Research Letters*, Vol. 59, No. 2, April – June 1988.

2.5.2-224 Nicholson, C., E. Roeloffs, and R.L. Wesson, “The Northeastern Ohio Earthquake of 31 January 1986: Was It Induced?” *Bulletin of the Seismological Society of America*, Vol. 78, No. 1, February 1988.

2.5.2-225 Hanks, T.C., and H. Kanamori, “A Moment Magnitude Scale,” *Journal of Geophysical Research*, Vol. 84, B5, 1979.

2.5.2-226 Hansen, M.C., “Earthquakes and Seismic Risk in Ohio,” *Ohio Geology*, Summer 1993.

2.5.2-227 Mereu, R.F., H.W. Asmis, B. Dunn, J. Brunet, D. Eaton, S. Dineva, and A. Yapp, “The Seismicity of the Western Lake Ontario Area: Results from the Southern Ontario Seismic Network (SOSN), 1992-2001,” *Seismological Research Letters*, Vol. 73, No. 4, July/August 2002.

2.5.2-228 Hansen, M.C., “January 1986 Northeastern Ohio Earthquake,” *Ohio Geology*, Ohio Seismic Network, Ohio Geological Survey, Summer 1986, http://www.dnr.state.oh.us/geosurvey/earthquakes/860131/860131/tabid/8365/Default.aspx, accessed 24 April 2008.

2.5.2-229 Hansen, M.C., “July 1986 Auglaize County Earthquake,” *Ohio Geology*, The Ohio Seismic Network, Ohio Geological Survey, Fall 1987, http://www.dnr.state.oh.us/geosurvey/earthquakes/860712/860712/tabid/8364/Default.aspx, accessed 24 April 2008.

2.5.2-230 Ohio Geological Survey, “September 25, 1998, Pymatuning Earthquake,” Ohio Seis, The Ohio Seismic Network, http://www.dnr.state.oh.us/geosurvey/earthquakes/980925/980925/tabid/8363/Default.aspx, accessed 24 April 2008.

2.5.2-231 Hansen, M.C., G.E. Larsen, E.M. Swinford, and L.J. Ruff, “Seismic Spotlight Shines on Ashtabula,” *Ohio Geology,* No. 3, 2001.

2.5.2-232 U.S. Geological Survey, Earthquake Hazards Program, “Magnitude 5.2 — Illinois,” 18 April 2008, http://earthquake.usgs.gov/eqcenter/eqinthenews/2008/us2008qza6/, accessed 29 April 2008.

2.5.2-233 U.S. Geological Survey, National Earthquake Information Center: M5.2 Mount Carmel, Illinois, Earthquake of 18 April 2008, 2008, ftp://hazards.cr.usgs.gov/maps/sigeqs/20080418/20080418.pdf, accessed 29 April 2008.

2.5.2-234 Bechtel Group, Inc., *Seismic Hazard Methodology for the Central and Eastern United States, Volume 9: Tectonic Interpretations by Bechtel Group, Inc.*, Technical Report NP-4726, (prepared for the Seismic Owners Group and the Electric Power Research Institute), 1986.

2.5.2-235 Dames & Moore, *Seismic Hazard Methodology for the Central and Eastern United States, Volume 6: Tectonic Interpretations by Dames & Moore*, Technical Report NP-4726, (prepared for the Seismic Owners Group and the Electric Power Research Institute), 1986.

2.5.2-236 Law Engineering Testing Company, *Seismic Hazard Methodology for the Central and Eastern United States, Volume 7: Tectonic Interpretations by Law Engineering Testing Company*, Technical Report NP-4726, (prepared for the Seismic Owners Group and the Electric Power Research Institute),1986.

2.5.2-237 Rondout Associates, *Seismic Hazard Methodology for the Central and Eastern United States, Volume 10: Tectonic Interpretations by Rondout Associates*, Technical Report NP-4726, (prepared for the Seismic Owners Group and the Electric Power Research Institute), 1986.

2.5.2-238 Weston Geophysical Corporation, *Seismic Hazard Methodology for the Central and Eastern United States, Volume 5: Tectonic Interpretations by Weston Geophysical Corporation*, Technical Report NP-4726, (prepared for the Seismic Owners Group and the Electric Power Research Institute), 1986.

2.5.2-239 Woodward-Clyde Consultants, *Seismic Hazard Methodology for the Central and Eastern United States, Volume 8: Tectonic Interpretations by Woodward-Clyde Consultants*, Technical Report NP-4726, (prepared for the Seismic Owners Group and the Electric Power Research Institute), 1986.

2.5.2-240 Frankel, A.D., M.D. Petersen, C.S. Mueller, K.M. Haller, R.L. Wheeler, E.V. Leyendecker, R.L. Wesson, S.C. Harmsen, C.H. Cramer, D.M. Perkins, and K.S. Rukstales, "Documentation for the 2002 Update of the National Seismic Hazard Maps," U.S. Geological Survey Open-File Report 02-420, 2002.

2.5.2-241 Petersen, M.D., A.D. Frankel, S.C. Harmsen, C.S. Mueller, K.M. Haller, R.L. Wheeler, R.L. Wesson, Y. Zeng, O.S. Boyd, D.M. Perkins, N. Luco, E.H. Field, C.J. Wills, and K.S. Rukstales, "Documentation for the 2008 Update of the United States National Seismic Hazard Maps," U.S. Geological Survey Open-File Report 2008-1128, 2008.

2.5.2-242 Frankel, A., C. Mueller, T. Barnhard, D. Perkins, E.V. Leyendecker, N. Dickman, S. Hanson, and M. Hopper, "National Seismic-Hazard Maps: Documentation," U.S. Geological Survey Open-File Report 96-532, 1996.

2.5.2-243 Exelon Generation Company (EGC), LLC, "Application for an Early Site Permit (ESP) for the Clinton ESP Site," September 25, 2003 (date of application submittal).

2.5.2-244 Tennessee Valley Authority, "Application for a Combined License (COL) for Two Westinghouse Advance Passive 1000 (AP1000) Pressurized Water Reactors (PWRs) Designated as Bellefonte Nuclear Station Units 3 & 4," October 30, 2007 (date of application submittal).

2.5.2-245 Bakun, W.H., and M.G. Hopper, "Magnitudes and Locations of the 1811 – 1812 New Madrid, Missouri, and the 1886 Charleston, South Carolina, Earthquakes," *Bulletin of the Seismological Society of America*, Vol. 94, No. 1, 2004.

2.5.2-246 Atkinson, G., B. Bakun, P. Bodin, D. Boore, C. Cramer, A. Frankel, P. Gasperini, J. Gomberg, T. Hanks, B. Herrmann, S. Hough, A. Johnston, S. Kenner, C. Langston, M. Linker, P. Mayne, M. Petersen, C. Powell, W. Prescott, E. Schweig, P. Segall, S. Stein, B. Stuart, M. Tuttle, and R. Van Arsdale, "Reassessing the New Madrid Seismic Zone," EOS, *Transactions of the American Geophysical Union*, Vol. 81, No. 35, 2000.

2.5.2-247 Hough, S.E., J.G. Armbruster, L. Seeber, and J.F. Hough, "On the Modified Mercalli Intensities and Magnitudes of the 1811 – 12 New Madrid Earthquakes," *Journal of Geophysical Research*, Vol. 105, 2000.

2.5.2-248 Johnston, A.C., "Seismic Moment Assessment of Earthquakes in Stable Continental Regions - III. New Madrid 1811 – 1812, Charleston 1886, and Lisbon 1755," *Geophysical Journal International*, Vol. 126, No. 3, 1996.

2.5.2-249 Youngs, R.R., and K.J. Coppersmith, "Implications of Fault Slip Rates and Earthquake Recurrence Models to Probabilistic Hazard Estimates," *Bulletin of the Seismological Society of America,* Vol. 75, 1985.

2.5.2-250 Youngs, R.R., F.H. Swan, and M.S. Power, "Use of Detailed Geologic Data in Regional PSHA: An Example from the Wasatch Front, Utah," in Von Thun, J.L., ed., *Earthquake Engineering and Soil Dynamics II — Recent Advances in Ground Motion Evaluation*, 1988.

2.5.2-251 Ellsworth, W.L., M.V. Matthews, R.M. Nadeau, S.P. Nishenko, P.A. Reasenberg, and R.W. Simpson, "A Physically Based Earthquake Recurrence Model for Estimation of Long-term Earthquake Probabilities," *Proceedings of the Workshop on Earthquake Recurrence: State of the Art and Directions for the Future*, Istituto Nazionale de Geofisica, Rome, Italy, February 1999.

2.5.2-252 Matthews, M.V., W.L. Ellsworth, and P.A. Reasenberg, "A Brownian Model for Recurrent Earthquakes," *Bulletin of the Seismological Society of America*, Vol. 92, 2002.

2.5.2-253 Exelon Generation Company (EGC), LLC, "Response to Request for Additional Information Letter No. 7," Exelon Generation Company, LLC, ESP application for Clinton site, October 11, 2004.

2.5.2-254 Exelon Generation Company (EGC), LLC, *ESP Site Safety Analysis Report*, Clinton Early Site Permit Application, Revision 4, April 14, 2006.

2.5.2-255 McGuire, R.K., G.R. Toro, and W.J. Silva, *Engineering Model of Earthquake Ground Motion for Eastern North America*, Electric Power Research Institute Technical Report NP-6074, 1988.

2.5.2-256 Boore, D.M., and G.M. Atkinson, “Stochastic Prediction of Ground Motion and Spectral Response Parameters at Hard-Rock Sites in Eastern North America,” *Bulletin of the Seismological Society of America*, Vol. 77, No. 2, 1987.

2.5.2-257 U.S. Nuclear Regulatory Commission, *Seismic Hazard Characterization of 69 Nuclear Plant Sites East of the Rocky Mountains: Questionnaires*, NUREG-5250, Vol. 7, Washington, DC, 1986.

2.5.2-258 Newmark, N.M., and W.J. Hall, “Earthquake Spectra and Design,” Earthquake Engineering Research Institute, 1982.

2.5.2-259 Electric Power Research Institute, *CEUS Ground Motion Project Final Report*, Technical Report 1009684, 2004.

2.5.2-260 U.S. Nuclear Regulatory Commission, *Recommendations for Probabilistic Seismic Hazard Analysis: Guidance on Uncertainty and Use of Experts*, NUREG-6372, Washington, DC,1997.

2.5.2-261 Silva, W., N. Gregor, and R. Darragh, “Development of Regional Hard Rock Attenuation Relations for Central and Eastern North America,” unpublished report by Pacific Engineering and Analysis, (1 November 2002), http://pacificengineering.org/rpts_page1.shtml, accessed 28 July 2008.

2.5.2-262 Atkinson, G.M., and D.M. Boore, “Ground Motion Relations for Eastern North America,” *Bulletin of the Seismological Society of America*, Vol. 85, No. 1, 1995.

2.5.2-263 Campbell, K.W., “Prediction of Strong Ground Motion Using the Hybrid Empirical Method and Its Use in the Development of Ground-Motion (Attenuation) Relations in Eastern North America,” *Bulletin of the Seismological Society of America*, Vol. 93, pp. 1012 – 1033; 2003; Vol. 94 erratum, p. 2418, 1994.

2.5.2-264 Silva, W., N. Gregor, and R. Darragh, “Development of Regional Hard Rock Attenuation Relations for Central and Eastern North America, Mid-Continent and Gulf Coast Areas,” unpublished report by Pacific Engineering and Analysis, (13 August 2003), http://pacificengineering.org/rpts_page1.shtml, accessed 28 July 2008.

2.5.2-265 Atkinson, G. M., and D.M. Boore, "Earthquake Ground-Motion Prediction Equations for Eastern North America," *Bulletin of the Seismological Society of America*, Vol. 96, No. 6, December 2006.

2.5.2-266 Tavakoli, B. and S. Pezeshk, "Empirical-Stochastic Ground-Motion Prediction for Eastern North America," *Bulletin of the Seismological Society of America*, Vol. 95, No. 6, December 2005.

2.5.2-267 Electric Power Research Institute, *Program on Technology Innovation: Truncation of the Lognormal Distribution and Value of the Standard Deviation for Ground Motion Models in the Central and Eastern United States*, Technical Report 1014381, August 2006.

2.5.2-268 Johnston, A.C., "Seismic Moment Assessment of Earthquakes in Stable Continental Regions — I: Instrumental Seismicity," *Geophysical Journal International*, Vol. 124, 1996.

2.5.2-269 Electric Power Research Institute, *Guidelines for Determining Design Basis Ground Motions*, Technical Report 102293, Vol. 1, 1993.

2.5.2-270 U.S. Nuclear Regulatory Commission, *Technical Basis for Revision of Regulatory Guidance on Design Ground Motions: Hazard and Risk Consistent Ground Motion Spectra Guidelines*, NUREG-6728, Washington, DC, 2001.

2.5.2-271 Baker, J.W., and C.A. Cornell, "Spectral Shape, Epsilon and Record Selection," *Earthquake Engineering & Structural Dynamics*, Vol. 35, No. 9, 2006.

2.5.2-272 Baker, J., and N. Jayaram, "Correlation of Spectral Acceleration Values from NGA Ground Motion Models," *Earthquake Spectra*, Vol. 24, pp. 299 – 317, 2008.

2.5.2-273 Baker, J.W., and C.A. Cornell, "Correlation of Response Spectral Values for Multicomponent Ground Motions," *Bulletin of the Seismological Society of America*, Vol. 96, No. 1, 2006.

2.5.2-274 Somerville, P.G., N. Collins, N.A. Abrahamson, R. Graves and C.K. Saikia, *Ground Motion Attenuation Relations for the Central and Eastern United States*, Report to U.S. Geological Survey, NEHRP External Research Program, Award No. 99-HQ-GR-0098, 2001.

2.5.2-275 Abrahamson, N.A., and W.J. Silva, "Summary of the Abrahamson & Silva NGA Ground Motion Relations," *Earthquake Spectra*, Vol. 24, pp. 67 – 97, 2008.

2.5.2-276 Boore, D.M., and G.M. Atkinson, "Ground Motion Prediction Equations for the Average Horizontal Component of PGA, PGV, and 5% Damped PSA at Spectral Periods between 0.01s and 10.0 s," *Earthquake Spectra*, Vol. 24, pp. 99 – 138, 2008.

2.5.2-277 Campbell, K.W., and Y. Bozorgnia, "NGA Ground Motion Relations for the Geometric Mean Horizontal Component of PGA, PGV, PGD, and 5% Damped Linear Elastic Response Spectra for Periods Ranging from 0.01 s to 10 s," *Earthquake Spectra*, Vol. 24, pp. 139 – 171, 2008.

2.5.2-278 Chiou, B.S.-J., and R.R. Youngs, "An NGA Model for the Average Horizontal Component of Peak Ground Motion and Response Spectra," *Earthquake Spectra*, Vol. 24, pp. 173 – 215, 2008.

2.5.2-279 Idriss, I.M., "An NGA Empirical Model for Estimating the Horizontal Spectral Values Generated by Shallow Crustal Earthquakes," *Earthquake Spectra*, Vol. 24, pp. 217 – 242, 2008.

2.5.2-280 GEOVision, Inc., *Final Report, Borehole And Surface Geophysics, Boreholes CB-C3, RB-C4, RB-C8, RB-C6, and TB-C5, Surface Arrays Near RW-C1, RB-C4, MW-393 and MW-381*, Report 7297-01, Rev 0, March 12, 2008.

2.5.2-281 Vucetic, M., and R. Dobry, "Effect of Soils Plasticity on Cyclic Response," *Journal of Geotechnical Engineering,* American Society of Civil Engineers, Vol. 117, No. 1, 1991.

2.5.2-282 Schnabel, P.B., J. Lysmer, and H.B. Seed, "SHAKE — A Computer Program for Earthquake Response Analysis of Horizontally Layered Sites," Earthquake Research Center, EERC 72-12, 1972.

2.5.2-283 Anderson, J.G., and S.E. Hough, “A Model for the Shape of the Fourier Amplitude Spectrum of Acceleration at High Frequencies,” *Bulletin of the Seismological Society of America*, Vol. 74, 1984.

2.5.2-284 Silva, W.J., and R. Darragh, “Engineering Characterization of Earthquake Strong Ground Motion Recorded at Rock Sites,” Electric Power Research Institute, TR-102261, 1995.

2.5.2-285 Electric Power Research Institute, *Assessment of a Performance-Based Approach for Determining the SSE Ground Motion for New Plant Sites*, Vol. 2, Seismic Hazard Results at 28 Sites, Final Report 1012045, May 2005.

2.5.2-286 Silva, W.J., N. Abrahamson, G. Toro, and C. Costantino, *Description and Validation of the Stochastic Ground Motion Model*, (report submitted to Brookhaven National Laboratory), 1996.

2.5.2-287 Silva, W.J., “Base Case and Recommended Limits of Modulus Reduction and Damping Relationships,” Data files EPRIRR1L.MAT, EPRIRR1U.MAT, EPRISR1.MAT, EPRISR1L.MAT, and EPRISR1U.MAT, transmitted March 18, 2007.

2.5.2-288 Hasek, M.J., *Properties, Behavior, and Construction Use of Controlled Low Strength Material (CLSM) (U)*: Engineering Studies Research Report K-ESR-G-00004, Rev 01, Geotechnical Engineering Group, Site Geotechnical Services Department, Savannah River Site, Aiken, SC, September, 2002.

2.5.2-289 Silva, W.J., and K. Lee, “WES RASCALS Code for Synthesizing Earthquake Ground Motions: State-of-the-Art for Assessing Earthquake Hazards in the United States Report 24,” Miscellaneous Paper S-73-1, U.S. Army Corps of Engineers Waterways Experiment Station, 1987.

2.5.2-290 Electric Power Research Institute, *Program on Technology Innovation: Use of Cumulative Absolute Velocity (CAV) in Determining Effects of Small Magnitude Earthquakes on Seismic Hazard Analyses*, Technical Report 1014099, August 2006.

2.5.2-291 GE-Hitachi Nuclear Energy, “ESBWR Design Control Document Tier 2, Chapter 2,” Revision 4, September 2007.

2.5.2-292 National Aeronautics and Space Administration/U.S. Geological Survey, “SRTM, Shuttle Radar Topography Mission, SRTM 30 data,” 2005, http://www2.jpl.nasa.gov/srtm/, accessed 11 January 2007.

2.5.2-293 National Geophysical Data Center, National Oceanic and Atmospheric Administration “Great Lakes Bathymetry,” http://www.ngdc.noaa.gov/mgg/greatlakes/greatlakes.html, accessed 17 August 2007.

2.5.2-294 National Geophysical Data Center, National Oceanic and Atmospheric Administration, “2-Minute Gridded Global Relief Data (ETOPO2v2) June, 2006,” http://www.ngdc.noaa.gov/mgg/fliers/01mgg04.html, accessed 1 January 2007.

2.5.2-295 Baranoski, M.T., “Structure Contour Map on the Precambrian Unconformity Surface in Ohio and Related Basement Features,” Ohio Geological Survey Map PG-23, 2002.

2.5.2-296 Van Schmus, W.R., “Tectonic Setting of the Midcontinent Rift System,” *Tectonophysics*, Vol. 213, 1992.

2.5.2-297 Easton, R.M., and T.R. Carter, “Geology of the Precambrian Basement beneath the Paleozoic of Southwestern Ontario,” in R.W. Ojakangas et al., eds., *Basement Tectonics*, Vol. 10, 1995.

2.5.2-298 Tanglis, C. comp., “Surface Faults in the Southwestern District, Southern Ontario,” Ontario Geological Survey, 1995.

2.5.2-299 Brigham, R.J., “Structural Geology of Southwestern Ontario and Southeastern Michigan,” Ontario Department of Mines and Northern Affairs, Petroleum Resource Section, Paper 71-2, 1971.

2.5.2-300 Ells, G.D., *Structures Associated with the Albion-Scipio Oil Field Trend*, Michigan Geological Survey Open-File Report 62-1, 1962.

2.5.2-301 Aangstrom Precision Corporation, Structure Contour Maps, Mt. Pleasant, Michigan, 1989:
(a) Dundee Residual Structure Contour Map, scale 1:600,000.
(b) Dundee Structure Contour Map, scale 1:600,000.
(c) Sunbury Shale Residual Structure Contour Map, scale 1:600,000.
(d) Sunbury Shale Structure Contour Map, scale 1:600,000.
(e) Traverse Limestone Residual Structure Contour Map, scale 1:600,000.
(f) Traverse Limestone Structure Contour Map, scale 1:600,000.

2.5.2-302 Root, S., "Recurrent Basement Faulting and Basin Evolution, West Virginia and Ohio: The Burning Springs — Cambridge Fault Zone," in van de Pluijm, B.A., and P.A. Catacosinos, eds., "Basement and Basins of Eastern North America," Boulder, Colorado, Geological Society of America Special Paper 308, 1996.

2.5.2-303 Gray, H.H., C.H. Ault, S.J. Keller, and D. Harper, "Bedrock Geologic Map of Indiana," Indiana Geological Survey Miscellaneous Map 48, 2002.

2.5.2-304 Slucher, E.R., E.M. Swinford, G.E. Larson, and D.M. Powers, "Bedrock Geologic Map of Ohio," Ohio Geological Survey, Map BG-1, version 6.0, 2006.

2.5.2-305 Johnston, A.C., and E.S. Schweig, "The Enigma of the New Madrid Earthquakes of 1811-1812," *Annual Review of Earth and Planetary Sciences,* Vol. 24, 1996.

2.5.2-306 Hough, S.E., and S. Martin, "Magnitude Estimates of Two Large Aftershocks of the 16 December 1811 New Madrid Earthquake," *Bulletin of the Seismological Society of America*, Vol. 92, No. 8, 2002.

## Table 2.5.2-201 Bechtel Team Seismic Sources

| Source | P* | Closest Distance to Fermi 3 Site (km) | EPRI (1989) Maximum Magnitude Distribution for Fermi 3 Site ($m_b$) | Maximum Magnitude Distribution Used in PSHA for Fermi 3 Site ($m_b$) |
|---|---|---|---|---|
| New Madrid Region (BEC-BZ0) | 1 | 484.1 | 5.7 (0.10), 6.0 (0.40), 6.3 (0.40), 6.6 (0.10) | **M** 7.0 (0.1), **M** 7.3 (0.4), **M** 7.5 (0.4), **M** 7.8 (0.1) |
| Northern Great Plains Region (BEC-BZ3) | 1 | 67.6 | 5.4 (0.10), 5.7 (0.40), 6.0 (0.40), 6.6 (0.10) | **M** 5.75 (0.02), **M** 6 (0.02), **M** 6.25 (0.16), **M** 6.5 (0.3), **M** 6.75 (0.26), **M** 7 (0.15), **M** 7.25 (0.07), **M** 7.5 (0.02) |
| Southern Eastern Craton Region (BEC-BZ6) | 1 | 0 | 5.4 (0.10), 5.7 (0.40), 6.0 (0.40), 6.6 (0.10) | 5.4 (0.10), 5.7 (0.40), 6.0 (0.40), 6.6 (0.10) |
| Frankfort-Bucyrus (BEC-27) | 0.12 | 80.2 | 5.4 (0.10), 5.7 (0.40), 6.0 (0.40), 6.6 (0.10) | 5.4 (0.10), 5.7 (0.40), 6.0 (0.40), 6.6 (0.10) |
| Southern Illinois Region (BEC-K) | 1 | 521.3 | 6.0 (0.10), 6.3 (0.40), 6.6 (0.50) | **M** 7.0 (0.1), **M** 7.3 (0.4), **M** 7.5 (0.4), **M** 7.8 (0.1) |
| Anna, Ohio, Area (BEC-N1) | 0.6 | 98.1 | 5.4 (0.10), 5.7 (0.40), 6.0 (0.40), 6.6 (0.10) | 5.4 (0.10), 5.7 (0.40), 6.0 (0.40), 6.6 (0.10) |

Notes:

P* = the probability that the source is included in the hazard model.

**M** = moment magnitude

(Weight) = relative contribution of the source

## Table 2.5.2-202 Dames & Moore Team Seismic Sources

| Source | P* | Closest Distance to Fermi 3 Site (km) | EPRI (1989) Maximum Magnitude Distribution for Fermi 3 Site ($m_b$) | Maximum Magnitude Distribution Used in PSHA for Fermi 3 Site ($m_b$) |
|---|---|---|---|---|
| Eastern Marginal Basin (DAM-8) | 0.08[a] | 106.3 | 5.6 (0.80), 7.2 (0.20) | 5.6 (0.80), 7.2 (0.20) |
| Anna, Ohio (DAM-12) | 1 | 127.7 | 6.8 (0.75), 7.2 (0.25) | 6.8 (0.75), 7.2 (0.25) |
| Findlay Arch/Algonquin Axis (DAM-14 and DAM-14B) | 1 (0.25 for 14, 0.75 for 14B) | 35.6 for 14<br>12.1 for 14B | 5.5 (0.75), 7.2 (0.25) for 14, 5.4 (0.80), 7.2 (0.20) for 14B | 5.5 (0.75), 7.2 (0.25) for 14, 5.4 (0.80), 7.2 (0.20) for 14B |
| Michigan Basin (DAM-15) | 1 | 42.1 | 5.3 (0.80), 7.2, (0.20) | 5.3 (0.80), 7.2, (0.20) |
| Southern Illinois/Southern Indiana/Fairfield Basin (DAM-18) | 1 | 436.1 | 6.6 (0.75), 7.2 (0.25) | **M** 7.0 (0.1), **M** 7.3 (0.4),<br>**M** 7.5 (0.4), **M** 7.8 (0.1) |
| Wisconsin-Michigan Block (DAM-70) | 1 | 0 | 5.1 (0.80), 7.2 (0.20) | 5.1 (0.80), 7.2 (0.20) |
| Southern Canada Province (DAM-73) | 1 | 66.1 | 5.3 (0.80), 7.2 (0.20) | 5.3 (0.80), 7.2 (0.20) |

Notes:

a. modified to 1 for Fermi 3 PSHA

P* = the probability that the source is included in the hazard model.

**M** = moment magnitude

(Weight) = relative contribution of the source

## Table 2.5.2-203 Law Engineering Team Seismic Sources

| Source | P* | Closest Distance to Fermi 3 Site (km) | EPRI (1989) Maximum Magnitude Distribution for Fermi 3 Site ($m_b$) | Maximum Magnitude Distribution Used in PSHA for Fermi 3 Site ($m_b$) |
|---|---|---|---|---|
| Wabash Valley Arm (LAW-07) | 1 | 374.5 | 5.5 (0.2), 6.0 (0.5), 6.8 (0.3) | **M** 7.0 (0.1), **M** 7.3 (0.4), **M** 7.5 (0.4), **M** 7.8 (0.1) |
| 111 Laurentian (LAW-111) | 1 | 19.7 | 5.5 (0.5), 6.0 (0.5) | 5.5 (0.5), 6.2 (0.5) |
| Ohio-Pennsylvania Block (LAW-112) | 1 | 19.9 | 4.6 (0.2), 5.1 (0.5), 5.5 (0.3) | 5.0 (0.5), 5.5 (0.5) |
| Wisconsin Block (LAW-114) | 1 | 0 | 4.6 (0.2), 5.1 (0.5), 5.5 (0.3) | 4.6 (0.2), 5.1 (0.5), 5.5 (0.3) |
| Indiana Block (LAW-115) | 1 | 17.4 | 5.2 (0.5), 5.5 (0.5) | 5.2 (0.5), 5.5 (0.5) |
| Illinois Block (LAW-116) | 1 | 303.6 | 5.2 (0.5), 5.5 (0.5) | **M** 5.75 (0.02), **M** 6 (0.02), **M** 6.25 (0.16), **M** 6.5 (0.3), **M** 6.75 (0.26), **M** 7 (0.15), **M** 7.25 (0.07), **M** 7.5 (0.02) |

Notes:

P* = the probability that the source is included in the hazard model.

**M** = moment magnitude

(Weight) = relative contribution of the source

## Table 2.5.2-204 Rondout Team Seismic Sources

| Source | P* | Closest Distance to Fermi 3 Site (km) | EPRI (1989) Maximum Magnitude Distribution for Fermi 3 Site ($m_b$) | Maximum Magnitude Distribution Used in PSHA for Fermi 3 Site ($m_b$) |
|---|---|---|---|---|
| New Madrid Rift Complex (RND-2) | 1 | 366.8 | 6.6 (0.30), 6.8 (0.60), 7.0 (0.10) | **M** 7.0 (0.1), **M** 7.3 (0.4), **M** 7.5 (0.4), **M** 7.8 (0.1) |
| Southern Illinois and Indiana (RND-4) | 1 | 310.8 | 6.6 (0.30), 6.8 (0.60), 7.0 (0.10) | **M** 7.0 (0.1), **M** 7.3 (0.4), **M** 7.5 (0.4), **M** 7.8 (0.1) |
| Anna, Ohio (RND-8) | 1 | 116.8 | 5.8 (0.15), 6.5 (0.60), 6.8 (0.25) | 5.8 (0.15), 6.5 (0.60), 6.8 (0.25) |
| Southeast Michigan (RND-10) | 0.95 | 0 | 5.8 (0.15), 6.5 (0.60), 6.8 (0.25) | 5.8 (0.15), 6.5 (0.60), 6.8 (0.25) |
| Northwestern Ohio (RND-11) | 0.87 | 14.9 | 5.2 (0.30), 6.3 (0.55), 6.5 (0.15) | 5.2 (0.30), 6.3 (0.55), 6.5 (0.15) |
| Cleveland, Ohio (RND-12) | 0.78 | 53.0 | 5.2 (0.30), 6.3 (0.55), 6.5 (0.15) | 5.2 (0.30), 6.3 (0.55), 6.5 (0.15) |
| Pre-Grenville Precambrian Craton (RND-52) | 1 | 89.5 | 4.8 (0.20), 5.5 (0.60), 5.8 (0.20) | **M** 5.75 (0.02), **M** 6 (0.02), **M** 6.25 (0.16), **M** 6.5 (0.3), **M** 6.75 (0.26), **M** 7 (0.15), **M** 7.25 (0.07), **M** 7.5 (0.02) |

Notes:

P* = the probability that the source is included in the hazard model.

**M** = moment magnitude

(Weight) = relative contribution of the source

## Table 2.5.2-205 Weston Geophysical Team Seismic Sources

| Source | P* | Closest Distance to Fermi 3 Site (km) | EPRI (1989) Maximum Magnitude Distribution for Fermi 3 Site ($m_b$) | Maximum Magnitude Distribution Used in PSHA for Fermi 3 Site ($m_b$) |
|---|---|---|---|---|
| Anna, Ohio (WGC-29) | 0.93 | 107.5 | 5.4 (0.19), 6.0 (0.68), 6.6 (0.13) | 5.4 (0.19), 6.0 (0.68), 6.6 (0.13) |
| Indiana Arm (WGC-33) | 1 | 361.8 | 6.0 (0.68), 6.6 (0.27), 7.2 (0.05) | **M** 7.0 (0.1), **M** 7.3 (0.4), **M** 7.5 (0.4), **M** 7.8 (0.1) |
| Northern Interior (WGC-100) | 1 | 99.2 | 5.4 (0.62), 6.0 (0.29), 6.6 (0.09) | 5.4 (0.62), 6.0 (0.29), 6.6 (0.09) |
| Southern Ontario–Ohio-Indiana (WGC-101) | 1 | 0 | 5.4 (0.19), 6.0 (0.68), 6.6 (0.13) | 5.4 (0.19), 6.0 (0.68), 6.6 (0.13) |
| North Central (WGC-105) | 1 | 44.9 | 5.4 (0.80), 6.0 (0.14), 6.6 (0.06) | **M** 5.75 (0.02), **M** 6 (0.02), **M** 6.25 (0.16), **M** 6.5 (0.3), **M** 6.75 (0.26), **M** 7 (0.15), **M** 7.25 (0.07), **M** 7.5 (0.02) |

Notes:

P* = the probability that the source is included in the hazard model.

**M** = moment magnitude

(Weight) = relative contribution of the source

## Table 2.5.2-206 Woodward-Clyde Team Seismic Sources

| Source | P* | Closest Distance to Fermi 3 Site (km) | EPRI (1989) Maximum Magnitude Distribution for Fermi 3 Site ($m_b$) | Maximum Magnitude Distribution Used in PSHA for Fermi 3 Site ($m_b$) |
|---|---|---|---|---|
| Attica, NY Intersection (WCC-34) | 1 | 381.9 | 5.6 (0.33), 6.3 (0.34), 7.4 (0.33) | 5.6 (0.33), 6.3 (0.34), 7.4 (0.33) |
| Northeastern Ohio Gravity Source (WCC-35) and NOTA | 0.548 | 107.4 | 5.3 (0.33), 6.0 (0.34), 6.8 (0.33) | 5.3 (0.33), 6.0 (0.34), 6.8 (0.33) |
| Michigan-Ohio Geophysical Anomaly (WCC-36) | 0.090 | 135.0 | 5.6 (0.33), 6.5 (0.34), 7.1 (0.33) | 5.6 (0.33), 6.5 (0.34), 7.1 (0.33) |
| Bowling Green–Auglaize Fault System (WCC-37) | 0.072 | 43.3 | 5.6 (0.33), 6.5 (0.34), 7.2 (0.33) | 5.6 (0.33), 6.5 (0.34), 7.2 (0.33) |
| Champaign-Anna Fault System (WCC-38) | 0.065 | 169.5 | 5.7 (0.33), 6.8 (0.34), 7.6 (0.33) | 5.7 (0.33), 6.8 (0.34), 7.6 (0.33) |
| Anna, Ohio Geophysical Intersection (WCC-39) and NOTA | 0.773 | 138.5 | 5.5 (0.33), 6.5 (0.34), 7.3 (0.33) | 5.5 (0.33), 6.5 (0.34), 7.3 (0.33) |
| Southern Indiana Arm (WCC-43) | 1 | 408.1 | 5.8 (0.33), 6.3 (0.34), 7.4 (0.33) | **M** 7.0 (0.1), **M** 7.3 (0.4), **M** 7.5 (0.4), **M** 7.8 (0.1) |
| New Madrid Loading Volume (WCC-44) | 1 | 369.4 | 5.6 (0.33), 6.3 (0.34), 6.9 (0.33) | **M** 7.0 (0.1), **M** 7.3 (0.4), **M** 7.5 (0.4), **M** 7.8 (0.1) |
| Background Zone 67 (WCC-B67) | 1 | 0 | 4.9 (0.17), 5.4 (0.28), 5.8 (0.27), 6.5 (0.28) | 5.0 (0.17), 5.4 (0.28), 5.8 (0.27), 6.5 (0.28) |

Notes:

NOTA = none of the above zone, a source with the same geometry.

P* = the probability that the source is included in the hazard model.

**M** = moment magnitude

(Weight) = relative contribution of the source

## Table 2.5.2-207 Magnitude Comparisons for New Madrid 1811/1812 Earthquake Sequence

| Study | NM1 | NM2 | NM3 |
|---|---|---|---|
| Johnston | **M** 8.1 ± 0.3 | **M** 7.8 ± 0.3 | **M** 8.0 ± 0.3 |
| Hough et al. | **M** 7.2 to 7.3 | **M** ~7.0[a] (located on the NN) | **M** 7.4 to 7.5 |
| Mueller and Pujol | - | - | **M** 7.2 to 7.4 (preferred **M** 7.2 to 7.3) |
| Bakun and Hopper | $\mathbf{M}_I$ 7.6 (**M** 7.2 to 7.9) (preferred model 3) | $\mathbf{M}_I$ 7.5 (**M** 7.1 to 7.8) (preferred model 3) | $\mathbf{M}_I$ 7.8 (**M** 7.4 to 8.1) (preferred model 3) |
| | $\mathbf{M}_I$ 7.2 (**M** 6.8 to 7.9) (model 1) | $\mathbf{M}_I$ 7.2 (**M** 6.8 to 7.8) (model 1) | $\mathbf{M}_I$ 7.4 (**M** 7.0 to 8.1) (model 1) |
| Mueller et al. | **M** 7.3 | **M** 6.8 (located within the Wabash Valley of southern Illinois/ southern Indiana) | **M** 7.5 |
| Johnston | **M** 7.8 to 7.9 | **M** 7.5 to 7.6 | **M** 7.7 to 7.8 |

Notes:

a. The estimated location and magnitude of this earthquake are revised in Mueller et al.

**M** = moment magnitude

(Weight) = relative contribution of the source

Source: Reference 2.5.2-244

## Table 2.5.2-208 Magnitude Distributions for Repeating Large-Magnitude New Madrid Earthquakes

| Earthquake Rupture Set | Magnitude for Individual Faults (moment magnitude [M]) | | | Weight |
|---|---|---|---|---|
| | New Madrid South | Reelfoot Thrust | New Madrid North | |
| 1 | 7.8 | 7.7 | 7.5 | 0.1667 |
| 2 | 7.9 | 7.8 | 7.6 | 0.1667 |
| 3 | 7.6 | 7.8 | 7.5 | 0.25 |
| 4 | 7.2 | 7.4 | 7.2 | 0.0833 |
| 5 | 7.2 | 7.4 | 7.0 | 0.1667 |
| 6 | 7.3 | 7.5 | 7.0 | 0.1667 |

Source: Reference 2.5.2-244

## Table 2.5.2-209 Earthquake Frequencies for Repeating Large-Magnitude Earthquakes

| Recurrence Model | Weight | Mean Repeat Time (years) | Equivalent Annual Frequency |
|---|---|---|---|
| New Madrid Poisson | 0.10108 | 160 | 6.26E-03 |
| | 0.24429 | 259 | 3.86E-03 |
| | 0.30926 | 407 | 2.46E-03 |
| | 0.24429 | 685 | 1.46E-03 |
| | 0.10108 | 1515 | 6.60E-04 |
| New Madrid Renewal, $\alpha$ = 0.3 | 0.10108 | 325 | 3.32E-03 |
| | 0.24429 | 401 | 9.96E-04 |
| | 0.30926 | 475 | 2.67E-04 |
| | 0.24429 | 562 | 4.98E-05 |
| | 0.10108 | 695 | 3.22E-06 |
| New Madrid Renewal, $\alpha$ = 0.5 | 0.10108 | 310 | 4.87E-03 |
| | 0.24429 | 430 | 2.19E-03 |
| | 0.30926 | 559 | 8.81E-04 |
| | 0.24429 | 728 | 2.49E-04 |
| | 0.10108 | 1008 | 2.72E-05 |
| New Madrid Renewal, $\alpha$ = 0.7 | 0.10108 | 318 | 4.53E-03 |
| | 0.24429 | 494 | 2.28E-03 |
| | 0.30926 | 701 | 1.03E-03 |
| | 0.24429 | 986 | 3.35E-04 |
| | 0.10108 | 1484 | 4.30E-05 |

Source: Reference 2.5.2-244

## Table 2.5.2-210 Estimates of Probability of Earthquake Detection for EPRI-SOG Completeness Regions in the Vicinity of the Fermi 3 Site

| Time Interval | | Probability of Detection $P_D$ | | | | | | | |
|---|---|---|---|---|---|---|---|---|---|
| Magnitude Interval ($m_b$*) | Earthquake Catalog | 1625 – 1780 | 1780 – 1860 | 1860 – 1910 | 1910 – 1950 | 1950 – 1975 | 1975 – 3/1985 | 3/1985 – 5/2008 | Equivalent Period of Completeness (yrs) |
| **Completeness Region 4** | | | | | | | | | |
| 3.3 to 3.9 | EPRI-SOG | | | 0.324 | 0.749 | 0.749 | 1.000 | | 75.0 |
| | Update | | | 0.776 | 0.942 | 0.942 | 1.000 | 1.000 | 133.4 |
| 3.9 to 4.5 | EPRI-SOG | | | 0.846 | 1.000 | 1.000 | 1.000 | | 117.5 |
| | Update | | | 1.000 | 1.000 | 1.000 | 1.000 | 1.000 | 148.3 |
| 4.5 to 5.1 | EPRI-SOG | | 0.432 | 1.000 | 1.000 | 1.000 | 1.000 | | 159.7 |
| | Update | | 0.631 | 1.000 | 1.000 | 1.000 | 1.000 | 1.000 | 198.8 |
| 5.1 to 5.7 | EPRI-SOG | | 0.723 | 1.000 | 1.000 | 1.000 | 1.000 | | 183.0 |
| | Update | | 0.892 | 1.000 | 1.000 | 1.000 | 1.000 | 1.000 | 219.7 |
| 5.7 to 6.3 | EPRI-SOG | | 0.931 | 1.000 | 1.000 | 1.000 | 1.000 | | 199.6 |
| | Update | | 0.918 | 1.000 | 1.000 | 1.000 | 1.000 | 1.000 | 221.8 |
| 6.3 to 6.9 | EPRI-SOG | | 1.000 | 1.000 | 1.000 | 1.000 | 1.000 | | 205.2 |
| | Update | | 0.957 | 1.000 | 1.000 | 1.000 | 1.000 | 1.000 | 224.9 |
| **Completeness Region 5** | | | | | | | | | |
| 3.3 to 3.9 | EPRI-SOG | | 0.156 | 0.360 | 0.735 | 0.889 | 1.000 | | 92.3 |
| | Update | | 0.389 | 1.000 | 1.000 | 1.000 | 1.000 | 1.000 | 179.5 |
| 3.9 to 4.5 | EPRI-SOG | | 0.356 | 0.708 | 1.000 | 1.000 | 1.000 | | 139.0 |
| | Update | | 0.763 | 1.000 | 1.000 | 1.000 | 1.000 | 1.000 | 209.4 |
| 4.5 to 5.1 | EPRI-SOG | 0.330 | 0.691 | 0.974 | 1.000 | 1.000 | 1.000 | | 230.3 |
| | Update | 0.307 | 0.793 | 1.000 | 1.000 | 1.000 | 1.000 | 1.000 | 259.4 |
| 5.1 to 5.7 | EPRI-SOG | 0.875 | 0.959 | 1.000 | 1.000 | 1.000 | 1.000 | | 337.5 |
| | Update | 0.976 | 0.976 | 1.000 | 1.000 | 1.000 | 1.000 | 1.000 | 377.7 |
| 5.7 to 6.3 | EPRI-SOG | 1.000 | 1.000 | 1.000 | 1.000 | 1.000 | 1.000 | | 360.2 |
| | Update | 1.000 | 1.000 | 1.000 | 1.000 | 1.000 | 1.000 | 1.000 | 383.3 |
| 6.3 to 6.9 | EPRI-SOG | 1.000 | 1.000 | 1.000 | 1.000 | 1.000 | 1.000 | | 360.2 |
| | Update | 1.000 | 1.000 | 1.000 | 1.000 | 1.000 | 1.000 | 1.000 | 383.3 |

## Table 2.5.2-211 PSHA Results for 0.5 Hz Spectral Acceleration on CEUS Generic Hard Rock for the FERMI 3 Site

| 0.5 Hz Spectral Acceleration (g) | Annual Exceedance Frequency | | | | | |
|---|---|---|---|---|---|---|
| | Mean | 5th% | 16th% | 50th% | 84th% | 95th% |
| 1.00E-05 | 8.52E-02 | 2.88E-02 | 3.98E-02 | 7.08E-02 | 1.32E-01 | 1.78E-01 |
| 1.00E-04 | 3.54E-02 | 1.15E-02 | 1.62E-02 | 2.88E-02 | 5.50E-02 | 8.13E-02 |
| 1.00E-03 | 6.62E-03 | 1.66E-03 | 2.75E-03 | 5.50E-03 | 1.02E-02 | 1.59E-02 |
| 2.00E-03 | 3.86E-03 | 7.76E-04 | 1.45E-03 | 3.24E-03 | 6.17E-03 | 9.12E-03 |
| 5.00E-03 | 1.75E-03 | 1.91E-04 | 4.27E-04 | 1.29E-03 | 3.09E-03 | 4.79E-03 |
| 1.00E-02 | 8.14E-04 | 3.98E-05 | 1.05E-04 | 4.27E-04 | 1.48E-03 | 2.95E-03 |
| 2.00E-02 | 3.13E-04 | 5.01E-06 | 1.62E-05 | 8.91E-05 | 5.25E-04 | 1.45E-03 |
| 3.00E-02 | 1.65E-04 | 1.18E-06 | 4.37E-06 | 2.88E-05 | 2.19E-04 | 8.13E-04 |
| 5.00E-02 | 6.91E-05 | 1.41E-07 | 6.61E-07 | 5.75E-06 | 5.89E-05 | 2.63E-04 |
| 1.00E-01 | 1.80E-05 | 7.59E-09 | 3.39E-08 | 5.13E-07 | 7.59E-06 | 3.55E-05 |
| 3.00E-01 | 8.52E-07 | <1.00E-10 | 1.32E-09 | 6.76E-09 | 1.66E-07 | 1.29E-06 |
| 1.00E+00 | 7.08E-09 | <1.00E-10 | <1.00E-10 | <1.00E-10 | 2.63E-09 | 2.34E-08 |

## Table 2.5.2-212 PSHA Results for 1 Hz Spectral Acceleration on CEUS Generic Hard Rock for the Fermi 3 Site

| 1 Hz Spectral Acceleration (g) | Annual Exceedance Frequency | | | | | |
|---|---|---|---|---|---|---|
| | Mean | 5th% | 16th% | 50th% | 84th% | 95th% |
| 1.00E-04 | 5.55E-02 | 2.04E-02 | 2.69E-02 | 4.68E-02 | 8.51E-02 | 1.23E-01 |
| 1.00E-03 | 1.27E-02 | 3.80E-03 | 5.89E-03 | 1.07E-02 | 1.95E-02 | 2.95E-02 |
| 3.00E-03 | 4.96E-03 | 1.23E-03 | 2.09E-03 | 4.27E-03 | 7.76E-03 | 1.12E-02 |
| 1.00E-02 | 1.52E-03 | 1.78E-04 | 3.80E-04 | 1.12E-03 | 2.63E-03 | 4.17E-03 |
| 2.00E-02 | 5.93E-04 | 3.55E-05 | 8.51E-05 | 3.16E-04 | 1.05E-03 | 2.14E-03 |
| 3.00E-02 | 3.03E-04 | 1.12E-05 | 3.02E-05 | 1.23E-04 | 4.90E-04 | 1.23E-03 |
| 5.00E-02 | 1.16E-04 | 2.09E-06 | 6.31E-06 | 3.02E-05 | 1.51E-04 | 4.79E-04 |
| 1.00E-01 | 2.49E-05 | 1.26E-07 | 5.25E-07 | 3.47E-06 | 2.29E-05 | 8.71E-05 |
| 2.00E-01 | 3.79E-06 | 7.08E-09 | 2.69E-08 | 3.09E-07 | 2.95E-06 | 1.20E-05 |
| 3.00E-01 | 1.09E-06 | 2.46E-09 | 5.62E-09 | 6.31E-08 | 8.32E-07 | 3.80E-06 |
| 5.00E-01 | 2.12E-07 | 9.12E-10 | 1.78E-09 | 8.71E-09 | 1.55E-07 | 9.12E-07 |
| 1.00E+00 | 2.30E-08 | <1.00E-10 | <1.00E-10 | 1.59E-09 | 1.45E-08 | 9.77E-08 |

## Table 2.5.2-213 PSHA Results for 2.5 Hz Spectral Acceleration on CEUS Generic Hard Rock for the Fermi 3 Site

| 2.5 Hz Spectral Acceleration (g) | Annual Exceedance Frequency | | | | | |
|---|---|---|---|---|---|---|
| | Mean | 5th% | 16th% | 50th% | 84th% | 95th% |
| 1.00E-04 | 8.03E-02 | 2.88E-02 | 3.89E-02 | 6.92E-02 | 1.23E-01 | 1.66E-01 |
| 1.00E-03 | 2.74E-02 | 1.05E-02 | 1.45E-02 | 2.34E-02 | 4.07E-02 | 5.89E-02 |
| 3.00E-03 | 1.18E-02 | 4.07E-03 | 6.03E-03 | 1.05E-02 | 1.74E-02 | 2.46E-02 |
| 1.00E-02 | 3.58E-03 | 9.12E-04 | 1.51E-03 | 3.09E-03 | 5.62E-03 | 7.94E-03 |
| 2.00E-02 | 1.45E-03 | 2.63E-04 | 4.68E-04 | 1.10E-03 | 2.46E-03 | 3.80E-03 |
| 5.00E-02 | 3.09E-04 | 2.82E-05 | 6.17E-05 | 1.62E-04 | 4.90E-04 | 1.10E-03 |
| 1.00E-01 | 7.75E-05 | 3.16E-06 | 9.33E-06 | 3.02E-05 | 1.05E-04 | 3.02E-04 |
| 2.00E-01 | 1.62E-05 | 2.34E-07 | 9.55E-07 | 5.13E-06 | 1.91E-05 | 7.24E-05 |
| 3.00E-01 | 6.14E-06 | 4.47E-08 | 2.09E-07 | 1.70E-06 | 7.24E-06 | 2.82E-05 |
| 5.00E-01 | 1.77E-06 | 6.92E-09 | 2.75E-08 | 3.47E-07 | 2.09E-06 | 7.76E-06 |
| 1.00E+00 | 3.01E-07 | 1.59E-09 | 2.95E-09 | 2.75E-08 | 3.16E-07 | 1.20E-06 |
| 3.00E+00 | 9.95E-09 | <1.00E-10 | <1.00E-10 | 1.41E-09 | 8.71E-09 | 4.27E-08 |

## Table 2.5.2-214 PSHA Results for 5 Hz Spectral Acceleration on CEUS Generic Hard Rock for the Fermi 3 Site

| 5 Hz Spectral Acceleration (g) | Annual Exceedance Frequency | | | | | |
|---|---|---|---|---|---|---|
| | Mean | 5th% | 16th% | 50th% | 84th% | 95th% |
| 1.00E-03 | 3.52E-02 | 1.51E-02 | 2.00E-02 | 3.09E-02 | 5.13E-02 | 7.08E-02 |
| 3.00E-03 | 1.69E-02 | 6.61E-03 | 9.33E-03 | 1.51E-02 | 2.40E-02 | 3.31E-02 |
| 1.00E-02 | 5.77E-03 | 1.74E-03 | 2.69E-03 | 5.01E-03 | 8.91E-03 | 1.20E-02 |
| 2.00E-02 | 2.45E-03 | 5.62E-04 | 9.33E-04 | 2.00E-03 | 3.98E-03 | 5.89E-03 |
| 3.00E-02 | 1.34E-03 | 2.57E-04 | 4.47E-04 | 1.00E-03 | 2.24E-03 | 3.63E-03 |
| 5.00E-02 | 5.82E-04 | 8.51E-05 | 1.62E-04 | 3.72E-04 | 9.55E-04 | 1.86E-03 |
| 1.00E-01 | 1.74E-04 | 1.51E-05 | 3.47E-05 | 9.33E-05 | 2.46E-04 | 6.46E-04 |
| 2.00E-01 | 4.86E-05 | 2.00E-06 | 5.89E-06 | 2.40E-05 | 6.31E-05 | 2.19E-04 |
| 3.00E-01 | 2.22E-05 | 5.37E-07 | 1.86E-06 | 1.02E-05 | 2.82E-05 | 9.77E-05 |
| 5.00E-01 | 7.95E-06 | 9.55E-08 | 3.98E-07 | 3.16E-06 | 9.77E-06 | 3.24E-05 |
| 1.00E+00 | 1.71E-06 | 8.71E-09 | 3.63E-08 | 4.57E-07 | 2.00E-06 | 6.61E-06 |
| 3.00E+00 | 8.37E-08 | 1.12E-09 | 1.70E-09 | 8.71E-09 | 8.13E-08 | 3.39E-07 |

## Table 2.5.2-215 PSHA Results for 10 Hz Spectral Acceleration on CEUS Generic Hard Rock for the Fermi 3 Site

| 10 Hz Spectral Acceleration (g) | Annual Exceedance Frequency | | | | | |
|---|---|---|---|---|---|---|
| | Mean | 5th% | 16th% | 50th% | 84th% | 95th% |
| 1.00E-03 | 3.50E-02 | 1.59E-02 | 2.04E-02 | 3.09E-02 | 4.90E-02 | 6.92E-02 |
| 3.00E-03 | 1.79E-02 | 7.24E-03 | 1.02E-02 | 1.62E-02 | 2.51E-02 | 3.39E-02 |
| 1.00E-02 | 6.93E-03 | 2.09E-03 | 3.24E-03 | 6.03E-03 | 1.05E-02 | 1.48E-02 |
| 2.00E-02 | 3.23E-03 | 7.59E-04 | 1.23E-03 | 2.57E-03 | 5.25E-03 | 7.76E-03 |
| 5.00E-02 | 8.83E-04 | 1.48E-04 | 2.63E-04 | 5.89E-04 | 1.45E-03 | 2.69E-03 |
| 1.00E-01 | 2.94E-04 | 3.47E-05 | 6.92E-05 | 1.70E-04 | 4.37E-04 | 1.07E-03 |
| 2.00E-01 | 9.36E-05 | 6.92E-06 | 1.59E-05 | 5.37E-05 | 1.26E-04 | 3.89E-04 |
| 3.00E-01 | 4.73E-05 | 2.34E-06 | 6.17E-06 | 2.57E-05 | 6.17E-05 | 1.95E-04 |
| 5.00E-01 | 1.96E-05 | 5.37E-07 | 1.74E-06 | 9.77E-06 | 2.46E-05 | 7.59E-05 |
| 1.00E+00 | 5.23E-06 | 4.90E-08 | 2.24E-07 | 2.04E-06 | 6.61E-06 | 1.95E-05 |
| 2.00E+00 | 1.07E-06 | 4.79E-09 | 2.04E-08 | 2.75E-07 | 1.35E-06 | 3.98E-06 |
| 5.00E+00 | 7.27E-08 | 1.12E-09 | 1.74E-09 | 9.12E-09 | 7.59E-08 | 2.82E-07 |

## Table 2.5.2-216 PSHA Results for 25 Hz Spectral Acceleration on CEUS Generic Hard Rock for the Fermi 3 Site

| 25 Hz Spectral Acceleration (g) | Annual Exceedance Frequency | | | | | |
|---|---|---|---|---|---|---|
| | Mean | 5th% | 16th% | 50th% | 84th% | 95th% |
| 1.00E-03 | 3.04E-02 | 1.29E-02 | 1.74E-02 | 2.63E-02 | 4.27E-02 | 6.17E-02 |
| 3.00E-03 | 1.65E-02 | 6.03E-03 | 8.71E-03 | 1.45E-02 | 2.29E-02 | 3.24E-02 |
| 1.00E-02 | 7.17E-03 | 1.86E-03 | 2.95E-03 | 5.75E-03 | 1.12E-02 | 1.70E-02 |
| 3.00E-02 | 2.39E-03 | 3.98E-04 | 6.76E-04 | 1.48E-03 | 4.07E-03 | 7.41E-03 |
| 1.00E-01 | 4.94E-04 | 4.68E-05 | 8.91E-05 | 2.34E-04 | 7.94E-04 | 1.95E-03 |
| 2.00E-01 | 1.72E-04 | 1.10E-05 | 2.57E-05 | 7.94E-05 | 2.40E-04 | 7.41E-04 |
| 3.00E-01 | 8.95E-05 | 4.37E-06 | 1.15E-05 | 4.17E-05 | 1.23E-04 | 3.80E-04 |
| 5.00E-01 | 3.90E-05 | 1.18E-06 | 3.72E-06 | 1.78E-05 | 5.37E-05 | 1.55E-04 |
| 1.00E+00 | 1.23E-05 | 1.23E-07 | 5.75E-07 | 4.37E-06 | 1.66E-05 | 4.47E-05 |
| 2.00E+00 | 3.43E-06 | 9.33E-09 | 7.41E-08 | 7.41E-07 | 4.47E-06 | 1.35E-05 |
| 5.00E+00 | 4.44E-07 | 1.38E-09 | 3.09E-09 | 3.98E-08 | 3.89E-07 | 2.00E-06 |
| 7.00E+00 | 1.80E-07 | 1.12E-09 | 1.62E-09 | 1.07E-08 | 1.32E-07 | 8.91E-07 |

## Table 2.5.2-217 PSHA Results for 100 Hz (PGA) Spectral Acceleration on CEUS Generic Hard Rock for the Fermi 3 Site

| 100 Hz Spectral Acceleration (g) | Annual Exceedance Frequency | | | | | |
|---|---|---|---|---|---|---|
| | Mean | 5th% | 16th% | 50th% | 84th% | 95th% |
| 1.00E-03 | 2.32E-02 | 9.33E-03 | 1.29E-02 | 2.04E-02 | 3.24E-02 | 4.79E-02 |
| 3.00E-03 | 1.09E-02 | 3.55E-03 | 5.37E-03 | 9.55E-03 | 1.62E-02 | 2.29E-02 |
| 1.00E-02 | 3.28E-03 | 6.61E-04 | 1.10E-03 | 2.46E-03 | 5.50E-03 | 8.71E-03 |
| 2.00E-02 | 1.26E-03 | 1.91E-04 | 3.47E-04 | 7.76E-04 | 2.19E-03 | 3.89E-03 |
| 3.00E-02 | 6.78E-04 | 8.71E-05 | 1.66E-04 | 3.89E-04 | 1.15E-03 | 2.29E-03 |
| 5.00E-02 | 3.03E-04 | 3.09E-05 | 6.31E-05 | 1.62E-04 | 4.68E-04 | 1.15E-03 |
| 1.00E-01 | 9.96E-05 | 6.17E-06 | 1.48E-05 | 5.37E-05 | 1.38E-04 | 4.17E-04 |
| 2.00E-01 | 3.32E-05 | 8.71E-07 | 3.09E-06 | 1.66E-05 | 4.47E-05 | 1.29E-04 |
| 3.00E-01 | 1.72E-05 | 2.24E-07 | 1.02E-06 | 7.24E-06 | 2.24E-05 | 6.46E-05 |
| 5.00E-01 | 7.08E-06 | 3.39E-08 | 2.29E-07 | 2.24E-06 | 9.55E-06 | 2.51E-05 |
| 1.00E+00 | 1.71E-06 | 3.24E-09 | 2.04E-08 | 3.02E-07 | 2.19E-06 | 6.92E-06 |
| 3.00E+00 | 7.71E-08 | <1.00E-10 | 1.32E-09 | 5.13E-09 | 5.75E-08 | 3.55E-07 |

## Table 2.5.2-218 Uniform Hazard Response Spectra for the Fermi 3 Site for Generic Hard Rock Conditions

| Period (sec) | Frequency (Hz) | Spectral Acceleration (g) for Annual Exceedance Frequency of: | | | |
|---|---|---|---|---|---|
| | | Mean $10^{-3}$ | Mean $10^{-4}$ | Mean $10^{-5}$ | Mean $10^{-6}$ |
| 0.01 | 100 | 0.0233 | 0.0997 | 0.4101 | 1.2088 |
| 0.04 | 25 | 0.0584 | 0.2799 | 1.1173 | 3.4735 |
| 0.1 | 10 | 0.0461 | 0.1922 | 0.7205 | 2.0545 |
| 0.2 | 5 | 0.0361 | 0.1359 | 0.4473 | 1.2438 |
| 0.4 | 2.5 | 0.0254 | 0.0886 | 0.2451 | 0.6288 |
| 1 | 1 | 0.0139 | 0.0537 | 0.1422 | 0.3080 |
| 2 | 0.5 | 0.0083 | 0.0402 | 0.1236 | 0.2832 |

## Table 2.5.2-219 Rock Hazard Reference and Deaggregation Earthquakes

| | Reference (Controlling) Earthquake | | Deaggregation Earthquakes | | |
|---|---|---|---|---|---|
| Hazard | Magnitude ($m_b$) | Distance (km) | Magnitude ($m_b$) | Distance (km) | Weight |
| Mean $10^{-3}$ 5 and 10 Hz | 6.1 | 139 | 5.4 | 52 | 0.440 |
| | | | 6.1 | 148 | 0.265 |
| | | | 7.1 | 566 | 0.295 |
| Mean $10^{-3}$ 1 and 2.5Hz | 6.8<br>7.0* | 328<br>479* | 5.4 | 33 | 0.126 |
| | | | 6.2 | 145 | 0.148 |
| | | | 7.1 | 582 | 0.726 |
| Mean $10^{-4}$ 5 and 10 Hz | 5.9 | 44 | 5.4 | 17.5 | 0.595 |
| | | | 6.3 | 71 | 0.224 |
| | | | 7.2 | 507 | 0.181 |
| Mean $10^{-4}$ 1 and 2.5Hz | 6.8<br>7.1* | 224<br>500* | 5.5 | 16.3 | 0.172 |
| | | | 6.3 | 58 | 0.117 |
| | | | 7.2 | 535 | 0.711 |
| Mean $10^{-5}$ 5 and 10 Hz | 5.8 | 13.7 | 5.5 | 9.7 | 0.687 |
| | | | 6.4 | 22 | 0.290 |
| | | | 7.4 | 600 | 0.023 |
| Mean $10^{-5}$ 1 and 2.5Hz | 6.7<br>7.2* | 107<br>504* | 5.6 | 10.2 | 0.220 |
| | | | 6.5 | 34 | 0.290 |
| | | | 7.3 | 598 | 0.490 |
| Mean $10^{-6}$ 5 and 10 Hz | 5.9 | 9.8 | 5.5 | 8.1 | 0.550 |
| | | | 6.4 | 11.5 | 0.442 |
| | | | 7.2 | 161 | 0.008 |
| Mean $10^{-6}$ 1 and 2.5Hz | 6.6<br>7.3* | 41<br>492* | 6.0 | 8.0 | 0.415 |
| | | | 6.6 | 32 | 0.306 |
| | | | 7.3 | 600 | 0.279 |

*computed using earthquakes with distances > 100 km

## Table 2.5.2-220 Site Response Analysis Profiles (Sheet 1 of 4)

| Layer Number | Thickness (ft.) | Median Shear Wave Velocity (fps) | Unit Weight (kips/ft.$^3$) | Material Curves | Soil/Rock Type |
|---|---|---|---|---|---|
| **GMRS Profile, Top of Profile Elevation 563 ft.** | | | | | |
| 1 | 5.5 | 1000 | 0.135 | PI 15 or PI 50 | Glacial Till |
| 2 | 5.5 | 1000 | 0.135 | PI 15 or PI 50 | Glacial Till |
| 3 | 10 | 6650 | 0.150 | Linear, $\kappa$ layer 1 | Bass Islands |
| 4 | 10 | 6650 | 0.150 | Linear, $\kappa$ layer 1 | Bass Islands |
| 5 | 10 | 6650 | 0.150 | Linear, $\kappa$ layer 1 | Bass Islands |
| 6 | 10 | 6650 | 0.150 | Linear, $\kappa$ layer 1 | Bass Islands |
| 7 | 11 | 6650 | 0.150 | Linear, $\kappa$ layer 1 | Bass Islands |
| 8 | 12 | 6650 | 0.150 | Linear, $\kappa$ layer 1 | Bass Islands |
| 9 | 12 | 6650 | 0.150 | Linear, $\kappa$ layer 1 | Bass Islands |
| 10 | 15 | 4600 | 0.150 | Linear, $\kappa$ layer 2 | Bass Islands |
| 11 | 20 | 3350 | 0.150 | Linear, $\kappa$ layer 3 | Salina F |
| 12 | 20 | 3350 | 0.150 | Linear, $\kappa$ layer 3 | Salina F |
| 13 | 20 | 3350 | 0.150 | Linear, $\kappa$ layer 3 | Salina F |
| 14 | 21 | 3350 | 0.150 | Linear, $\kappa$ layer 3 | Salina F |
| 15 | 21 | 4050 | 0.150 | Linear, $\kappa$ layer 4 | Salina F |
| 16 | 21 | 4050 | 0.150 | Linear, $\kappa$ layer 4 | Salina F |
| 17 | 10 | 5600 | 0.150 | Linear, $\kappa$ layer 5 | Salina E |
| 18 | 20 | 9450 | 0.150 | Linear, $\kappa$ layer 6 | Salina E |
| 19 | 21 | 9450 | 0.150 | Linear, $\kappa$ layer 6 | Salina E |
| 20 | 21 | 9450 | 0.150 | Linear, $\kappa$ layer 6 | Salina E |
| 21 | 21 | 9450 | 0.150 | Linear, $\kappa$ layer 6 | Salina E |
| 22 | 45 | 9000 | 0.160 | Linear, $\kappa$ layer 7 | Salina C |
| 23 | 45 | 9000 | 0.160 | Linear, $\kappa$ layer 7 | Salina C |
| Halfspace | | 9300 | 0.169 | 0.1% Damping | Salina B |

## Table 2.5.2-220 Site Response Analysis Profiles (Sheet 2 of 4)

| Layer Number | Thickness (ft.) | Median Shear Wave Velocity (fps) | Unit Weight (kips/ft.$^3$) | Material Curves | Soil/Rock Type |
|---|---|---|---|---|---|
| **R/FB FIRS Profile, Top of Profile Elevation 524 ft.** | | | | | |
| 1 | 11 | 6650 | 0.150 | Linear, $\kappa$ layer 1 | Bass Islands |
| 2 | 12 | 6650 | 0.150 | Linear, $\kappa$ layer 1 | Bass Islands |
| 3 | 12 | 6650 | 0.150 | Linear, $\kappa$ layer 1 | Bass Islands |
| 4 | 12 | 6650 | 0.150 | Linear, $\kappa$ layer 1 | Bass Islands |
| 5 | 15 | 4600 | 0.150 | Linear, $\kappa$ layer 2 | Bass Islands |
| 6 | 20 | 3350 | 0.150 | Linear, $\kappa$ layer 3 | Salina F |
| 7 | 20 | 3350 | 0.150 | Linear, $\kappa$ layer 3 | Salina F |
| 8 | 20 | 3350 | 0.150 | Linear, $\kappa$ layer 3 | Salina F |
| 9 | 21 | 3350 | 0.150 | Linear, $\kappa$ layer 3 | Salina F |
| 10 | 21 | 4050 | 0.150 | Linear, $\kappa$ layer 4 | Salina F |
| 11 | 21 | 4050 | 0.150 | Linear, $\kappa$ layer 4 | Salina F |
| 12 | 10 | 5600 | 0.150 | Linear, $\kappa$ layer 5 | Salina E |
| 13 | 20 | 9450 | 0.150 | Linear, $\kappa$ layer 6 | Salina E |
| 14 | 21 | 9450 | 0.150 | Linear, $\kappa$ layer 6 | Salina E |
| 15 | 21 | 9450 | 0.150 | Linear, $\kappa$ layer 6 | Salina E |
| 16 | 21 | 9450 | 0.150 | Linear, $\kappa$ layer 6 | Salina E |
| 17 | 45 | 9000 | 0.160 | Linear, $\kappa$ layer 7 | Salina C |
| 18 | 45 | 9000 | 0.160 | Linear, $\kappa$ layer 7 | Salina C |
| Halfspace | | 9300 | 0.169 | 0.1% Damping | Salina B |

## Table 2.5.2-220 Site Response Analysis Profiles (Sheet 3 of 4)

| Layer Number | Thickness (ft.) | Median Shear Wave Velocity (fps) | Unit Weight (kips/ft.$^3$) | Material Curves | Soil/Rock Type |
|---|---|---|---|---|---|
| **CB FIRS Profile, Top of Profile Elevation 540 ft.** | | | | | |
| 1 | 8 | 6650 | 0.150 | Linear, $\kappa$ layer 1 | Bass Islands |
| 2 | 10 | 6650 | 0.150 | Linear, $\kappa$ layer 1 | Bass Islands |
| 3 | 10 | 6650 | 0.150 | Linear, $\kappa$ layer 1 | Bass Islands |
| 4 | 11 | 6650 | 0.150 | Linear, $\kappa$ layer 1 | Bass Islands |
| 5 | 12 | 6650 | 0.150 | Linear, $\kappa$ layer 1 | Bass Islands |
| 6 | 12 | 6650 | 0.150 | Linear, $\kappa$ layer 1 | Bass Islands |
| 7 | 15 | 4600 | 0.150 | Linear, $\kappa$ layer 2 | Bass Islands |
| 8 | 20 | 3350 | 0.150 | Linear, $\kappa$ layer 3 | Salina F |
| 9 | 20 | 3350 | 0.150 | Linear, $\kappa$ layer 3 | Salina F |
| 10 | 20 | 3350 | 0.150 | Linear, $\kappa$ layer 3 | Salina F |
| 11 | 21 | 3350 | 0.150 | Linear, $\kappa$ layer 3 | Salina F |
| 12 | 21 | 4050 | 0.150 | Linear, $\kappa$ layer 4 | Salina F |
| 13 | 21 | 4050 | 0.150 | Linear, $\kappa$ layer 4 | Salina F |
| 14 | 10 | 5600 | 0.150 | Linear, $\kappa$ layer 5 | Salina E |
| 15 | 20 | 9450 | 0.150 | Linear, $\kappa$ layer 6 | Salina E |
| 16 | 21 | 9450 | 0.150 | Linear, $\kappa$ layer 6 | Salina E |
| 17 | 21 | 9450 | 0.150 | Linear, $\kappa$ layer 6 | Salina E |
| 18 | 21 | 9450 | 0.150 | Linear, $\kappa$ layer 6 | Salina E |
| 19 | 45 | 9000 | 0.160 | Linear, $\kappa$ layer 7 | Salina C |
| 20 | 45 | 9000 | 0.160 | Linear, $\kappa$ layer 7 | Salina C |
| Halfspace | | 9300 | 0.169 | 0.1% Damping | Salina B |

## Table 2.5.2-220 Site Response Analysis Profiles (Sheet 4 of 4)

| Layer Number | Thickness (ft.) | Median Shear Wave Velocity (fps) | Unit Weight (kips/ft.$^3$) | Material Curves | Soil/Rock Type |
|---|---|---|---|---|---|
| **FWSC FIRS Profile, Top of Profile Elevation 582 ft.** | | | | | |
| 1 | 10 | 3600 | 0.145 | Lean concrete backfill | N/A |
| 2 | 10 | 3600 | 0.145 | Lean concrete backfill | N/A |
| 3 | 10 | 3600 | 0.145 | Lean concrete backfill | N/A |
| 4 | 10 | 6650 | 0.150 | Linear, $\kappa$ layer 1 | Bass Islands |
| 5 | 10 | 6650 | 0.150 | Linear, $\kappa$ layer 1 | Bass Islands |
| 6 | 10 | 6650 | 0.150 | Linear, $\kappa$ layer 1 | Bass Islands |
| 7 | 10 | 6650 | 0.150 | Linear, $\kappa$ layer 1 | Bass Islands |
| 8 | 11 | 6650 | 0.150 | Linear, $\kappa$ layer 1 | Bass Islands |
| 9 | 12 | 6650 | 0.150 | Linear, $\kappa$ layer 1 | Bass Islands |
| 10 | 12 | 6650 | 0.150 | Linear, $\kappa$ layer 1 | Bass Islands |
| 11 | 15 | 4600 | 0.150 | Linear, $\kappa$ layer 2 | Bass Islands |
| 12 | 20 | 3350 | 0.150 | Linear, $\kappa$ layer 3 | Salina F |
| 13 | 20 | 3350 | 0.150 | Linear, $\kappa$ layer 3 | Salina F |
| 14 | 20 | 3350 | 0.150 | Linear, $\kappa$ layer 3 | Salina F |
| 15 | 21 | 3350 | 0.150 | Linear, $\kappa$ layer 3 | Salina F |
| 16 | 21 | 4050 | 0.150 | Linear, $\kappa$ layer 4 | Salina F |
| 17 | 21 | 4050 | 0.150 | Linear, $\kappa$ layer 4 | Salina F |
| 18 | 10 | 5600 | 0.150 | Linear, $\kappa$ layer 5 | Salina E |
| 19 | 20 | 9450 | 0.150 | Linear, $\kappa$ layer 6 | Salina E |
| 20 | 21 | 9450 | 0.150 | Linear, $\kappa$ layer 6 | Salina E |
| 21 | 21 | 9450 | 0.150 | Linear, $\kappa$ layer 6 | Salina E |
| 22 | 21 | 9450 | 0.150 | Linear, $\kappa$ layer 6 | Salina E |
| 23 | 45 | 9000 | 0.160 | Linear, $\kappa$ layer 7 | Salina C |
| 24 | 45 | 9000 | 0.160 | Linear, $\kappa$ layer 7 | Salina C |
| Halfspace | | 9300 | 0.169 | 0.1% Damping | Salina B |

## Table 2.5.2-221 Rock Damping Values for Site Response Analyses

| Layer | Thickness (ft.) | $V_s$ (fps) | 1% Damping | | 2% Damping | | 3% Damping | |
|---|---|---|---|---|---|---|---|---|
| | | | Damping Ratio (%) | $\kappa$ (sec) | Damping Ratio (%) | $\kappa$ (sec) | Damping Ratio (%) | $\kappa$ (sec) |
| Bass Islands 1 | 75 | 6650 | 0.52% | 0.0001 | 1.03% | 0.0002 | 1.55% | 0.0003 |
| Bass Islands 2 | 15 | 4600 | 0.75% | 0.0000 | 1.49% | 0.0001 | 2.24% | 0.0001 |
| Salina F 1 | 81 | 3350 | 1.03% | 0.0005 | 2.05% | 0.0010 | 3.08% | 0.0015 |
| Salina F 2 | 42 | 4050 | 0.85% | 0.0002 | 1.70% | 0.0004 | 2.55% | 0.0005 |
| Salina E 1 | 10 | 5600 | 0.61% | 0.0000 | 1.23% | 0.0000 | 1.84% | 0.0001 |
| Salina E 2 | 83 | 9450 | 0.36% | 0.0001 | 0.73% | 0.0001 | 1.09% | 0.0002 |
| Salina C | 90 | 9000 | 0.38% | 0.0001 | 0.76% | 0.0002 | 1.15% | 0.0002 |
| | | | | Total 0.001 | | Total 0.002 | | Total 0.003 |

## Table 2.5.2-222 Time History Data Sets from McGuire et al. (2001) Used for Each Deaggregation Earthquake (Sheet 1 of 2)

| Hazard Level | Deaggregation Earthquakes (DE) | | | | |
|---|---|---|---|---|---|
| | Designation | Magnitude ($m_b$) | Distance (km) | Weight | NUREG/CR-6728 CEUS Data Set |
| Mean $10^{-3}$ 5 and 10 Hz | HF DEL | **5.4** | **52** | **0.440** | **M** 4.5–6, D 0–50 km |
| | HF DEM | **6.1** | **148** | **0.265** | **M** 6–7, D 100–200 km |
| | HF DEH | **7.1** | **566** | **0.295** | **M** >7, D 100–200 km |
| Mean $10^{-3}$ 1 and 2.5 Hz | LF DEL | **5.4** | **33** | **0.126** | **M** 4.5–6, D 0-50 km |
| | LF DEM | **6.2** | **145** | **0.148** | **M** 6–7, D 100–200 km |
| | LF DEH | **7.1** | **582** | **0.726** | **M** >7, D 100-200 km |
| Mean $10^{-4}$ 5 and 10 Hz | HF DEL | **5.4** | **17.5** | **0.595** | **M** 4.5–6, D 0–50 km |
| | HF DEM | **6.3** | **71** | **0.224** | **M** 6–7, D 50–100 km |
| | HF DEH | **7.2** | **507** | **0.181** | **M** >7, D 100–200 km |
| Mean $10^{-4}$ 1 and 2.5 Hz | LF DEL | **5.5** | **16.3** | **0.172** | **M** 4.5–6, D 0–50 km |
| | LF DEM | **6.3** | **58** | **0.117** | **M** 6–7, D 50-100 km |
| | LF DEH | **7.2** | **535** | **0.711** | **M** >7, D 100–200 km |
| Mean $10^{-5}$ 5 and 10 Hz | HF DEL | **5.5** | **9.7** | **0.687** | **M** 4.5–6, D 0–50 km |
| | HF DEM | **6.4** | **22** | **0.290** | **M** 6–7, D 10–50 km |
| | HF DEH | **7.4** | **600** | **0.023** | **M** >7, D 100–200 km |
| Mean $10^{-5}$ 1 and 2.5 Hz | LF DEL | **5.6** | **10.2** | **0.220** | **M** 4.5–6, D 0–50 km |
| | LF DEM | **6.5** | **34** | **0.290** | **M** 6–7, D 10–50 km |
| | LF DEH | **7.3** | **598** | **0.490** | **M** >7, D 100-200 km |

## Table 2.5.2-222 Time History Data Sets from McGuire et al. (2001) Used for Each Deaggregation Earthquake (Sheet 2 of 2)

| Hazard Level | Deaggregation Earthquakes (DE) | | | | |
|---|---|---|---|---|---|
| | Designation | Magnitude ($m_b$) | Distance (km) | Weight | NUREG/CR-6728 CEUS Data Set |
| Mean $10^{-6}$ 5 and 10 Hz | HF DEL | 5.5 | 8.1 | 0.550 | **M** 4.5–6, D 0–50 km |
| | HF DEM | 6.4 | 11.5 | 0.442 | **M** 6–7, D 10–50 km |
| | HF DEH | 7.2 | 161 | 0.008 | **M** >7, D 100–200 km |
| Mean $10^{-6}$ 1 and 2.5 Hz | LF DEL | 6.0 | 8.0 | 0.415 | **M** 4.5–6, D 0–50 km |
| | LF DEM | 6.6 | 32 | 0.306 | **M** 6–7, D 10–50 km |
| | LF DEH | 7.3 | 600 | 0.279 | **M** >7, D 100–200 km |

## Table 2.5.2-223 GMRS for the Fermi 3 Site (Sheet 1 of 4)

| Spectral Frequency (Hz) | 5% Damped Spectral Acceleration (g) | | | | |
|---|---|---|---|---|---|
| | $10^{-4}$ UHRS | $10^{-5}$ UHRS | Horizontal GMRS | Vertical/Horizontal | Vertical GMRS |
| 100.000 | 0.1448 | 0.8961 | 0.4032 | 1.0000 | 0.4032 |
| 60.241 | 0.2306 | 1.3941 | 0.6274 | 1.1374 | 0.7136 |
| 50.000 | 0.2537 | 1.5810 | 0.7115 | 1.1244 | 0.7999 |
| 40.000 | 0.3063 | 1.9208 | 0.8644 | 1.0426 | 0.9012 |
| 33.343 | 0.3625 | 2.1925 | 0.9866 | 0.9675 | 0.9546 |
| 30.303 | 0.4026 | 2.3975 | 1.0789 | 0.9400 | 1.0142 |
| 25.000 | 0.4944 | 2.9339 | 1.3202 | 0.8800 | 1.1618 |
| 23.810 | 0.5108 | 2.9987 | 1.3494 | 0.8681 | 1.1715 |
| 22.727 | 0.5238 | 3.0406 | 1.3683 | 0.8569 | 1.1725 |
| 21.739 | 0.5239 | 3.0395 | 1.3678 | 0.8461 | 1.1574 |
| 20.833 | 0.5136 | 2.9631 | 1.3334 | 0.8355 | 1.1141 |
| 20.000 | 0.5036 | 2.9190 | 1.3136 | 0.8255 | 1.0843 |
| 18.182 | 0.4571 | 2.7955 | 1.2580 | 0.8069 | 1.0151 |
| 16.667 | 0.4146 | 2.6288 | 1.1829 | 0.7984 | 0.9444 |
| 15.385 | 0.3832 | 2.4173 | 1.0878 | 0.7906 | 0.8600 |
| 14.286 | 0.3541 | 2.2422 | 1.0090 | 0.7834 | 0.7905 |
| 13.343 | 0.3431 | 2.1279 | 0.9575 | 0.7769 | 0.7439 |
| 12.500 | 0.3331 | 2.0262 | 0.9118 | 0.7708 | 0.7028 |
| 11.765 | 0.3240 | 1.9351 | 0.8708 | 0.7651 | 0.6662 |
| 11.111 | 0.3157 | 1.8530 | 0.8338 | 0.7597 | 0.6335 |
| 10.526 | 0.3080 | 1.7785 | 0.8003 | 0.7547 | 0.6040 |
| 10.000 | 0.3008 | 1.7106 | 0.7698 | 0.7500 | 0.5773 |
| 9.091 | 0.2902 | 1.5777 | 0.7100 | 0.7500 | 0.5325 |
| 8.343 | 0.2808 | 1.4653 | 0.6594 | 0.7500 | 0.4946 |
| 7.692 | 0.2724 | 1.3691 | 0.6161 | 0.7500 | 0.4621 |
| 7.143 | 0.2648 | 1.2856 | 0.5785 | 0.7500 | 0.4339 |
| 6.667 | 0.2580 | 1.2125 | 0.5456 | 0.7500 | 0.4092 |

## Table 2.5.2-223 GMRS for the Fermi 3 Site (Sheet 2 of 4)

| Spectral Frequency (Hz) | 5% Damped Spectral Acceleration (g) | | | | |
|---|---|---|---|---|---|
| | $10^{-4}$ UHRS | $10^{-5}$ UHRS | Horizontal GMRS | Vertical/Horizontal | Vertical GMRS |
| 6.250 | 0.2518 | 1.1478 | 0.5165 | 0.7500 | 0.3874 |
| 5.882 | 0.2461 | 1.0902 | 0.4906 | 0.7500 | 0.3680 |
| 5.556 | 0.2408 | 1.0386 | 0.4674 | 0.7500 | 0.3505 |
| 5.263 | 0.2359 | 0.9920 | 0.4466 | 0.7500 | 0.3350 |
| 5.000 | 0.2314 | 0.9497 | 0.4296 | 0.7500 | 0.3222 |
| 4.545 | 0.2203 | 0.8822 | 0.4011 | 0.7500 | 0.3008 |
| 4.167 | 0.2107 | 0.8247 | 0.3766 | 0.7500 | 0.2825 |
| 3.846 | 0.2022 | 0.7752 | 0.3555 | 0.7500 | 0.2666 |
| 3.571 | 0.1966 | 0.7404 | 0.3408 | 0.7500 | 0.2556 |
| 3.343 | 0.1892 | 0.7068 | 0.3258 | 0.7500 | 0.2444 |
| 3.125 | 0.1773 | 0.6559 | 0.3029 | 0.7500 | 0.2272 |
| 2.941 | 0.1652 | 0.6053 | 0.2801 | 0.7500 | 0.2101 |
| 2.778 | 0.1533 | 0.5549 | 0.2574 | 0.7500 | 0.1931 |
| 2.632 | 0.1431 | 0.5140 | 0.2388 | 0.7500 | 0.1791 |
| 2.500 | 0.1329 | 0.4740 | 0.2205 | 0.7500 | 0.1654 |
| 2.381 | 0.1226 | 0.4364 | 0.2031 | 0.7500 | 0.1523 |
| 2.273 | 0.1138 | 0.4048 | 0.1884 | 0.7500 | 0.1413 |
| 2.174 | 0.1053 | 0.3758 | 0.1748 | 0.7500 | 0.1311 |
| 2.083 | 0.0997 | 0.3557 | 0.1655 | 0.7500 | 0.1241 |
| 2.000 | 0.0935 | 0.3339 | 0.1553 | 0.7500 | 0.1165 |
| 1.818 | 0.0805 | 0.2888 | 0.1342 | 0.7500 | 0.1007 |
| 1.667 | 0.0707 | 0.2551 | 0.1184 | 0.7500 | 0.0888 |
| 1.538 | 0.0632 | 0.2281 | 0.1059 | 0.7500 | 0.0794 |
| 1.429 | 0.0571 | 0.2062 | 0.0957 | 0.7500 | 0.0718 |
| 1.343 | 0.0525 | 0.1901 | 0.0882 | 0.7500 | 0.0661 |
| 1.250 | 0.0495 | 0.1801 | 0.0835 | 0.7500 | 0.0626 |
| 1.176 | 0.0467 | 0.1706 | 0.0790 | 0.7500 | 0.0592 |

## Table 2.5.2-223 GMRS for the Fermi 3 Site (Sheet 3 of 4)

| Spectral Frequency (Hz) | 5% Damped Spectral Acceleration (g) | | | | |
|---|---|---|---|---|---|
| | $10^{-4}$ UHRS | $10^{-5}$ UHRS | Horizontal GMRS | Vertical/Horizontal | Vertical GMRS |
| 1.111 | 0.0447 | 0.1637 | 0.0758 | 0.7500 | 0.0568 |
| 1.053 | 0.0426 | 0.1564 | 0.0723 | 0.7500 | 0.0542 |
| 1.000 | 0.0407 | 0.1505 | 0.0695 | 0.7500 | 0.0521 |
| 0.909 | 0.0379 | 0.1455 | 0.0667 | 0.7500 | 0.0500 |
| 0.833 | 0.0357 | 0.1411 | 0.0643 | 0.7500 | 0.0482 |
| 0.769 | 0.0336 | 0.1371 | 0.0621 | 0.7500 | 0.0466 |
| 0.714 | 0.0319 | 0.1346 | 0.0606 | 0.7500 | 0.0454 |
| 0.667 | 0.0306 | 0.1327 | 0.0597 | 0.7500 | 0.0448 |
| 0.625 | 0.0294 | 0.1304 | 0.0587 | 0.7500 | 0.0440 |
| 0.588 | 0.0281 | 0.1285 | 0.0578 | 0.7500 | 0.0434 |
| 0.556 | 0.0273 | 0.1271 | 0.0572 | 0.7500 | 0.0429 |
| 0.526 | 0.0263 | 0.1250 | 0.0563 | 0.7500 | 0.0422 |
| 0.500 | 0.0255 | 0.1238 | 0.0557 | 0.7500 | 0.0418 |
| 0.455 | 0.0235 | 0.1152 | 0.0518 | 0.7500 | 0.0389 |
| 0.417 | 0.0219 | 0.1082 | 0.0487 | 0.7500 | 0.0365 |
| 0.385 | 0.0205 | 0.1022 | 0.0460 | 0.7500 | 0.0345 |
| 0.357 | 0.0194 | 0.0977 | 0.0440 | 0.7500 | 0.0330 |
| 0.343 | 0.0184 | 0.0936 | 0.0421 | 0.7500 | 0.0316 |
| 0.313 | 0.0176 | 0.0898 | 0.0404 | 0.7500 | 0.0303 |
| 0.294 | 0.0168 | 0.0861 | 0.0387 | 0.7500 | 0.0290 |
| 0.278 | 0.0162 | 0.0828 | 0.0373 | 0.7500 | 0.0280 |
| 0.263 | 0.0155 | 0.0801 | 0.0360 | 0.7500 | 0.0270 |
| 0.250 | 0.0150 | 0.0775 | 0.0349 | 0.7500 | 0.0262 |
| 0.238 | 0.0145 | 0.0751 | 0.0338 | 0.7500 | 0.0254 |
| 0.227 | 0.0140 | 0.0731 | 0.0329 | 0.7500 | 0.0247 |
| 0.217 | 0.0136 | 0.0710 | 0.0319 | 0.7500 | 0.0240 |
| 0.208 | 0.0131 | 0.0691 | 0.0311 | 0.7500 | 0.0233 |

## Table 2.5.2-223 GMRS for the Fermi 3 Site (Sheet 4 of 4)

| Spectral Frequency (Hz) | 5% Damped Spectral Acceleration (g) | | | | |
|---|---|---|---|---|---|
| | $10^{-4}$ UHRS | $10^{-5}$ UHRS | Horizontal GMRS | Vertical/Horizontal | Vertical GMRS |
| 0.200 | 0.0127 | 0.0675 | 0.0304 | 0.7500 | 0.0228 |
| 0.182 | 0.0118 | 0.0639 | 0.0287 | 0.7500 | 0.0216 |
| 0.167 | 0.0111 | 0.0604 | 0.0272 | 0.7500 | 0.0204 |
| 0.154 | 0.0105 | 0.0574 | 0.0258 | 0.7500 | 0.0194 |
| 0.143 | 0.0099 | 0.0547 | 0.0246 | 0.7500 | 0.0184 |
| 0.133 | 0.0094 | 0.0524 | 0.0236 | 0.7500 | 0.0177 |
| 0.125 | 0.0089 | 0.0504 | 0.0227 | 0.7500 | 0.0170 |
| 0.118 | 0.0085 | 0.0486 | 0.0219 | 0.7500 | 0.0164 |
| 0.111 | 0.0082 | 0.0472 | 0.0212 | 0.7500 | 0.0159 |
| 0.100 | 0.0076 | 0.0442 | 0.0199 | 0.7500 | 0.0149 |

## Table 2.5.2-224 R/FB FIRS for the Fermi 3 Site (Sheet 1 of 4)

| Spectral Frequency (Hz) | 5% Damped Spectral Acceleration (g) | | | | |
|---|---|---|---|---|---|
| | $10^{-4}$ UHRS | $10^{-5}$ UHRS | Horizontal FIRS | Vertical/Horizontal | Vertical FIRS |
| 100.000 | 0.0760 | 0.4854 | 0.2185 | 1.0000 | 0.2185 |
| 60.241 | 0.1248 | 0.8124 | 0.3656 | 1.1374 | 0.4158 |
| 50.000 | 0.1448 | 0.9595 | 0.4318 | 1.1244 | 0.4855 |
| 40.000 | 0.1544 | 1.0237 | 0.4607 | 1.0426 | 0.4803 |
| 33.343 | 0.1532 | 1.0120 | 0.4554 | 0.9675 | 0.4406 |
| 30.303 | 0.1551 | 1.0325 | 0.4646 | 0.9400 | 0.4367 |
| 25.000 | 0.1591 | 1.0749 | 0.4837 | 0.8800 | 0.4257 |
| 23.810 | 0.1613 | 1.0815 | 0.4867 | 0.8681 | 0.4225 |
| 22.727 | 0.1635 | 1.0878 | 0.4895 | 0.8569 | 0.4195 |
| 21.739 | 0.1656 | 1.0938 | 0.4922 | 0.8461 | 0.4165 |
| 20.833 | 0.1677 | 1.0997 | 0.4948 | 0.8355 | 0.4135 |
| 20.000 | 0.1697 | 1.1053 | 0.4974 | 0.8255 | 0.4106 |
| 18.182 | 0.1744 | 1.1185 | 0.5033 | 0.8069 | 0.4061 |
| 16.667 | 0.1788 | 1.1307 | 0.5088 | 0.7984 | 0.4062 |
| 15.385 | 0.1806 | 1.1041 | 0.4968 | 0.7906 | 0.3928 |
| 14.286 | 0.1822 | 1.0937 | 0.4922 | 0.7834 | 0.3856 |
| 13.343 | 0.1837 | 1.0841 | 0.4879 | 0.7769 | 0.3790 |
| 12.500 | 0.1851 | 1.0752 | 0.4839 | 0.7708 | 0.3729 |
| 11.765 | 0.1864 | 1.0670 | 0.4801 | 0.7651 | 0.3673 |
| 11.111 | 0.1877 | 1.0592 | 0.4766 | 0.7597 | 0.3621 |
| 10.526 | 0.1889 | 1.0519 | 0.4734 | 0.7547 | 0.3573 |
| 10.000 | 0.1901 | 1.0451 | 0.4703 | 0.7500 | 0.3527 |
| 9.091 | 0.1937 | 1.0236 | 0.4606 | 0.7500 | 0.3455 |
| 8.343 | 0.1971 | 1.0044 | 0.4520 | 0.7500 | 0.3390 |
| 7.692 | 0.2002 | 0.9871 | 0.4442 | 0.7500 | 0.3331 |
| 7.143 | 0.2032 | 0.9713 | 0.4371 | 0.7500 | 0.3278 |
| 6.667 | 0.2060 | 0.9568 | 0.4306 | 0.7500 | 0.3229 |
| 6.250 | 0.2086 | 0.9434 | 0.4246 | 0.7500 | 0.3184 |

## Table 2.5.2-224 R/FB FIRS for the Fermi 3 Site (Sheet 2 of 4)

| Spectral Frequency (Hz) | 5% Damped Spectral Acceleration (g) | | | | |
|---|---|---|---|---|---|
| | $10^{-4}$ UHRS | $10^{-5}$ UHRS | Horizontal FIRS | Vertical/Horizontal | Vertical FIRS |
| 5.882 | 0.2112 | 0.9311 | 0.4190 | 0.7500 | 0.3142 |
| 5.556 | 0.2136 | 0.9196 | 0.4138 | 0.7500 | 0.3104 |
| 5.263 | 0.2159 | 0.9088 | 0.4090 | 0.7500 | 0.3068 |
| 5.000 | 0.2181 | 0.8987 | 0.4062 | 0.7500 | 0.3047 |
| 4.545 | 0.2196 | 0.8653 | 0.3946 | 0.7500 | 0.2960 |
| 4.167 | 0.2128 | 0.8256 | 0.3777 | 0.7500 | 0.2833 |
| 3.846 | 0.2011 | 0.7678 | 0.3524 | 0.7500 | 0.2643 |
| 3.571 | 0.1863 | 0.7008 | 0.3226 | 0.7500 | 0.2419 |
| 3.343 | 0.1723 | 0.6427 | 0.2964 | 0.7500 | 0.2223 |
| 3.125 | 0.1573 | 0.5807 | 0.2683 | 0.7500 | 0.2013 |
| 2.941 | 0.1446 | 0.5294 | 0.2450 | 0.7500 | 0.1838 |
| 2.778 | 0.1338 | 0.4841 | 0.2246 | 0.7500 | 0.1684 |
| 2.632 | 0.1252 | 0.4495 | 0.2089 | 0.7500 | 0.1566 |
| 2.500 | 0.1168 | 0.4150 | 0.1932 | 0.7500 | 0.1449 |
| 2.381 | 0.1085 | 0.3849 | 0.1793 | 0.7500 | 0.1345 |
| 2.273 | 0.1013 | 0.3600 | 0.1676 | 0.7500 | 0.1257 |
| 2.174 | 0.0949 | 0.3382 | 0.1574 | 0.7500 | 0.1180 |
| 2.083 | 0.0901 | 0.3210 | 0.1494 | 0.7500 | 0.1120 |
| 2.000 | 0.0851 | 0.3036 | 0.1413 | 0.7500 | 0.1060 |
| 1.818 | 0.0746 | 0.2670 | 0.1242 | 0.7500 | 0.0931 |
| 1.667 | 0.0664 | 0.2389 | 0.1110 | 0.7500 | 0.0832 |
| 1.538 | 0.0598 | 0.2149 | 0.0998 | 0.7500 | 0.0749 |
| 1.429 | 0.0543 | 0.1954 | 0.0907 | 0.7500 | 0.0681 |
| 1.343 | 0.0502 | 0.1816 | 0.0843 | 0.7500 | 0.0632 |
| 1.250 | 0.0475 | 0.1729 | 0.0801 | 0.7500 | 0.0601 |
| 1.176 | 0.0451 | 0.1647 | 0.0763 | 0.7500 | 0.0572 |
| 1.111 | 0.0432 | 0.1583 | 0.0733 | 0.7500 | 0.0549 |
| 1.053 | 0.0413 | 0.1518 | 0.0702 | 0.7500 | 0.0527 |

## Table 2.5.2-224 R/FB FIRS for the Fermi 3 Site (Sheet 3 of 4)

| Spectral Frequency (Hz) | 5% Damped Spectral Acceleration (g) | | | | |
|---|---|---|---|---|---|
| | $10^{-4}$ UHRS | $10^{-5}$ UHRS | Horizontal FIRS | Vertical/Horizontal | Vertical FIRS |
| 1.000 | 0.0397 | 0.1464 | 0.0677 | 0.7500 | 0.0507 |
| 0.909 | 0.0371 | 0.1421 | 0.0652 | 0.7500 | 0.0489 |
| 0.833 | 0.0350 | 0.1379 | 0.0629 | 0.7500 | 0.0472 |
| 0.769 | 0.0330 | 0.1347 | 0.0610 | 0.7500 | 0.0458 |
| 0.714 | 0.0314 | 0.1323 | 0.0596 | 0.7500 | 0.0447 |
| 0.667 | 0.0301 | 0.1304 | 0.0587 | 0.7500 | 0.0440 |
| 0.625 | 0.0289 | 0.1283 | 0.0578 | 0.7500 | 0.0433 |
| 0.588 | 0.0278 | 0.1266 | 0.0570 | 0.7500 | 0.0427 |
| 0.556 | 0.0269 | 0.1251 | 0.0563 | 0.7500 | 0.0422 |
| 0.526 | 0.0260 | 0.1232 | 0.0554 | 0.7500 | 0.0416 |
| 0.500 | 0.0252 | 0.1220 | 0.0549 | 0.7500 | 0.0412 |
| 0.455 | 0.0233 | 0.1137 | 0.0512 | 0.7500 | 0.0384 |
| 0.417 | 0.0217 | 0.1070 | 0.0481 | 0.7500 | 0.0361 |
| 0.385 | 0.0203 | 0.1010 | 0.0454 | 0.7500 | 0.0341 |
| 0.357 | 0.0192 | 0.0961 | 0.0433 | 0.7500 | 0.0324 |
| 0.343 | 0.0182 | 0.0919 | 0.0413 | 0.7500 | 0.0310 |
| 0.313 | 0.0173 | 0.0880 | 0.0396 | 0.7500 | 0.0297 |
| 0.294 | 0.0165 | 0.0843 | 0.0379 | 0.7500 | 0.0285 |
| 0.278 | 0.0159 | 0.0809 | 0.0364 | 0.7500 | 0.0273 |
| 0.263 | 0.0152 | 0.0780 | 0.0351 | 0.7500 | 0.0263 |
| 0.250 | 0.0147 | 0.0755 | 0.0340 | 0.7500 | 0.0255 |
| 0.238 | 0.0142 | 0.0731 | 0.0329 | 0.7500 | 0.0247 |
| 0.227 | 0.0137 | 0.0710 | 0.0319 | 0.7500 | 0.0240 |
| 0.217 | 0.0132 | 0.0689 | 0.0310 | 0.7500 | 0.0233 |
| 0.208 | 0.0128 | 0.0670 | 0.0302 | 0.7500 | 0.0226 |
| 0.200 | 0.0124 | 0.0654 | 0.0294 | 0.7500 | 0.0221 |
| 0.182 | 0.0115 | 0.0617 | 0.0278 | 0.7500 | 0.0208 |
| 0.167 | 0.0108 | 0.0581 | 0.0262 | 0.7500 | 0.0196 |

## Table 2.5.2-224 R/FB FIRS for the Fermi 3 Site (Sheet 4 of 4)

| Spectral Frequency (Hz) | 5% Damped Spectral Acceleration (g) | | | | |
|---|---|---|---|---|---|
| | $10^{-4}$ UHRS | $10^{-5}$ UHRS | Horizontal FIRS | Vertical/Horizontal | Vertical FIRS |
| 0.154 | 0.0102 | 0.0551 | 0.0248 | 0.7500 | 0.0186 |
| 0.143 | 0.0096 | 0.0523 | 0.0235 | 0.7500 | 0.0176 |
| 0.133 | 0.0091 | 0.0500 | 0.0225 | 0.7500 | 0.0169 |
| 0.125 | 0.0087 | 0.0481 | 0.0216 | 0.7500 | 0.0162 |
| 0.118 | 0.0079 | 0.0449 | 0.0202 | 0.7500 | 0.0152 |
| 0.111 | 0.0074 | 0.0419 | 0.0188 | 0.7500 | 0.0141 |
| 0.100 | 0.0079 | 0.0449 | 0.0202 | 0.7500 | 0.0152 |

## Table 2.5.2-225 CB FIRS for the Fermi 3 Site (Sheet 1 of 4)

| Spectral Frequency (Hz) | 5% Damped Spectral Acceleration (g) | | | | |
|---|---|---|---|---|---|
| | $10^{-4}$ UHRS | $10^{-5}$ UHRS | Horizontal FIRS | Vertical/Horizontal | Vertical FIRS |
| 100.000 | 0.0746 | 0.4722 | 0.2125 | 1.0000 | 0.2125 |
| 60.241 | 0.1232 | 0.8003 | 0.3601 | 1.1374 | 0.4096 |
| 50.000 | 0.1472 | 0.9801 | 0.4410 | 1.1244 | 0.4959 |
| 40.000 | 0.1683 | 1.1318 | 0.5093 | 1.0426 | 0.5310 |
| 33.343 | 0.1670 | 1.1187 | 0.5034 | 0.9675 | 0.4871 |
| 30.303 | 0.1666 | 1.1068 | 0.4981 | 0.9400 | 0.4682 |
| 25.000 | 0.1658 | 1.0831 | 0.4874 | 0.8800 | 0.4289 |
| 23.810 | 0.1668 | 1.0779 | 0.4851 | 0.8681 | 0.4211 |
| 22.727 | 0.1677 | 1.0730 | 0.4829 | 0.8569 | 0.4138 |
| 21.739 | 0.1686 | 1.0683 | 0.4808 | 0.8461 | 0.4068 |
| 20.833 | 0.1695 | 1.0639 | 0.4787 | 0.8355 | 0.4000 |
| 20.000 | 0.1703 | 1.0596 | 0.4768 | 0.8255 | 0.3936 |
| 18.182 | 0.1723 | 1.0498 | 0.4724 | 0.8069 | 0.3812 |
| 16.667 | 0.1741 | 1.0408 | 0.4684 | 0.7984 | 0.3739 |
| 15.385 | 0.1758 | 1.0327 | 0.4647 | 0.7906 | 0.3674 |
| 14.286 | 0.1774 | 1.0141 | 0.4563 | 0.7834 | 0.3575 |
| 13.343 | 0.1789 | 1.0065 | 0.4529 | 0.7769 | 0.3519 |
| 12.500 | 0.1803 | 0.9994 | 0.4497 | 0.7708 | 0.3466 |
| 11.765 | 0.1816 | 0.9928 | 0.4468 | 0.7651 | 0.3418 |
| 11.111 | 0.1828 | 0.9867 | 0.4440 | 0.7597 | 0.3373 |
| 10.526 | 0.1840 | 0.9809 | 0.4414 | 0.7547 | 0.3331 |
| 10.000 | 0.1852 | 0.9754 | 0.4389 | 0.7500 | 0.3292 |
| 9.091 | 0.1887 | 0.9570 | 0.4307 | 0.7500 | 0.3230 |
| 8.343 | 0.1920 | 0.9406 | 0.4233 | 0.7500 | 0.3175 |
| 7.692 | 0.1951 | 0.9257 | 0.4166 | 0.7500 | 0.3124 |
| 7.143 | 0.1980 | 0.9121 | 0.4105 | 0.7500 | 0.3078 |
| 6.667 | 0.2008 | 0.8997 | 0.4049 | 0.7500 | 0.3036 |
| 6.250 | 0.2034 | 0.8882 | 0.3997 | 0.7500 | 0.2998 |
| 5.882 | 0.2058 | 0.8775 | 0.3949 | 0.7500 | 0.2962 |

## Table 2.5.2-225 CB FIRS for the Fermi 3 Site (Sheet 2 of 4)

| Spectral Frequency (Hz) | 5% Damped Spectral Acceleration (g) | | | | |
|---|---|---|---|---|---|
| | $10^{-4}$ UHRS | $10^{-5}$ UHRS | Horizontal FIRS | Vertical/Horizontal | Vertical FIRS |
| 5.556 | 0.2082 | 0.8676 | 0.3913 | 0.7500 | 0.2935 |
| 5.263 | 0.2105 | 0.8583 | 0.3888 | 0.7500 | 0.2916 |
| 5.000 | 0.2126 | 0.8496 | 0.3864 | 0.7500 | 0.2898 |
| 4.545 | 0.2139 | 0.8396 | 0.3832 | 0.7500 | 0.2874 |
| 4.167 | 0.2139 | 0.8256 | 0.3781 | 0.7500 | 0.2836 |
| 3.846 | 0.2049 | 0.7820 | 0.3589 | 0.7500 | 0.2692 |
| 3.571 | 0.1936 | 0.7295 | 0.3357 | 0.7500 | 0.2518 |
| 3.343 | 0.1821 | 0.6798 | 0.3134 | 0.7500 | 0.2351 |
| 3.125 | 0.1695 | 0.6244 | 0.2886 | 0.7500 | 0.2165 |
| 2.941 | 0.1562 | 0.5711 | 0.2644 | 0.7500 | 0.1983 |
| 2.778 | 0.1437 | 0.5190 | 0.2409 | 0.7500 | 0.1806 |
| 2.632 | 0.1333 | 0.4775 | 0.2220 | 0.7500 | 0.1665 |
| 2.500 | 0.1237 | 0.4399 | 0.2048 | 0.7500 | 0.1536 |
| 2.381 | 0.1146 | 0.4065 | 0.1893 | 0.7500 | 0.1420 |
| 2.273 | 0.1064 | 0.3782 | 0.1761 | 0.7500 | 0.1320 |
| 2.174 | 0.0991 | 0.3529 | 0.1642 | 0.7500 | 0.1232 |
| 2.083 | 0.0941 | 0.3344 | 0.1557 | 0.7500 | 0.1168 |
| 2.000 | 0.0886 | 0.3153 | 0.1468 | 0.7500 | 0.1101 |
| 1.818 | 0.0770 | 0.2759 | 0.1283 | 0.7500 | 0.0962 |
| 1.667 | 0.0680 | 0.2451 | 0.1138 | 0.7500 | 0.0853 |
| 1.538 | 0.0609 | 0.2194 | 0.1019 | 0.7500 | 0.0764 |
| 1.429 | 0.0553 | 0.1996 | 0.0927 | 0.7500 | 0.0695 |
| 1.343 | 0.0513 | 0.1852 | 0.0860 | 0.7500 | 0.0645 |
| 1.250 | 0.0483 | 0.1757 | 0.0814 | 0.7500 | 0.0611 |
| 1.176 | 0.0457 | 0.1670 | 0.0773 | 0.7500 | 0.0580 |
| 1.111 | 0.0438 | 0.1605 | 0.0743 | 0.7500 | 0.0557 |
| 1.053 | 0.0418 | 0.1536 | 0.0710 | 0.7500 | 0.0533 |
| 1.000 | 0.0401 | 0.1479 | 0.0684 | 0.7500 | 0.0513 |
| 0.909 | 0.0374 | 0.1431 | 0.0656 | 0.7500 | 0.0492 |

## Table 2.5.2-225 CB FIRS for the Fermi 3 Site (Sheet 3 of 4)

| Spectral Frequency (Hz) | 5% Damped Spectral Acceleration (g) | | | | |
|---|---|---|---|---|---|
| | $10^{-4}$ UHRS | $10^{-5}$ UHRS | Horizontal FIRS | Vertical/Horizontal | Vertical FIRS |
| 0.833 | 0.0352 | 0.1390 | 0.0634 | 0.7500 | 0.0475 |
| 0.769 | 0.0332 | 0.1357 | 0.0614 | 0.7500 | 0.0461 |
| 0.714 | 0.0316 | 0.1331 | 0.0599 | 0.7500 | 0.0449 |
| 0.667 | 0.0303 | 0.1312 | 0.0590 | 0.7500 | 0.0443 |
| 0.625 | 0.0291 | 0.1291 | 0.0581 | 0.7500 | 0.0436 |
| 0.588 | 0.0279 | 0.1273 | 0.0573 | 0.7500 | 0.0429 |
| 0.556 | 0.0270 | 0.1258 | 0.0566 | 0.7500 | 0.0425 |
| 0.526 | 0.0261 | 0.1238 | 0.0557 | 0.7500 | 0.0418 |
| 0.500 | 0.0253 | 0.1227 | 0.0552 | 0.7500 | 0.0414 |
| 0.455 | 0.0233 | 0.1142 | 0.0514 | 0.7500 | 0.0385 |
| 0.417 | 0.0217 | 0.1072 | 0.0482 | 0.7500 | 0.0362 |
| 0.385 | 0.0204 | 0.1014 | 0.0456 | 0.7500 | 0.0342 |
| 0.357 | 0.0192 | 0.0964 | 0.0434 | 0.7500 | 0.0325 |
| 0.343 | 0.0183 | 0.0921 | 0.0415 | 0.7500 | 0.0311 |
| 0.313 | 0.0174 | 0.0883 | 0.0397 | 0.7500 | 0.0298 |
| 0.294 | 0.0166 | 0.0846 | 0.0381 | 0.7500 | 0.0286 |
| 0.278 | 0.0159 | 0.0813 | 0.0366 | 0.7500 | 0.0274 |
| 0.263 | 0.0153 | 0.0784 | 0.0353 | 0.7500 | 0.0265 |
| 0.250 | 0.0147 | 0.0759 | 0.0341 | 0.7500 | 0.0256 |
| 0.238 | 0.0142 | 0.0735 | 0.0331 | 0.7500 | 0.0248 |
| 0.227 | 0.0137 | 0.0713 | 0.0321 | 0.7500 | 0.0241 |
| 0.217 | 0.0132 | 0.0692 | 0.0311 | 0.7500 | 0.0234 |
| 0.208 | 0.0128 | 0.0673 | 0.0303 | 0.7500 | 0.0227 |
| 0.200 | 0.0124 | 0.0656 | 0.0295 | 0.7500 | 0.0221 |
| 0.182 | 0.0116 | 0.0618 | 0.0278 | 0.7500 | 0.0209 |
| 0.167 | 0.0108 | 0.0582 | 0.0262 | 0.7500 | 0.0196 |
| 0.154 | 0.0102 | 0.0553 | 0.0249 | 0.7500 | 0.0186 |
| 0.143 | 0.0096 | 0.0525 | 0.0236 | 0.7500 | 0.0177 |
| 0.133 | 0.0091 | 0.0503 | 0.0226 | 0.7500 | 0.0170 |

## Table 2.5.2-225 CB FIRS for the Fermi 3 Site (Sheet 4 of 4)

| Spectral Frequency (Hz) | 5% Damped Spectral Acceleration (g) | | | | |
|---|---|---|---|---|---|
| | $10^{-4}$ UHRS | $10^{-5}$ UHRS | Horizontal FIRS | Vertical/Horizontal | Vertical FIRS |
| 0.125 | 0.0087 | 0.0484 | 0.0218 | 0.7500 | 0.0163 |
| 0.118 | 0.0083 | 0.0466 | 0.0210 | 0.7500 | 0.0157 |
| 0.111 | 0.0079 | 0.0451 | 0.0203 | 0.7500 | 0.0152 |
| 0.100 | 0.0074 | 0.0421 | 0.0189 | 0.7500 | 0.0142 |

## Table 2.5.2-226 FWSC FIRS for the Fermi 3 Site (Sheet 1 of 4)

| Spectral Frequency (Hz) | 5% Damped Spectral Acceleration (g) | | | | |
|---|---|---|---|---|---|
| | $10^{-4}$ UHRS | $10^{-5}$ UHRS | Horizontal FIRS | Vertical/Horizontal | Vertical FIRS |
| 100.000 | 0.0937 | 0.6266 | 0.2820 | 1.0000 | 0.2820 |
| 60.241 | 0.1475 | 1.0026 | 0.4511 | 1.1374 | 0.5131 |
| 50.000 | 0.1814 | 1.2427 | 0.5592 | 1.1244 | 0.6288 |
| 40.000 | 0.2347 | 1.6223 | 0.7300 | 1.0426 | 0.7612 |
| 33.343 | 0.2673 | 1.8570 | 0.8356 | 0.9675 | 0.8085 |
| 30.303 | 0.2842 | 1.9772 | 0.8897 | 0.9400 | 0.8364 |
| 25.000 | 0.3217 | 2.2439 | 1.0098 | 0.8800 | 0.8886 |
| 23.810 | 0.3041 | 2.1018 | 0.9458 | 0.8681 | 0.8211 |
| 22.727 | 0.2883 | 1.9747 | 0.8886 | 0.8569 | 0.7615 |
| 21.739 | 0.2740 | 1.8604 | 0.8372 | 0.8461 | 0.7084 |
| 20.833 | 0.2609 | 1.7572 | 0.7907 | 0.8355 | 0.6607 |
| 20.000 | 0.2490 | 1.6636 | 0.7486 | 0.8255 | 0.6180 |
| 18.182 | 0.2232 | 1.4640 | 0.6588 | 0.8069 | 0.5316 |
| 16.667 | 0.2020 | 1.3027 | 0.5862 | 0.7984 | 0.4680 |
| 15.385 | 0.2010 | 1.2252 | 0.5514 | 0.7906 | 0.4359 |
| 14.286 | 0.2002 | 1.1966 | 0.5385 | 0.7834 | 0.4219 |
| 13.343 | 0.1994 | 1.1705 | 0.5267 | 0.7769 | 0.4092 |
| 12.500 | 0.1986 | 1.1467 | 0.5160 | 0.7708 | 0.3977 |
| 11.765 | 0.1980 | 1.1247 | 0.5061 | 0.7651 | 0.3872 |
| 11.111 | 0.1973 | 1.1043 | 0.4970 | 0.7597 | 0.3776 |
| 10.526 | 0.1967 | 1.0854 | 0.4885 | 0.7547 | 0.3686 |
| 10.000 | 0.1961 | 1.0678 | 0.4805 | 0.7500 | 0.3604 |
| 9.091 | 0.1965 | 1.0269 | 0.4621 | 0.7500 | 0.3466 |
| 8.343 | 0.1969 | 0.9910 | 0.4460 | 0.7500 | 0.3345 |
| 7.692 | 0.1972 | 0.9590 | 0.4316 | 0.7500 | 0.3237 |
| 7.143 | 0.1975 | 0.9304 | 0.4187 | 0.7500 | 0.3140 |
| 6.667 | 0.1978 | 0.9045 | 0.4070 | 0.7500 | 0.3053 |
| 6.250 | 0.1981 | 0.8809 | 0.3964 | 0.7500 | 0.2973 |

## Table 2.5.2-226 FWSC FIRS for the Fermi 3 Site (Sheet 2 of 4)

| Spectral Frequency (Hz) | 5% Damped Spectral Acceleration (g) | | | | |
|---|---|---|---|---|---|
| | $10^{-4}$ UHRS | $10^{-5}$ UHRS | Horizontal FIRS | Vertical/Horizontal | Vertical FIRS |
| 5.882 | 0.1983 | 0.8593 | 0.3867 | 0.7500 | 0.2900 |
| 5.556 | 0.1985 | 0.8394 | 0.3777 | 0.7500 | 0.2833 |
| 5.263 | 0.1988 | 0.8210 | 0.3709 | 0.7500 | 0.2782 |
| 5.000 | 0.1990 | 0.8040 | 0.3648 | 0.7500 | 0.2736 |
| 4.545 | 0.1968 | 0.7787 | 0.3549 | 0.7500 | 0.2662 |
| 4.167 | 0.1949 | 0.7564 | 0.3460 | 0.7500 | 0.2595 |
| 3.846 | 0.1931 | 0.7364 | 0.3380 | 0.7500 | 0.2535 |
| 3.571 | 0.1912 | 0.7190 | 0.3310 | 0.7500 | 0.2482 |
| 3.343 | 0.1881 | 0.6982 | 0.3223 | 0.7500 | 0.2417 |
| 3.125 | 0.1791 | 0.6581 | 0.3044 | 0.7500 | 0.2283 |
| 2.941 | 0.1686 | 0.6147 | 0.2847 | 0.7500 | 0.2136 |
| 2.778 | 0.1578 | 0.5698 | 0.2644 | 0.7500 | 0.1983 |
| 2.632 | 0.1478 | 0.5296 | 0.2462 | 0.7500 | 0.1846 |
| 2.500 | 0.1375 | 0.4881 | 0.2273 | 0.7500 | 0.1705 |
| 2.381 | 0.1272 | 0.4507 | 0.2100 | 0.7500 | 0.1575 |
| 2.273 | 0.1176 | 0.4172 | 0.1943 | 0.7500 | 0.1457 |
| 2.174 | 0.1091 | 0.3878 | 0.1805 | 0.7500 | 0.1354 |
| 2.083 | 0.1025 | 0.3649 | 0.1698 | 0.7500 | 0.1274 |
| 2.000 | 0.0960 | 0.3424 | 0.1593 | 0.7500 | 0.1195 |
| 1.818 | 0.0824 | 0.2947 | 0.1370 | 0.7500 | 0.1028 |
| 1.667 | 0.0719 | 0.2595 | 0.1204 | 0.7500 | 0.0903 |
| 1.538 | 0.0641 | 0.2312 | 0.1073 | 0.7500 | 0.0805 |
| 1.429 | 0.0579 | 0.2088 | 0.0969 | 0.7500 | 0.0727 |
| 1.343 | 0.0532 | 0.1922 | 0.0892 | 0.7500 | 0.0669 |
| 1.250 | 0.0499 | 0.1813 | 0.0840 | 0.7500 | 0.0630 |
| 1.176 | 0.0471 | 0.1720 | 0.0796 | 0.7500 | 0.0597 |
| 1.111 | 0.0449 | 0.1646 | 0.0762 | 0.7500 | 0.0571 |
| 1.053 | 0.0429 | 0.1577 | 0.0729 | 0.7500 | 0.0547 |

## Table 2.5.2-226 FWSC FIRS for the Fermi 3 Site (Sheet 3 of 4)

| Spectral Frequency (Hz) | 5% Damped Spectral Acceleration (g) | | | | |
|---|---|---|---|---|---|
| | $10^{-4}$ UHRS | $10^{-5}$ UHRS | Horizontal FIRS | Vertical/Horizontal | Vertical FIRS |
| 1.000 | 0.0410 | 0.1514 | 0.0699 | 0.7500 | 0.0525 |
| 0.909 | 0.0381 | 0.1459 | 0.0669 | 0.7500 | 0.0502 |
| 0.833 | 0.0357 | 0.1413 | 0.0644 | 0.7500 | 0.0483 |
| 0.769 | 0.0337 | 0.1377 | 0.0623 | 0.7500 | 0.0468 |
| 0.714 | 0.0320 | 0.1350 | 0.0608 | 0.7500 | 0.0456 |
| 0.667 | 0.0306 | 0.1327 | 0.0597 | 0.7500 | 0.0448 |
| 0.625 | 0.0294 | 0.1306 | 0.0588 | 0.7500 | 0.0441 |
| 0.588 | 0.0282 | 0.1286 | 0.0579 | 0.7500 | 0.0434 |
| 0.556 | 0.0273 | 0.1272 | 0.0572 | 0.7500 | 0.0429 |
| 0.526 | 0.0263 | 0.1250 | 0.0562 | 0.7500 | 0.0422 |
| 0.500 | 0.0255 | 0.1238 | 0.0557 | 0.7500 | 0.0418 |
| 0.455 | 0.0235 | 0.1150 | 0.0518 | 0.7500 | 0.0388 |
| 0.417 | 0.0218 | 0.1081 | 0.0487 | 0.7500 | 0.0365 |
| 0.385 | 0.0205 | 0.1022 | 0.0460 | 0.7500 | 0.0345 |
| 0.357 | 0.0193 | 0.0973 | 0.0438 | 0.7500 | 0.0328 |
| 0.343 | 0.0184 | 0.0932 | 0.0419 | 0.7500 | 0.0314 |
| 0.313 | 0.0175 | 0.0893 | 0.0402 | 0.7500 | 0.0301 |
| 0.294 | 0.0167 | 0.0856 | 0.0385 | 0.7500 | 0.0289 |
| 0.278 | 0.0160 | 0.0822 | 0.0370 | 0.7500 | 0.0278 |
| 0.263 | 0.0154 | 0.0793 | 0.0357 | 0.7500 | 0.0268 |
| 0.250 | 0.0148 | 0.0768 | 0.0345 | 0.7500 | 0.0259 |
| 0.238 | 0.0143 | 0.0744 | 0.0335 | 0.7500 | 0.0251 |
| 0.227 | 0.0138 | 0.0722 | 0.0325 | 0.7500 | 0.0244 |
| 0.217 | 0.0134 | 0.0701 | 0.0315 | 0.7500 | 0.0236 |
| 0.208 | 0.0129 | 0.0681 | 0.0307 | 0.7500 | 0.0230 |
| 0.200 | 0.0125 | 0.0664 | 0.0299 | 0.7500 | 0.0224 |
| 0.182 | 0.0117 | 0.0627 | 0.0282 | 0.7500 | 0.0211 |
| 0.167 | 0.0109 | 0.0591 | 0.0266 | 0.7500 | 0.0200 |

## Table 2.5.2-226 FWSC FIRS for the Fermi 3 Site (Sheet 4 of 4)

| Spectral Frequency (Hz) | 5% Damped Spectral Acceleration (g) | | | | |
|---|---|---|---|---|---|
| | $10^{-4}$ UHRS | $10^{-5}$ UHRS | Horizontal FIRS | Vertical/Horizontal | Vertical FIRS |
| 0.154 | 0.0103 | 0.0561 | 0.0253 | 0.7500 | 0.0189 |
| 0.143 | 0.0097 | 0.0533 | 0.0240 | 0.7500 | 0.0180 |
| 0.133 | 0.0092 | 0.0511 | 0.0230 | 0.7500 | 0.0172 |
| 0.125 | 0.0087 | 0.0490 | 0.0221 | 0.7500 | 0.0165 |
| 0.118 | 0.0083 | 0.0472 | 0.0213 | 0.7500 | 0.0159 |
| 0.111 | 0.0080 | 0.0459 | 0.0206 | 0.7500 | 0.0155 |
| 0.100 | 0.0074 | 0.0428 | 0.0192 | 0.7500 | 0.0144 |

## Figure 2.5.2-201 Earthquake Catalog for Mid-Continent Region

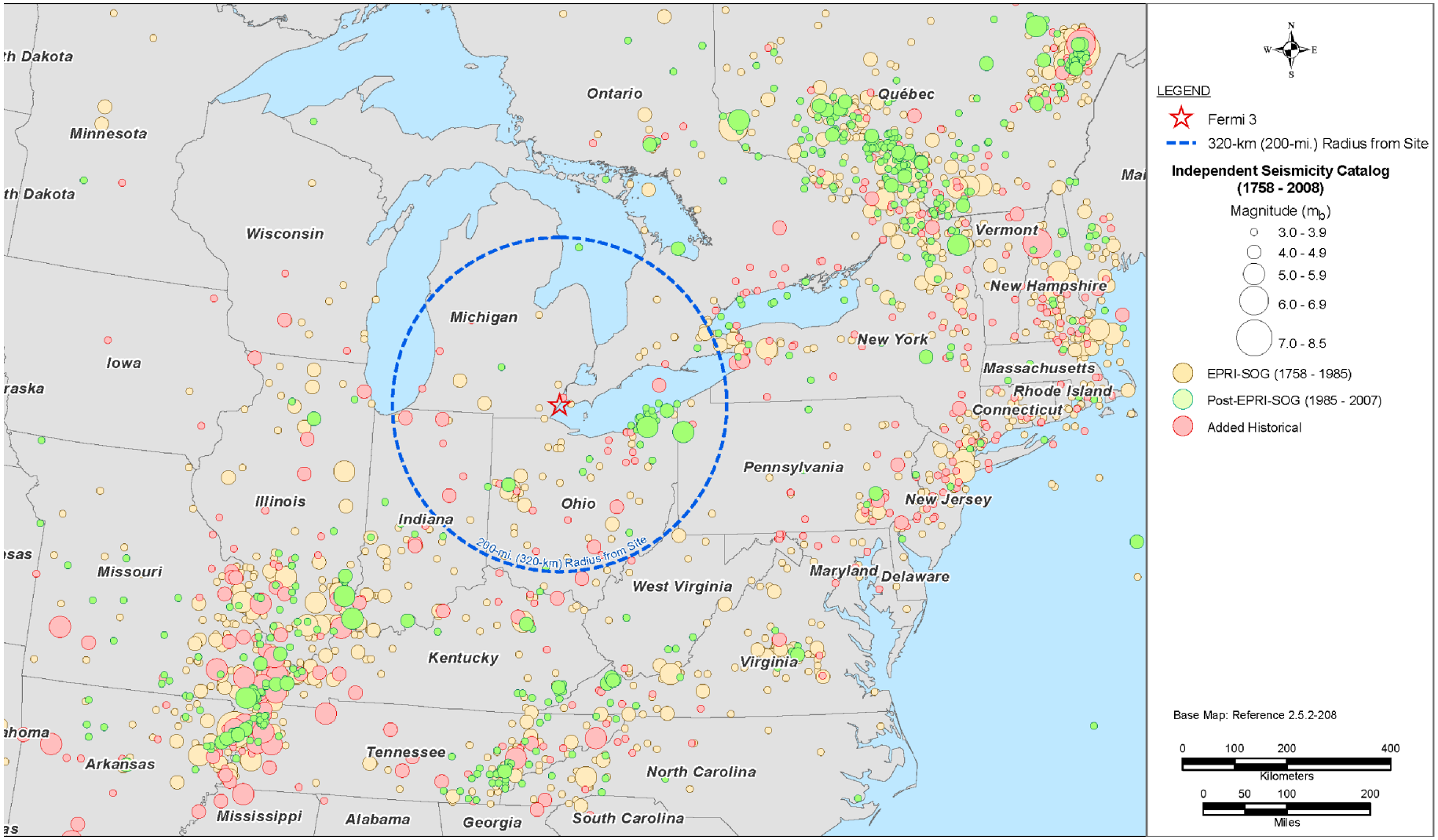

## Figure 2.5.2-202 Location of Earthquakes within 320 km (200 mi.) of the Fermi 3 Site

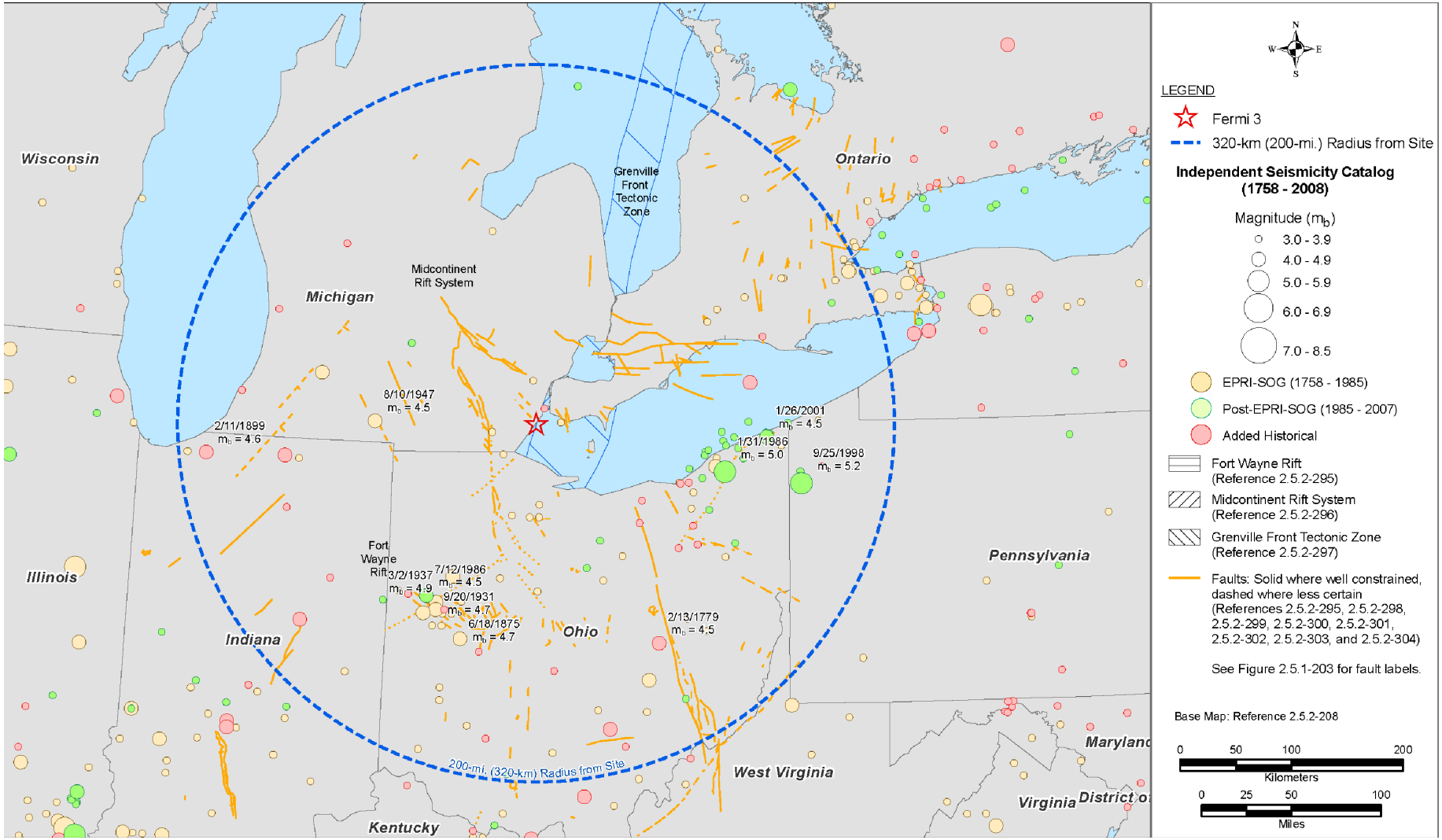

## Figure 2.5.2-203 Location of Earthquakes within 80 km (50 mi.) of the Fermi 3 Site

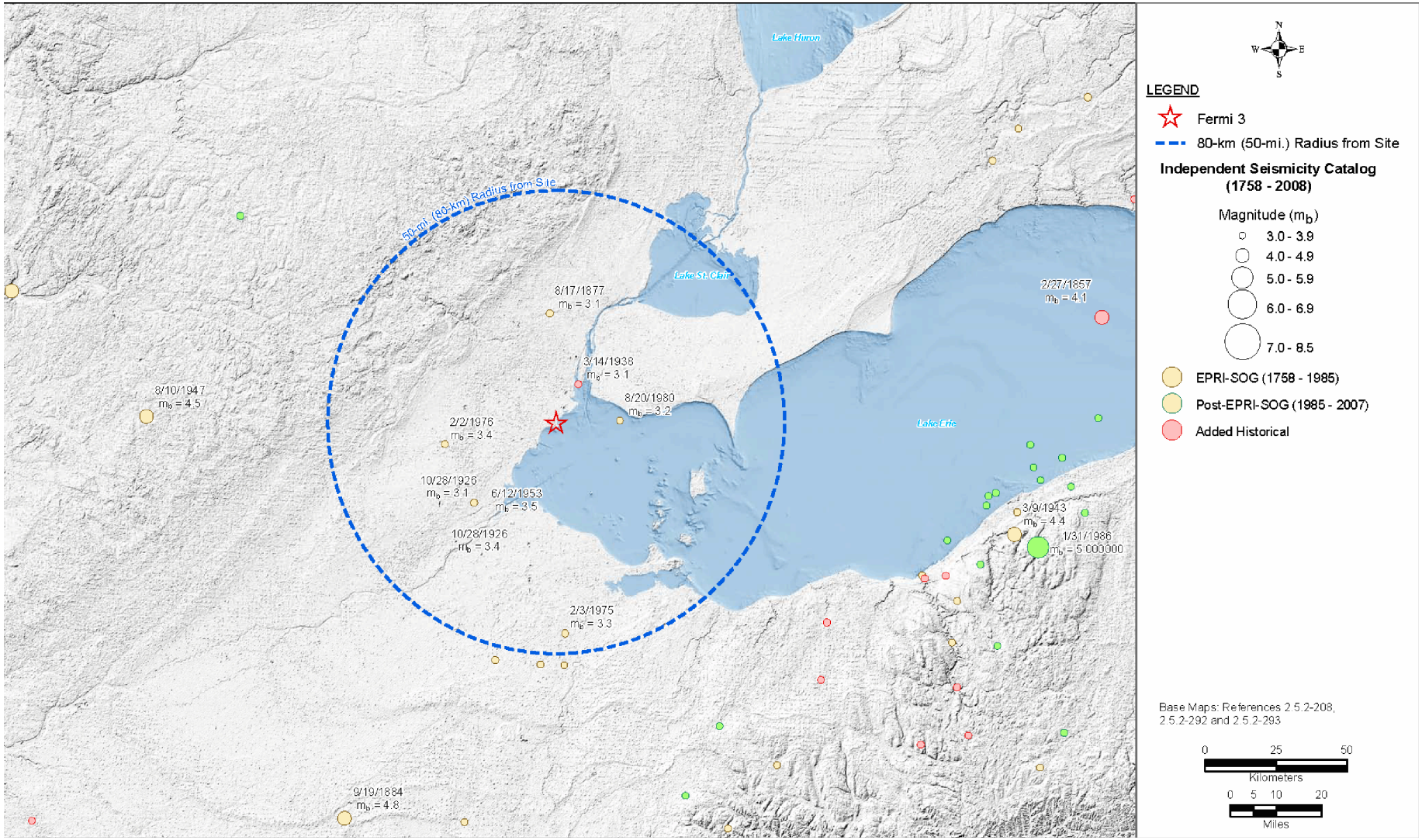

## Figure 2.5.2-204 Bechtel EPRI-SOG Seismic Sources

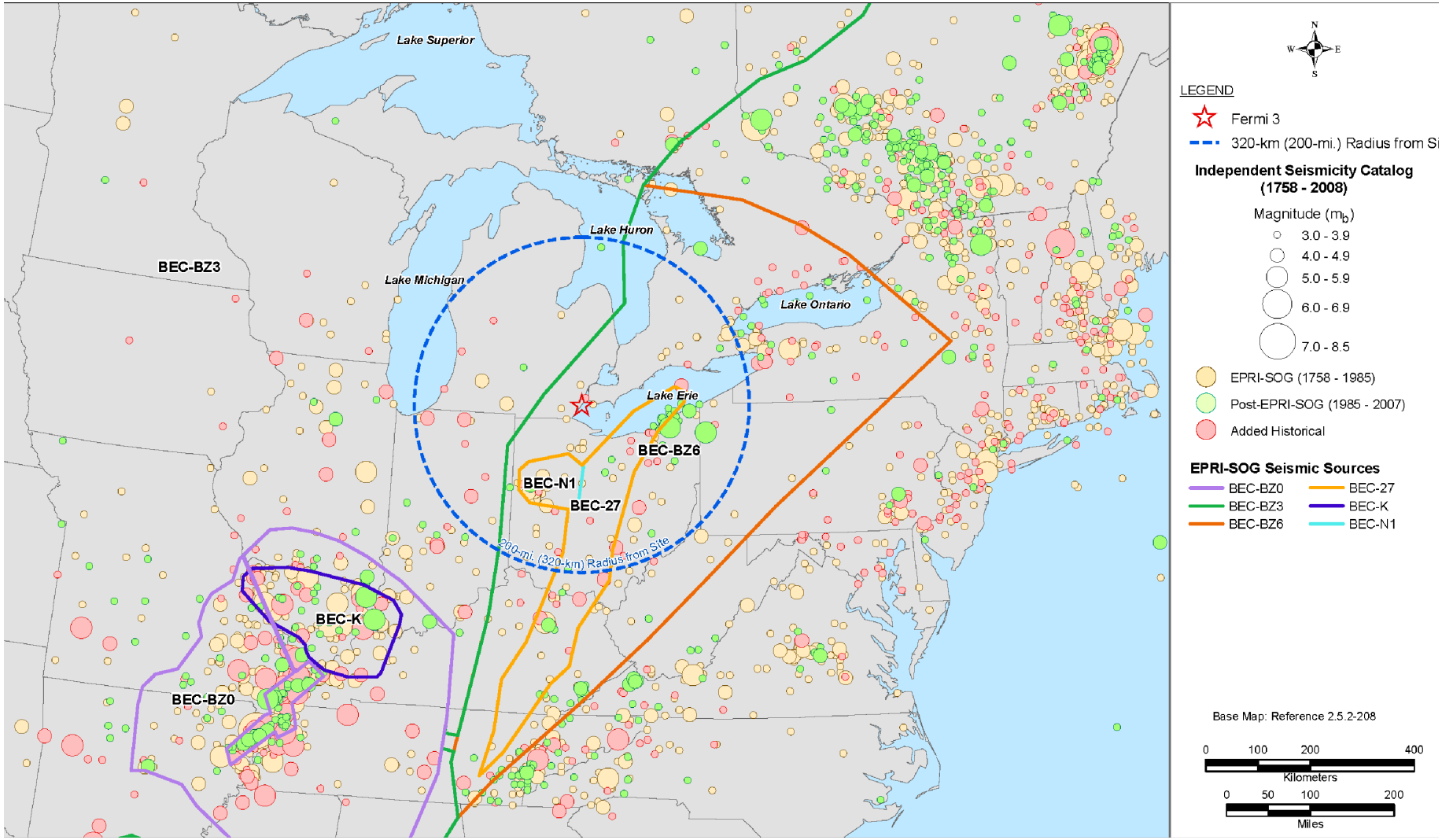

## Figure 2.5.2-205 Dames & Moore EPRI-SOG Seismic Sources

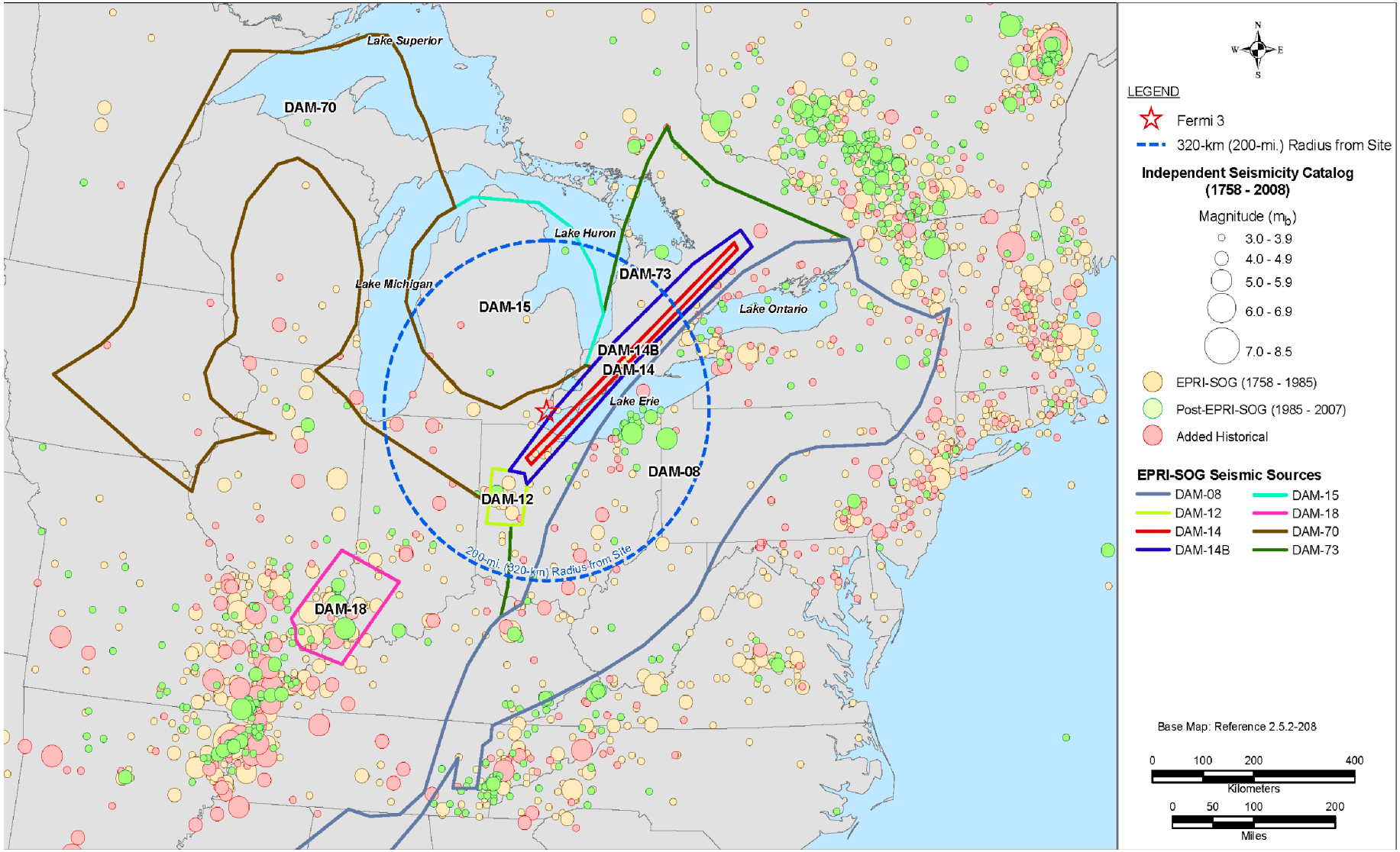

## Figure 2.5.2-206 Law Engineering EPRI-SOG Seismic Sources

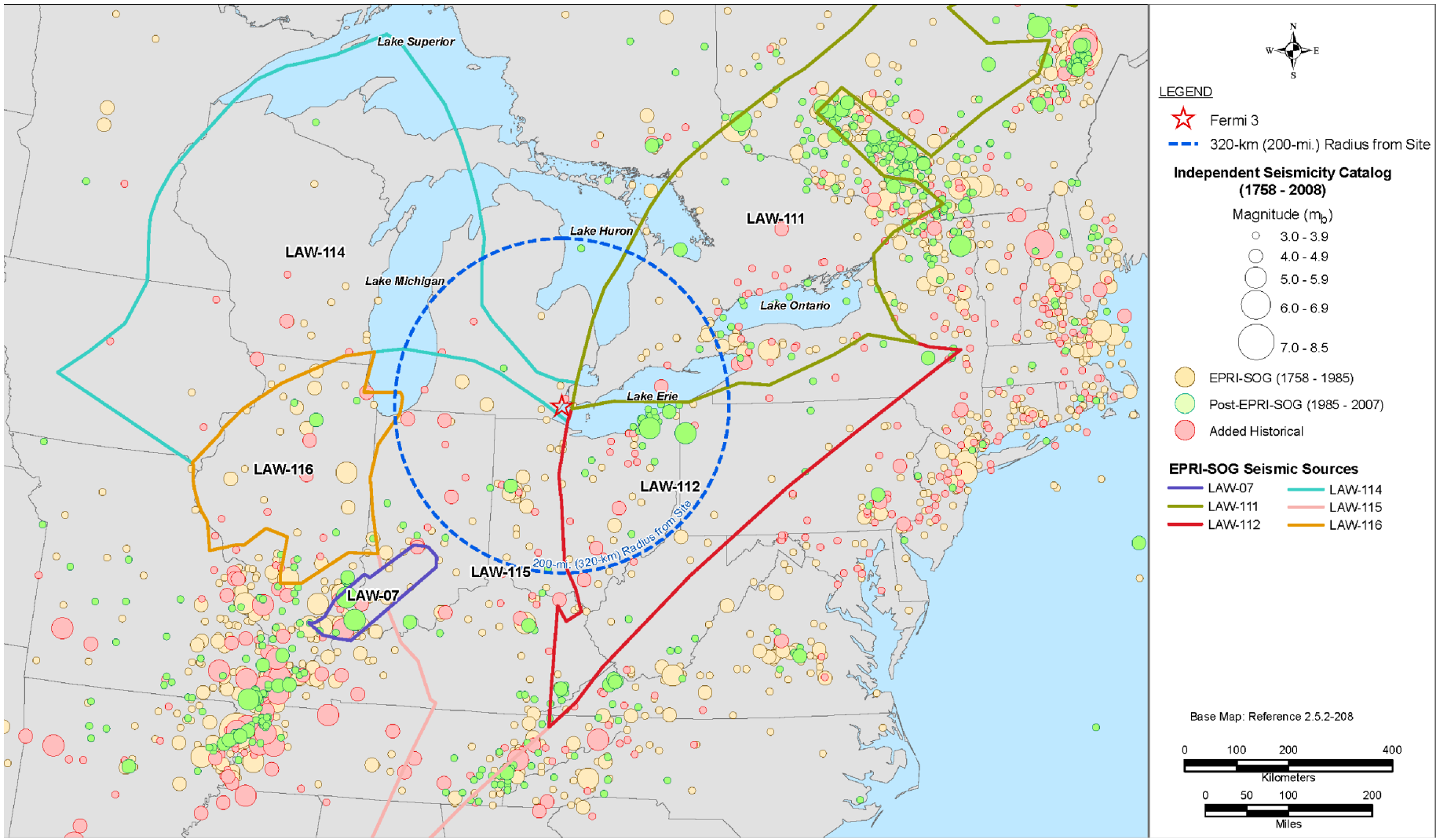

## Figure 2.5.2-207 Rondout Associates EPRI-SOG Seismic Sources

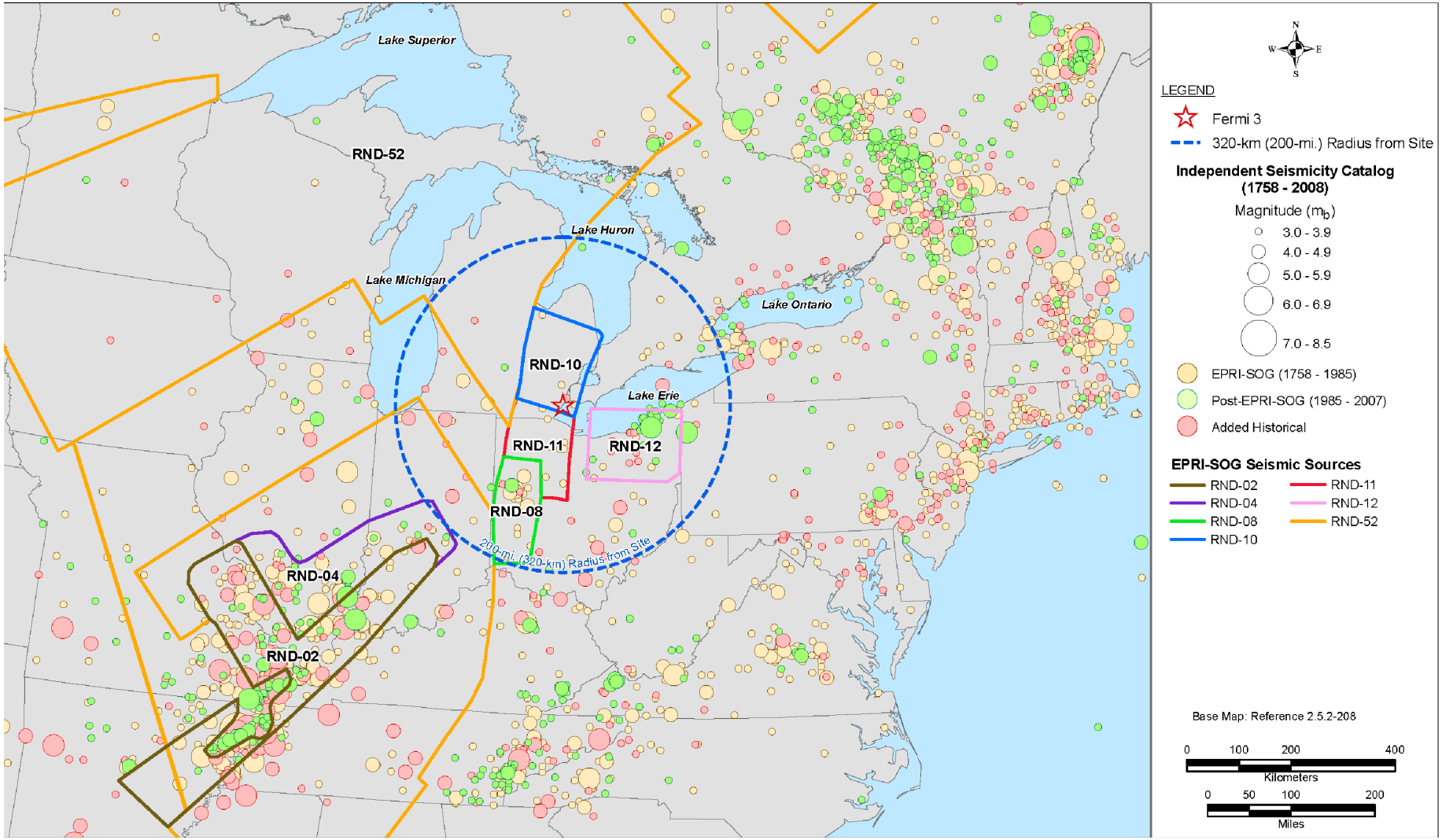

## Figure 2.5.2-208 Weston Geophysical EPRI-SOG Seismic Sources

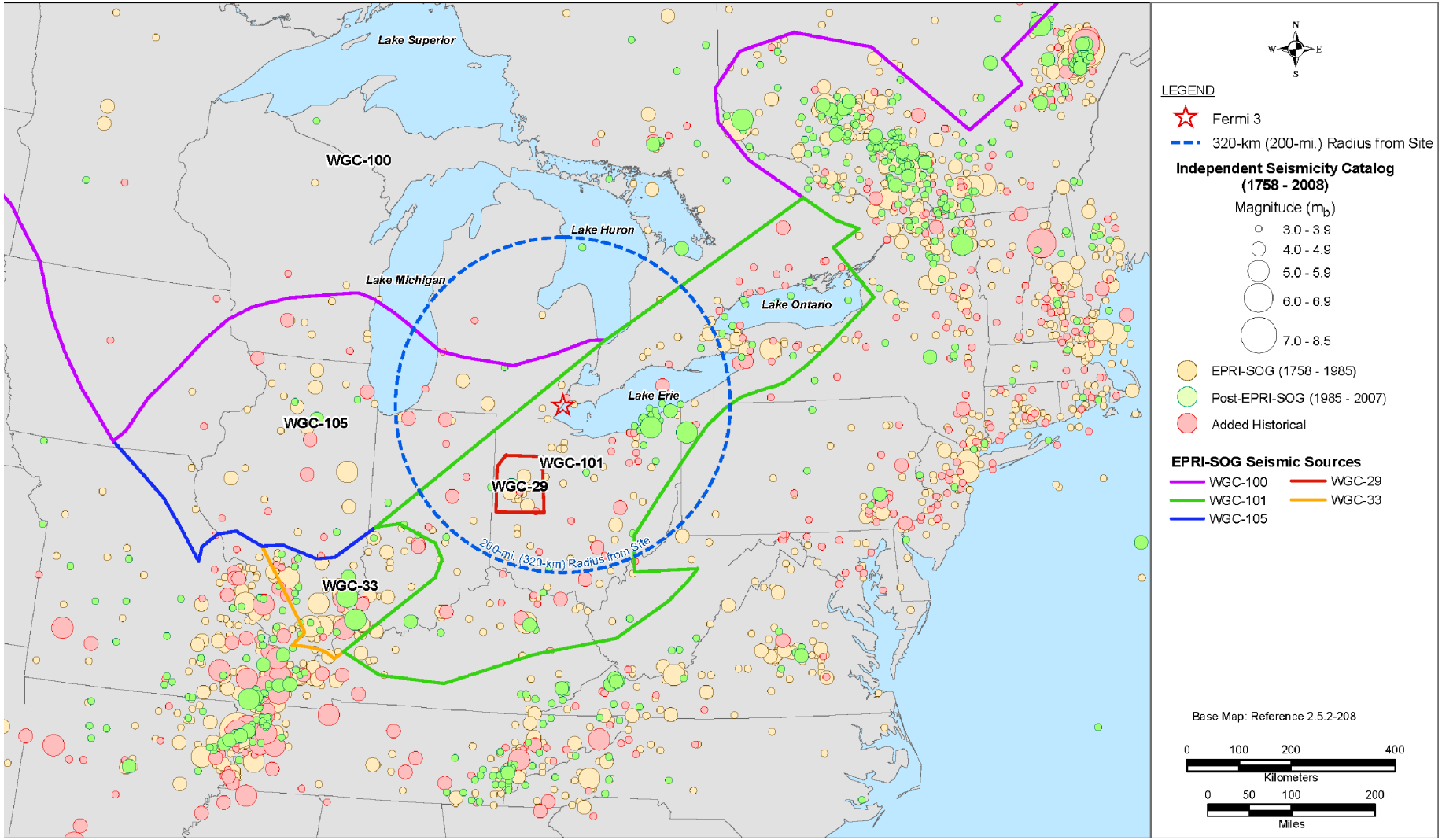

## Figure 2.5.2-209 Woodward-Clyde Consultants EPRI-SOG Seismic Sources

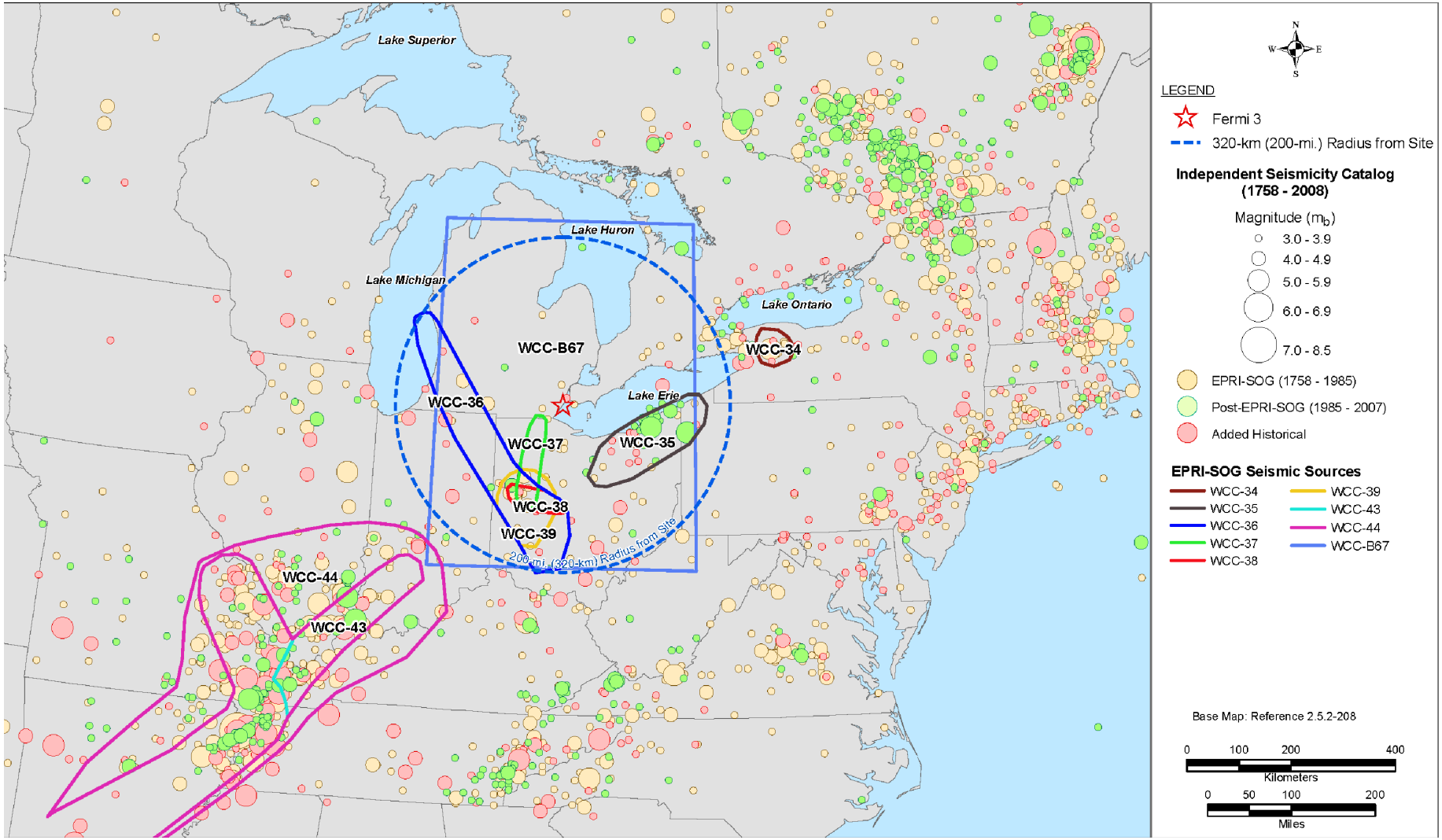

**Figure 2.5.2-210 USGS National Seismic Hazard Mapping Project Source Model**

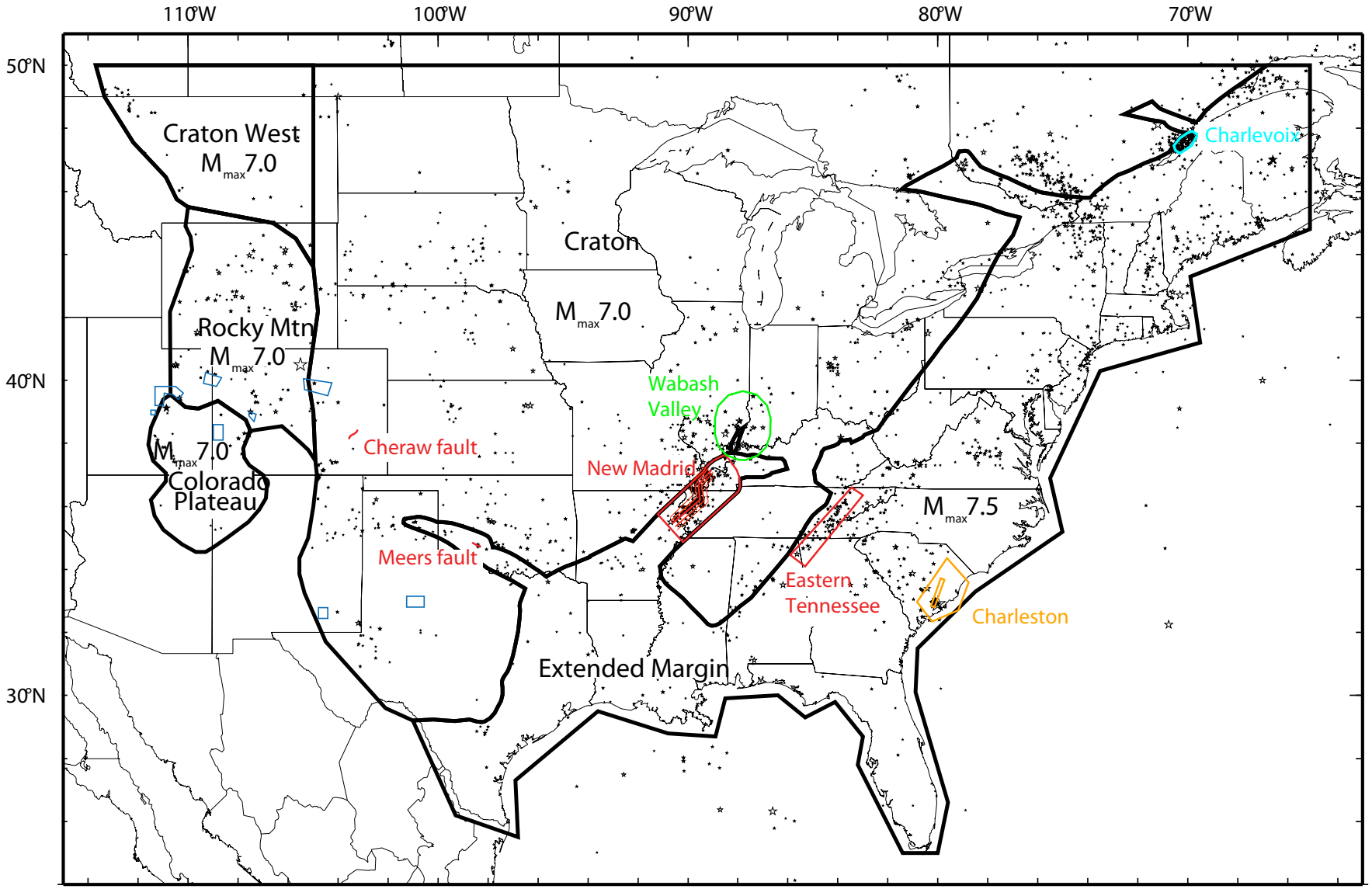

**Figure 2.5.2-211 Source Characterization Logic Tree for Repeating Large-Magnitude New Madrid Earthquakes**

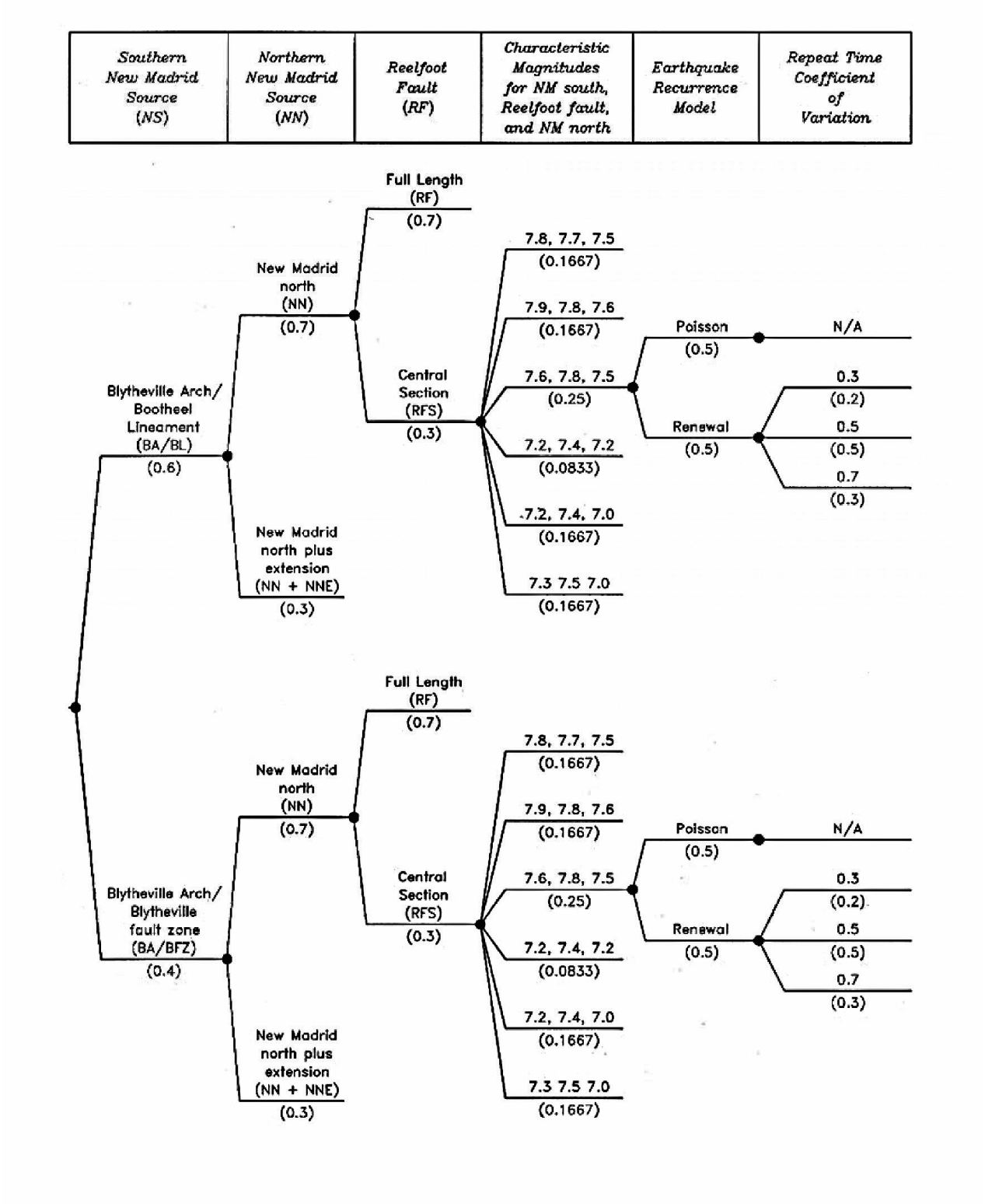

## Figure 2.5.2-212 Central Fault System of New Madrid Seismic Zone

(a) Fault segmentation of the NMSZ. Seismicity of the NMSZ, the Blytheville arch, and the Bootheel lineament/NNfault (left) yield the seven segments (right) identified as: BA, Blytheville arch; BFZ, Blytheville fault zone; BL, Bootheel lineament; NW, New Madrid west; NN, New Madrid north; RF, Reelfoot fault; and RS, Reelfoot south. Segments NW and RS are defined solely from seismicity.

(b) Possible fault rupture scenarios (S#1, S#2, S#3) for the1811/1812 D1, J1, and F1 earthquake sequences, using the seven fault segments of (a). Based on historical and physical constraints, the D1 principal event must rupture BA, and the F1 principal event must rupture RF in all scenarios. S#1 is the favored scenario.

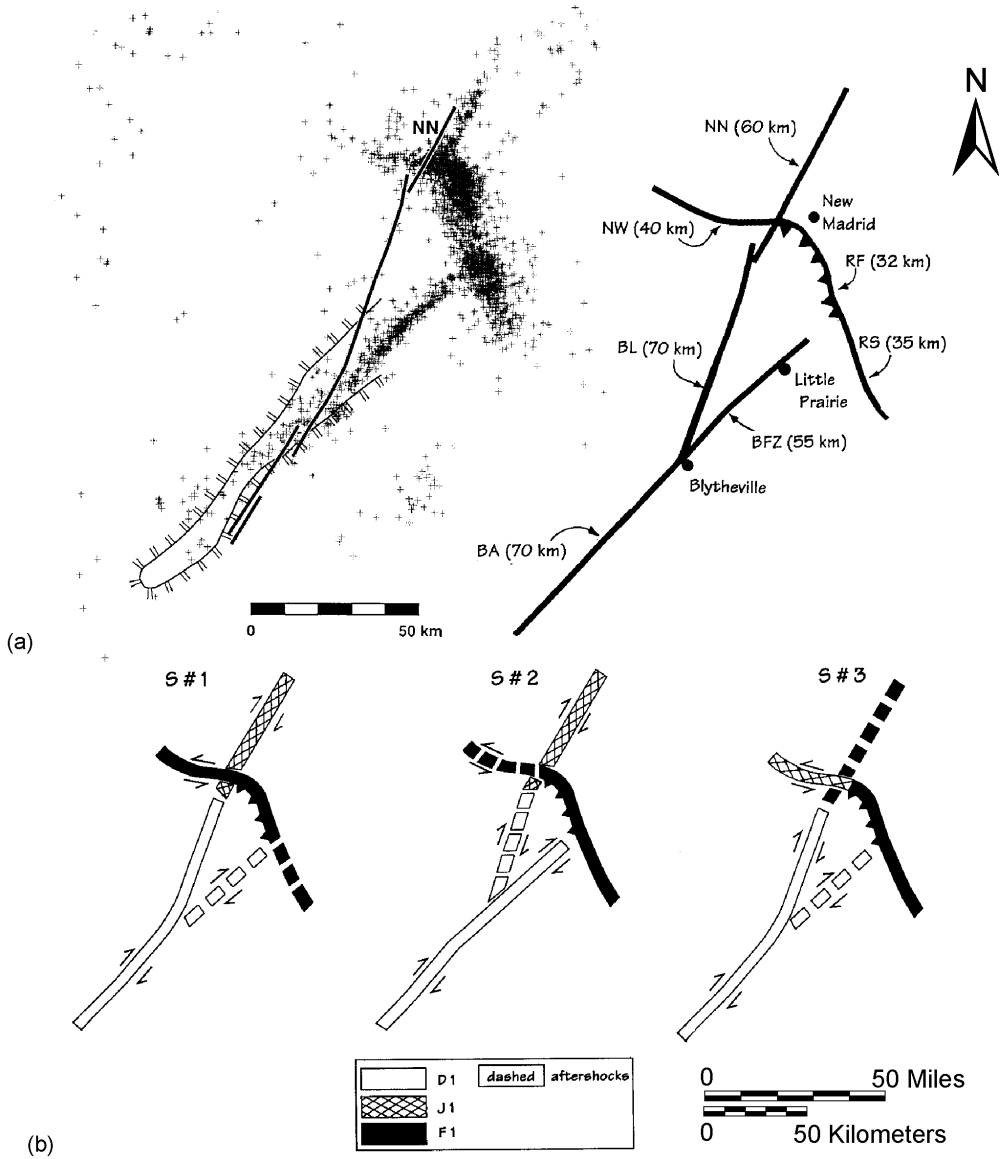

**Figure 2.5.2-213 Location of New Madrid Seismic Zone as Illuminated by Seismicity between 1974 and 1996**

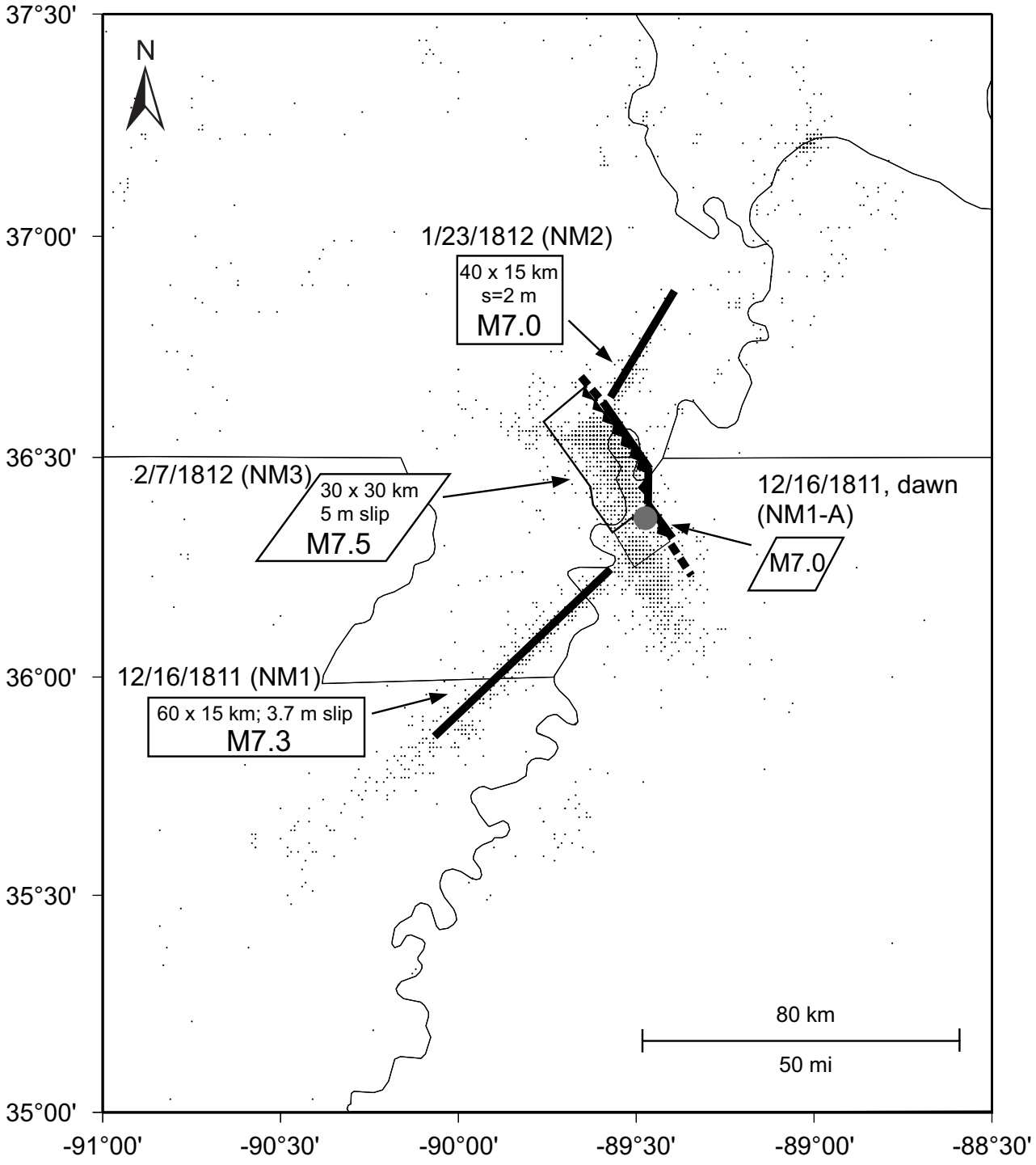

**Figure 2.5.2-214 Earthquake Recurrence Rates for New Madrid Seismic Sources**

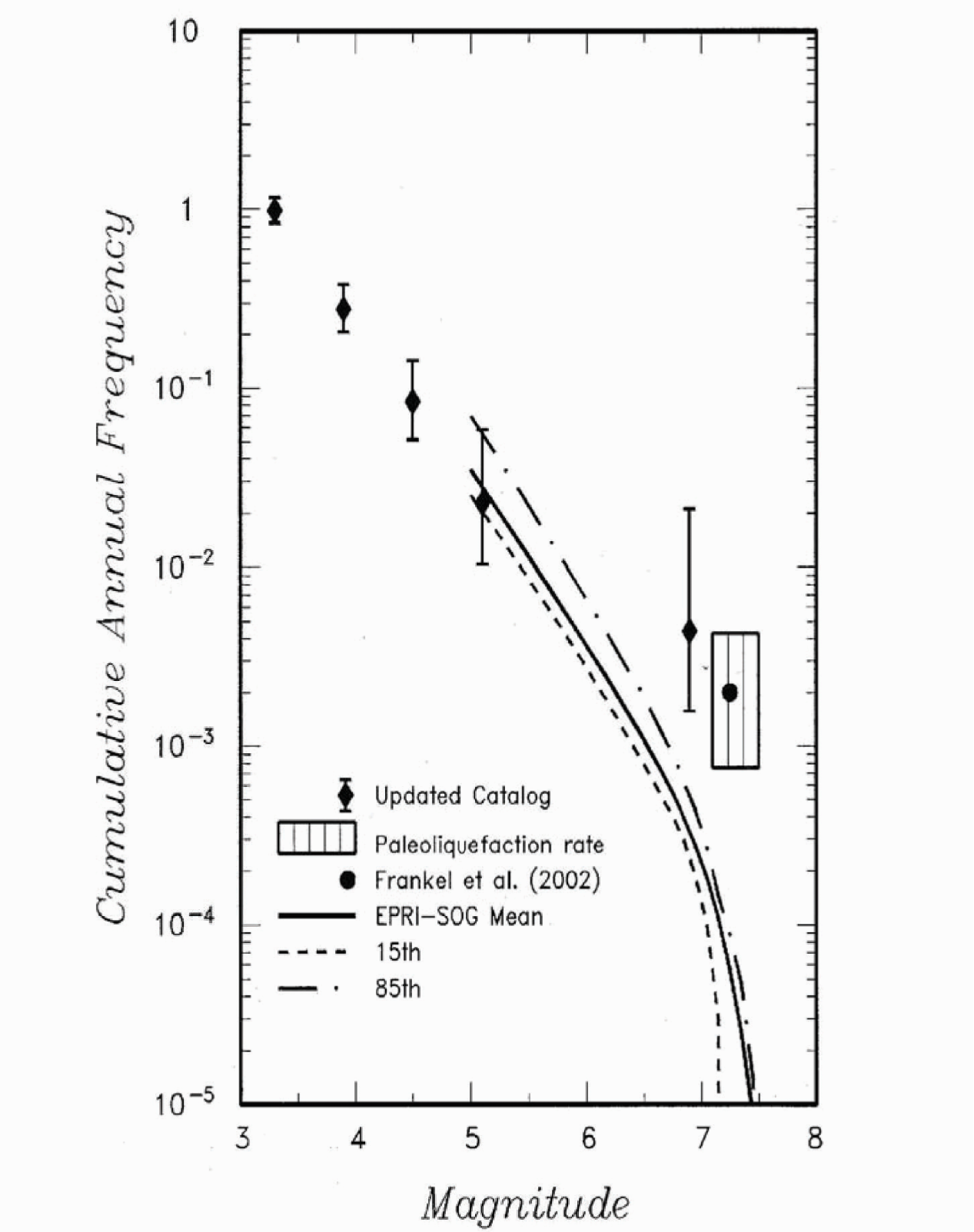

**Figure 2.5.2-215 Distributions for Mean Repeat Time for Repeating Large-Magnitude New Madrid Earthquakes**

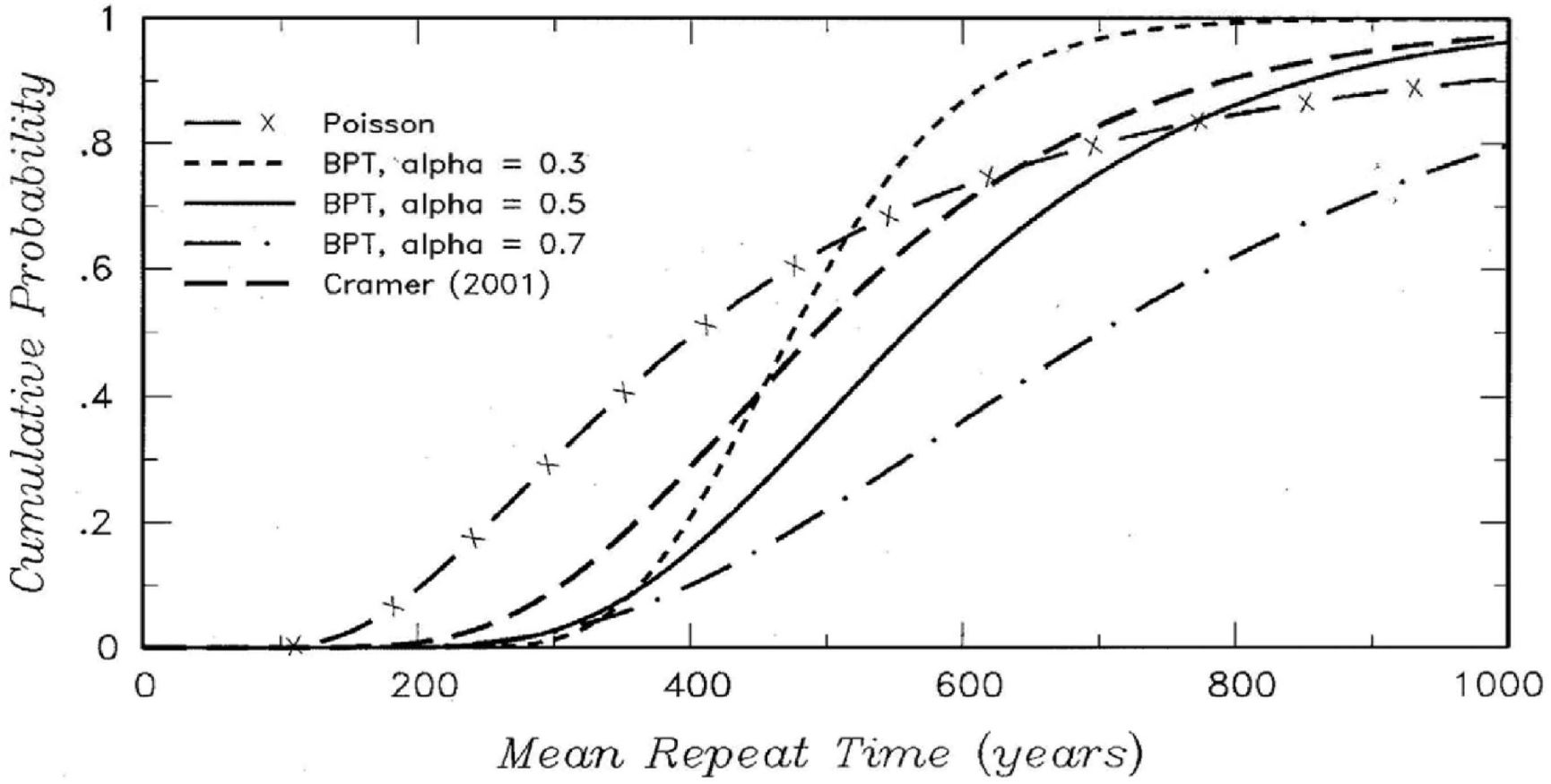

**Figure 2.5.2-216 Earthquake Rupture Sequences for Repeating Large-Magnitude New Madrid Earthquakes**

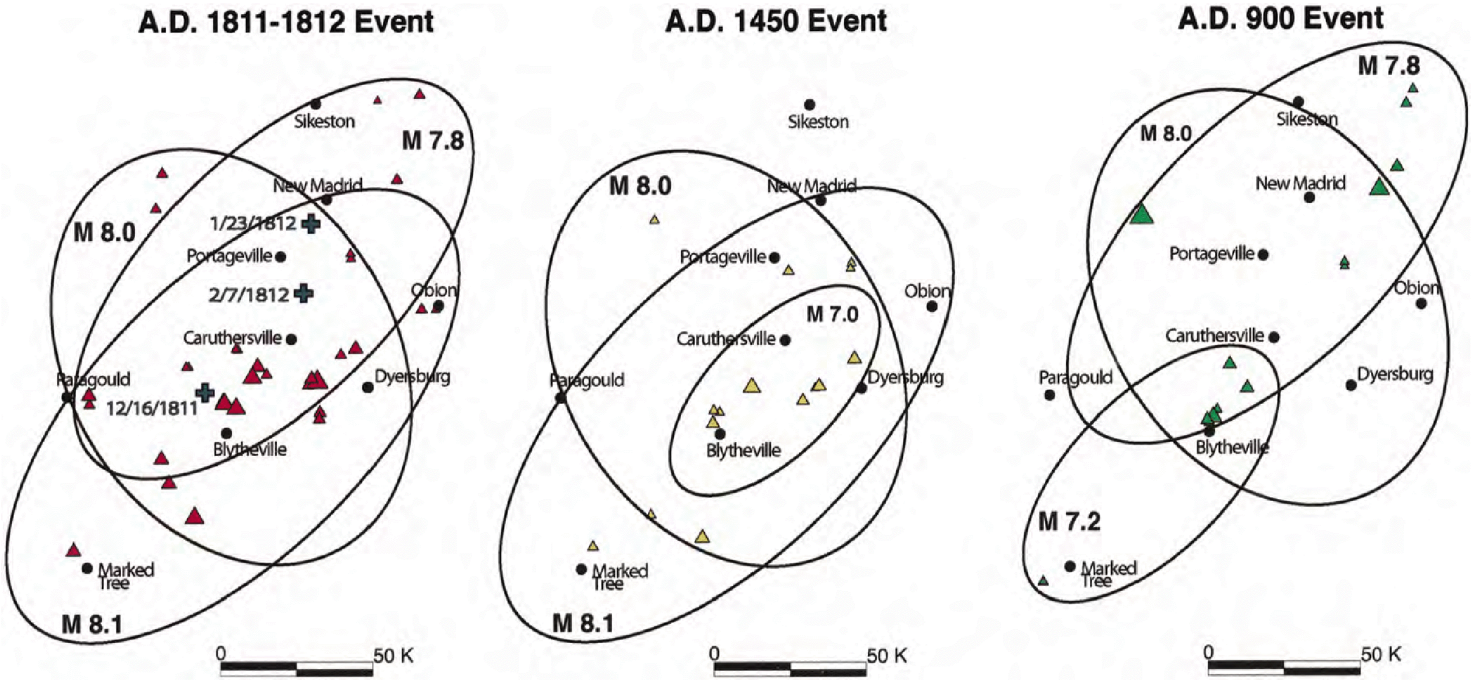


Note:
Triangles indicate the location and relative size of sand blows for each sequence of earthquakes. The ovals represent the liquefaction fields for each event in the rupture sequences as interpreted from the spatial distribution and stratigraphy of sand blows. Liquefaction fields for the 1811/1812 earthquakes are proportional in size to the estimated magnitudes derived by Johnston (1996). Magnitudes of individual earthquakes in A.D. 1450 and A.D. 900 are inferred on the basis of liquefaction fields compared with those for the 1811/1812 earthquakes.

**Figure 2.5.2-217 EPRI-SOG Catalog Completeness Regions**

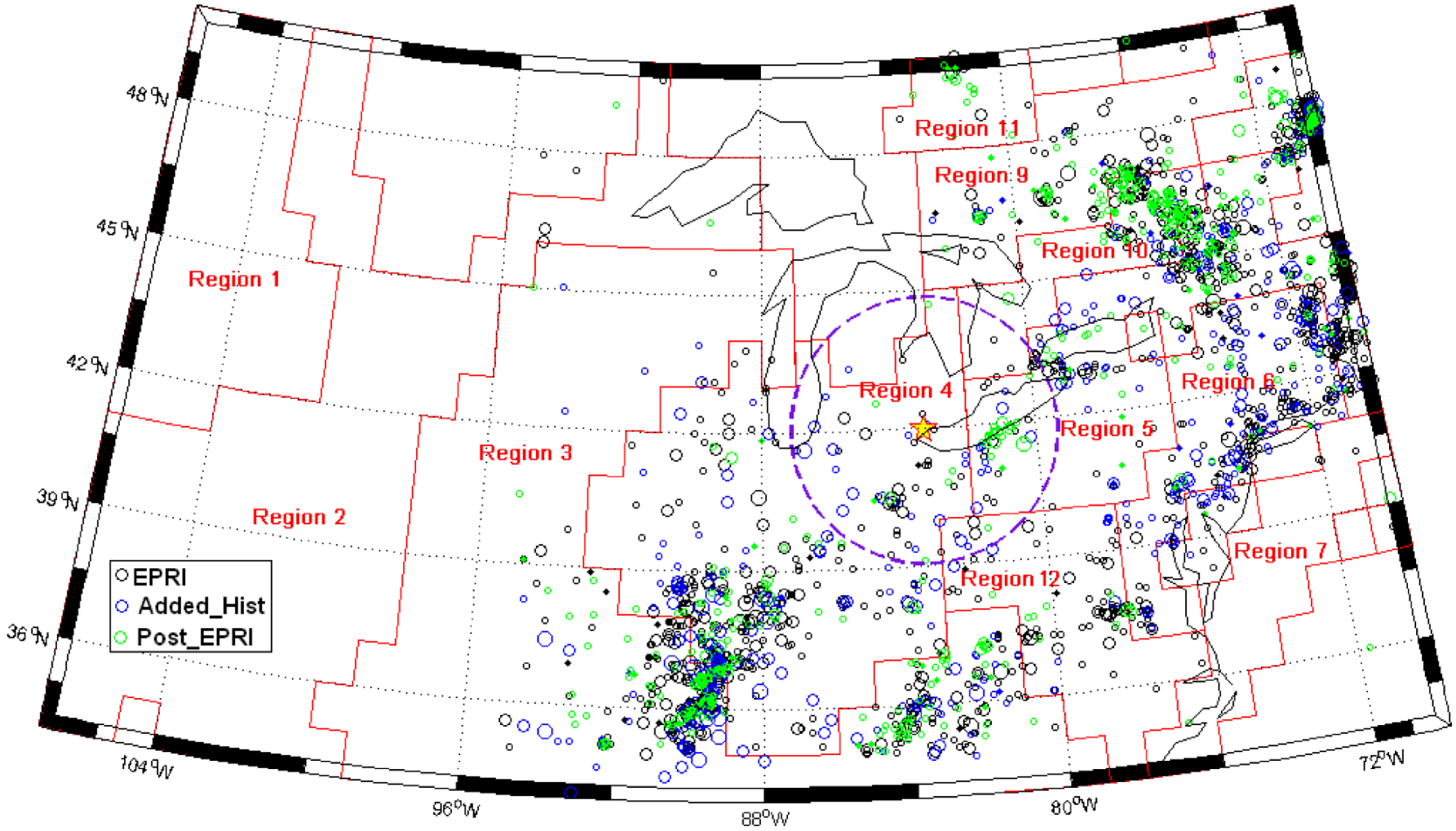

**Figure 2.5.2-218 Effect of Updated Catalog on Earthquake Occurrence Rates within Completeness Region 4**

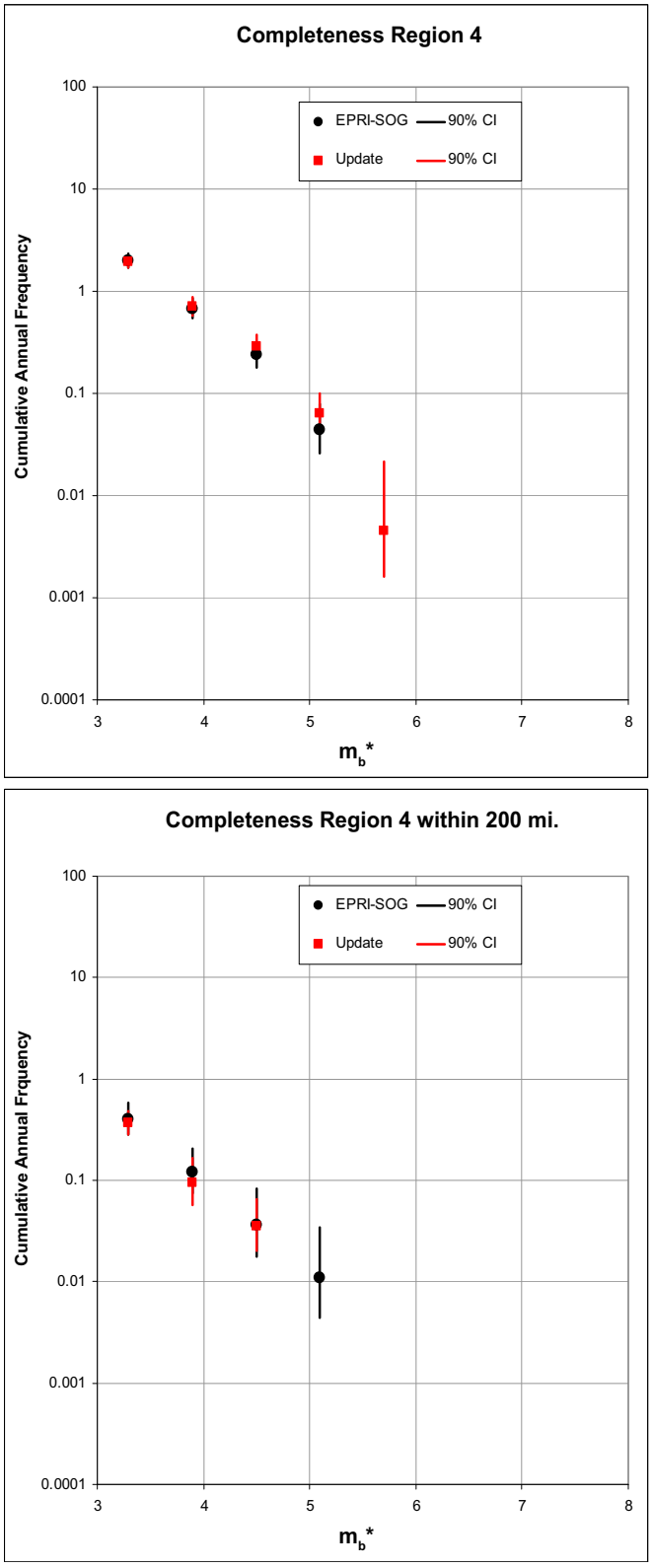

**Figure 2.5.2-219 Effect of Updated Catalog on Earthquake Occurrence Rates within Completeness Region 5**

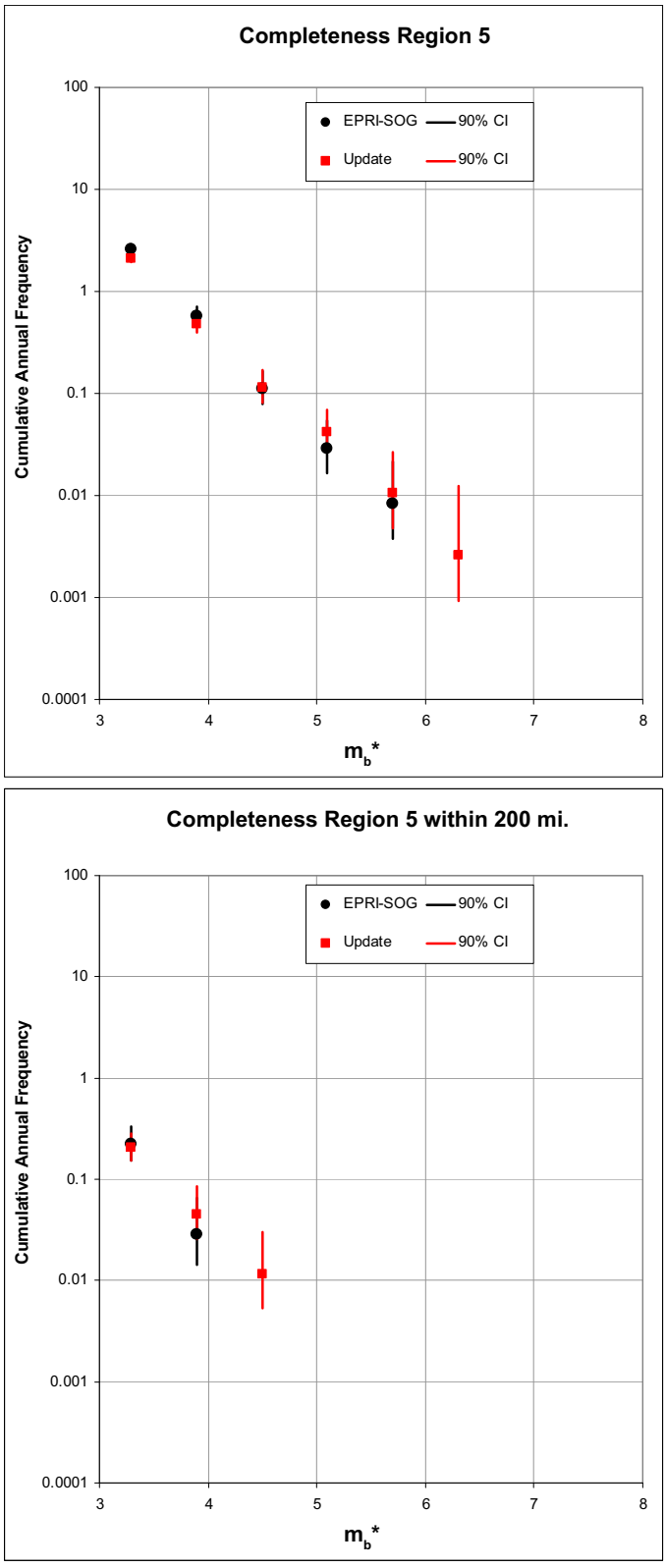

**Figure 2.5.2-220 Ground Motion Characterization Logic Tree Used in the PSHA for the Fermi 3 Site**

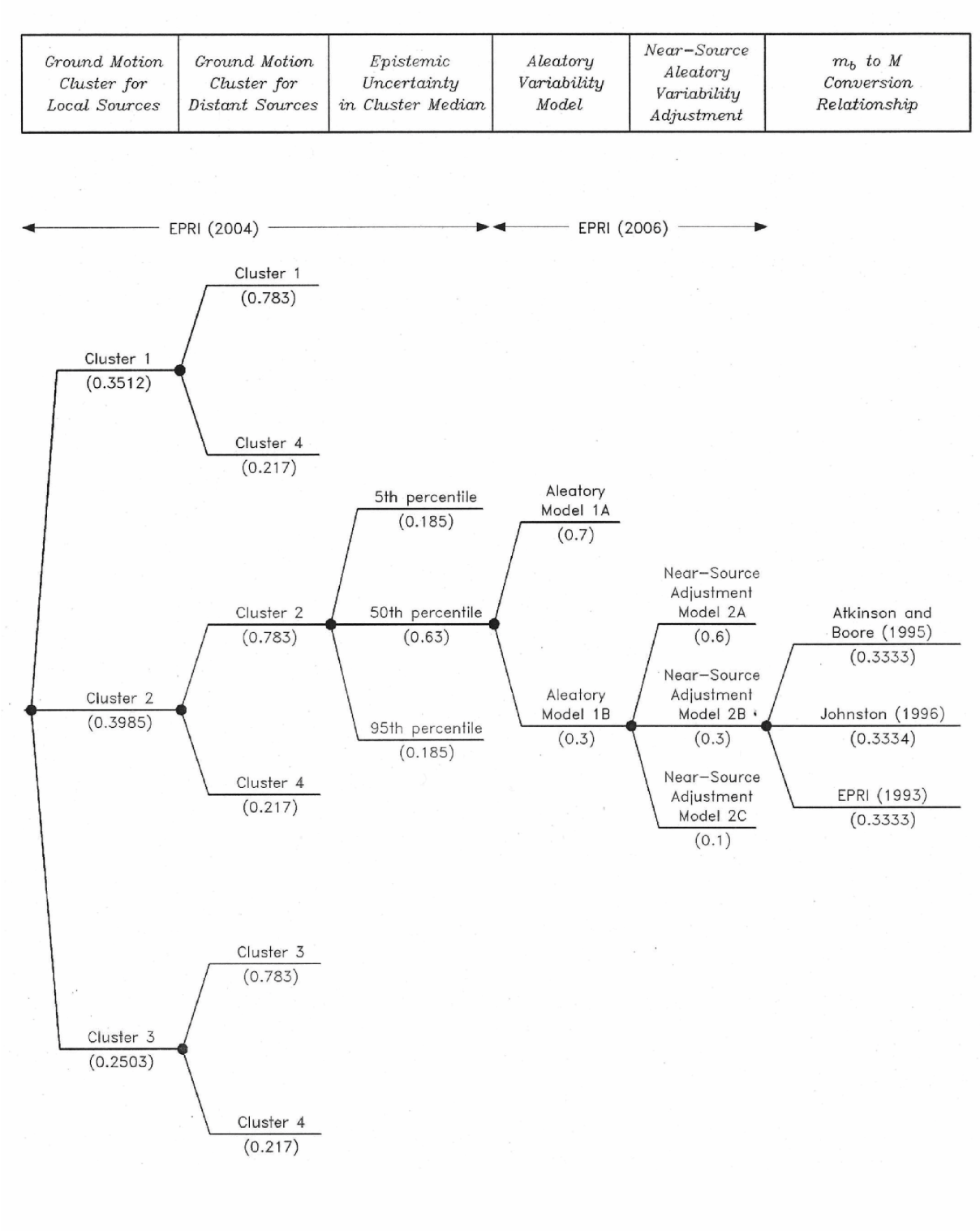

**Figure 2.5.2-221 Comparison of Median Ground Motion Models Used in the PSHA with Recently Published Models**

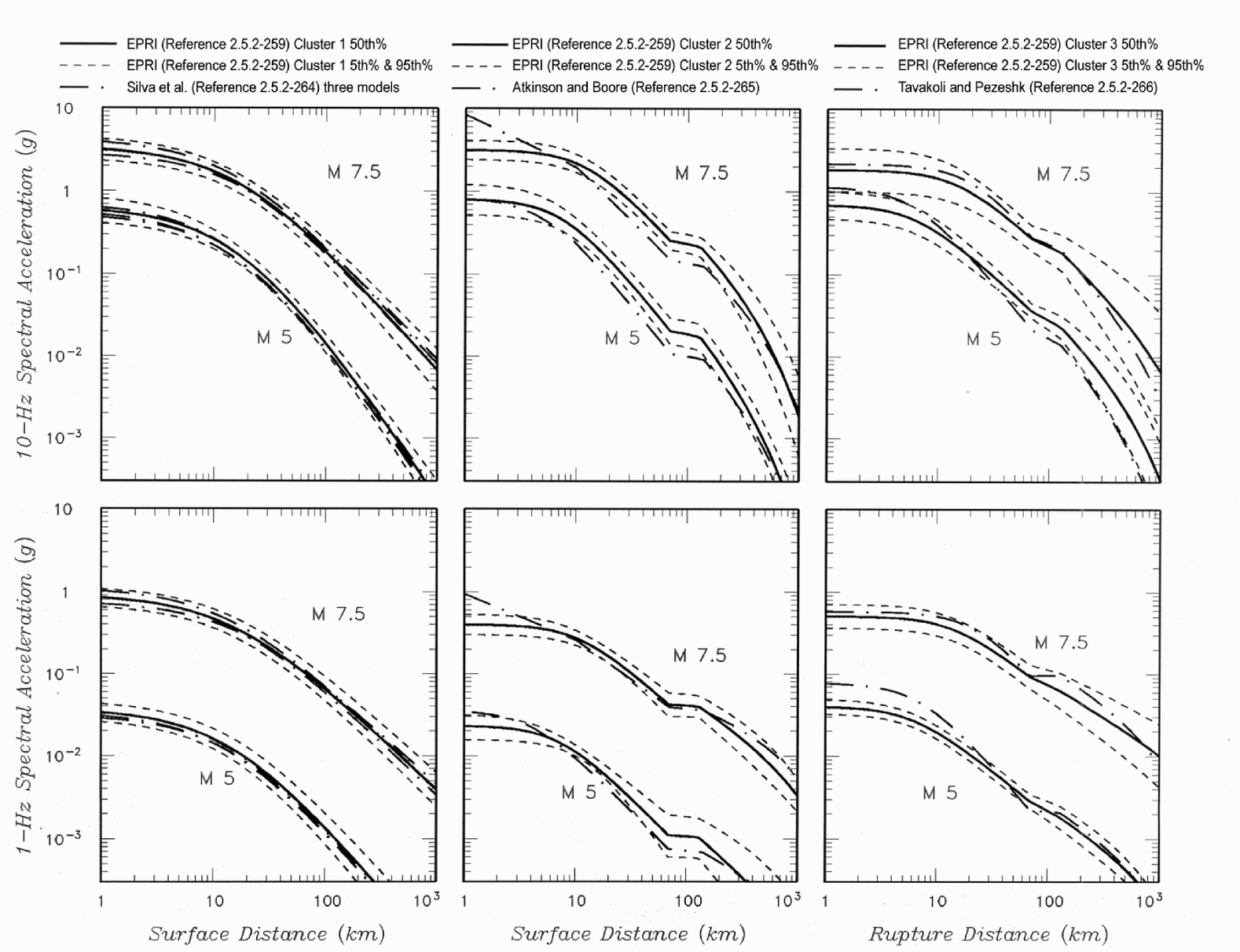

**Figure 2.5.2-222 Mean Hazard Curves for the Bechtel Team Sources**

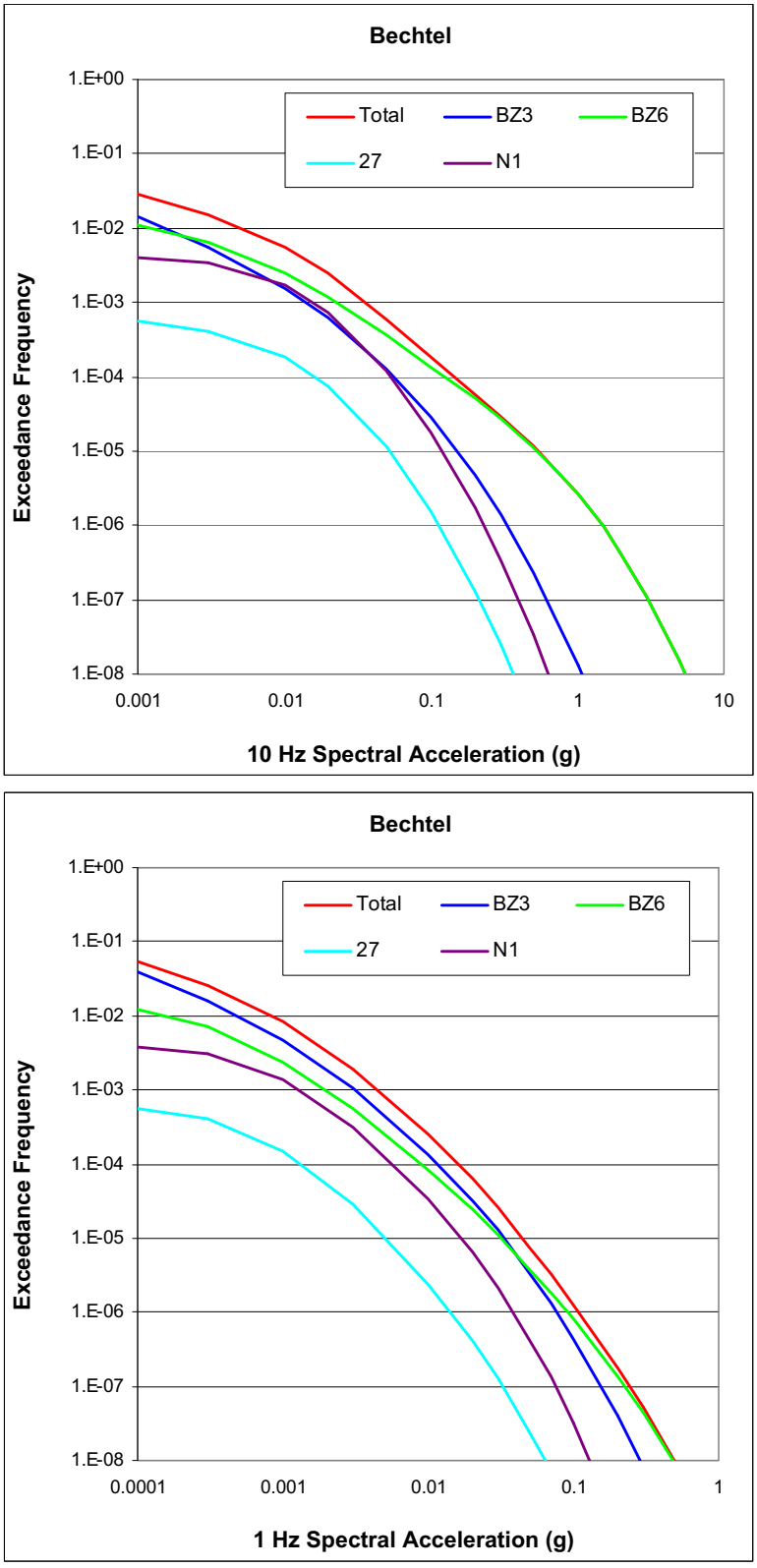

**Figure 2.5.2-223 Mean Hazard Curves for the Dames & Moore Team Sources**

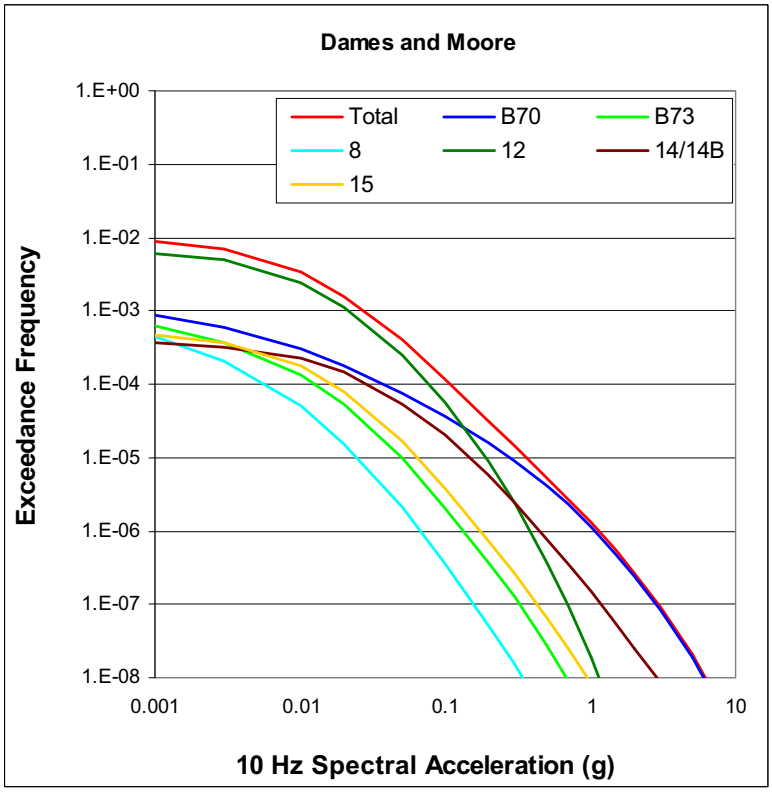


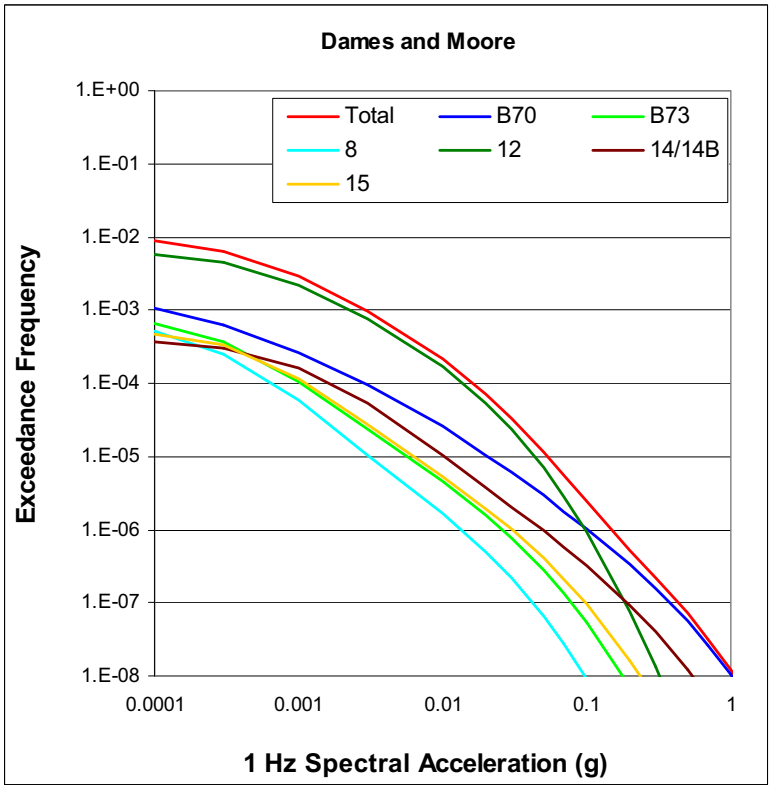

**Figure 2.5.2-224 Mean Hazard Curves for the Law Engineering Team Sources**

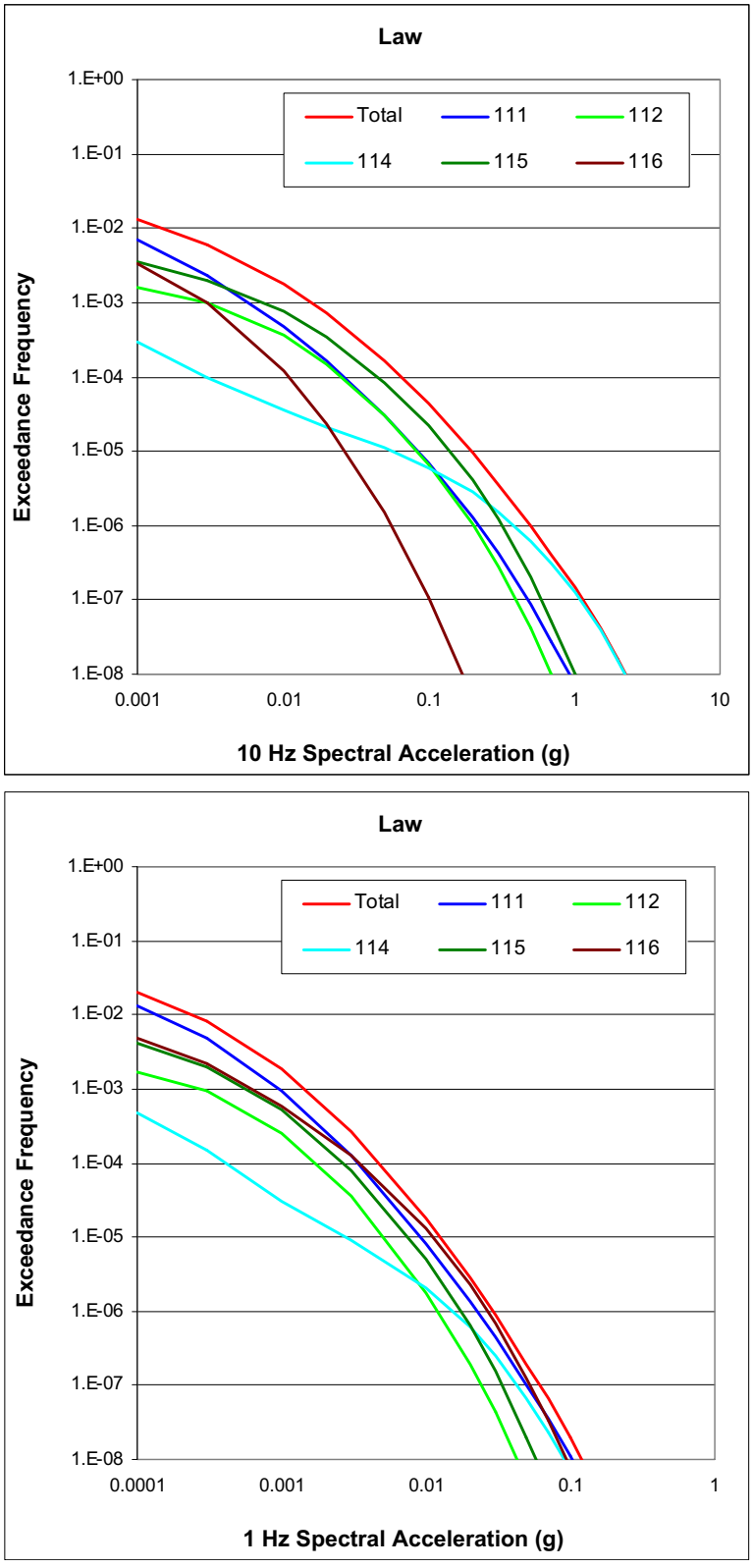

**Figure 2.5.2-225 Mean Hazard Curves for the Rondout Associates Team Sources**

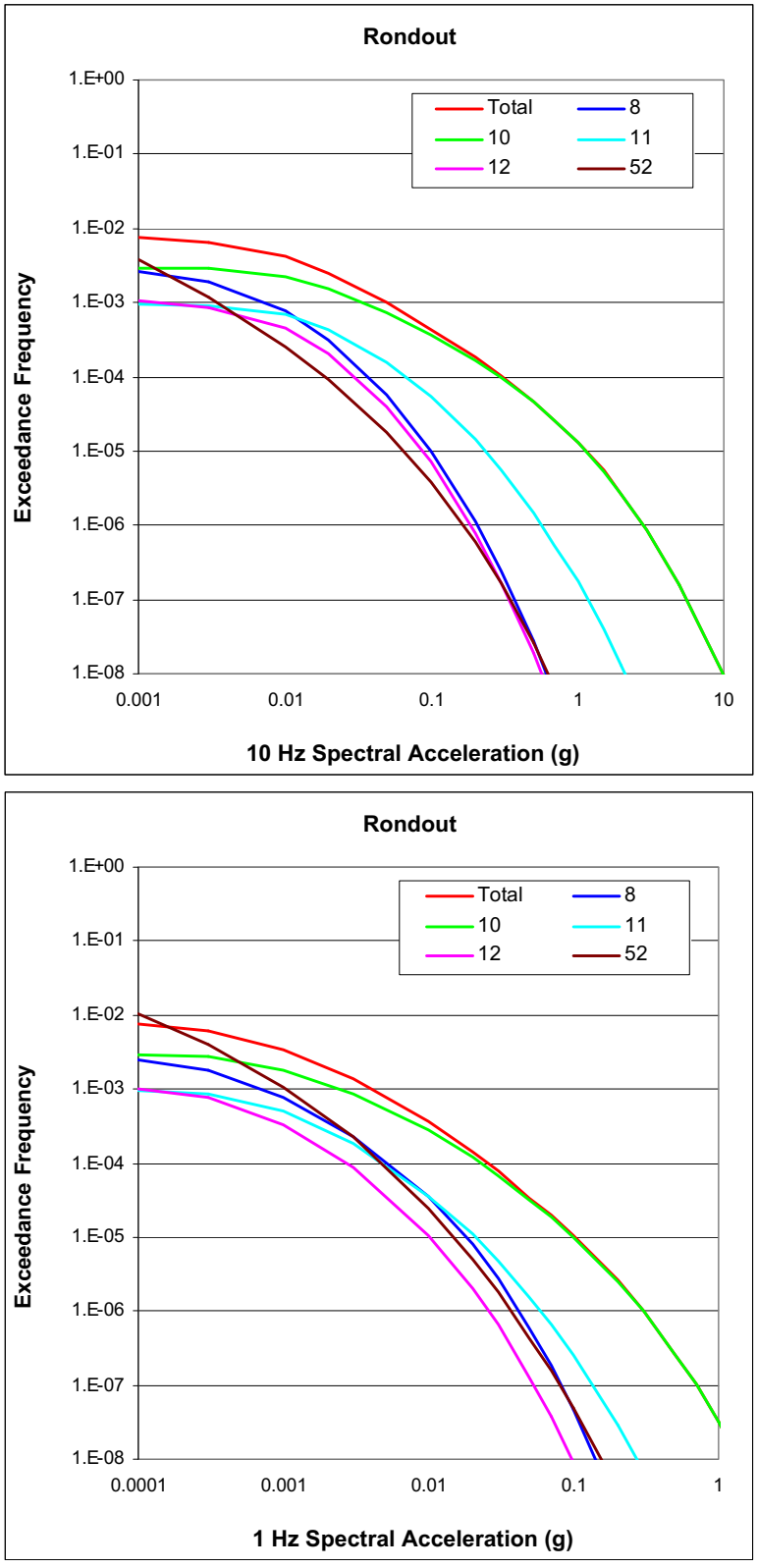

**Figure 2.5.2-226 Mean Hazard Curves for the Weston Geophysical Team Sources**

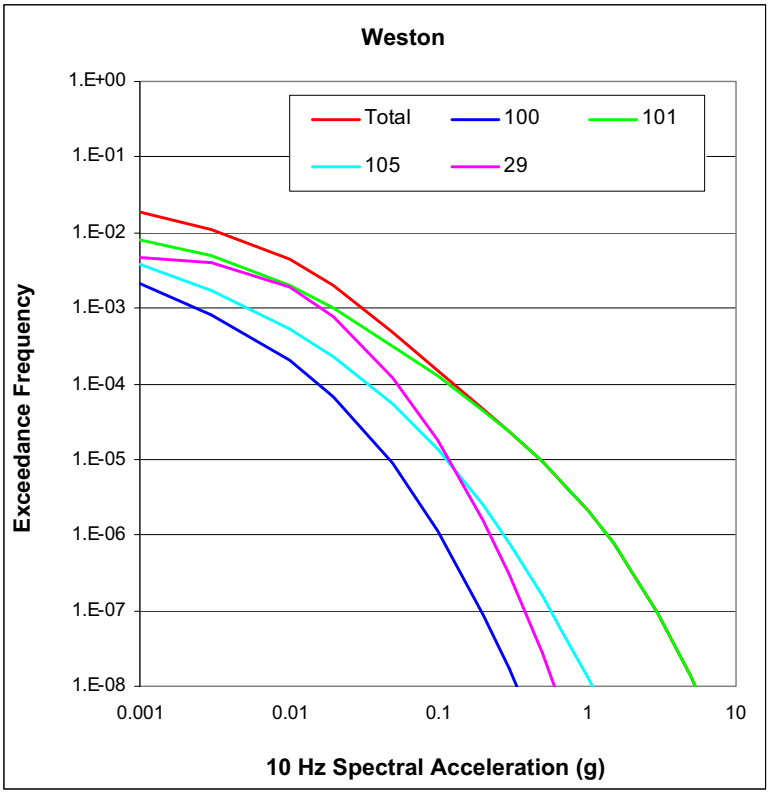


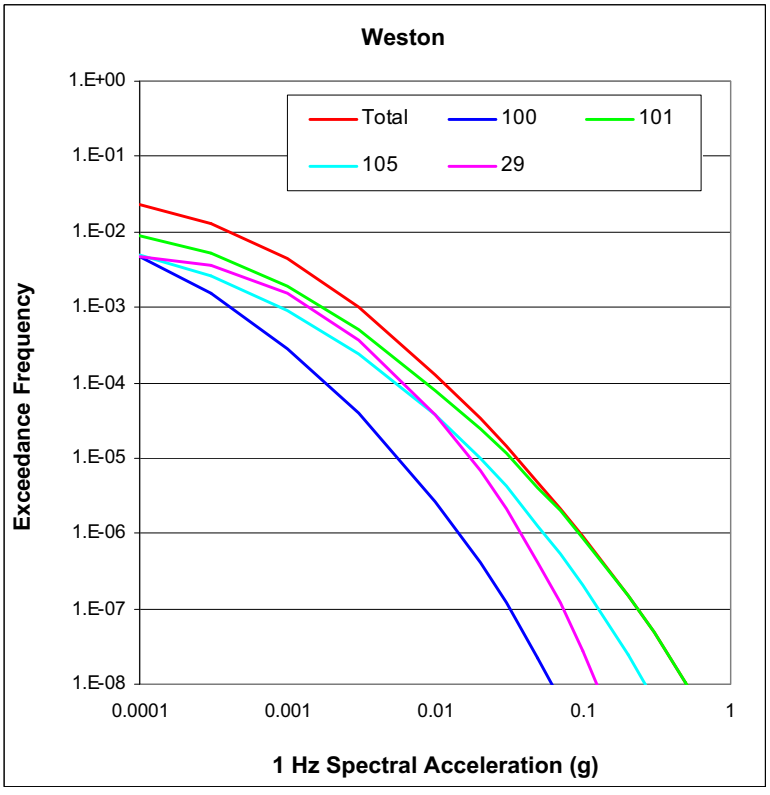

**Figure 2.5.2-227 Mean Hazard Curves for the Woodward-Clyde Consultants Team Sources**

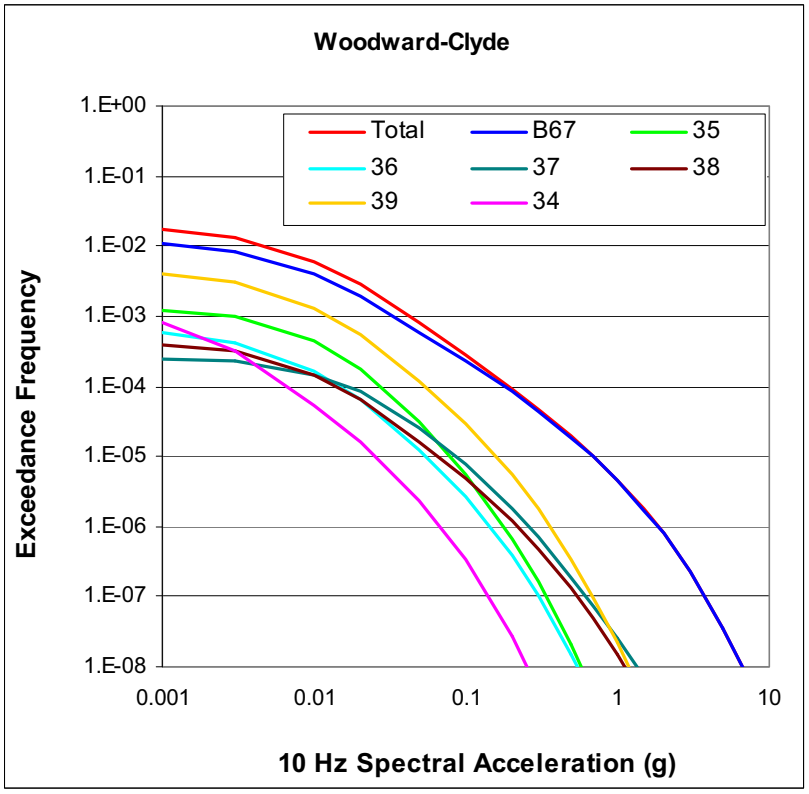


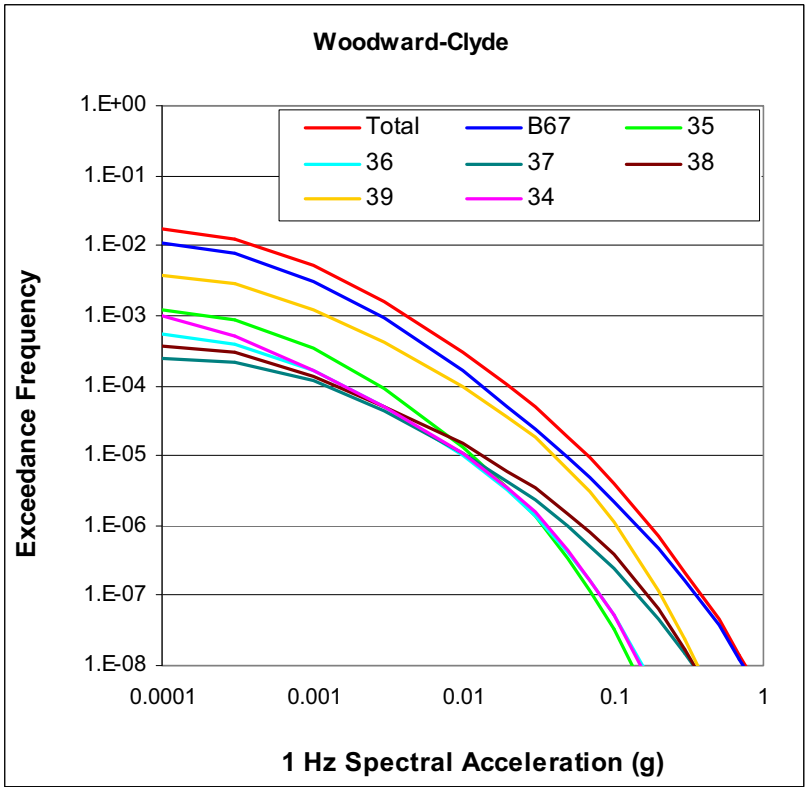

**Figure 2.5.2-228 Effect of Update of EPRI-SOG and Additional Sources on the Seismic Hazard for the Fermi 3 Site**

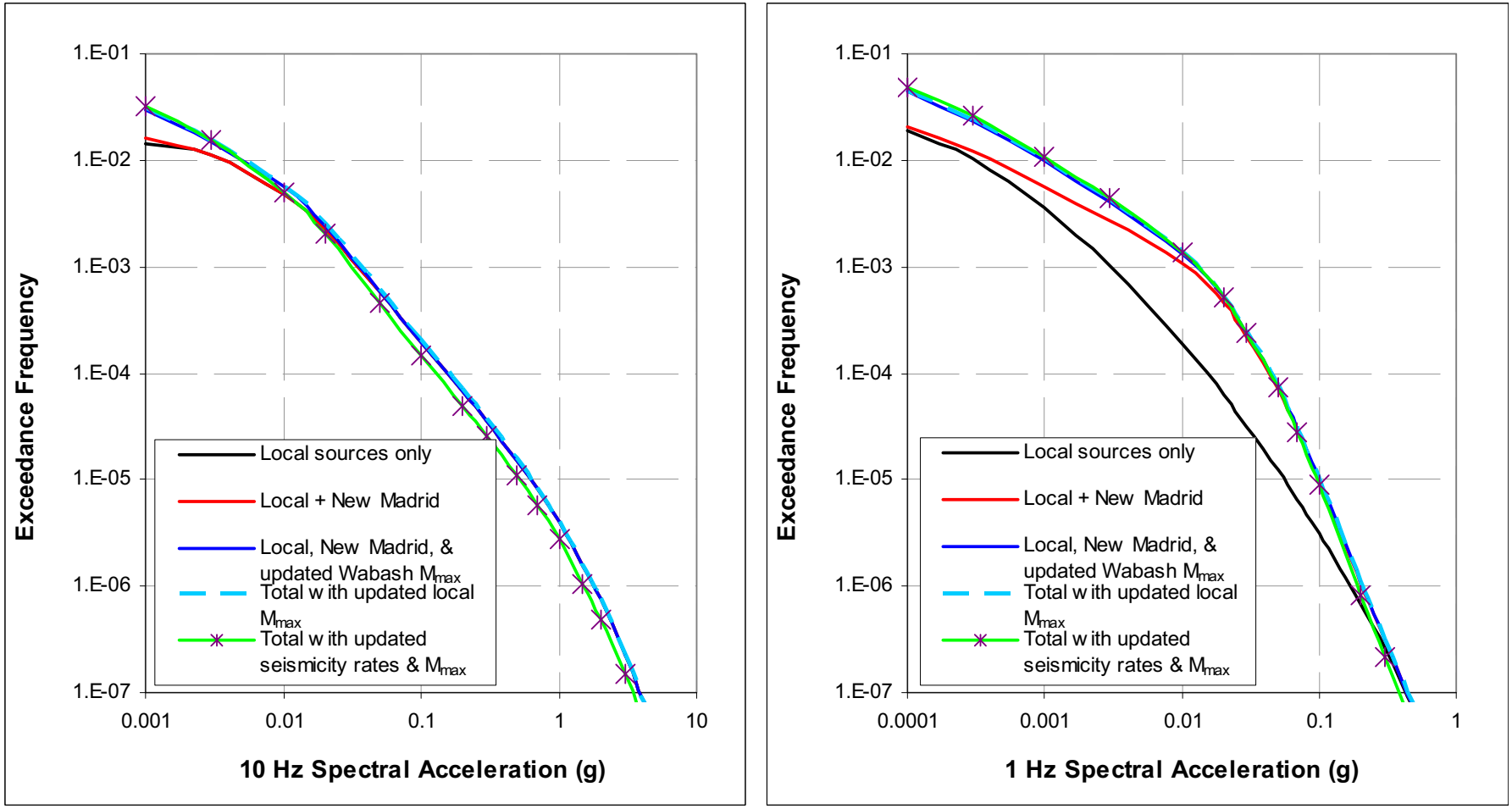

**Figure 2.5.2-229 Generic CEUS Hard Rock Hazard Results for 0.5-Hz Spectral Accelerations for the Fermi 3 Site**

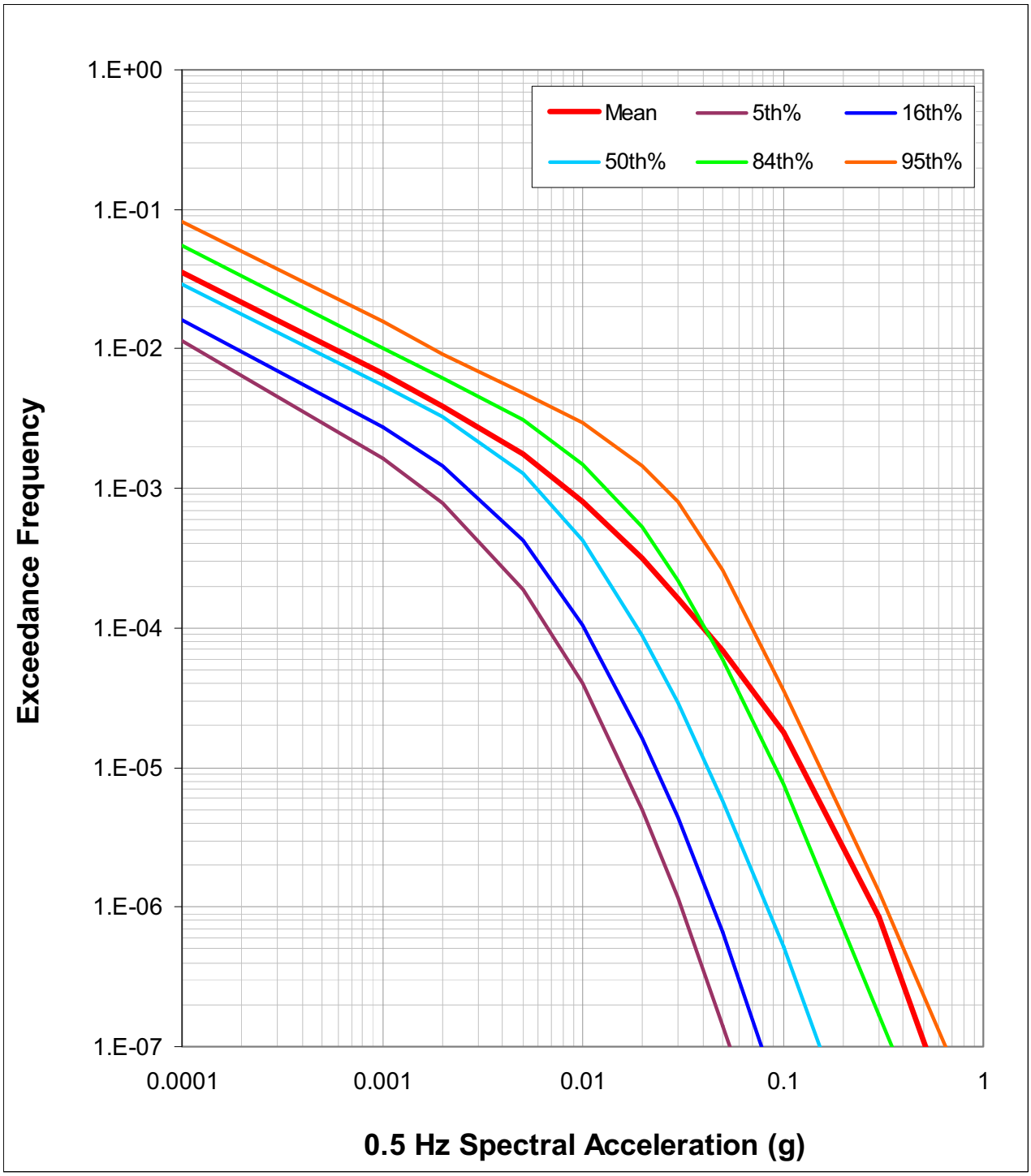

**Figure 2.5.2-230 Generic CEUS Hard Rock Hazard Results for 1-Hz Spectral Accelerations for the Fermi 3 Site**

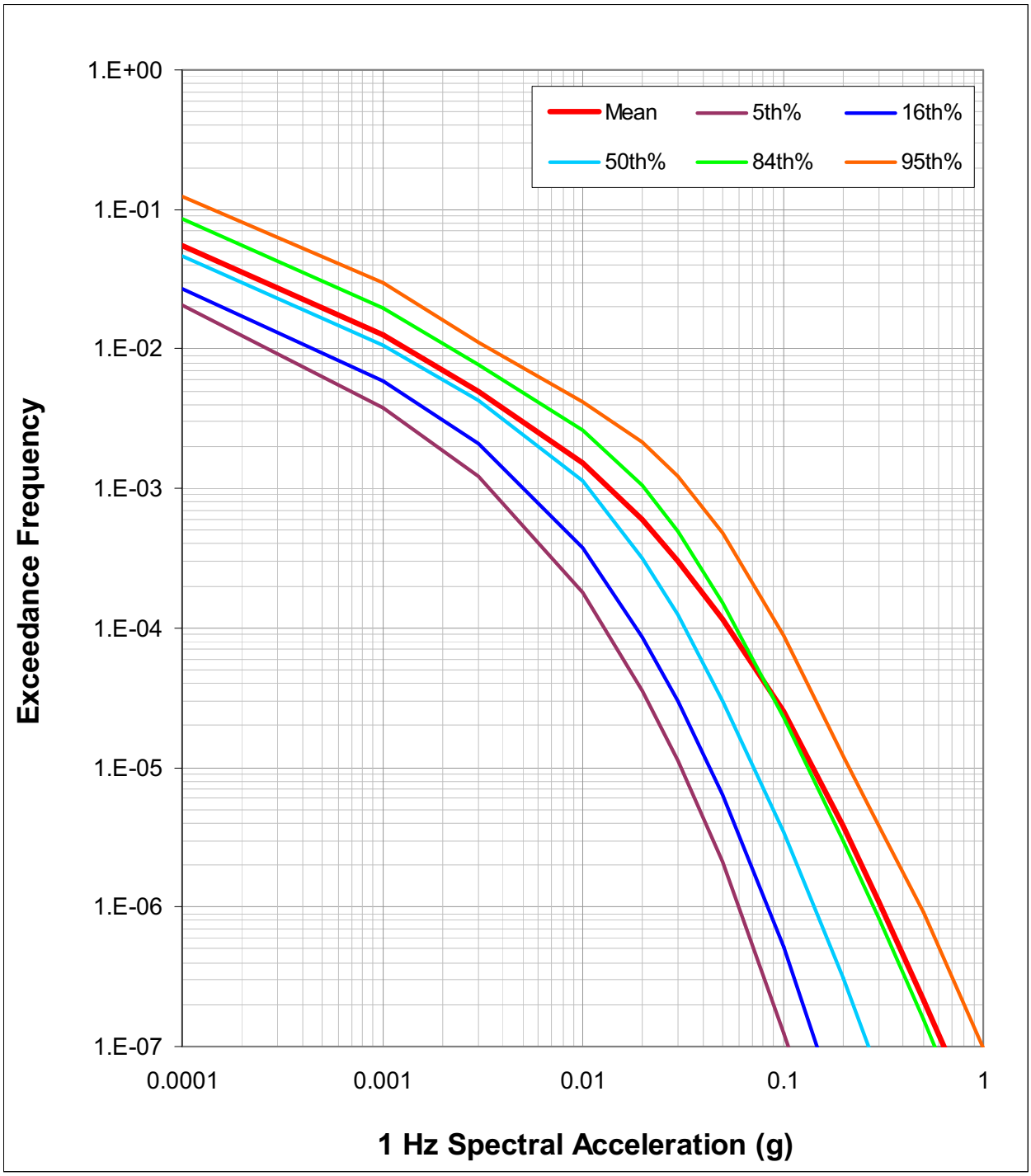

**Figure 2.5.2-231 Generic CEUS Hard Rock Hazard Results for 2.5-Hz Spectral Accelerations for the Fermi 3 Site**

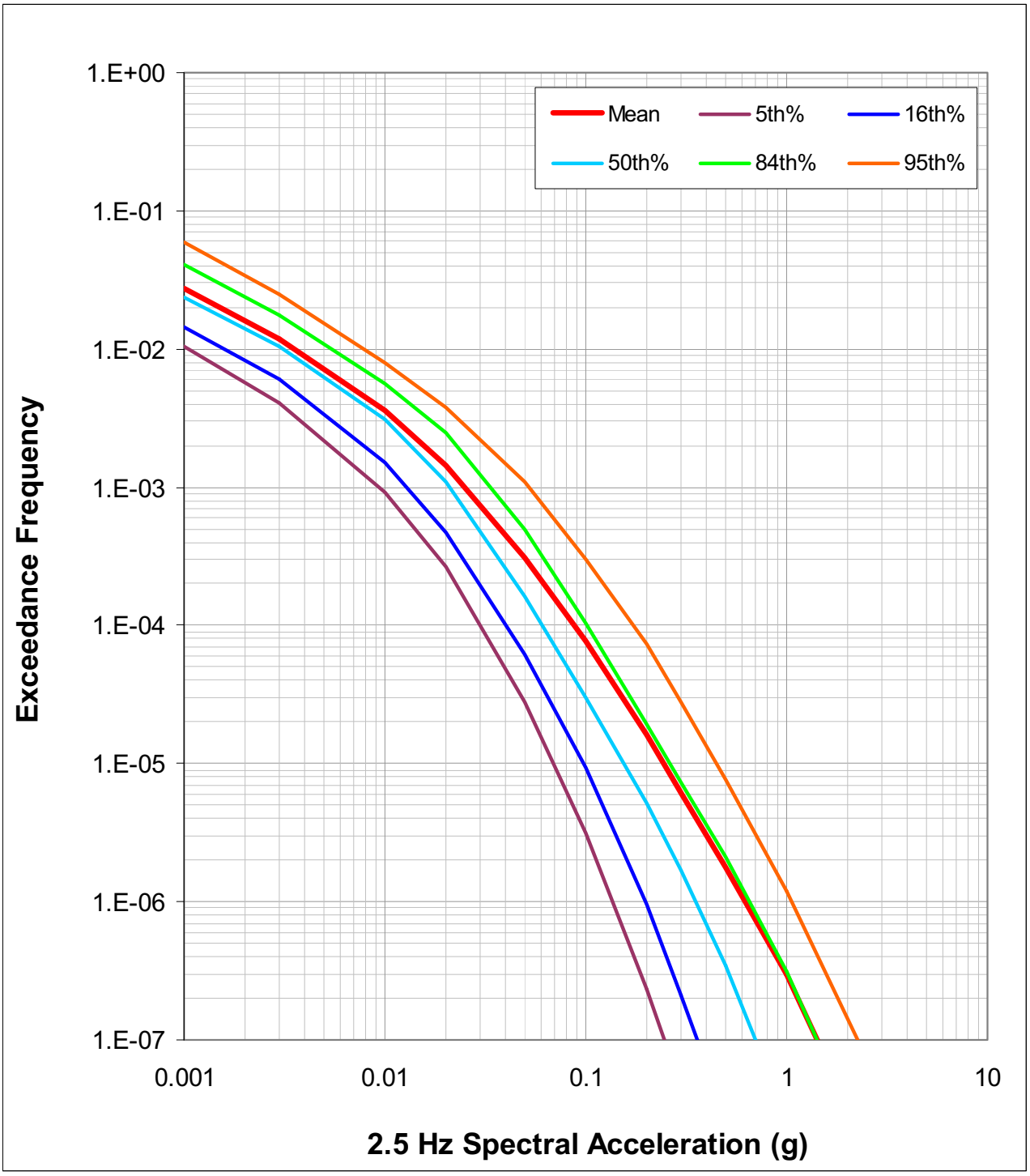

**Figure 2.5.2-232 Generic CEUS Hard Rock Hazard Results for 5-Hz Spectral Accelerations for the Fermi 3 Site**

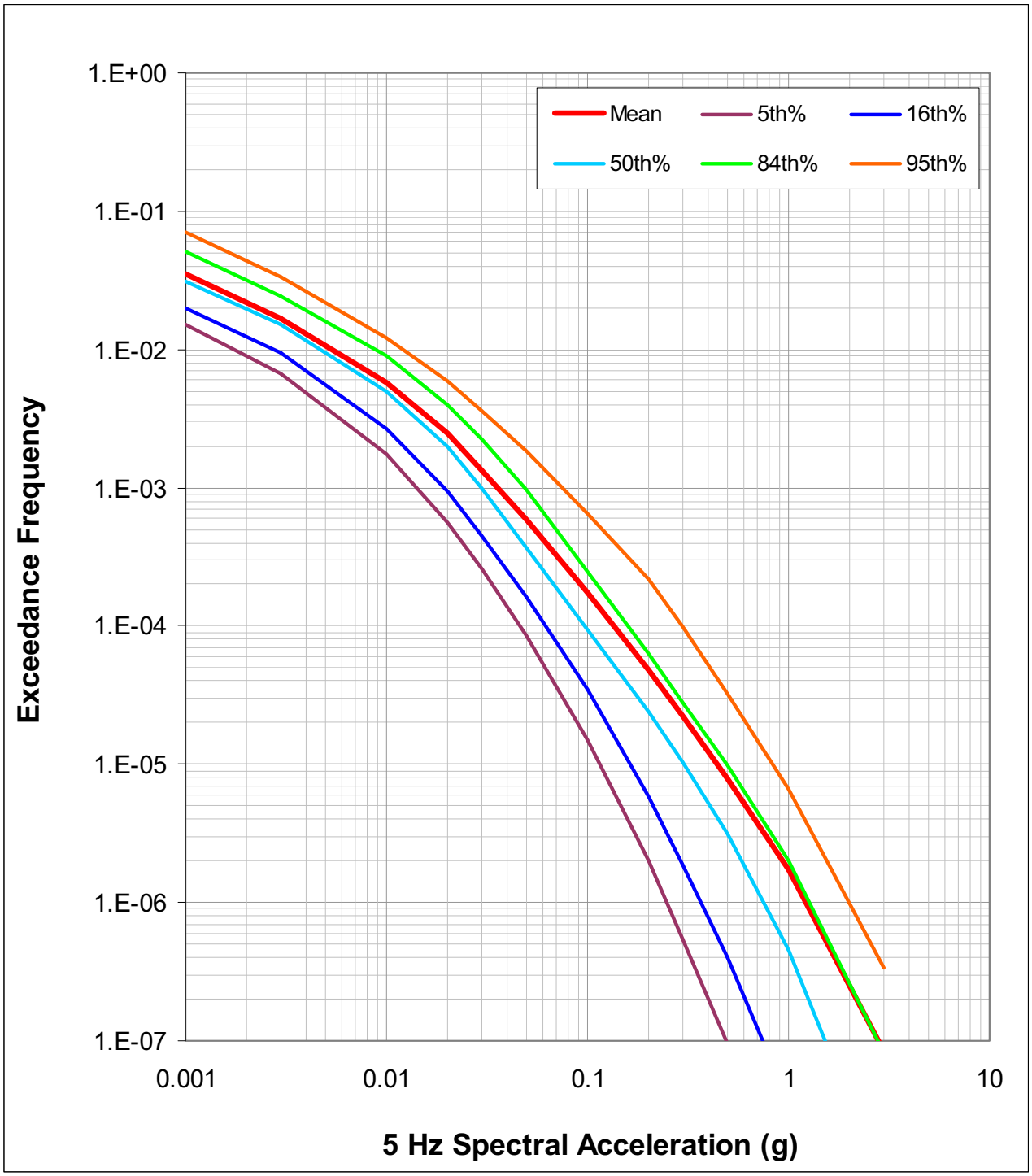

**Figure 2.5.2-233 Generic CEUS Hard Rock Hazard Results for 10-Hz Spectral Accelerations for the Fermi 3 Site**

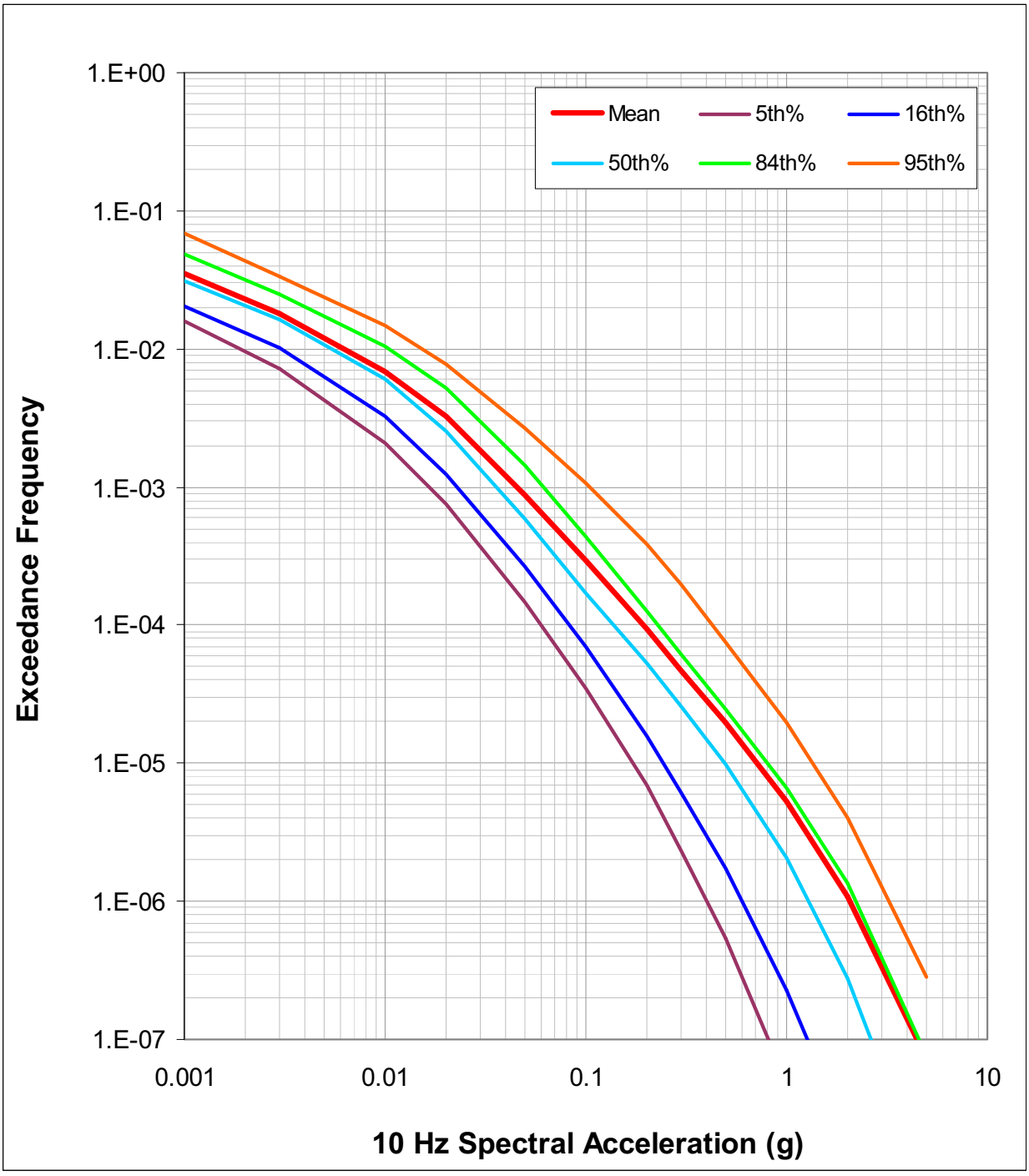

**Figure 2.5.2-234 Generic CEUS Hard Rock Hazard Results for 25-Hz Spectral Accelerations for the Fermi 3 Site**

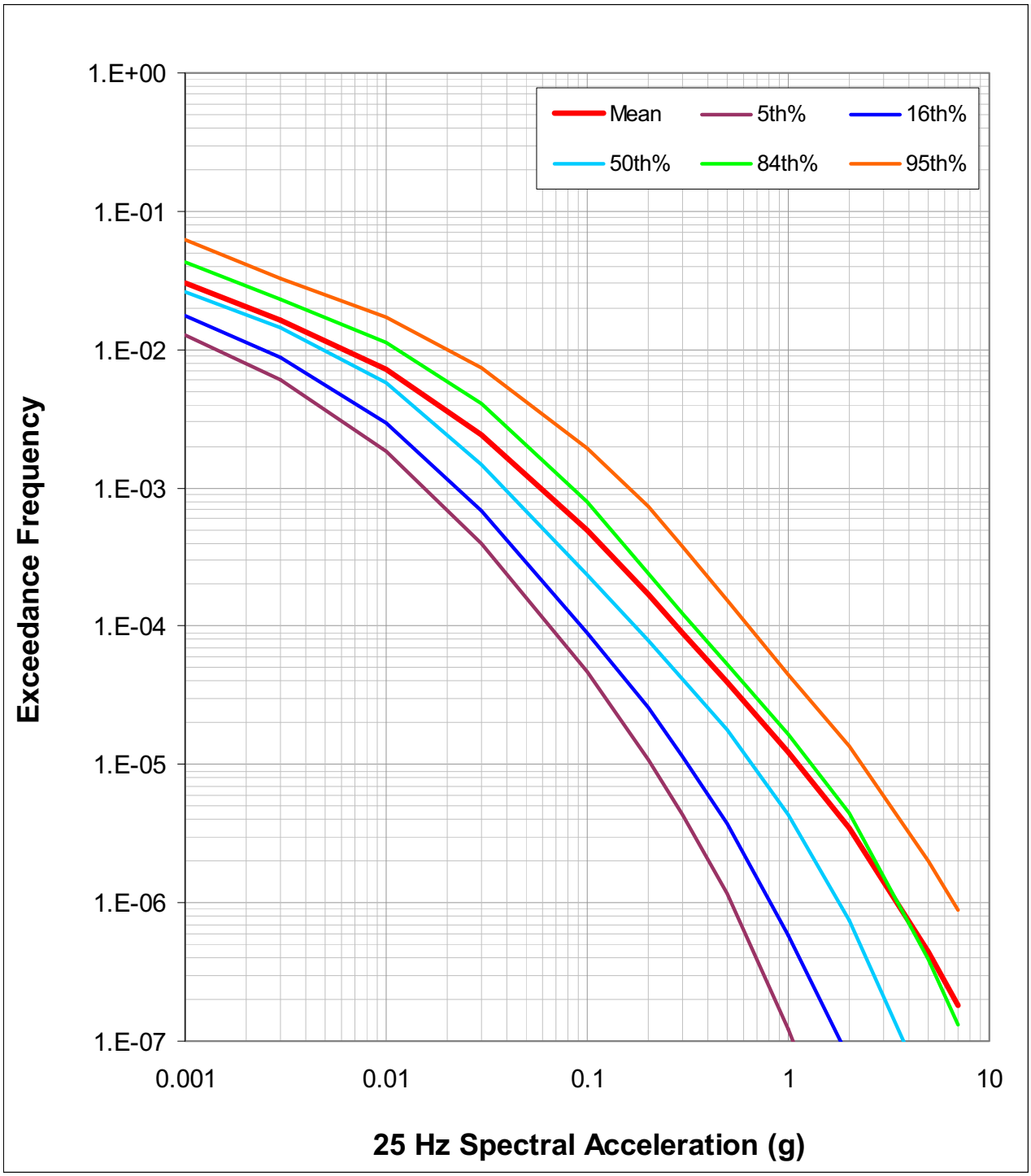

**Figure 2.5.2-235 Generic CEUS Hard Rock Hazard Results for 100-Hz Spectral Accelerations for the Fermi 3 Site**

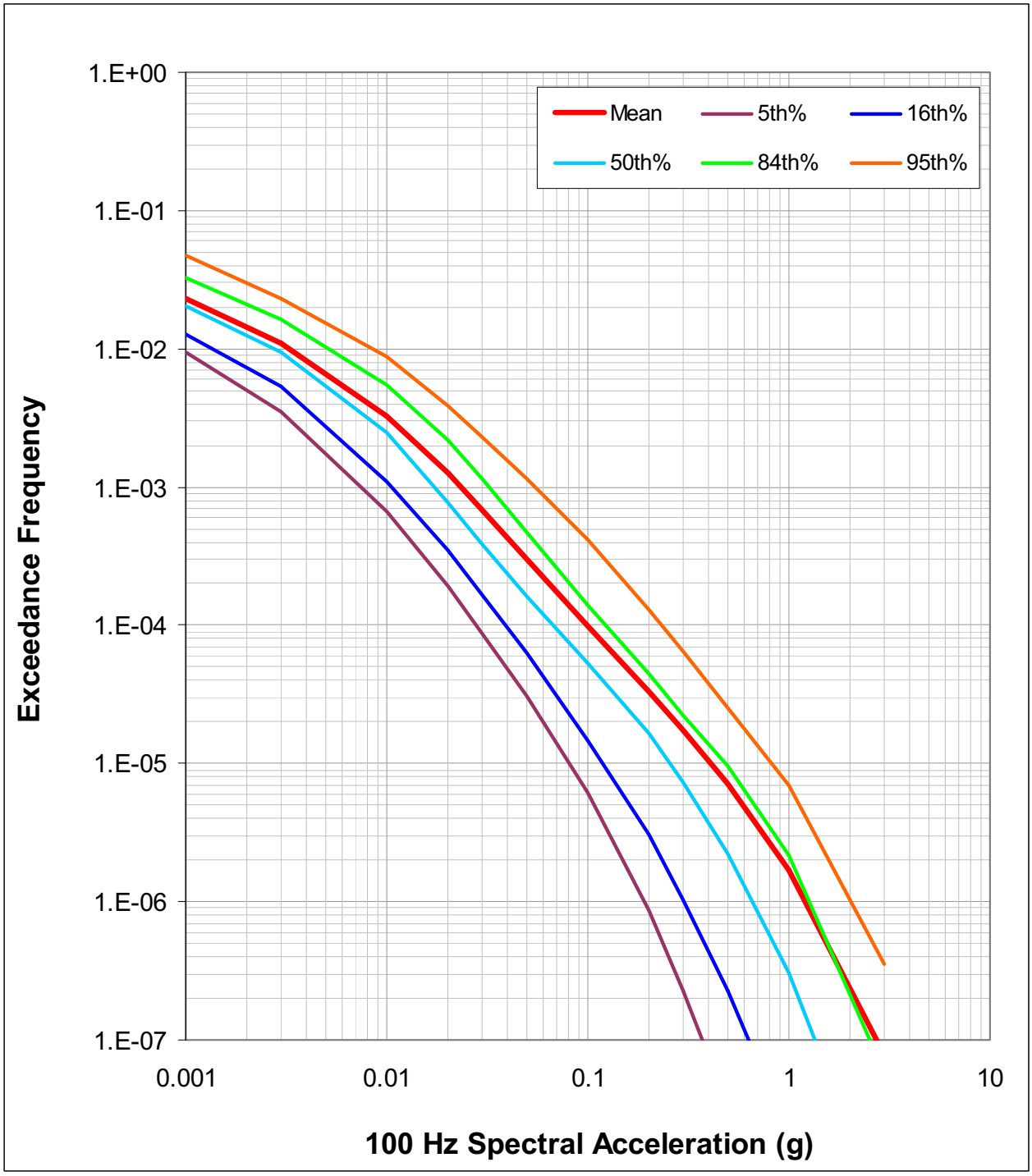

**Figure 2.5.2-236 Contribution of the Updated EPRI-SOG Model and the New Madrid/Wabash Valley Sources to the Total Mean Hazard at the Fermi 3 Site**

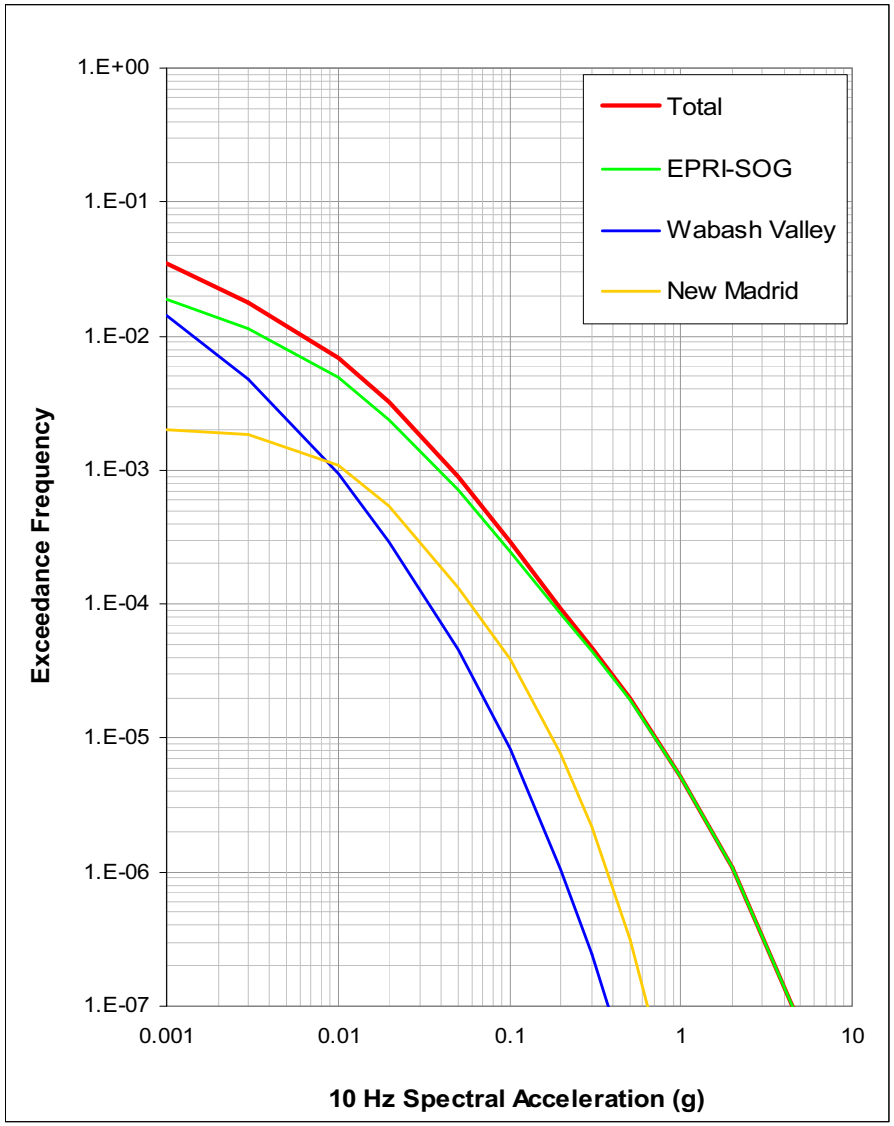


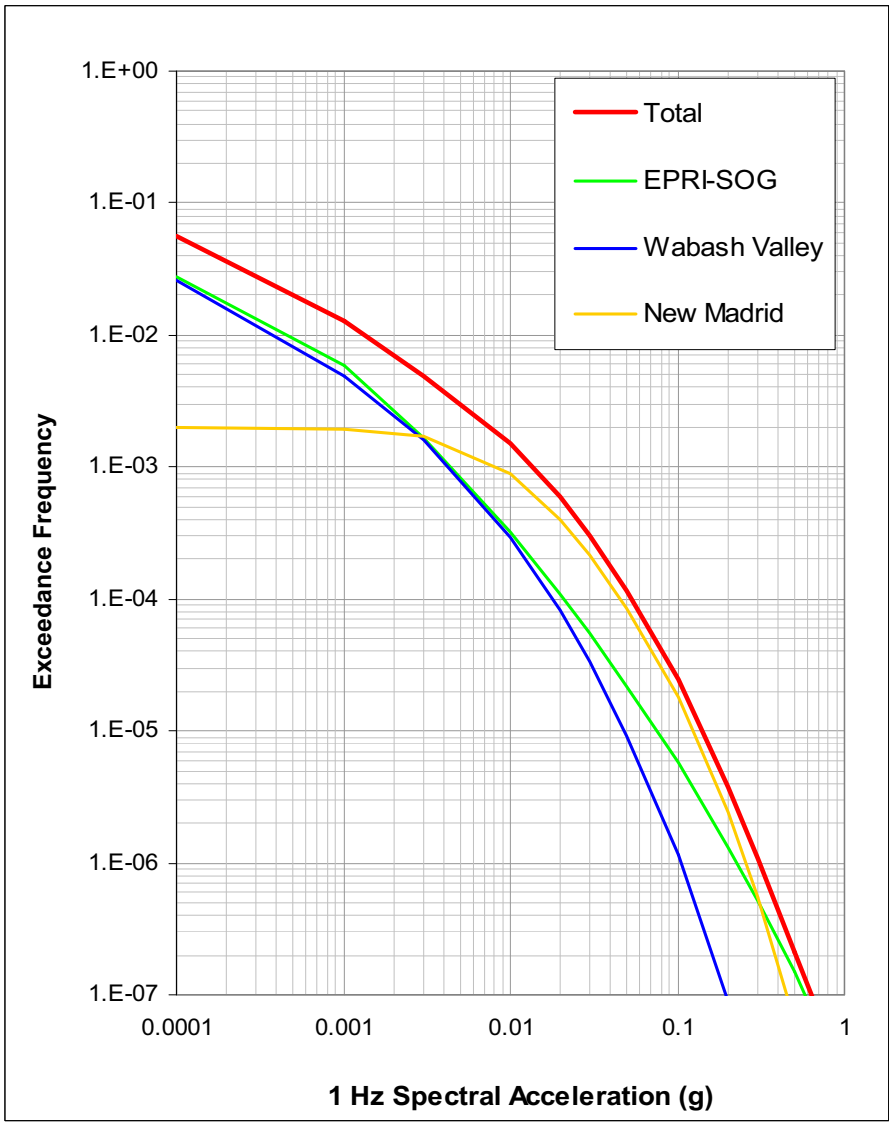

**Figure 2.5.2-237 Effect of Alternative EPRI (2004) Ground Motion Cluster Median Models on the Hazard Computed for the Fermi 3 Site**

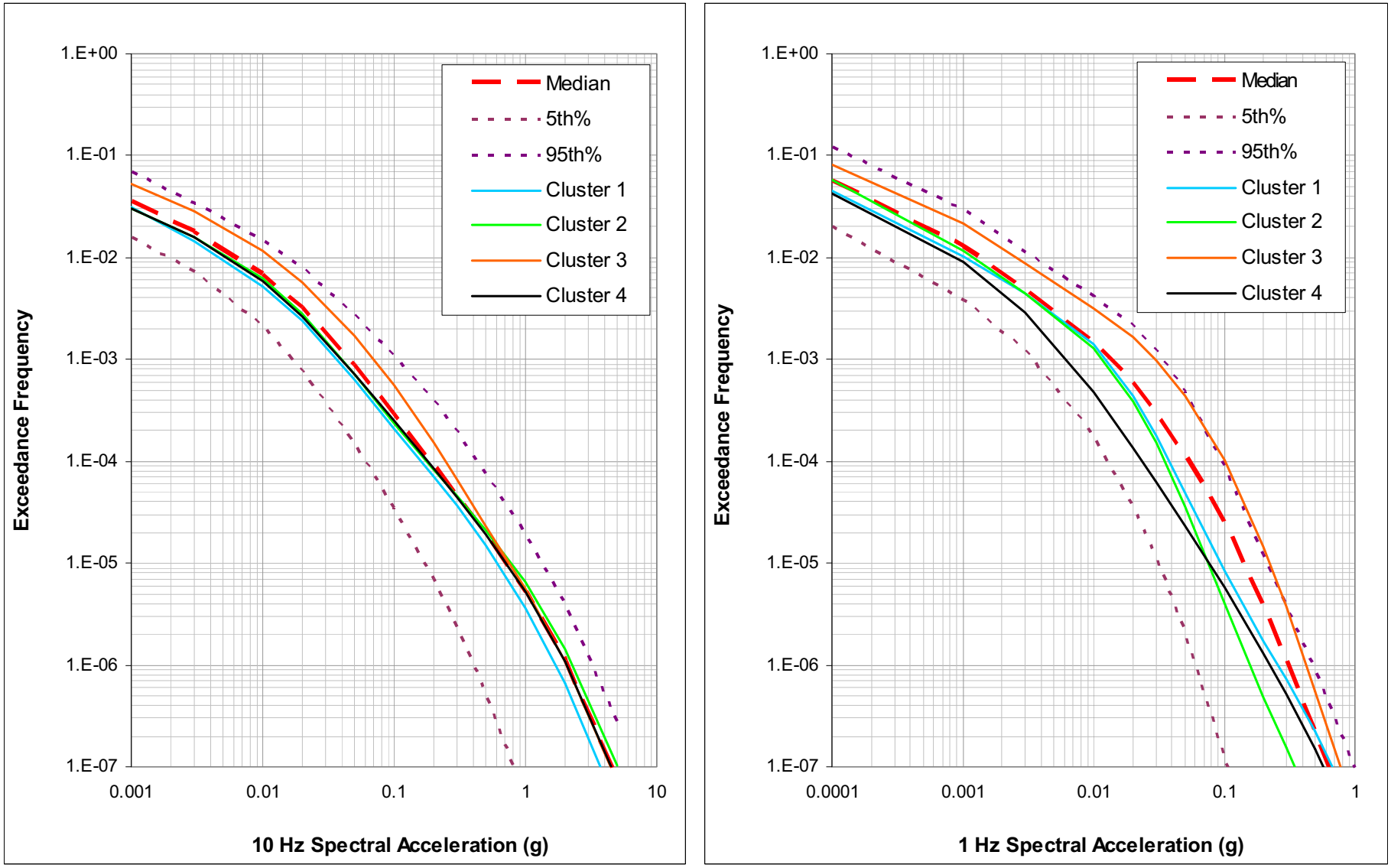

**Figure 2.5.2-238 Effect of Uncertainty in the EPRI (2004) Ground Motion Cluster Median Models on the Hazard Computed for the Fermi 3 Site**

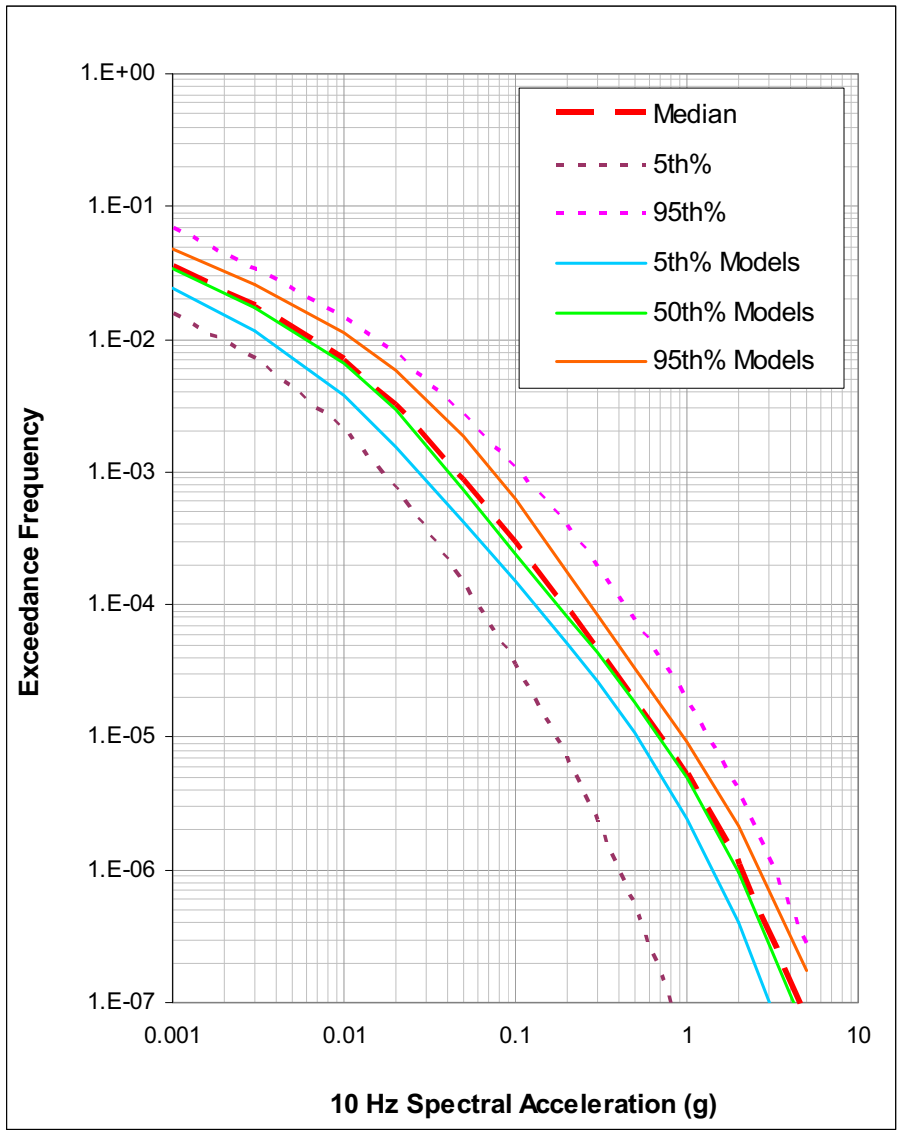


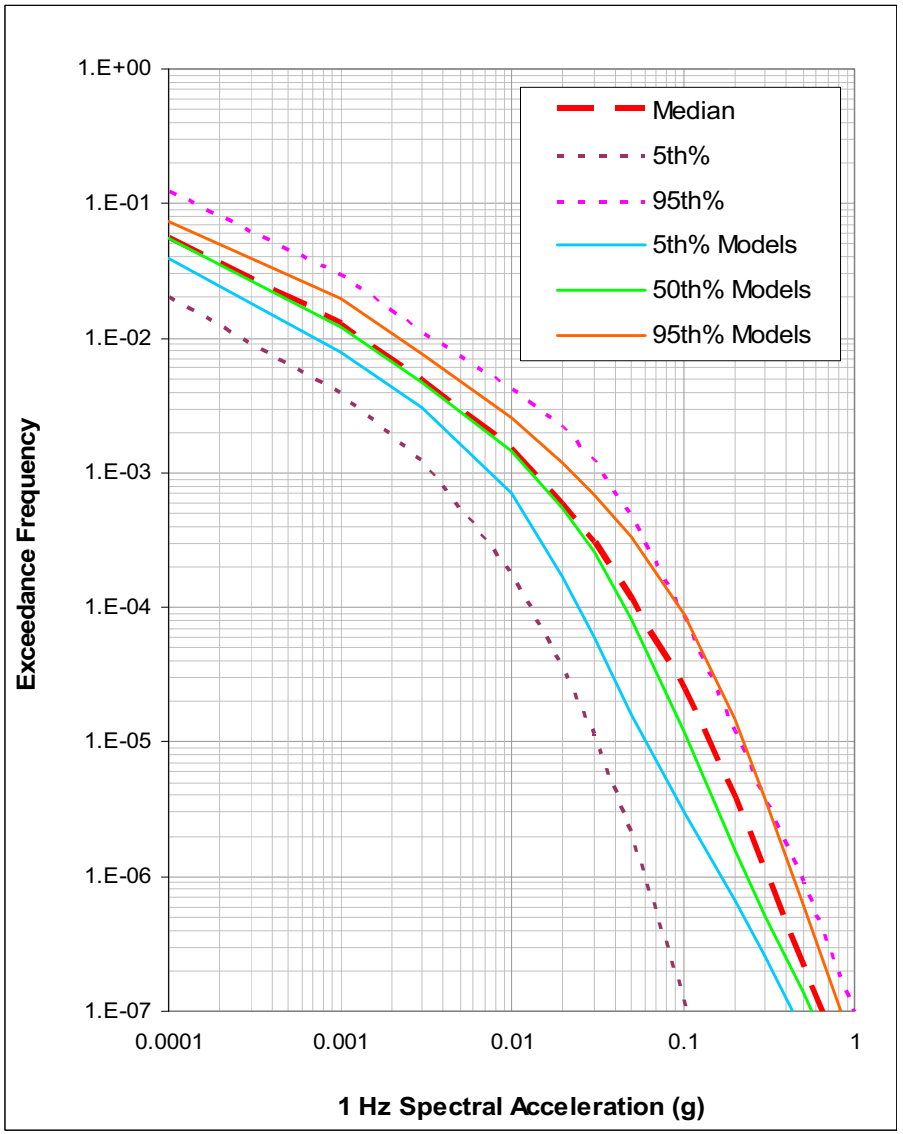

**Figure 2.5.2-239 Effect of Alternative $m_b$-M Conversion Relationships on the Hazard Computed for the Fermi 3 Site**

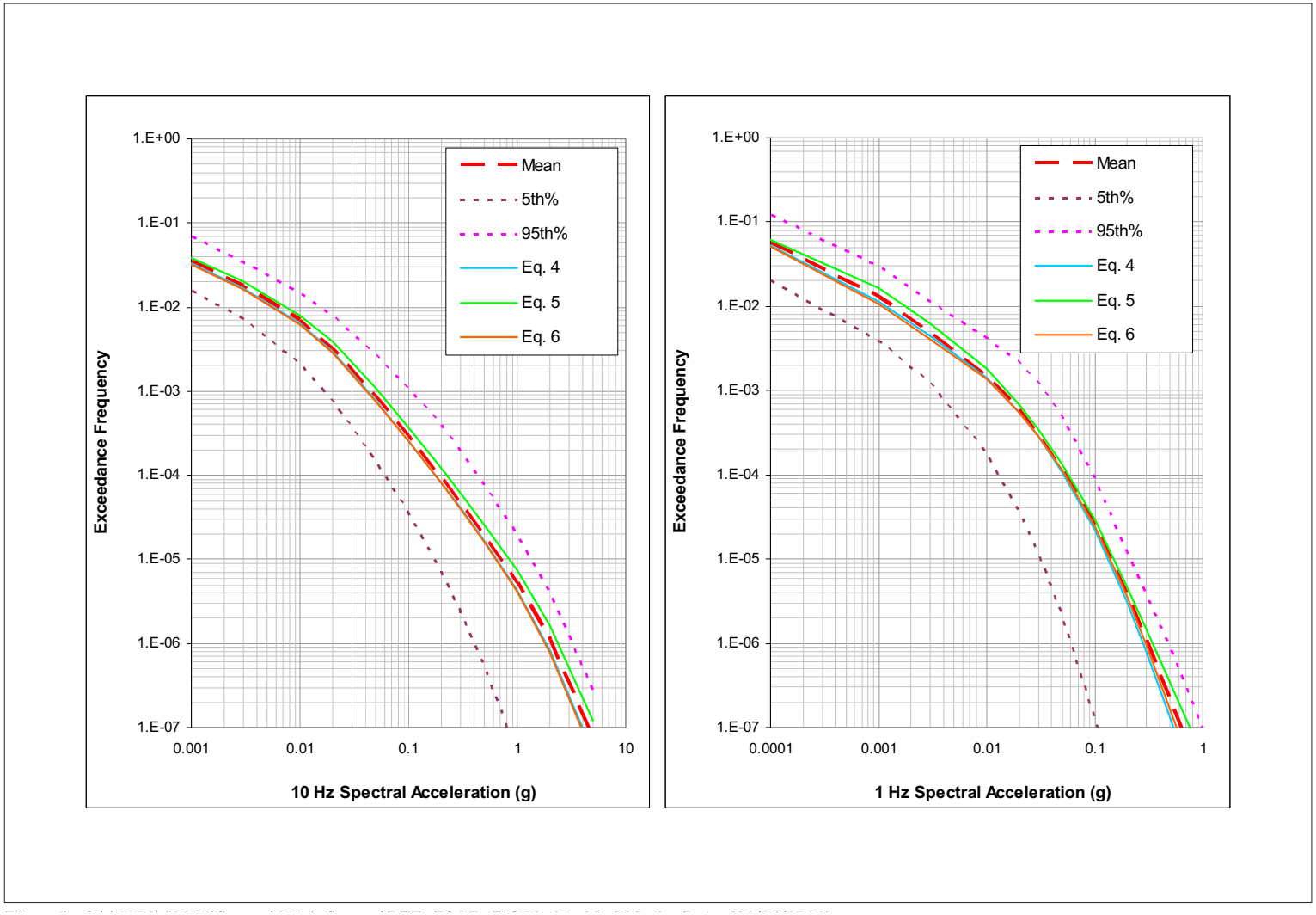

**Figure 2.5.2-240 Uncertainty in the Hazard for the Fermi 3 Site from the Updated EPRI-SOG Seismic Sources and Comparison of Individual Team Mean Hazard Results**

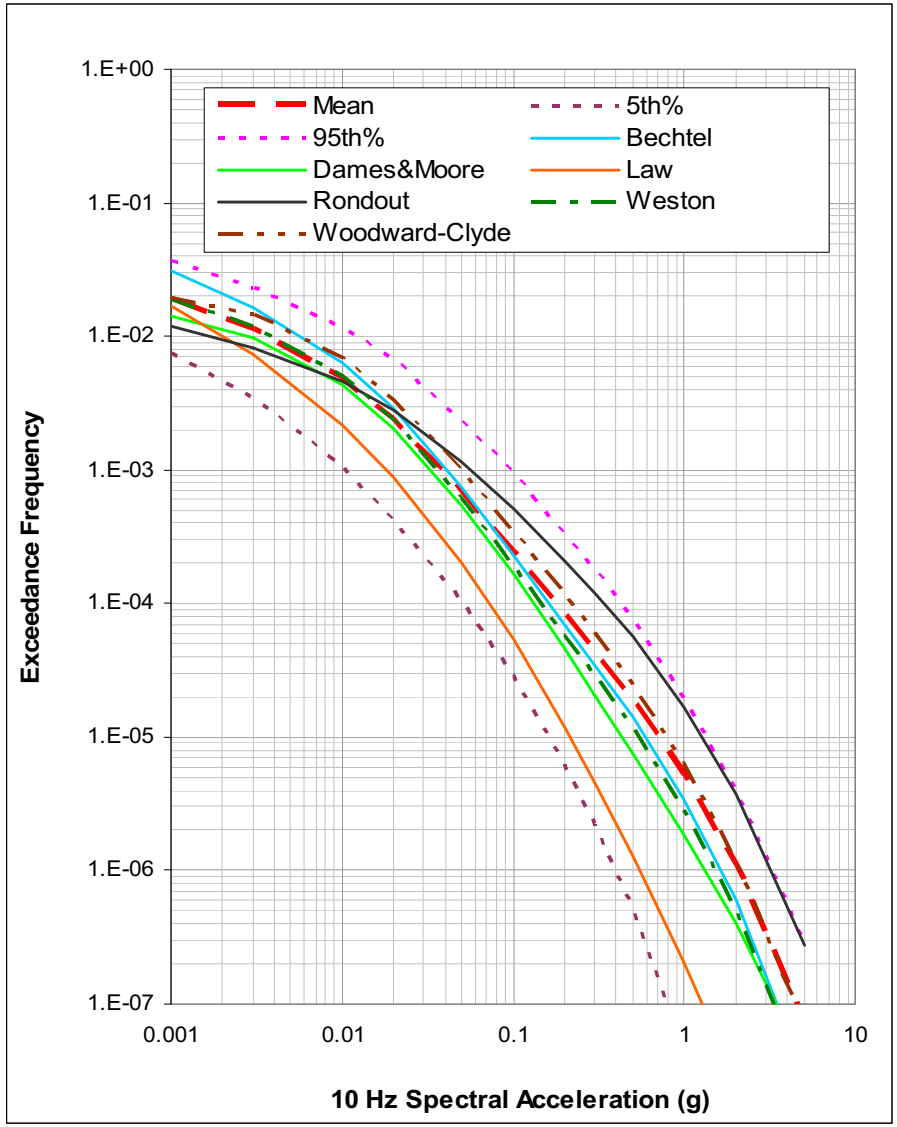


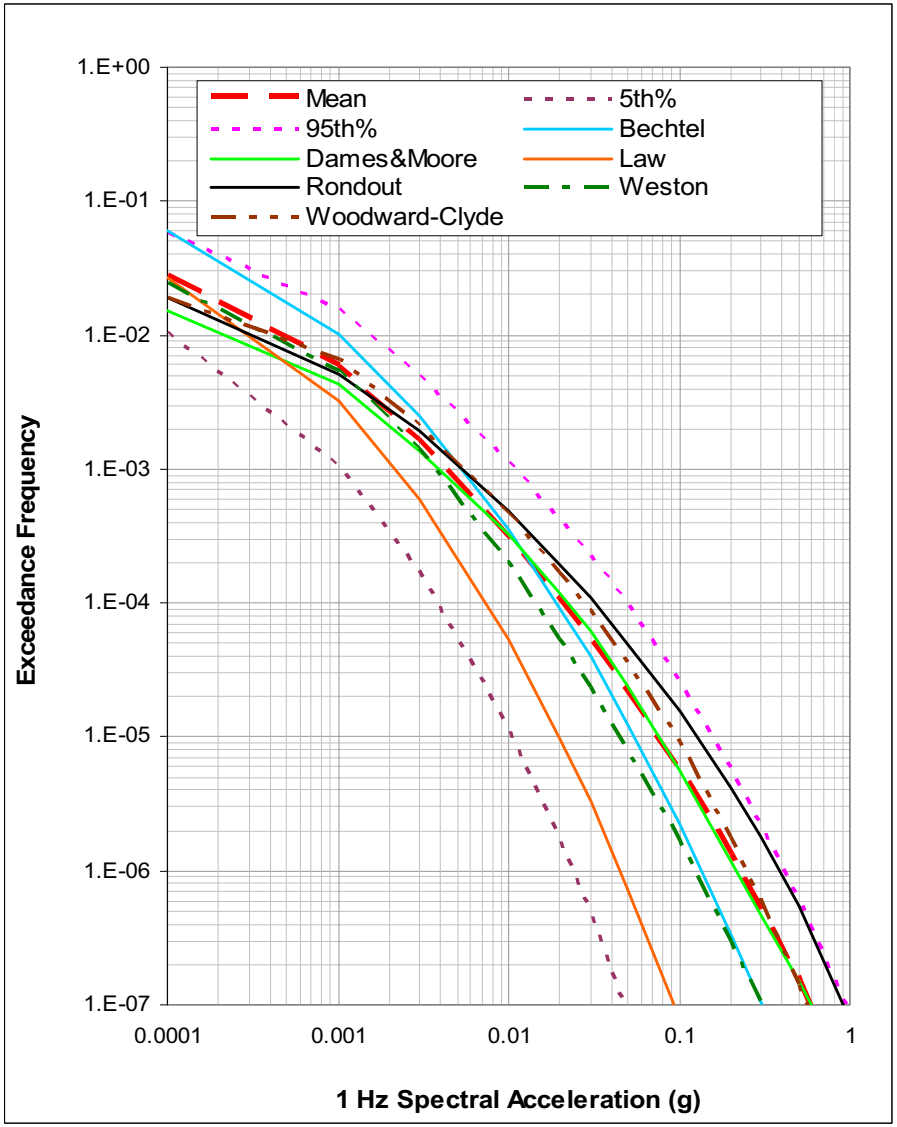

**Figure 2.5.2-241 Uniform Hazard Response Spectra for the Fermi 3 Site and Generic Hard Rock Conditions**

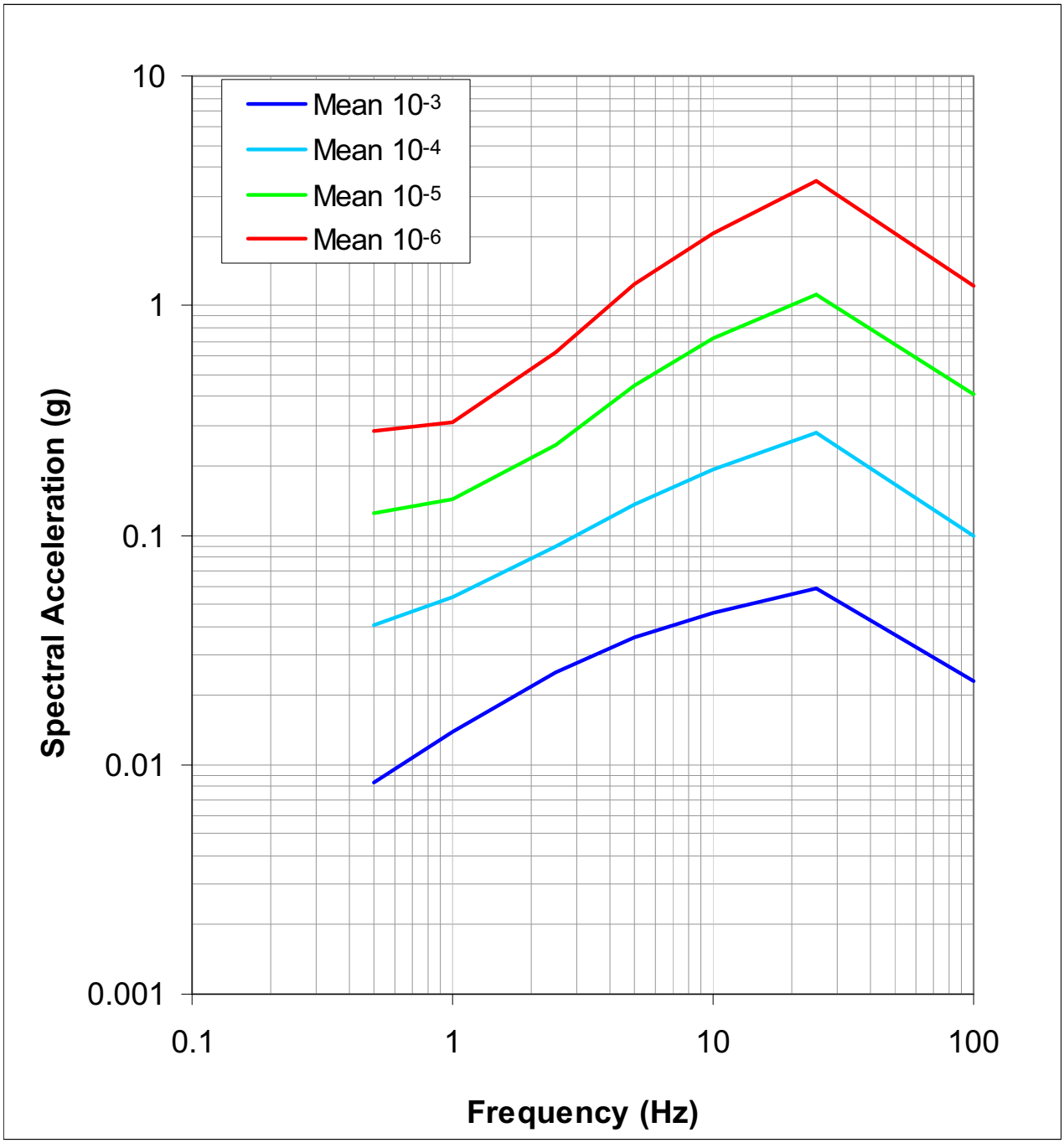

**Figure 2.5.2-242 Deaggregation of Mean $10^{-3}$ Hazard**

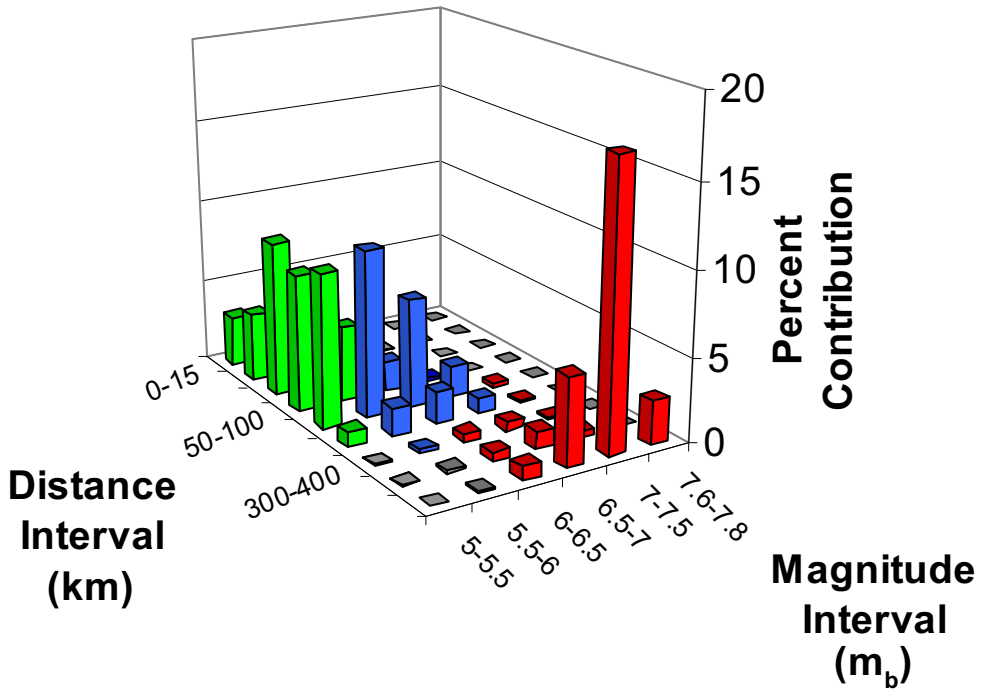


**1 and 2.5 Hz**

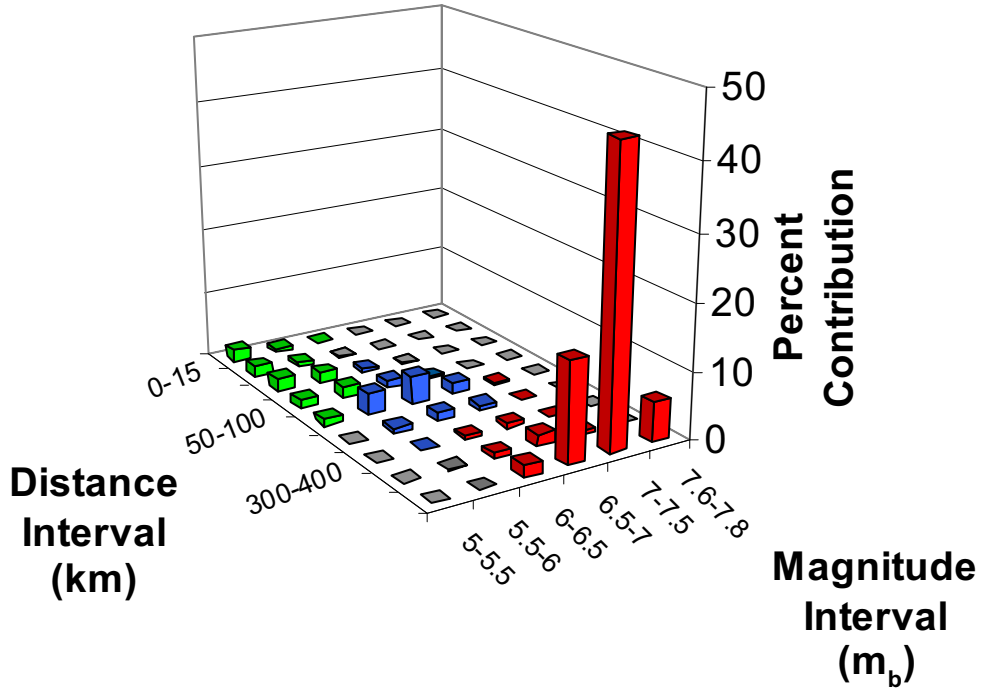

**Figure 2.5.2-243 Deaggregation of Mean $10^{-4}$ Hazard**

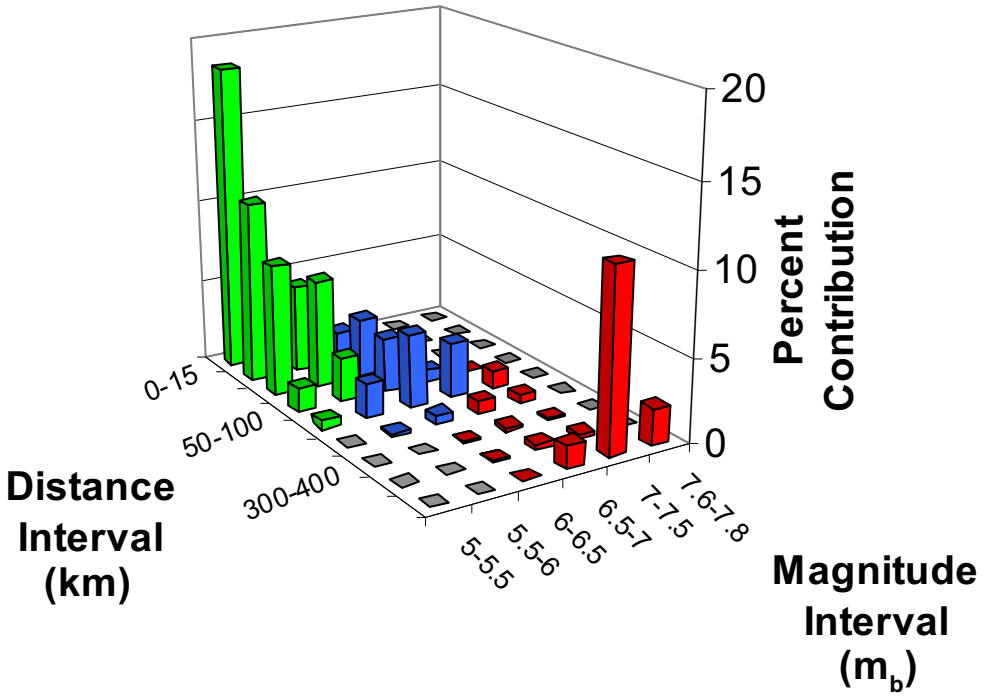


**1 and 2.5 Hz**

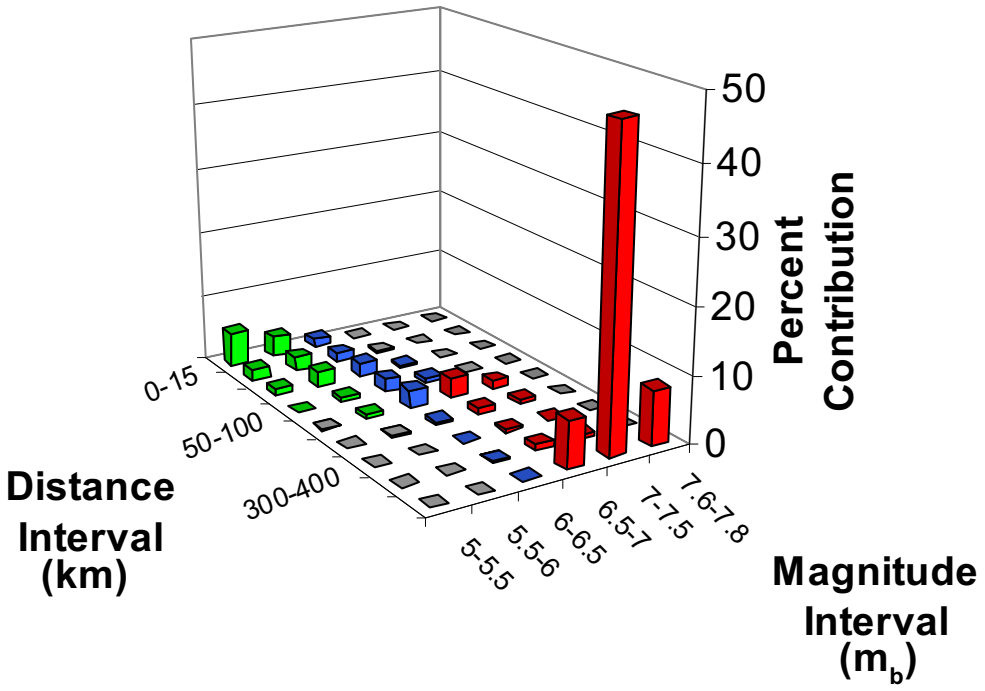

**Figure 2.5.2-244 Deaggregation of Mean $10^{-5}$ Hazard**

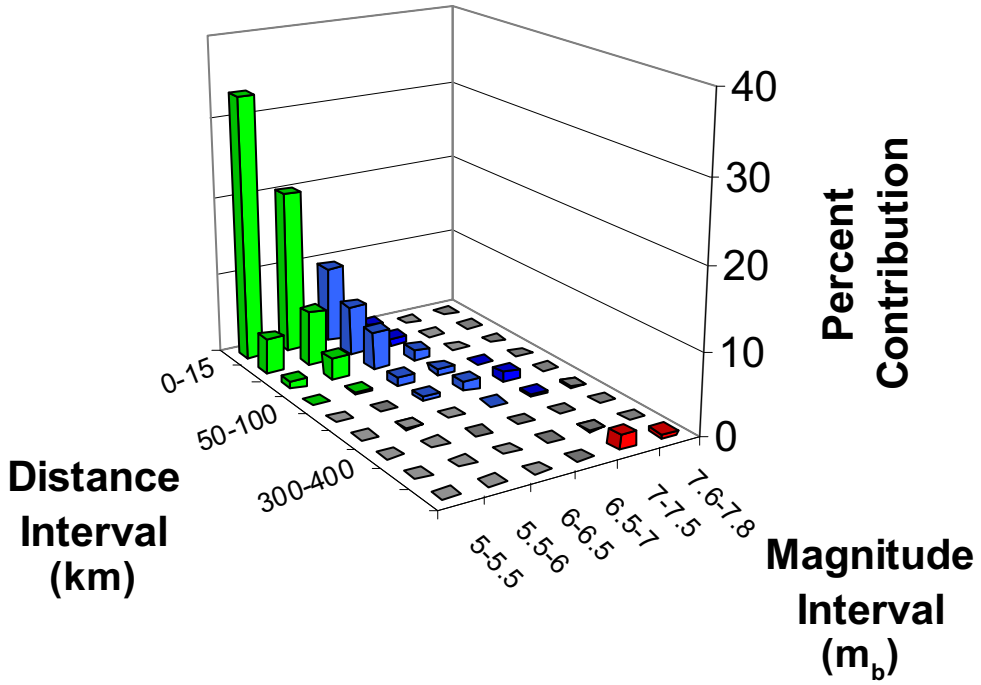


**1 and 2.5 Hz**

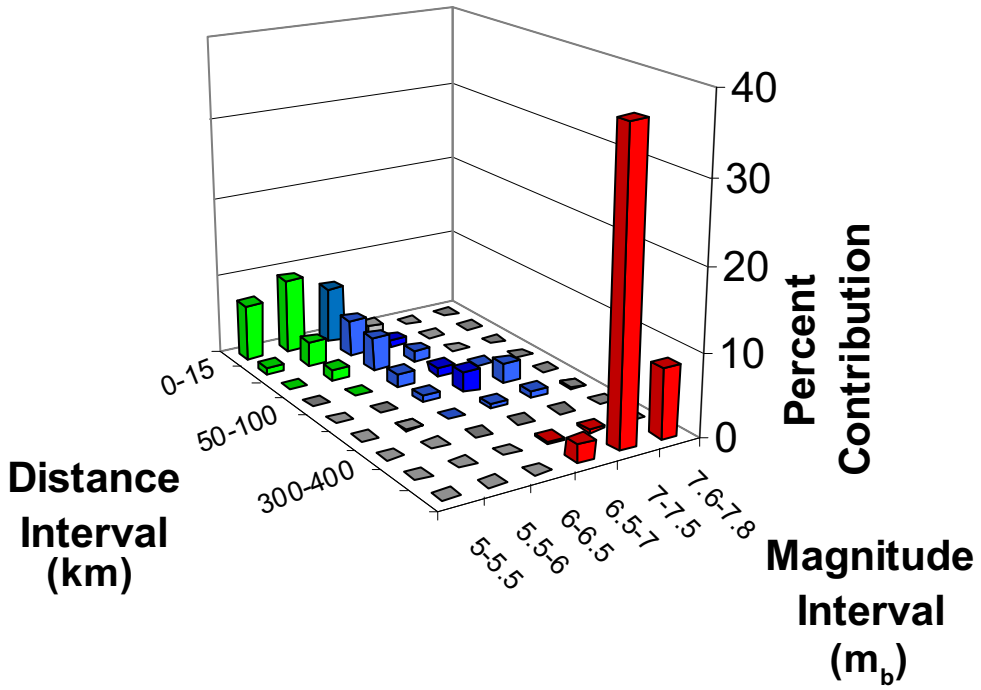

**Figure 2.5.2-245 Deaggregation of Mean $10^{-6}$ Hazard**

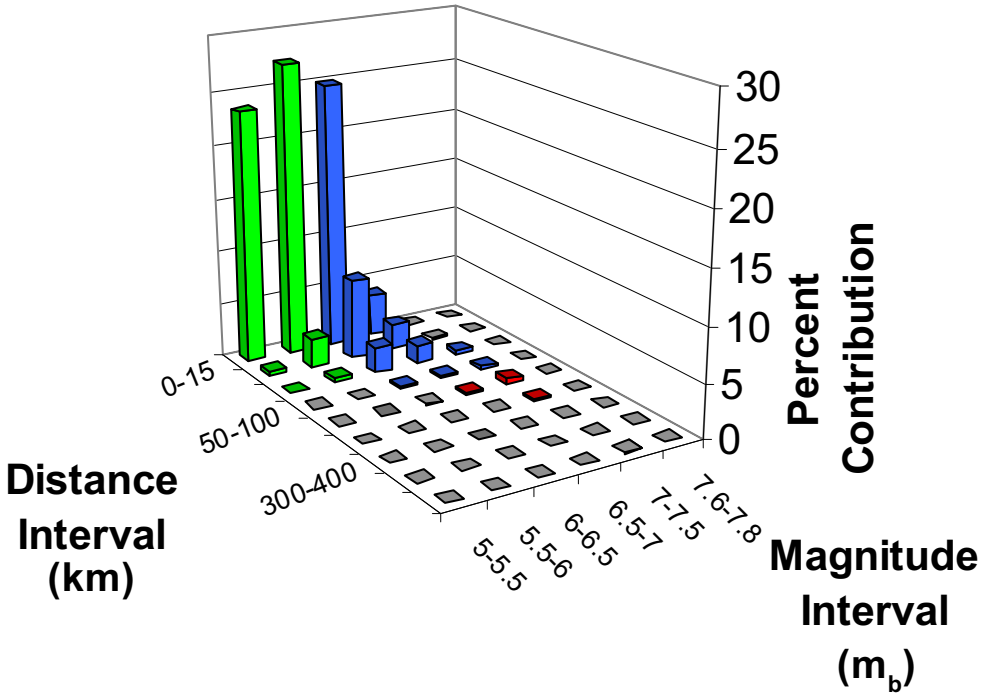


**1 and 2.5 Hz**

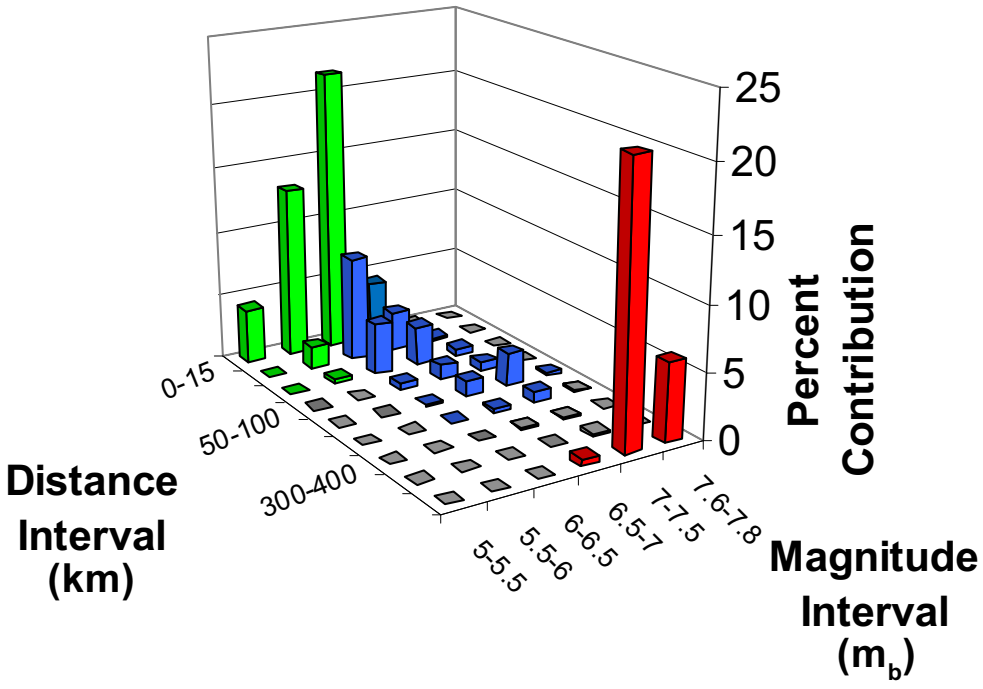

**Figure 2.5.2-246 Mean $10^{-3}$ UHRS, RE, and DE Spectra**

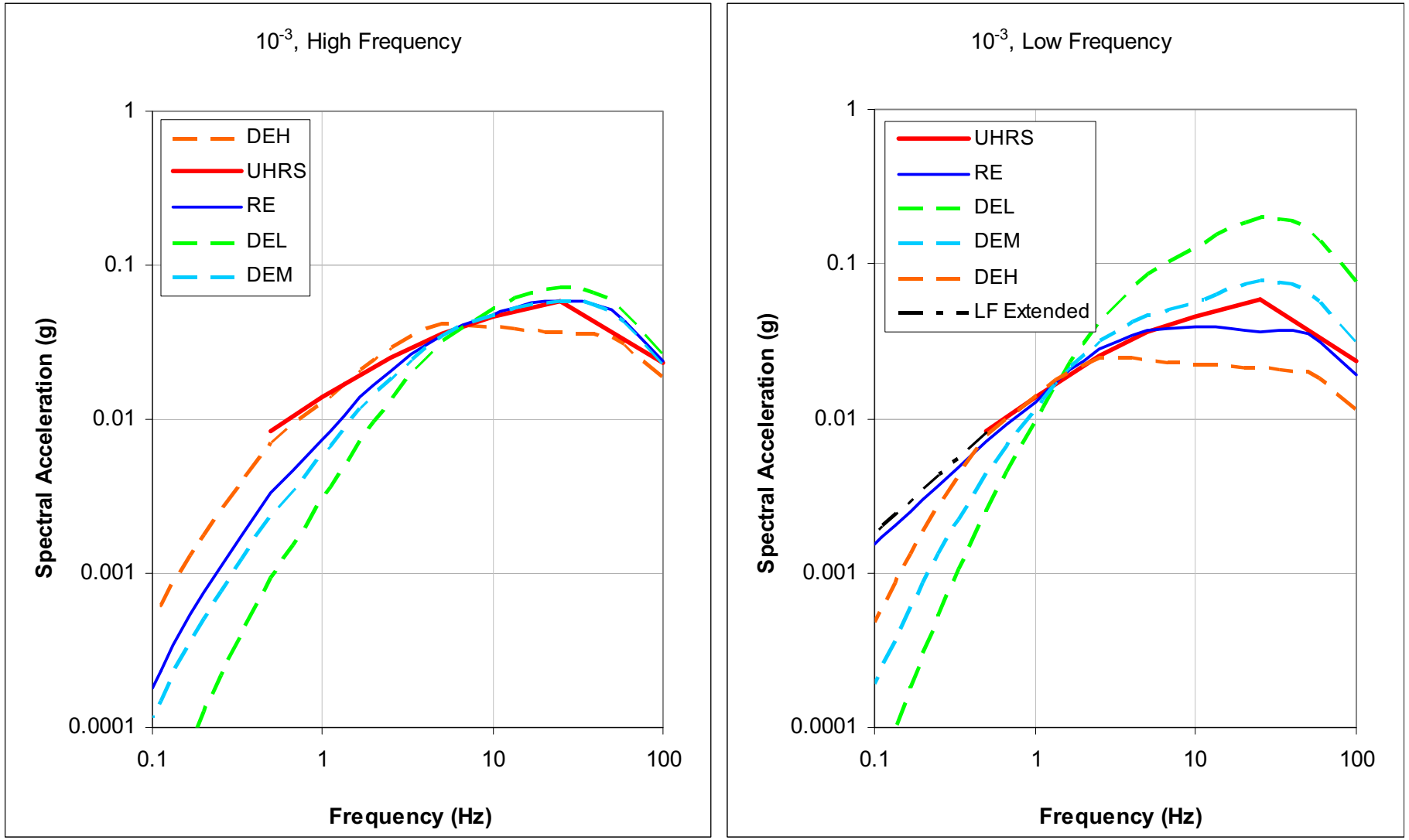

**Figure 2.5.2-247 Mean $10^{-4}$ UHRS, RE, and DE Spectra**

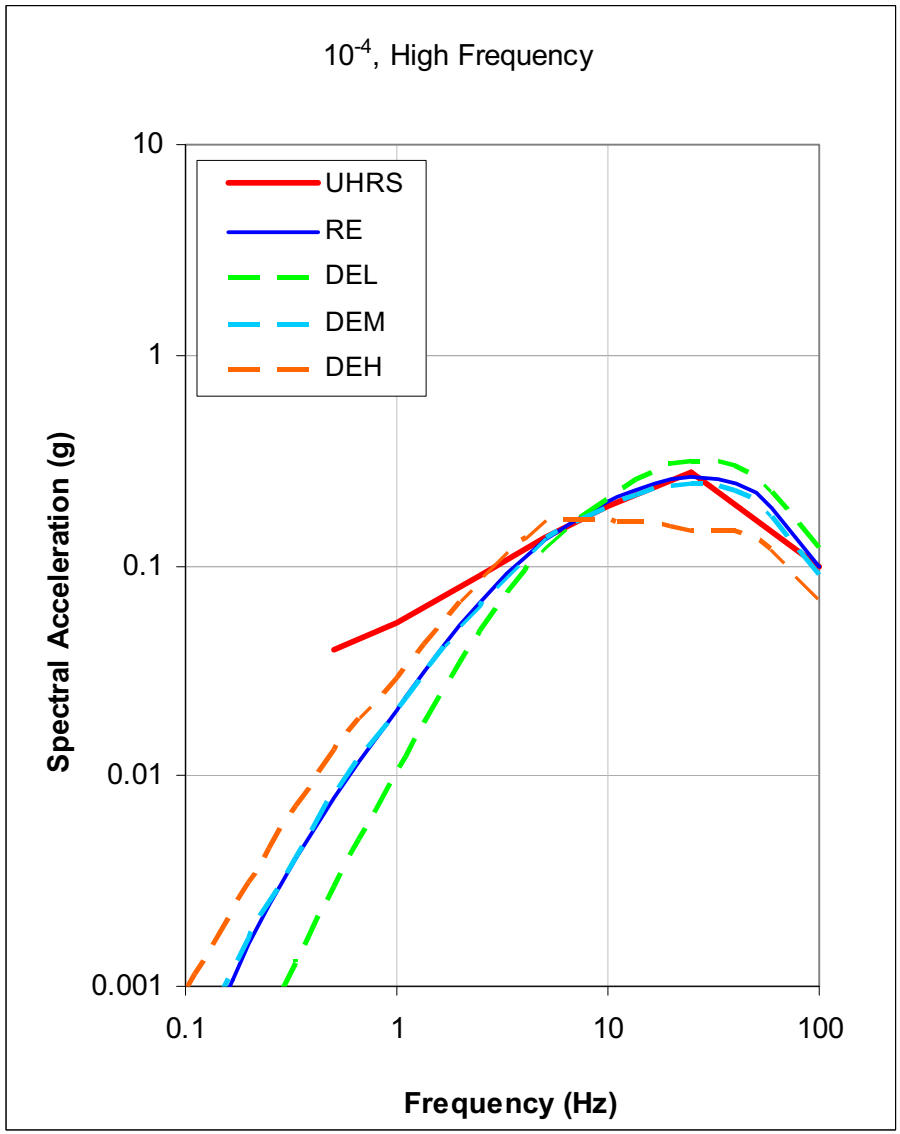


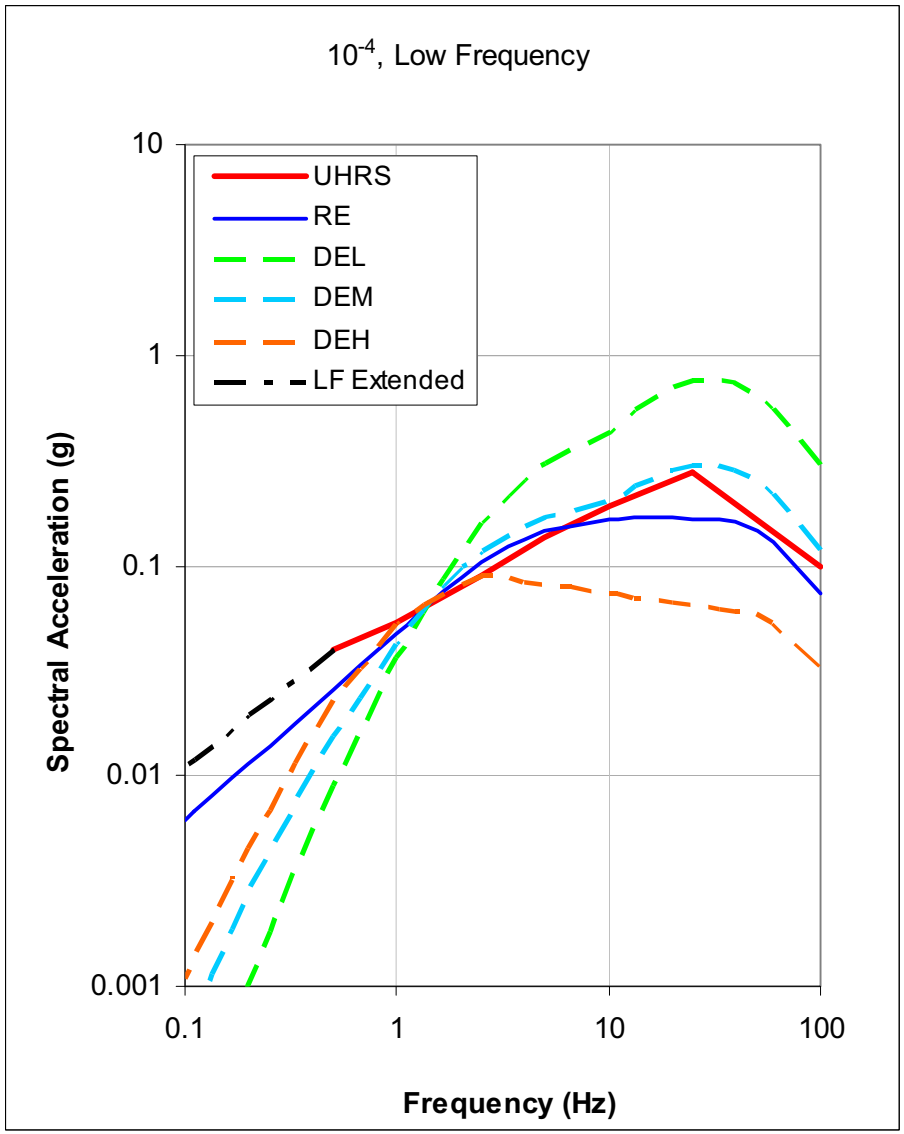

**Figure 2.5.2-248 Mean $10^{-5}$ UHRS, RE, and DE Spectra**

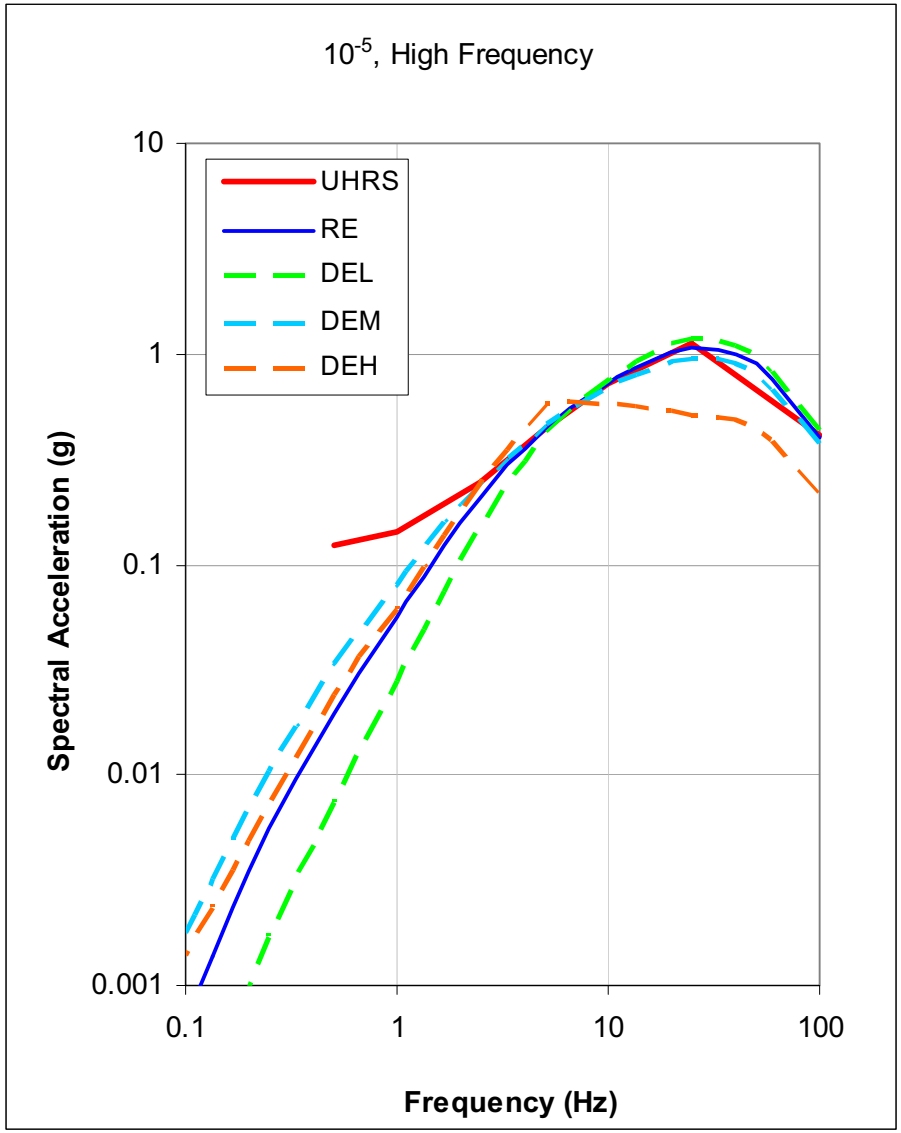


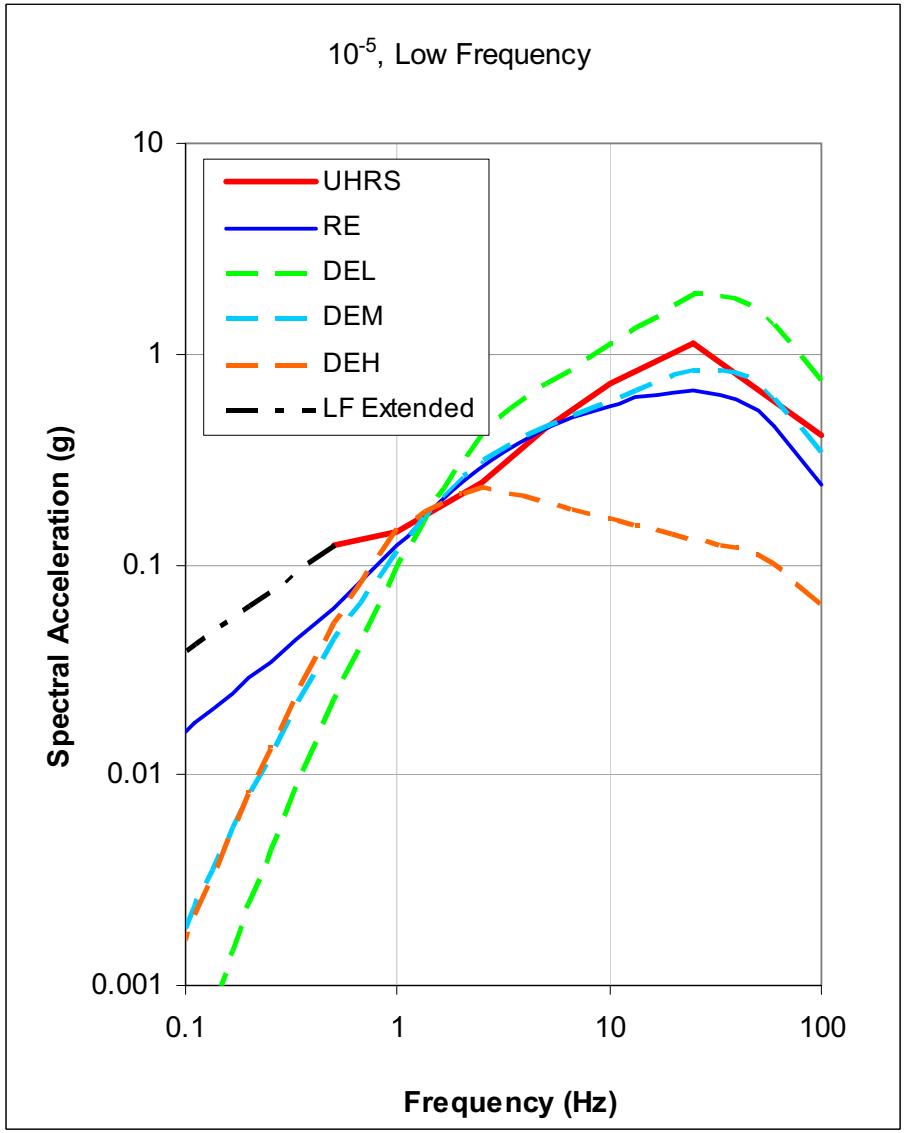

**Figure 2.5.2-249 Mean $10^{-6}$ UHRS, RE, and DE Spectra**

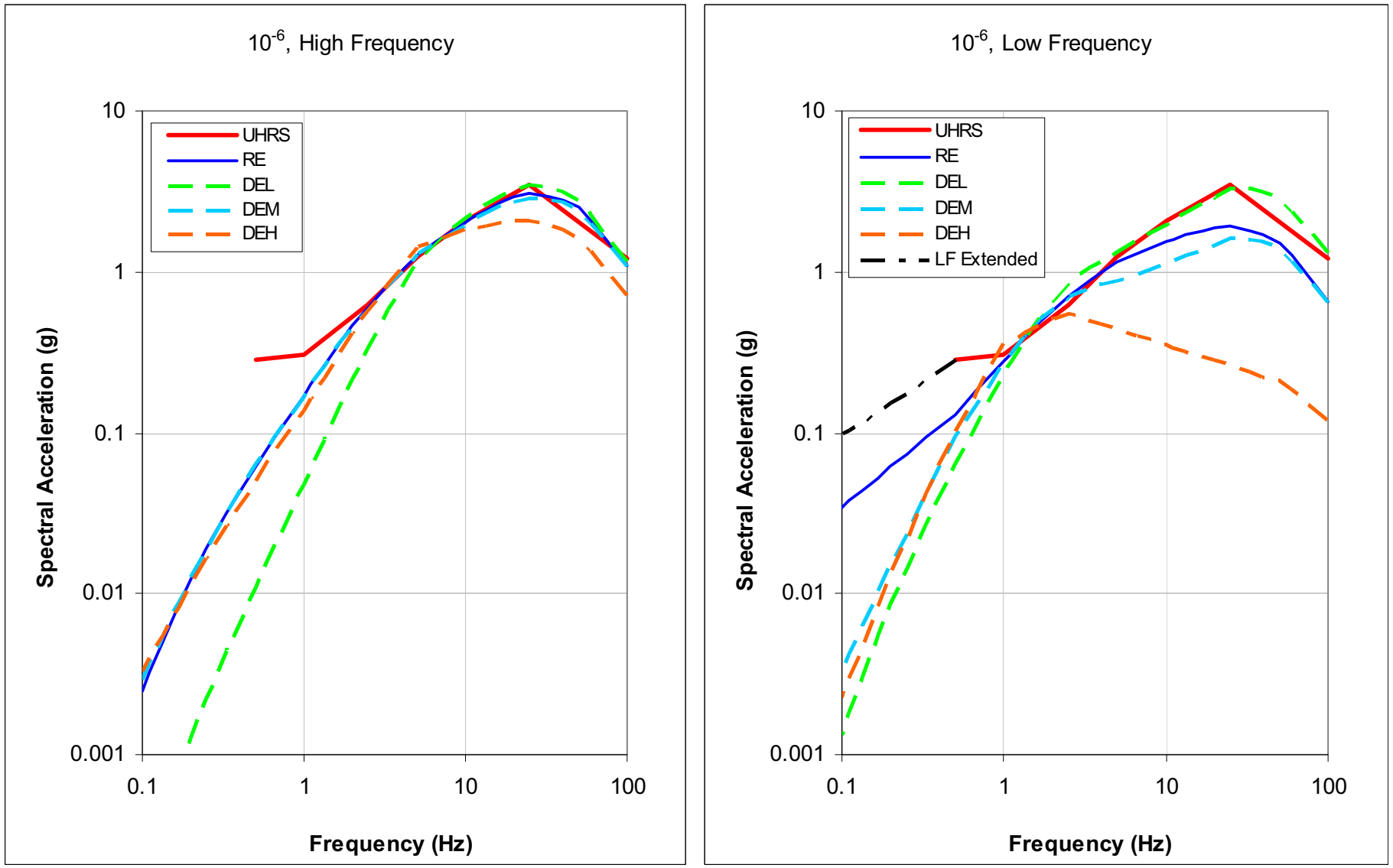

**Figure 2.5.2-250 Extension of Response Spectra to 0.1 Hz**

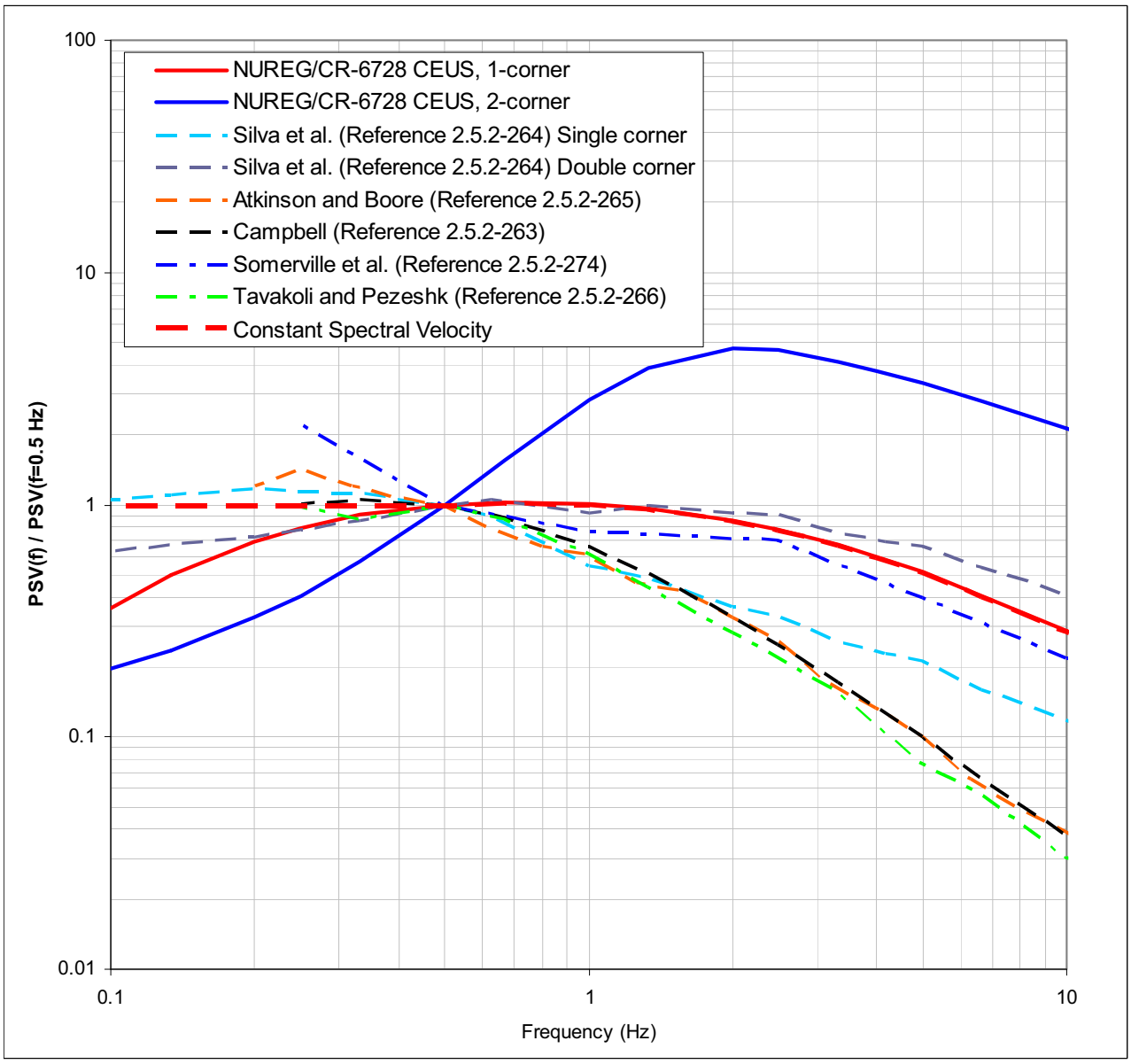

**Figure 2.5.2-251 Shear Wave Velocity Data for Boring TB-C5**

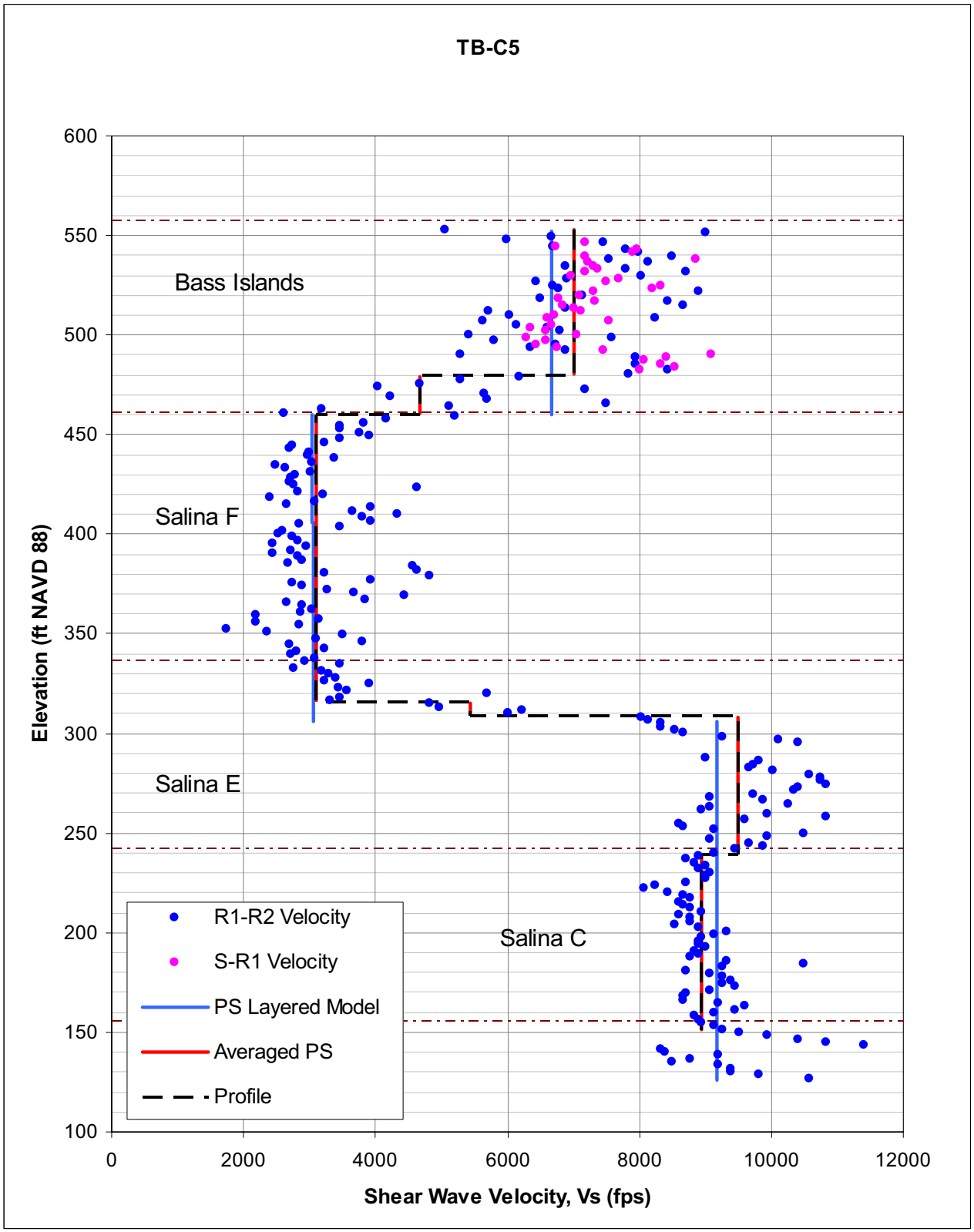

**Figure 2.5.2-252 Shear Wave Velocity Data for Boring RB-C8**

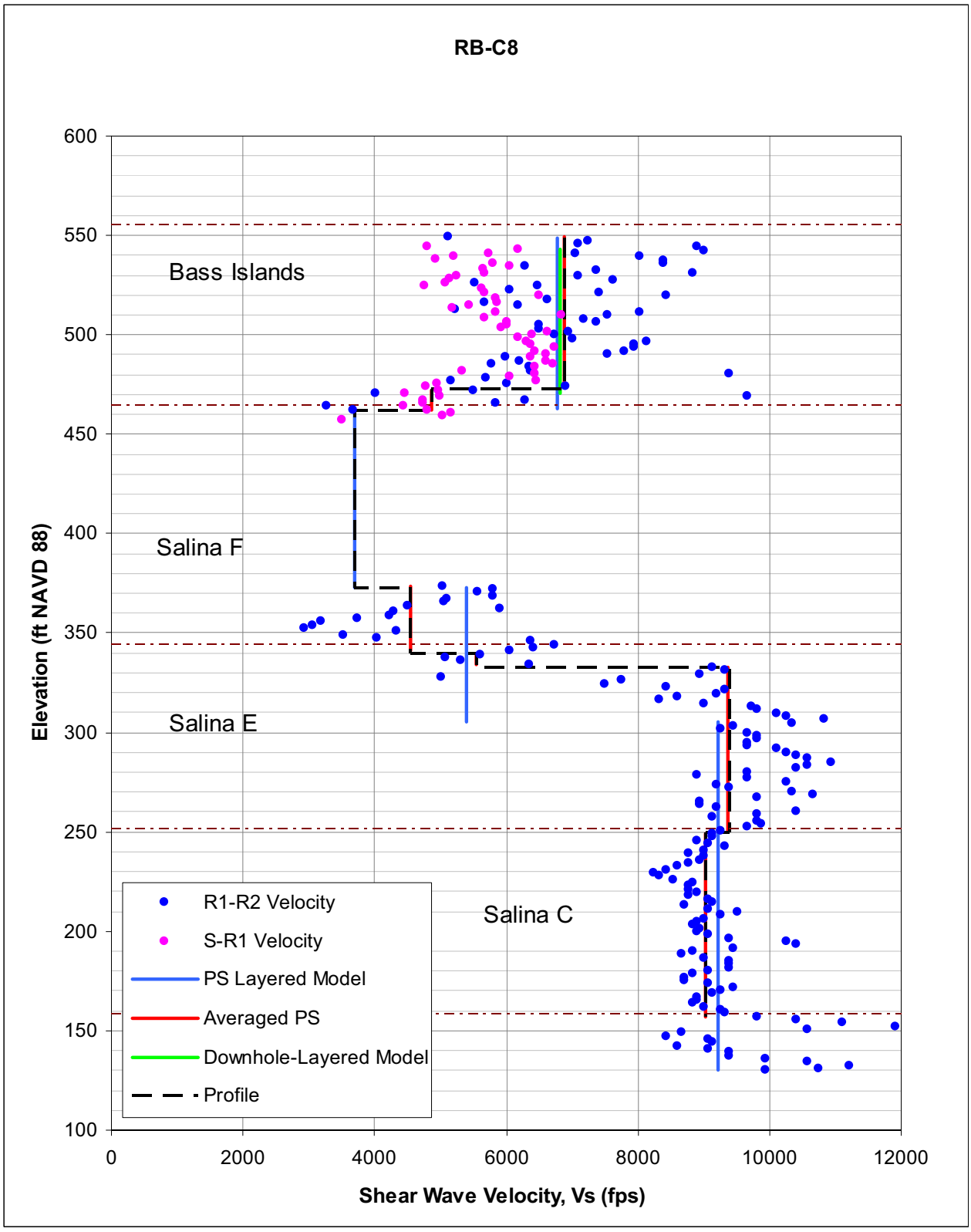

**Figure 2.5.2-253 Shear Wave Velocity Data for Boring CB-C3**

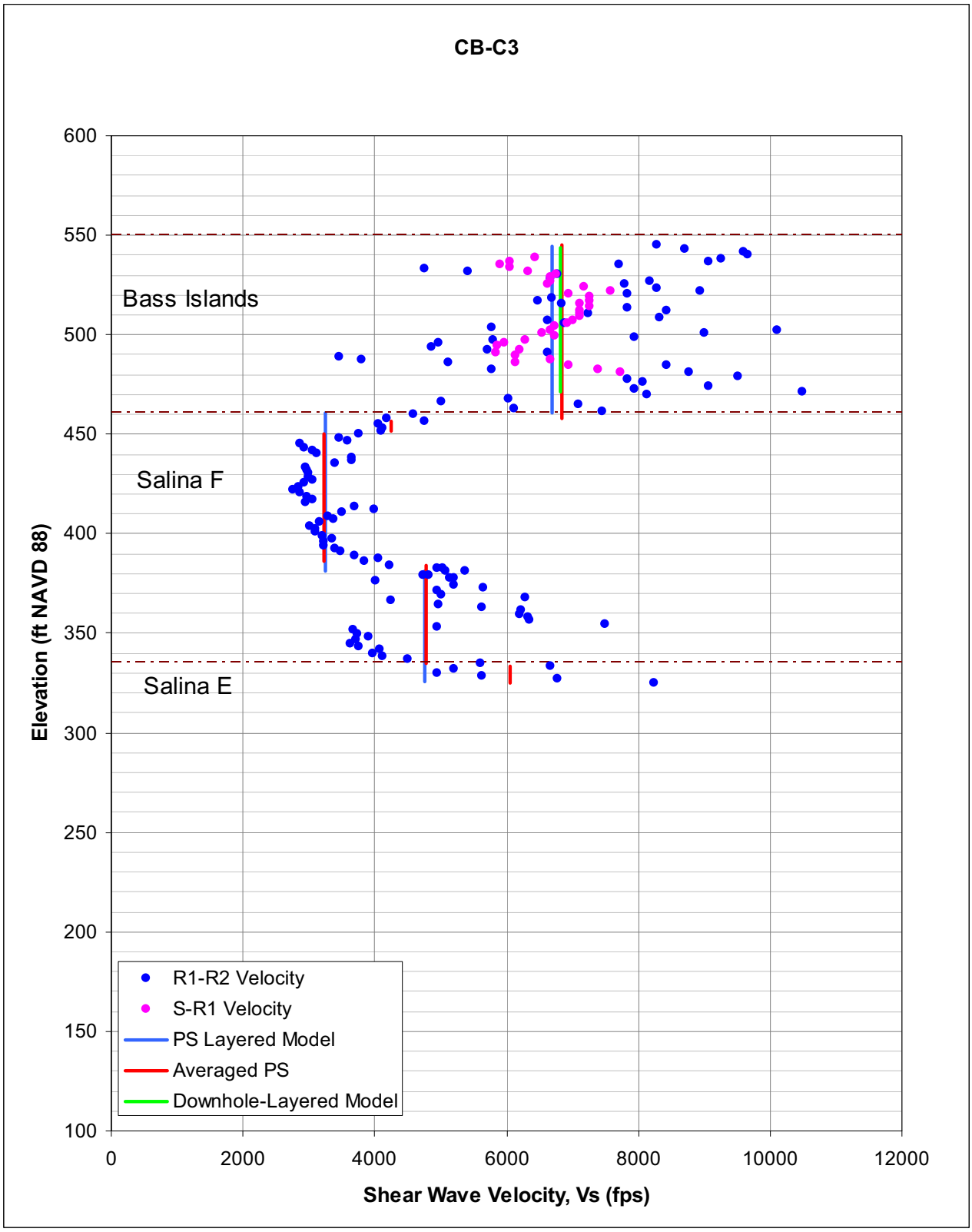

**Figure 2.5.2-254 Shear Wave Velocity Data for Boring RB-C4**

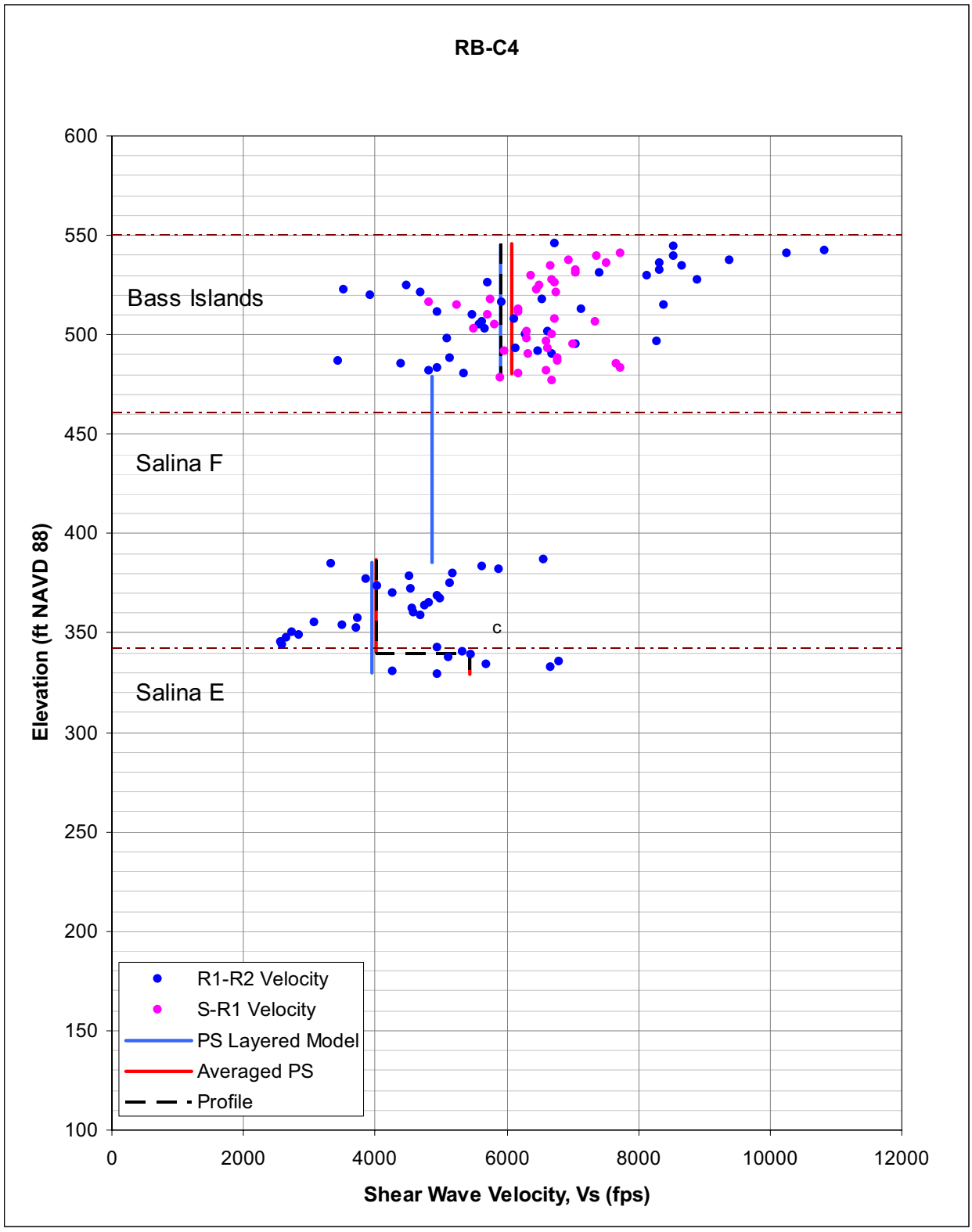

**Figure 2.5.2-255 Geometric Mean Velocity Profile for Fermi 3 Site**

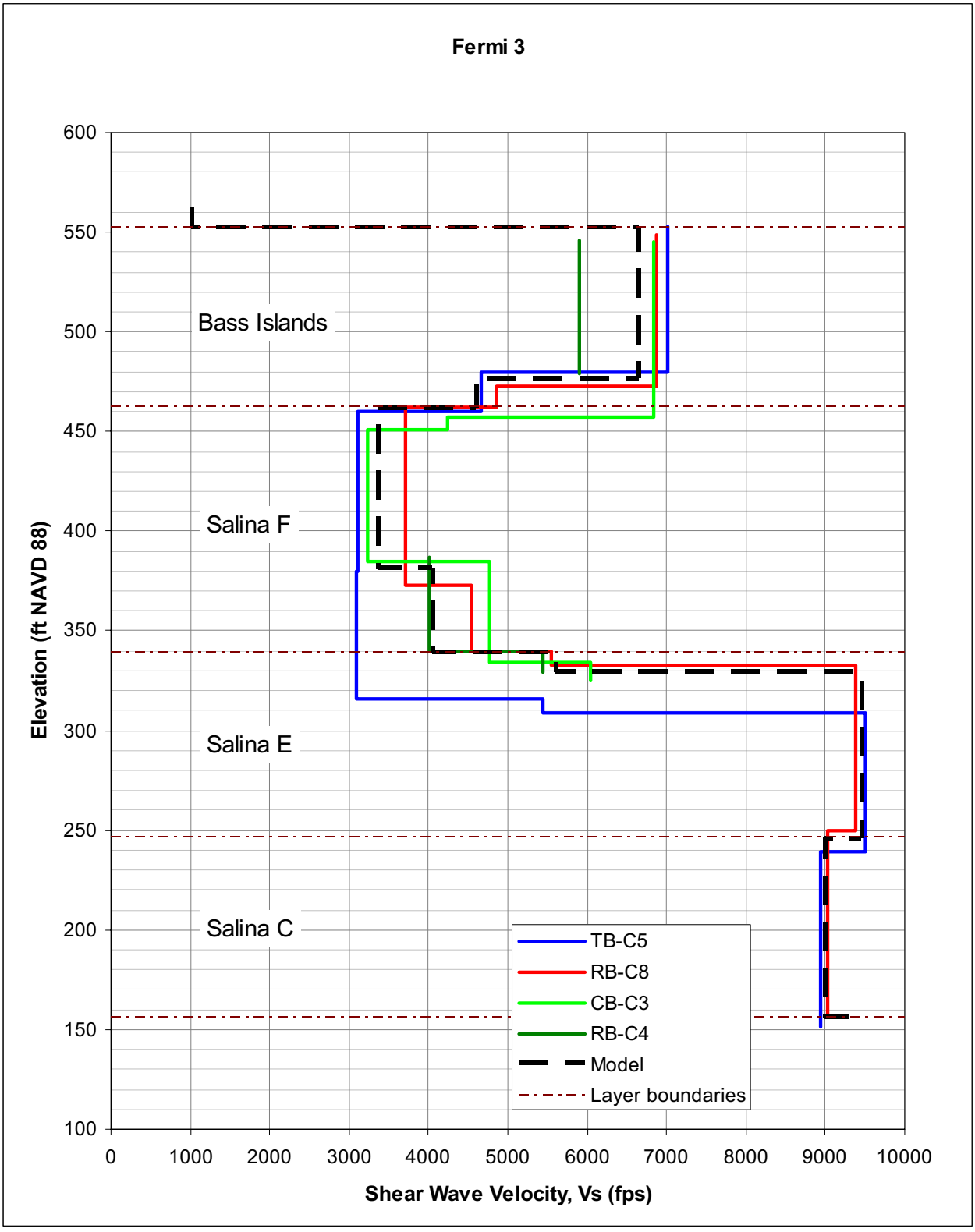

**Figure 2.5.2-256 Modulus Reduction and Damping Relationships Used for the Glacial Till and Lean Concrete Backfill**

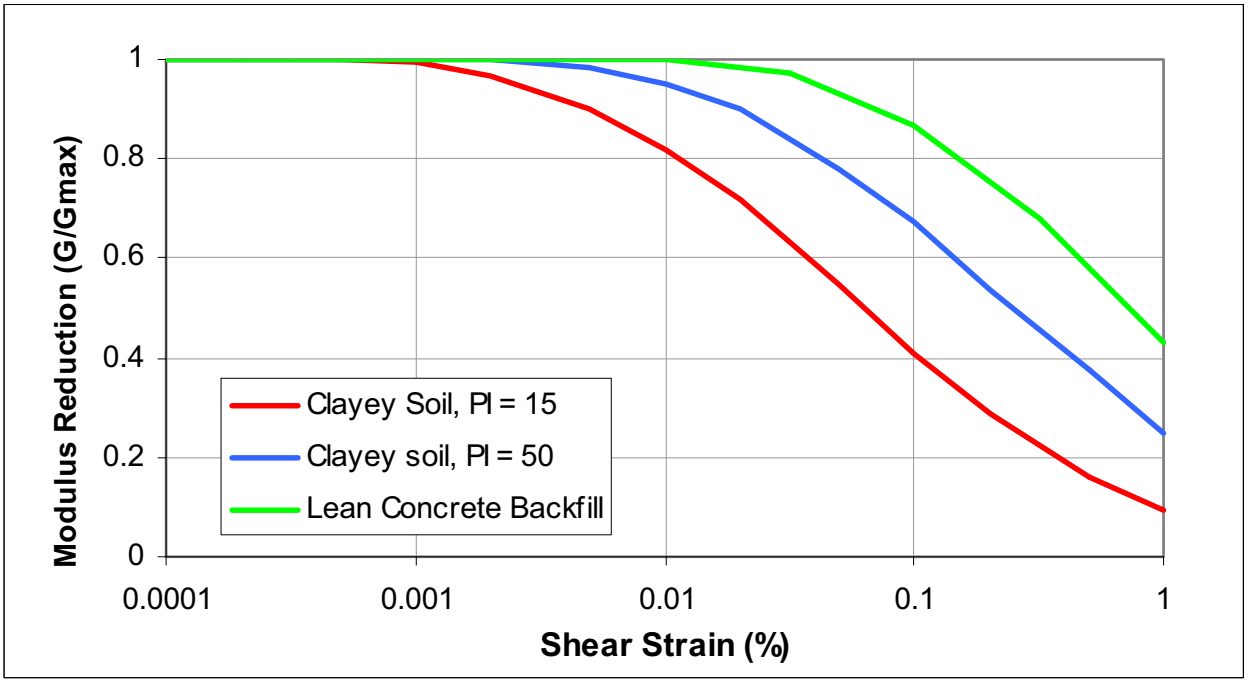


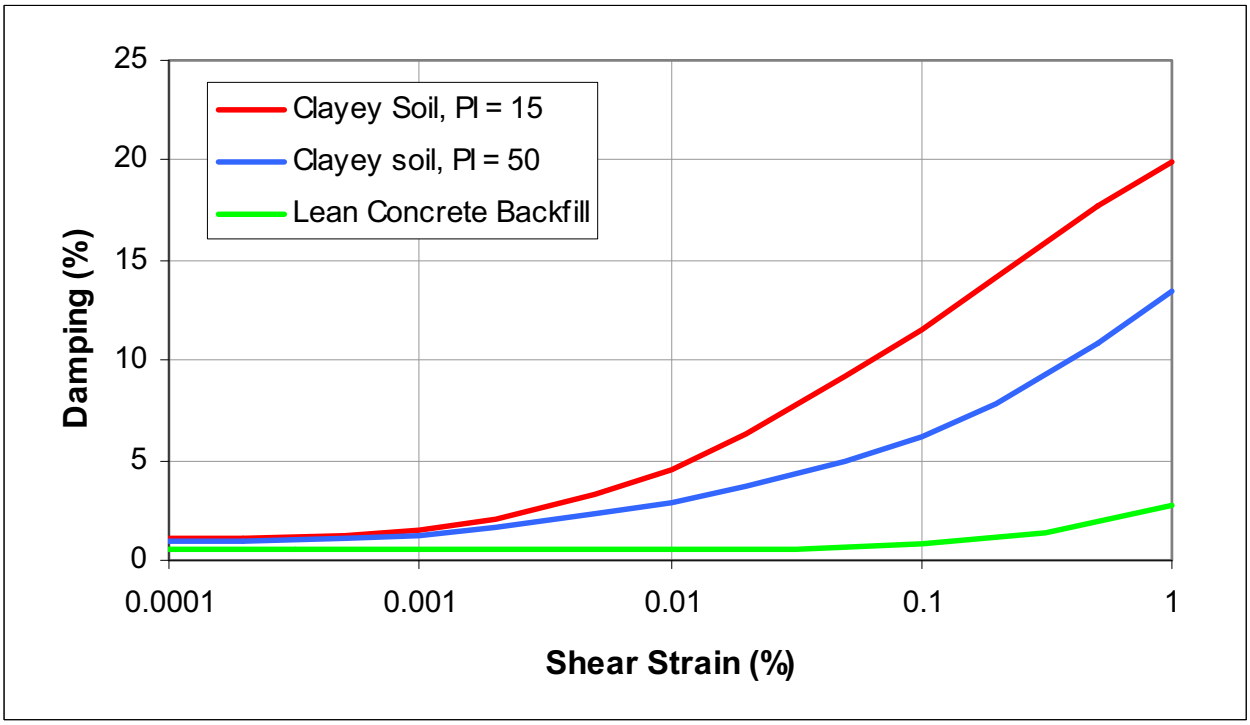

**Figure 2.5.2-257 Estimation of Scattering *κ***

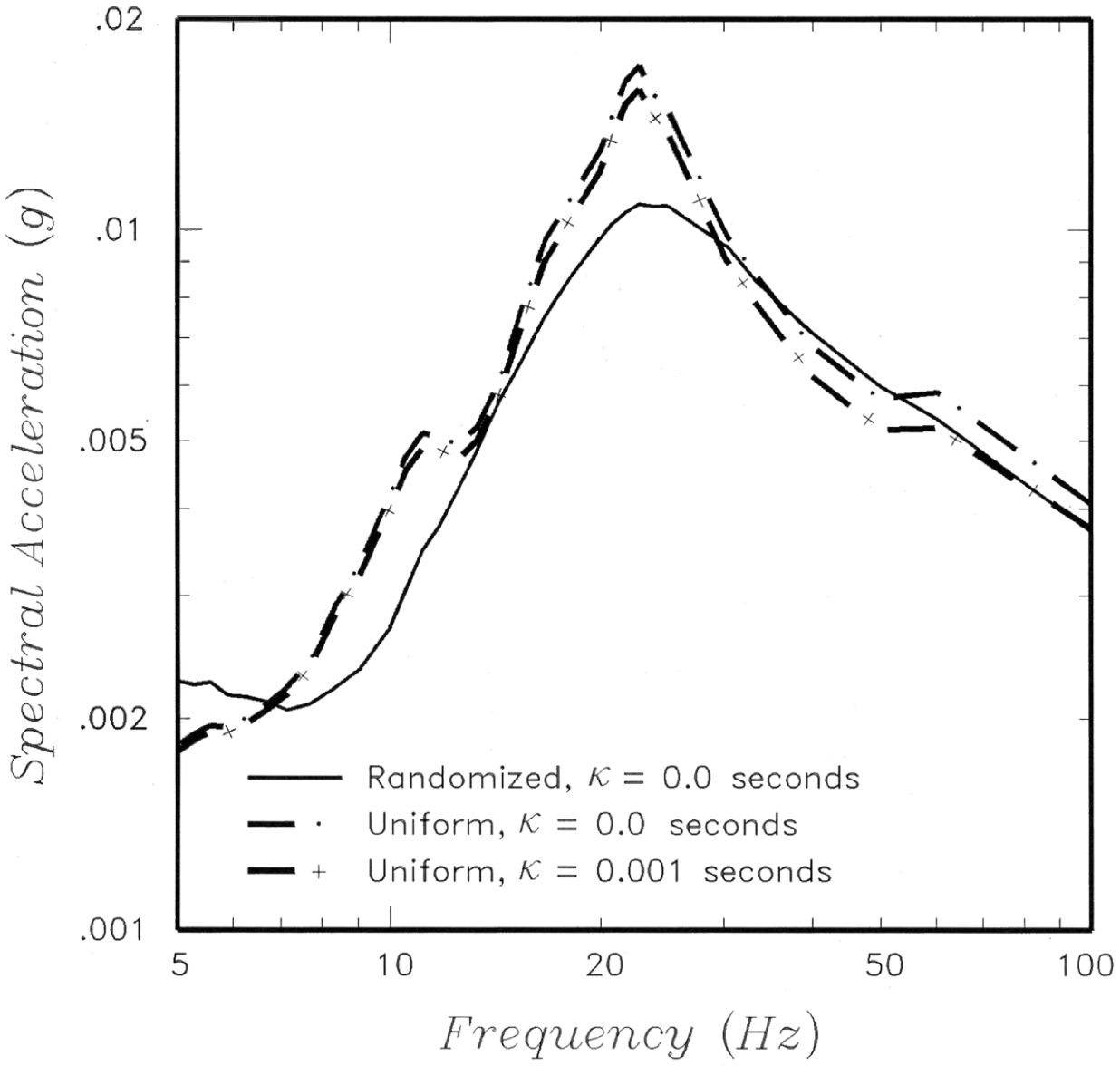

**Figure 2.5.2-258 Randomized Shear Wave Velocity Profiles 1–30**

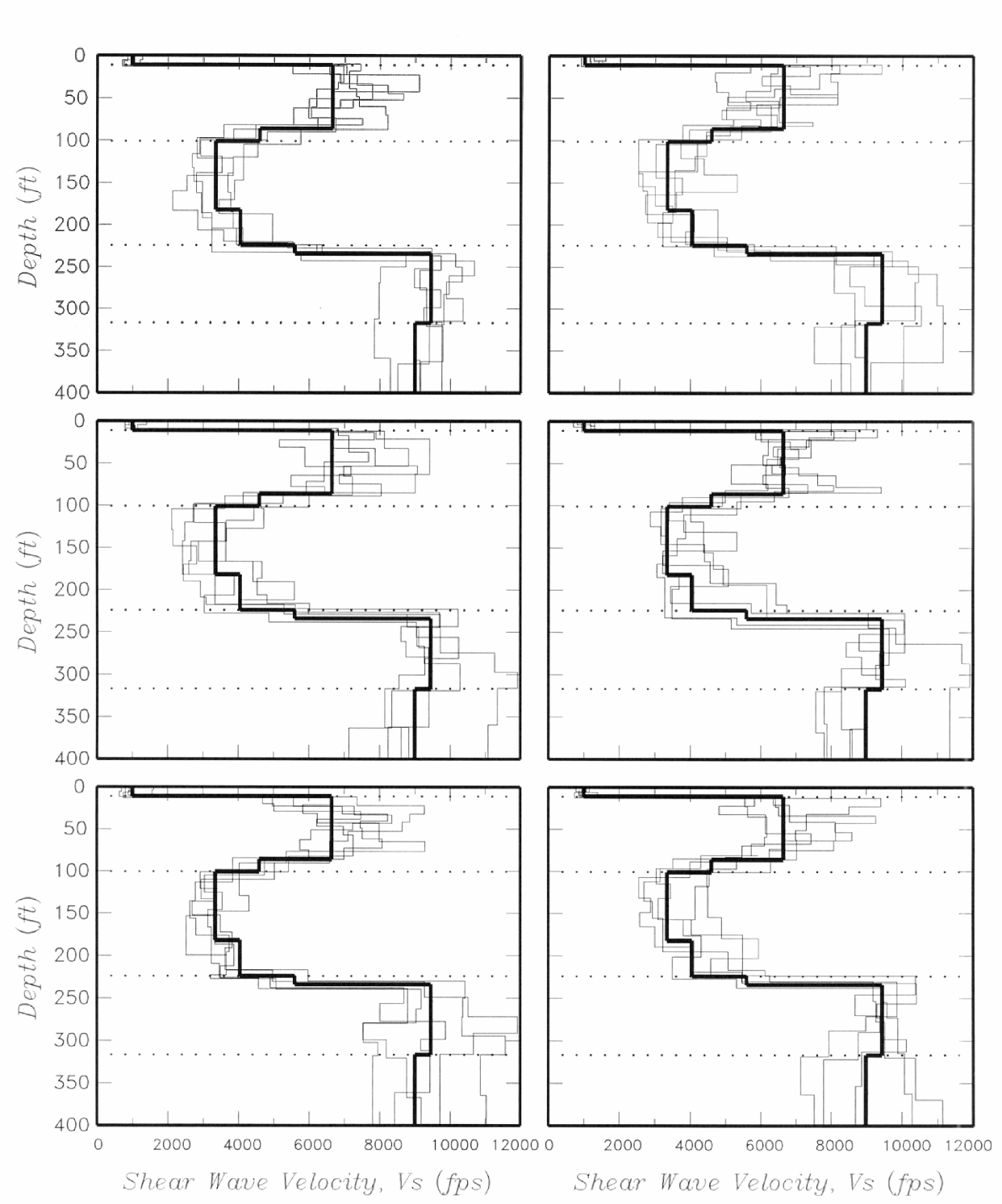

**Figure 2.5.2-259 Randomized Shear Wave Velocity Profiles 31–60**

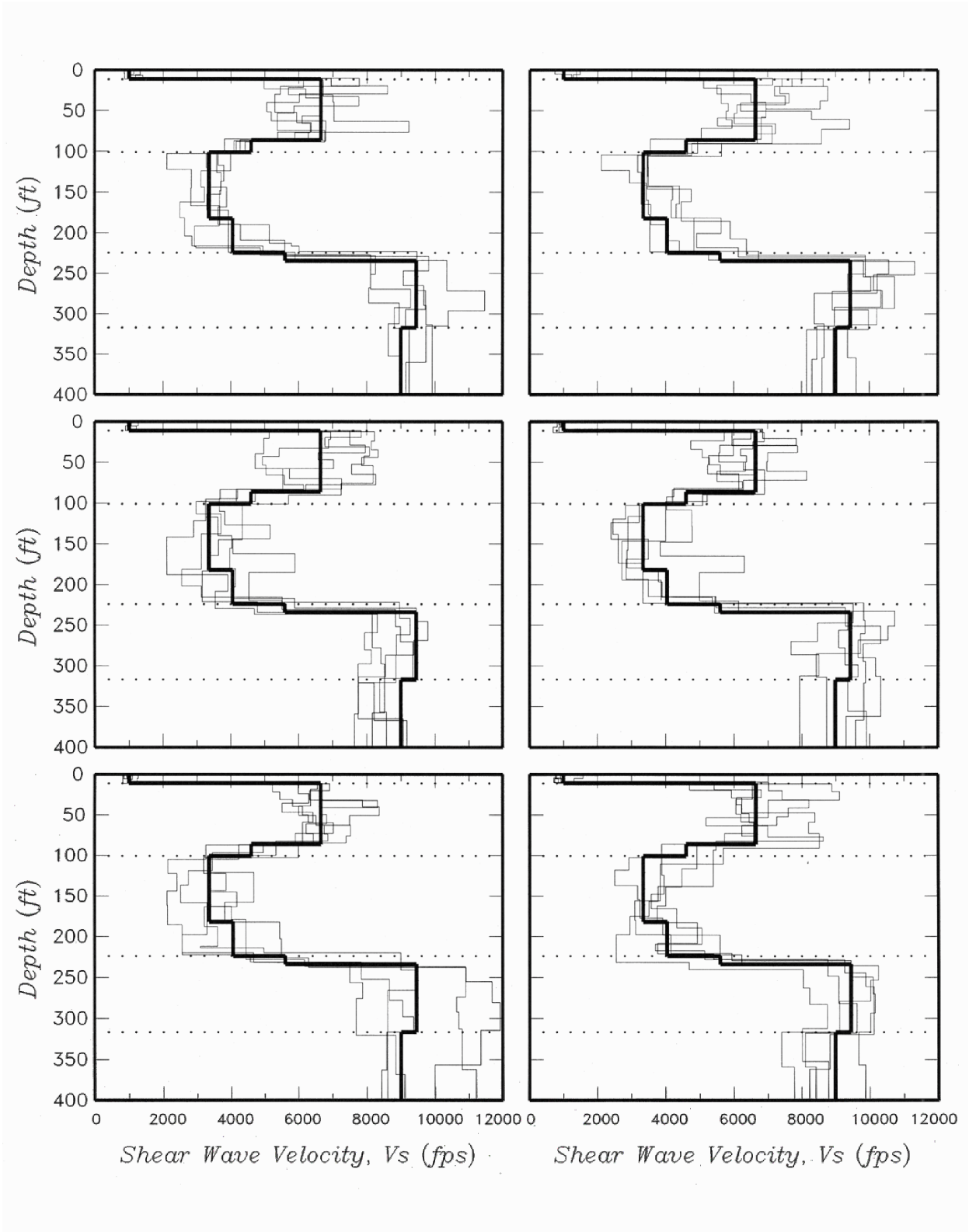

**Figure 2.5.2-260 Statistics of Randomized Shear Wave Velocity Profiles**

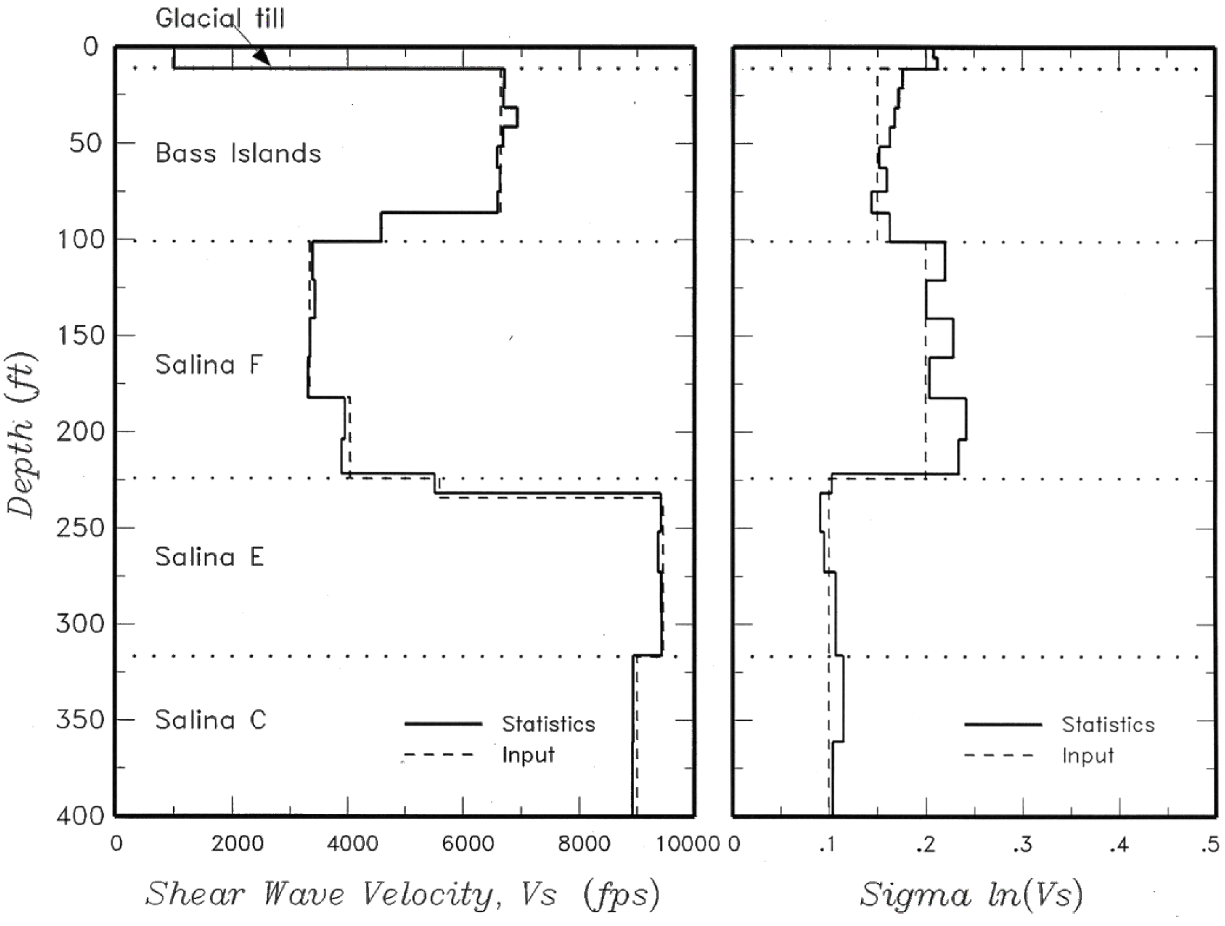

**Figure 2.5.2-261 Randomized Shear Modulus (G) Reduction and Damping Relationships for Clayey Soils with a PI of 15 Used for Glacial Till**

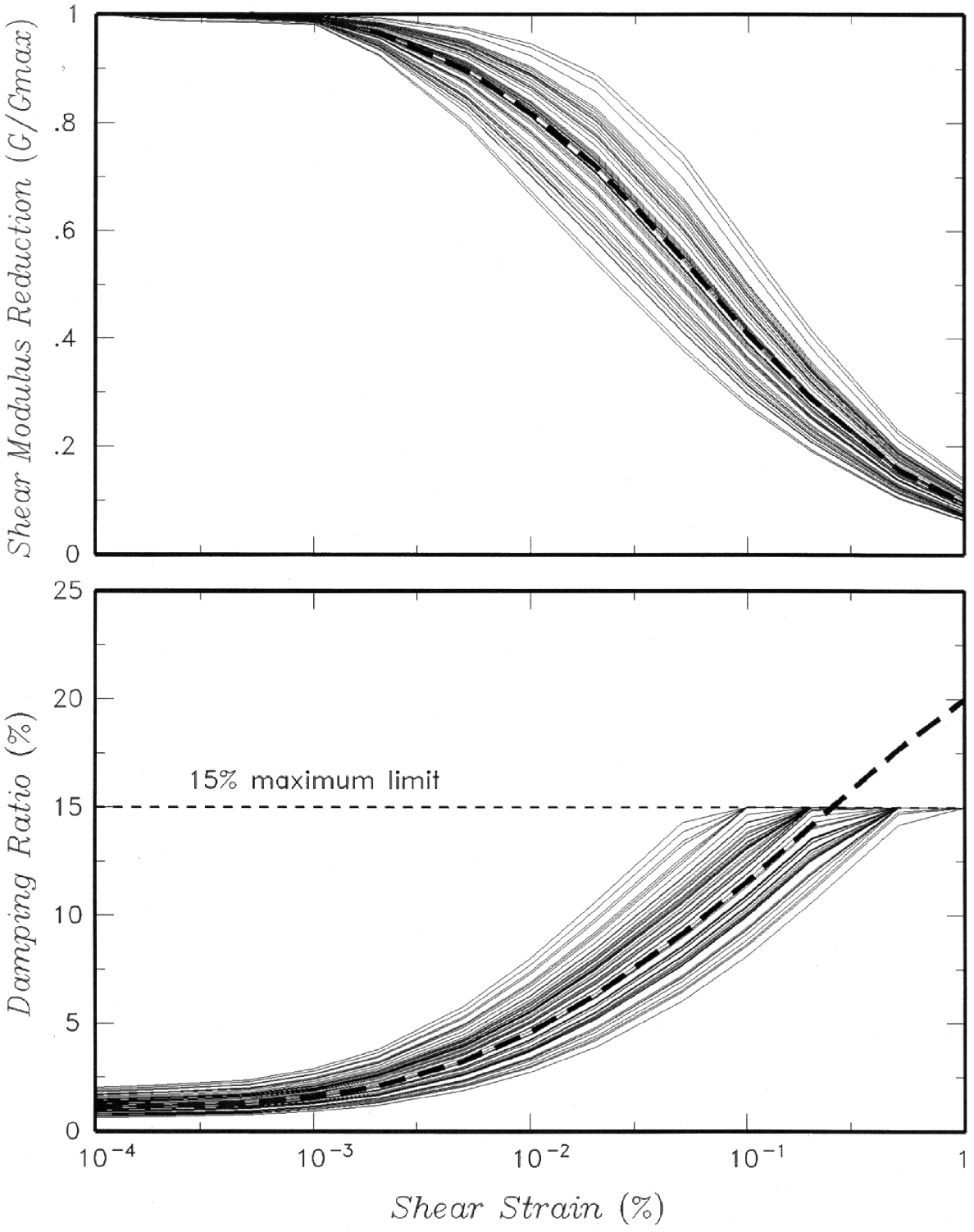

**Figure 2.5.2-262 Randomized Shear Modulus (G) Reduction and Damping Relationships for Clayey Soils with a PI of 50 Used for Glacial Till**

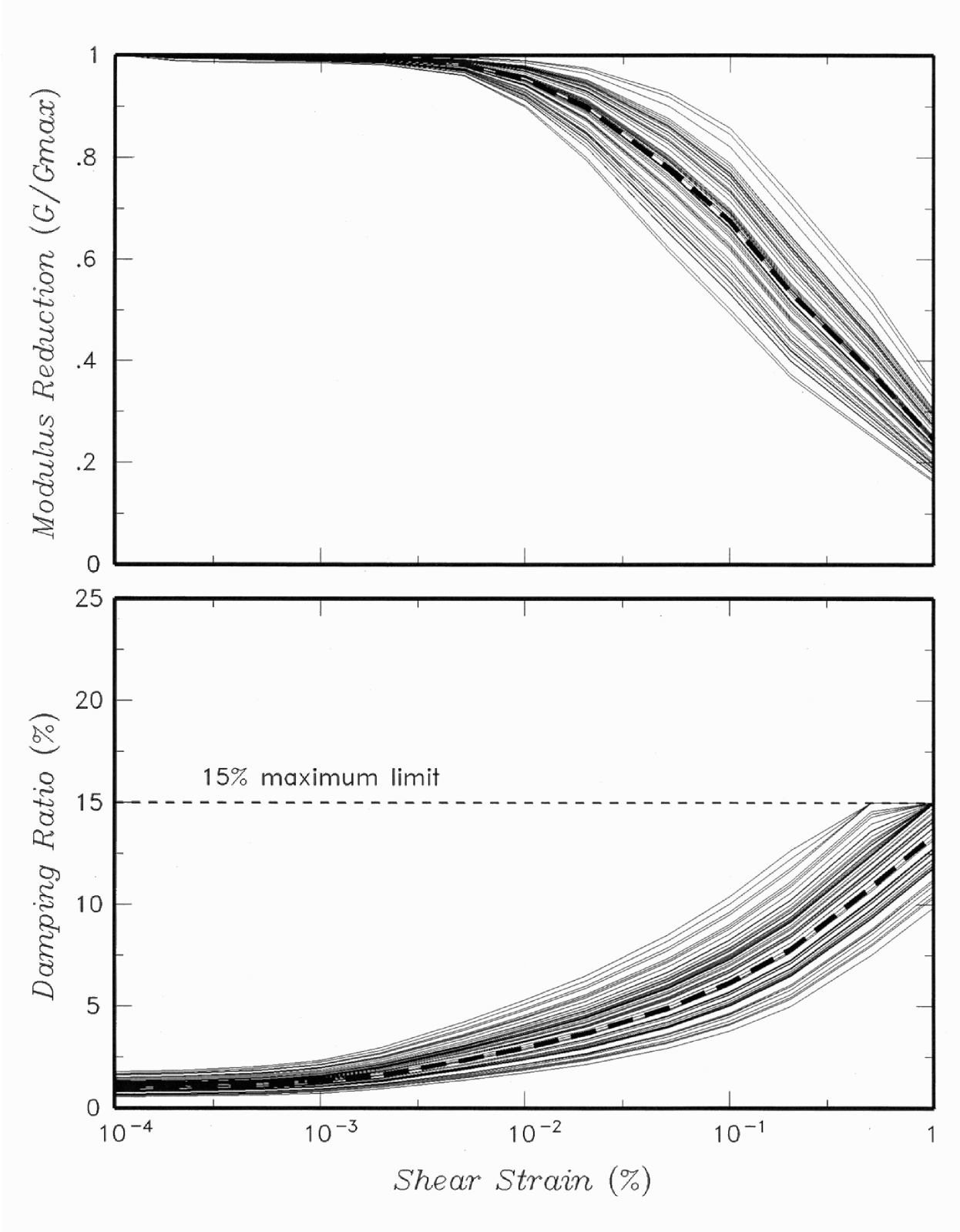

**Figure 2.5.2-263 Randomized Shear Modulus (G) Reduction and Damping Relationships Used for Lean Concrete Backfill**

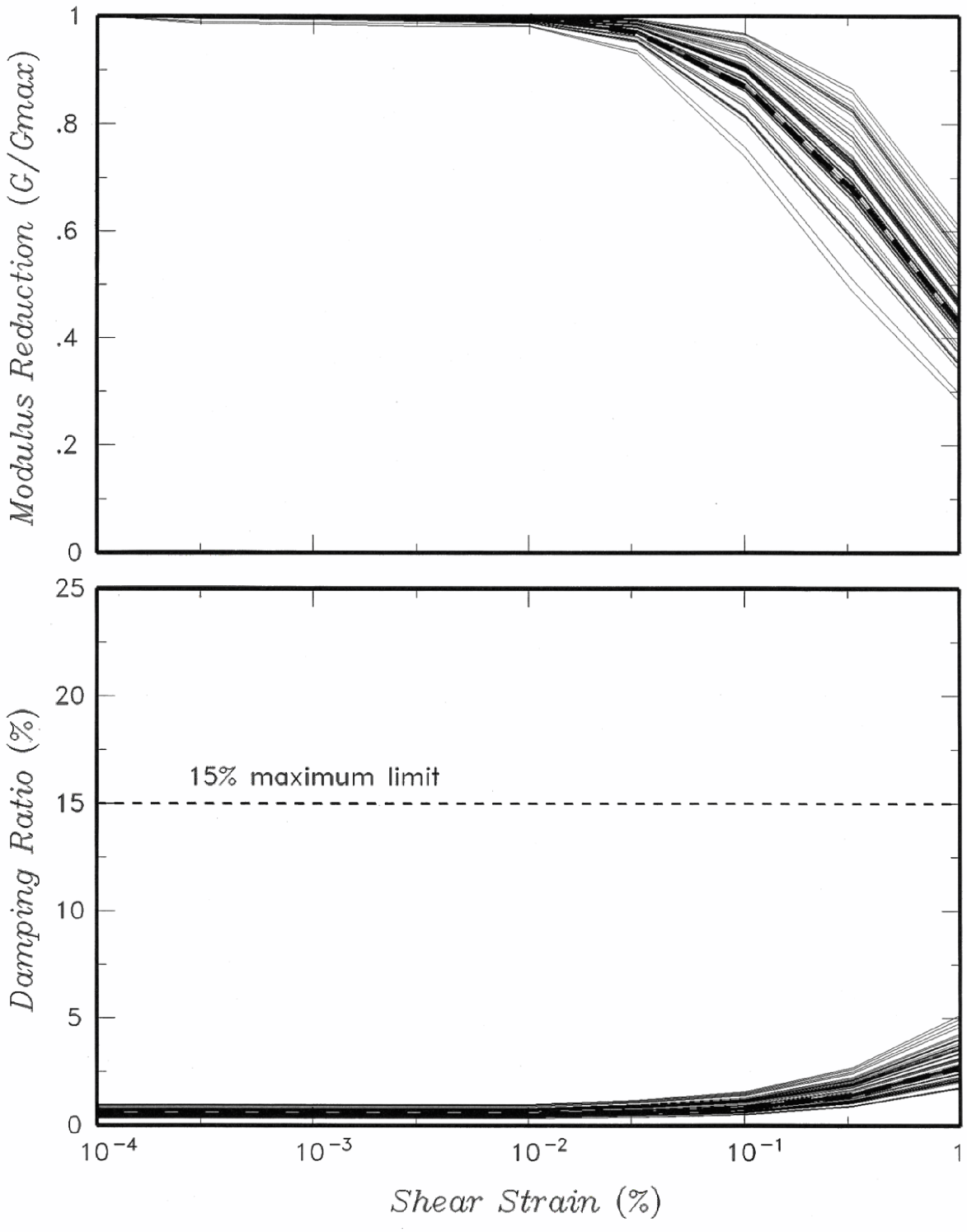

**Figure 2.5.2-264 Example Response Spectra of Time Histories Used for Site Response Analyses**

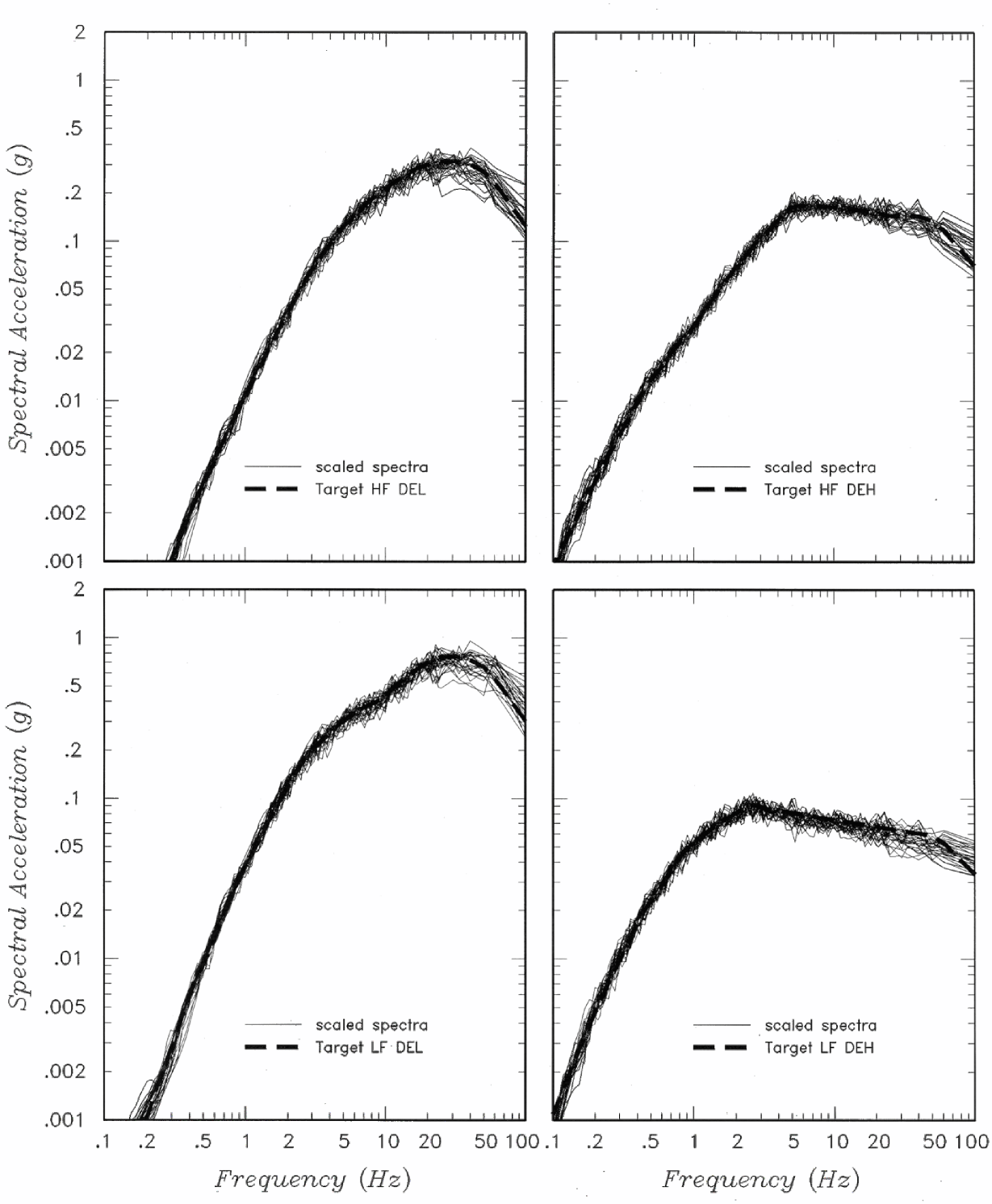

**Figure 2.5.2-265 Statistics of Site Amplification for the Fermi 3 GMRS Profile**

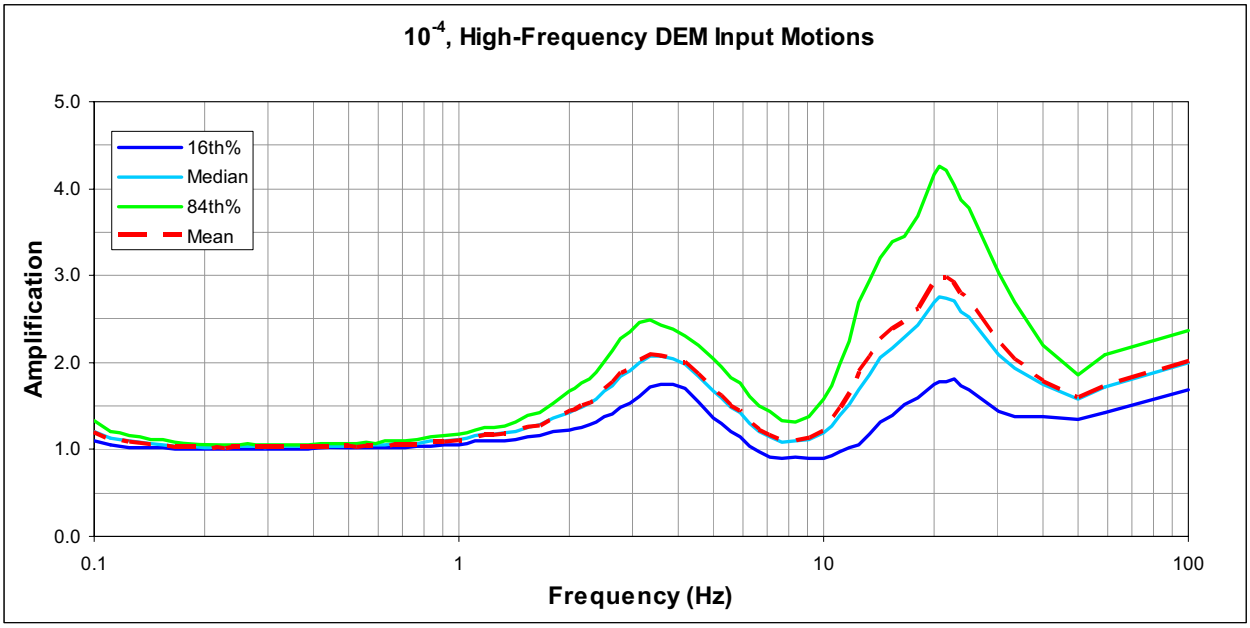


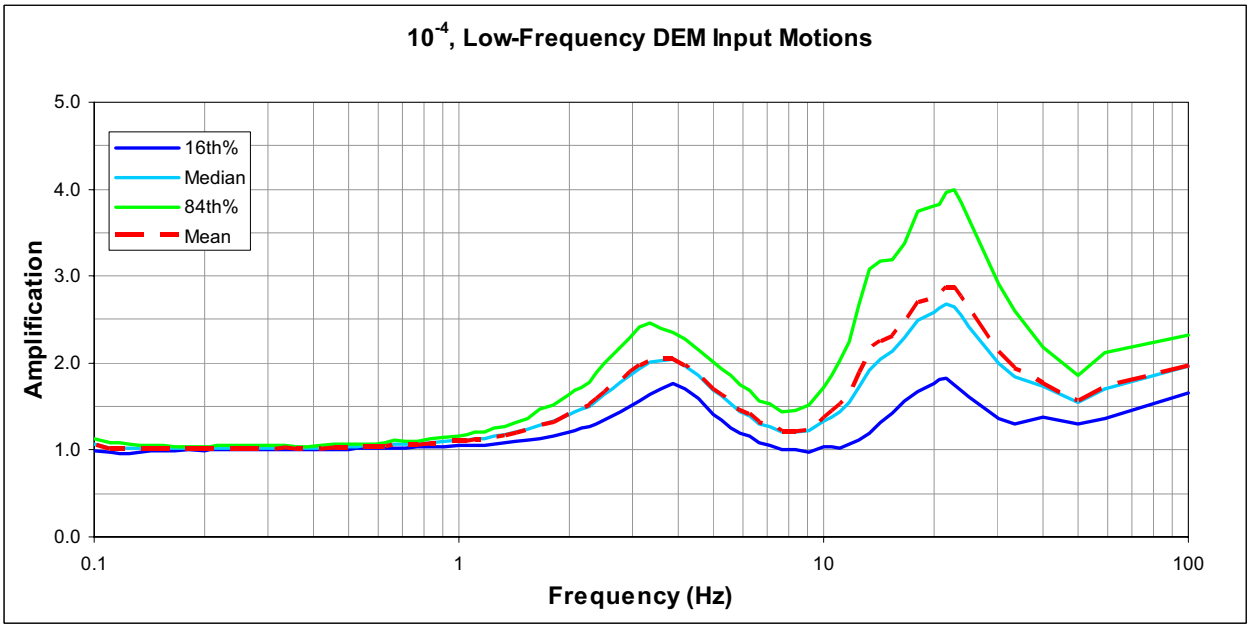

**Figure 2.5.2-266 Site Response Logic Tree**

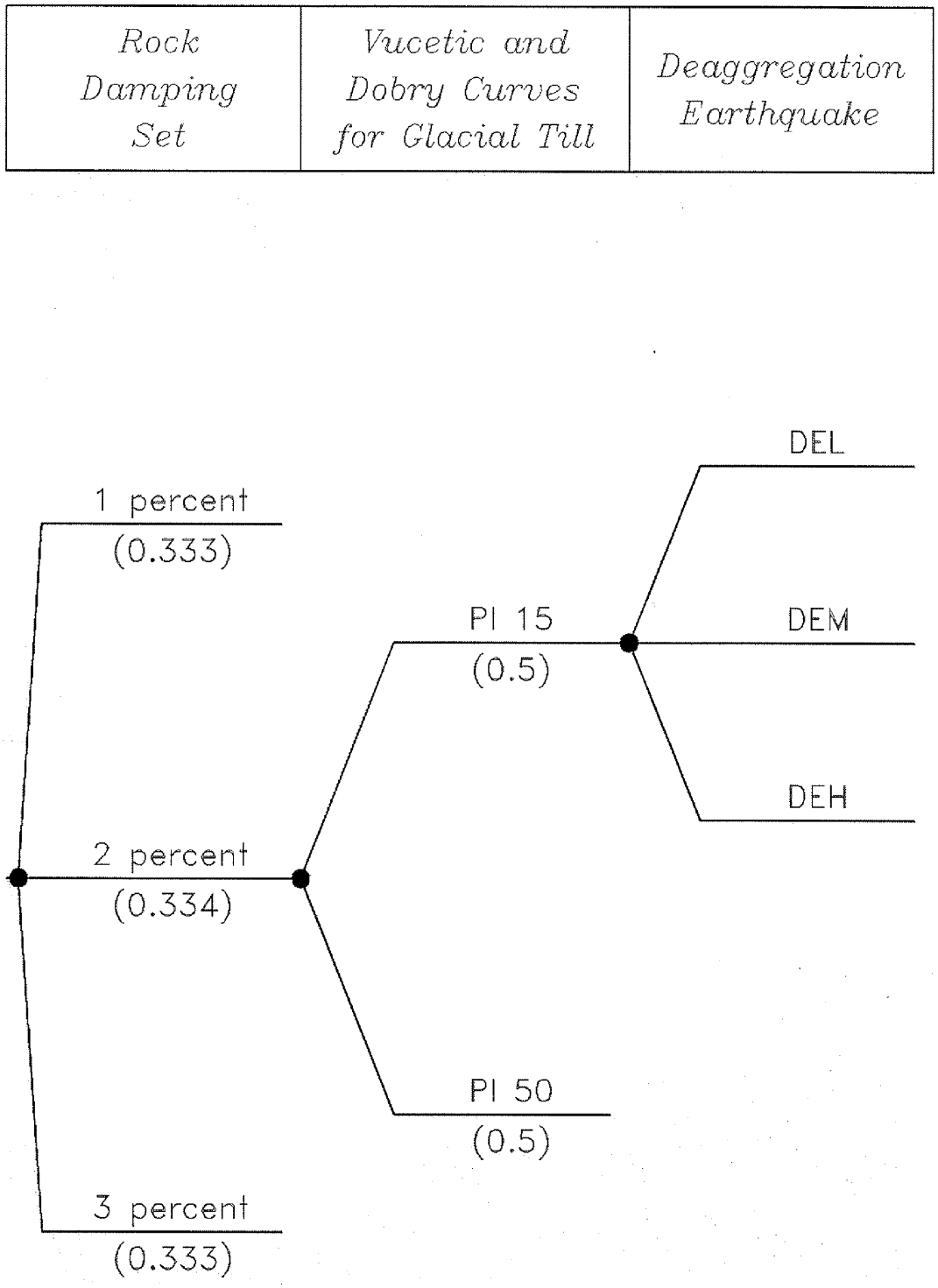

**Figure 2.5.2-267 Sensitivity of GMRS Profile Mean Site Amplification to Damping Assigned to the Rock Layers**

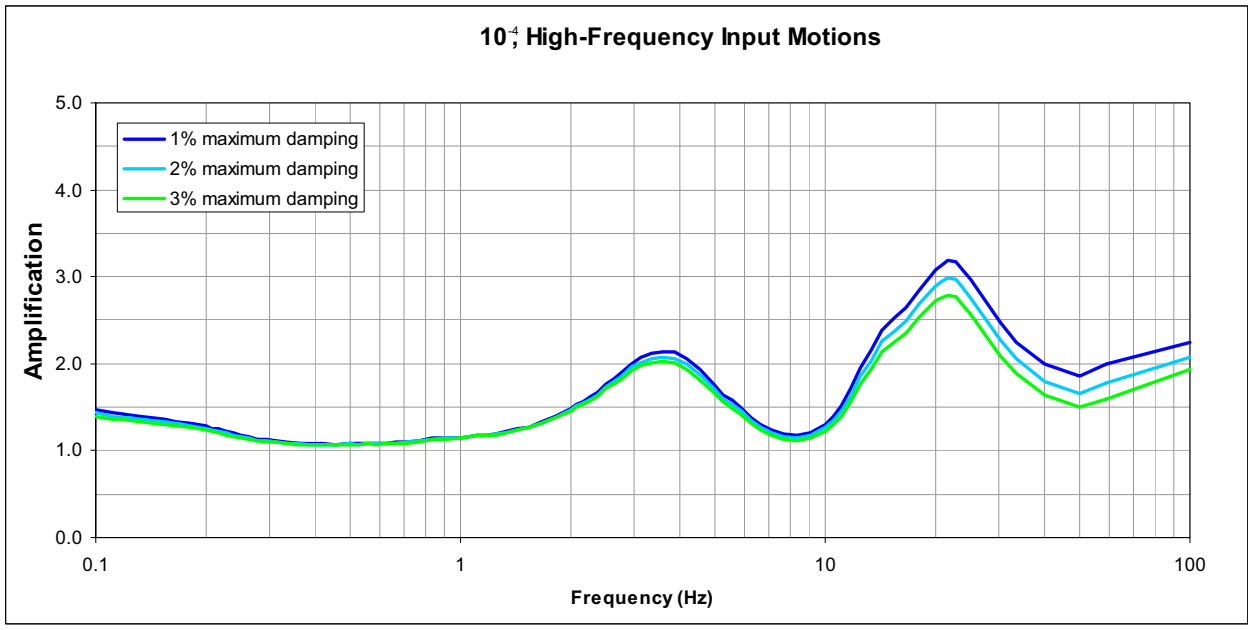


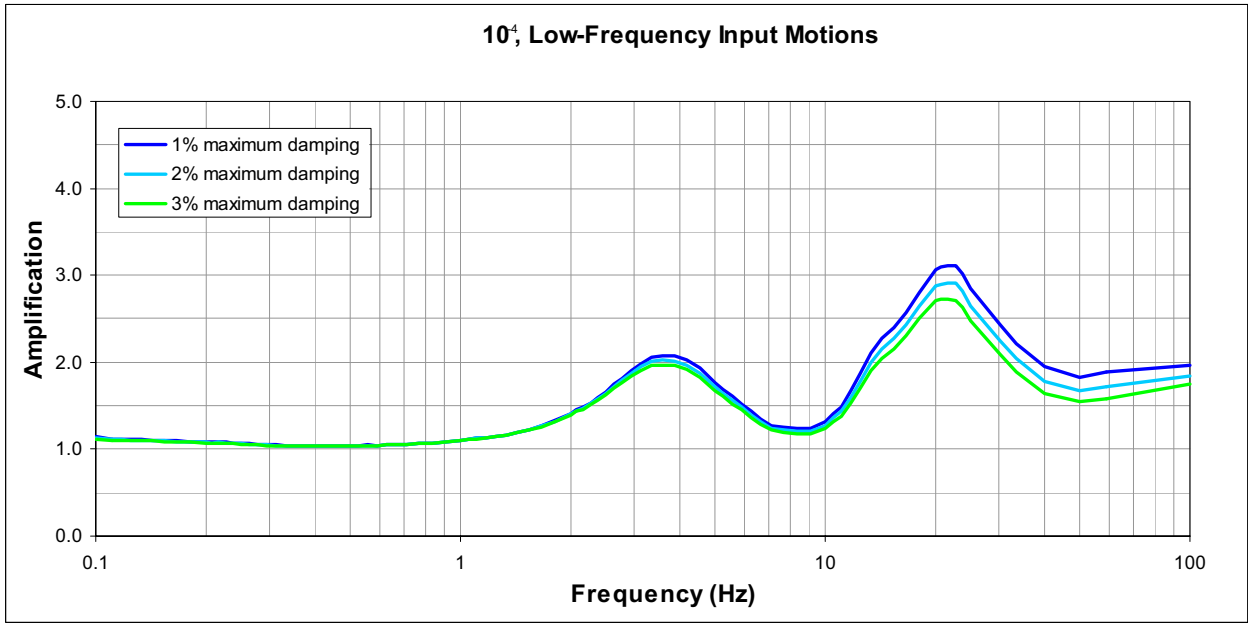

**Figure 2.5.2-268 Sensitivity of GMRS Profile Mean Site Amplification to Modulus Reduction and Damping Relationships for Glacical Till**

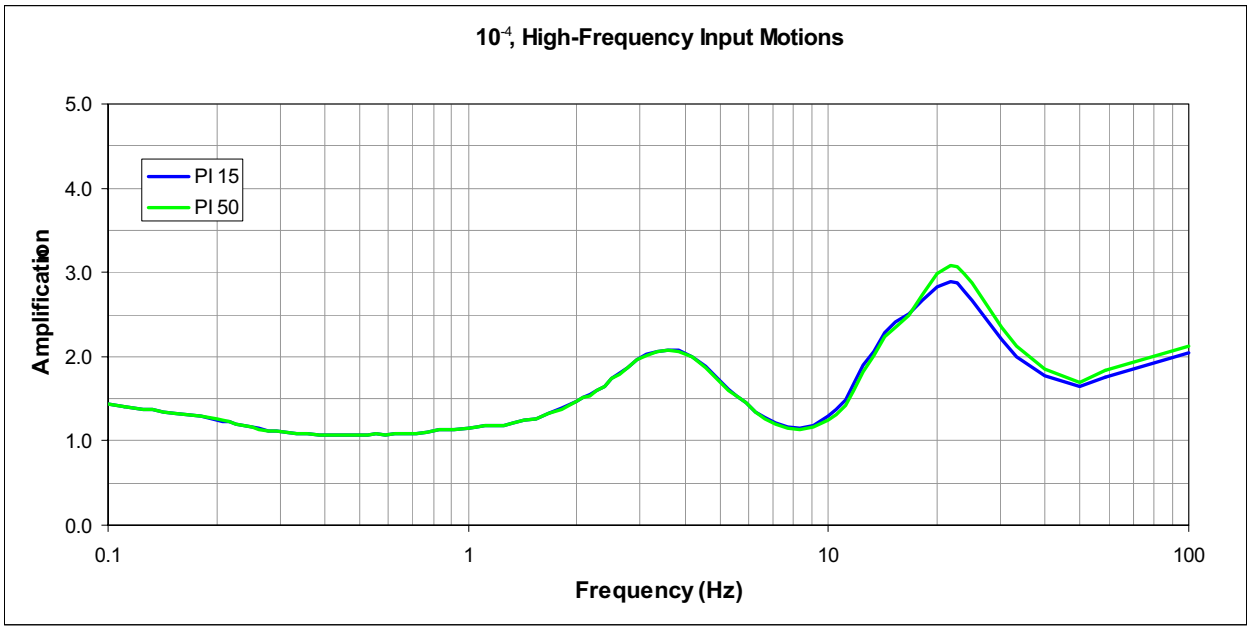


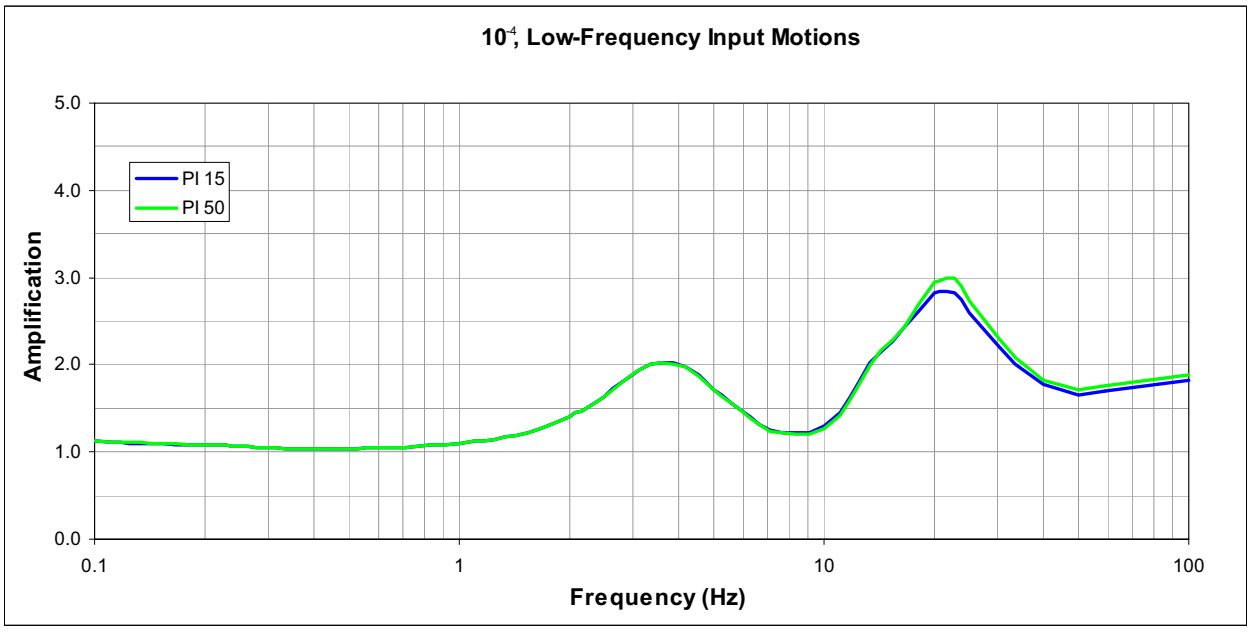

**Figure 2.5.2-269 Sensitivity of GMRS Profile Mean Site Amplification to Deaggregation Earthquake Motions**

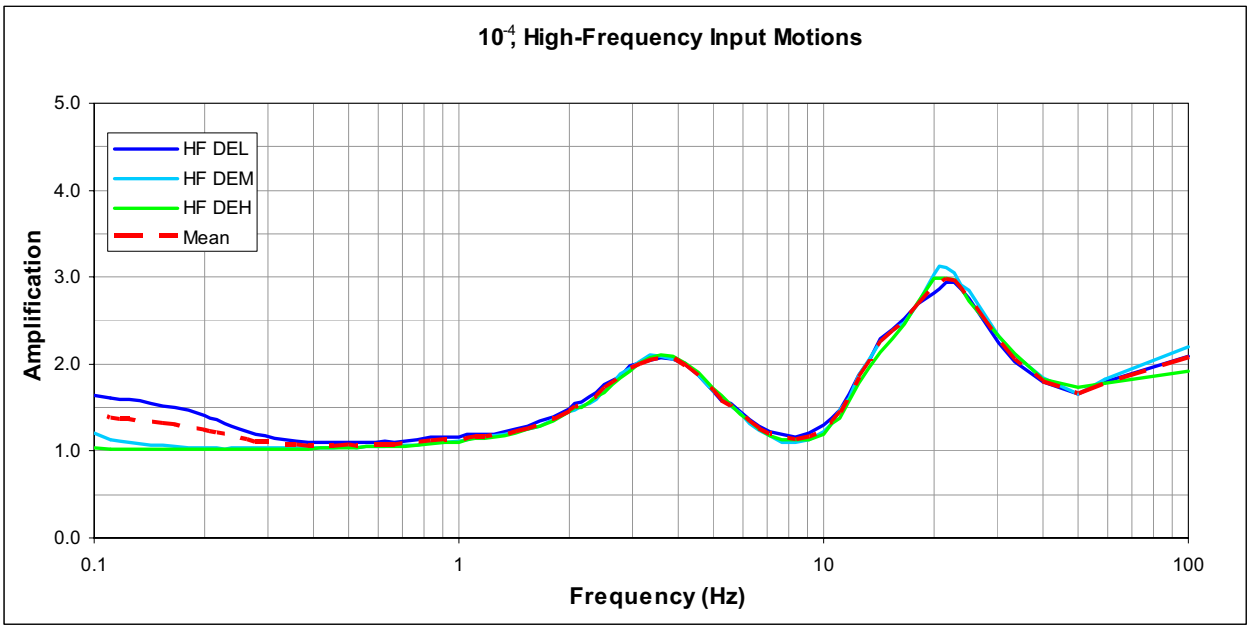


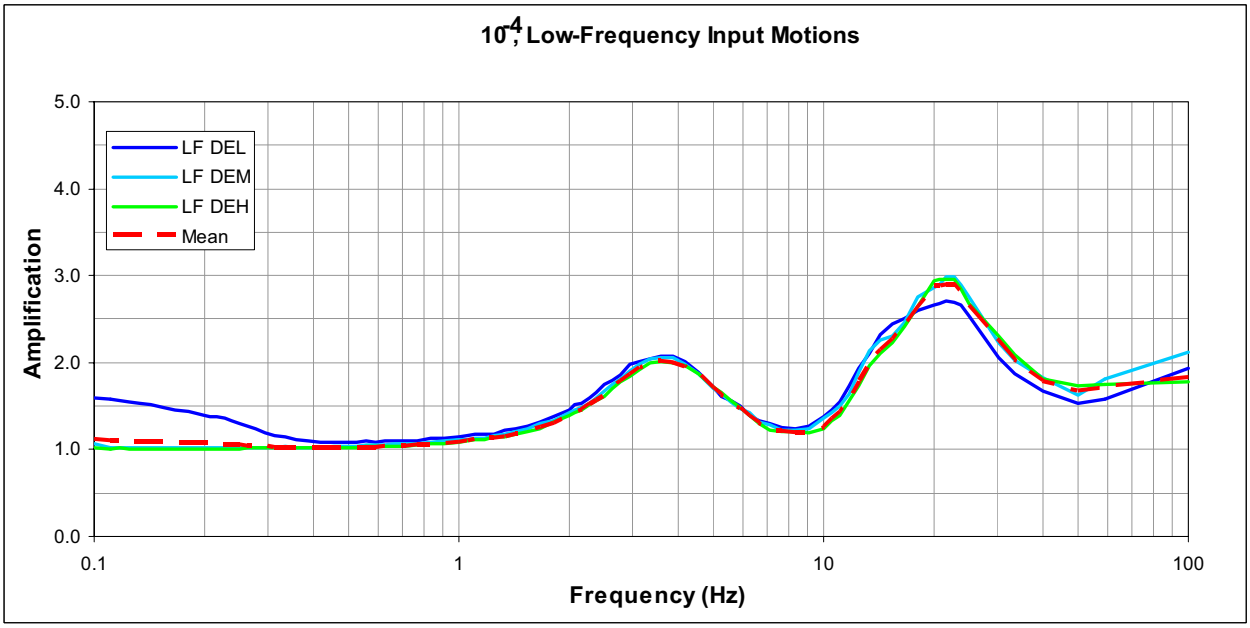

## Figure 2.5.2-270 GMRS Amplification Functions for the Fermi 3 Site

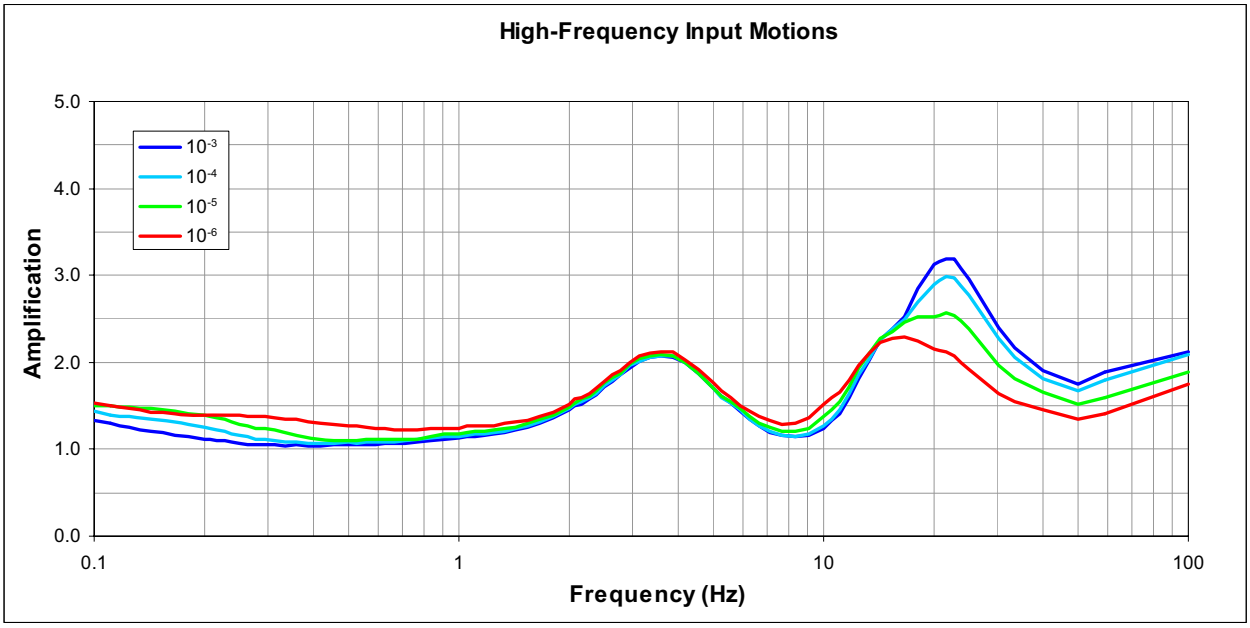


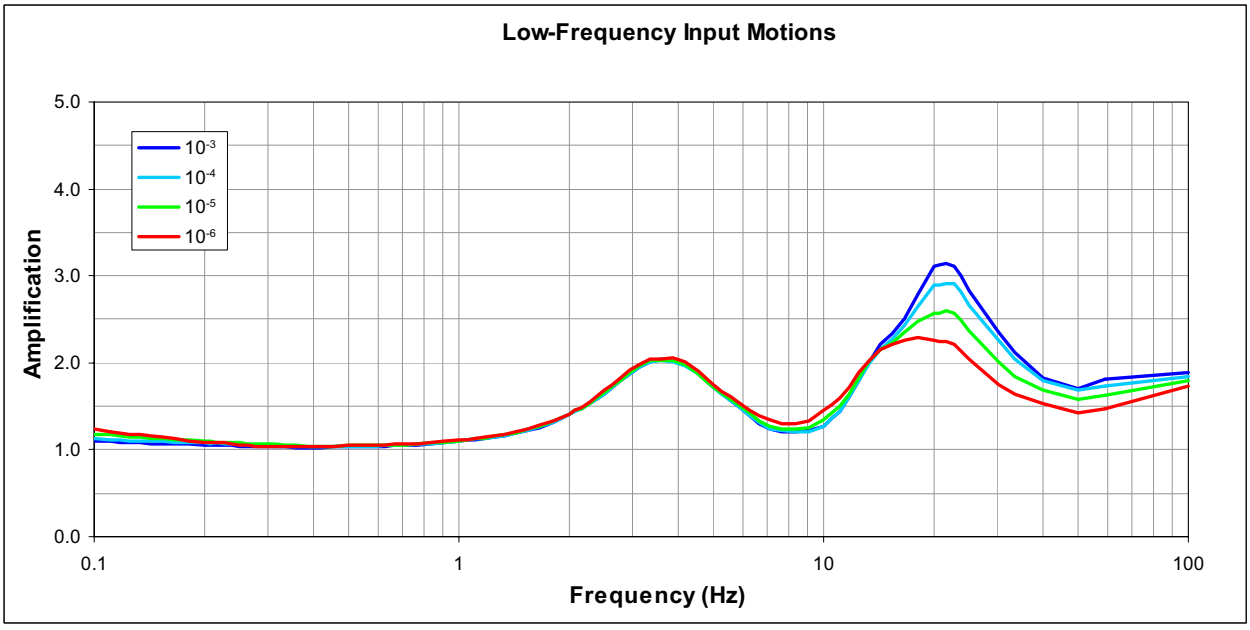

**Figure 2.5.2-271 Statistics of Effective Strain for the GMRS Profile and $10^{-4}$ Motions**

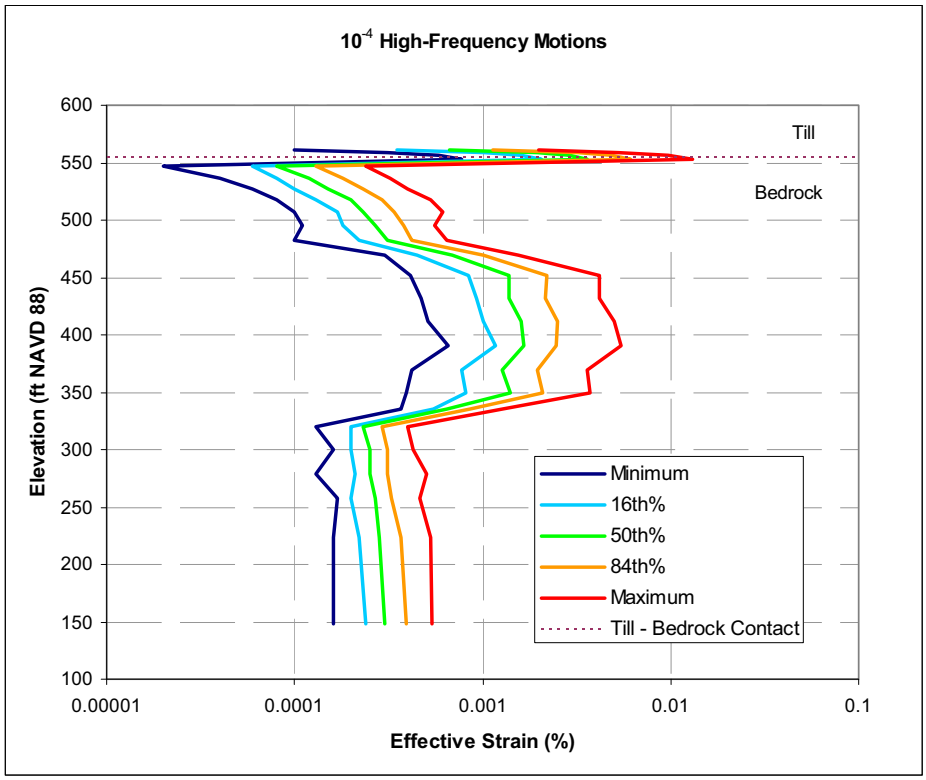


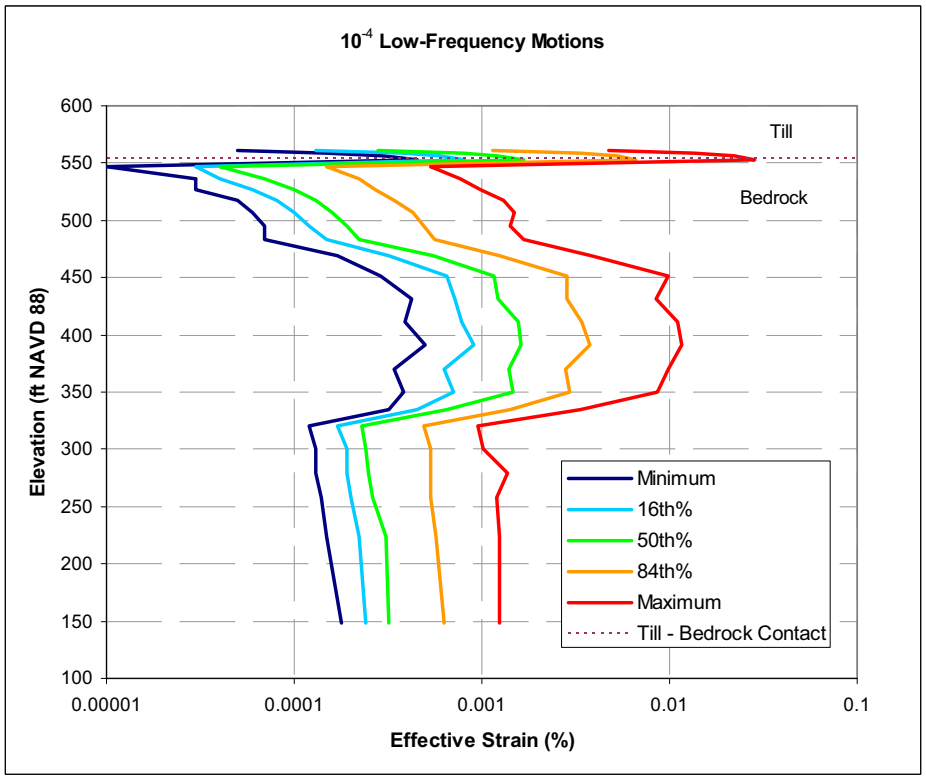

**Figure 2.5.2-272 Statistics of Effective Strain for the GMRS Profile and $10^{-5}$ Motions**

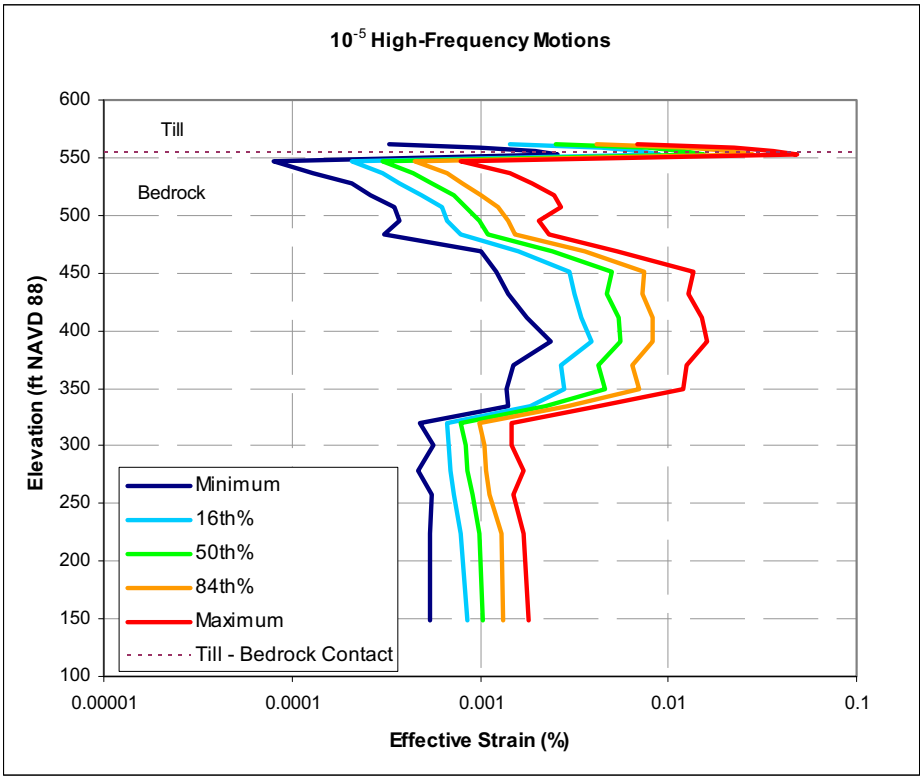


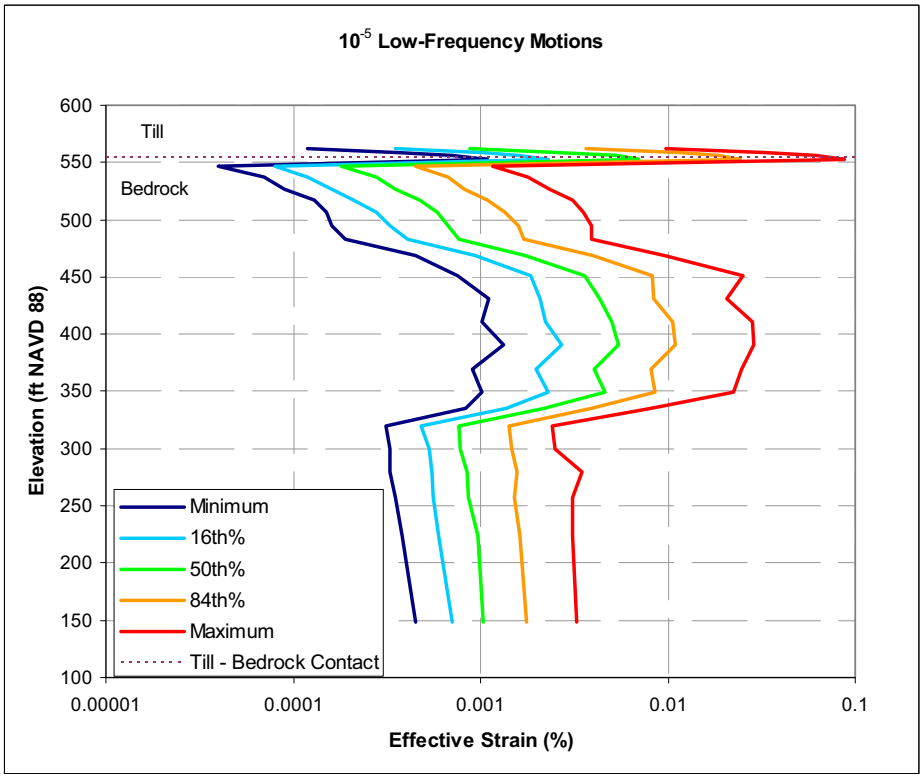

## Figure 2.5.2-273 R/FB FIRS Amplification Functions for the Fermi 3 Site

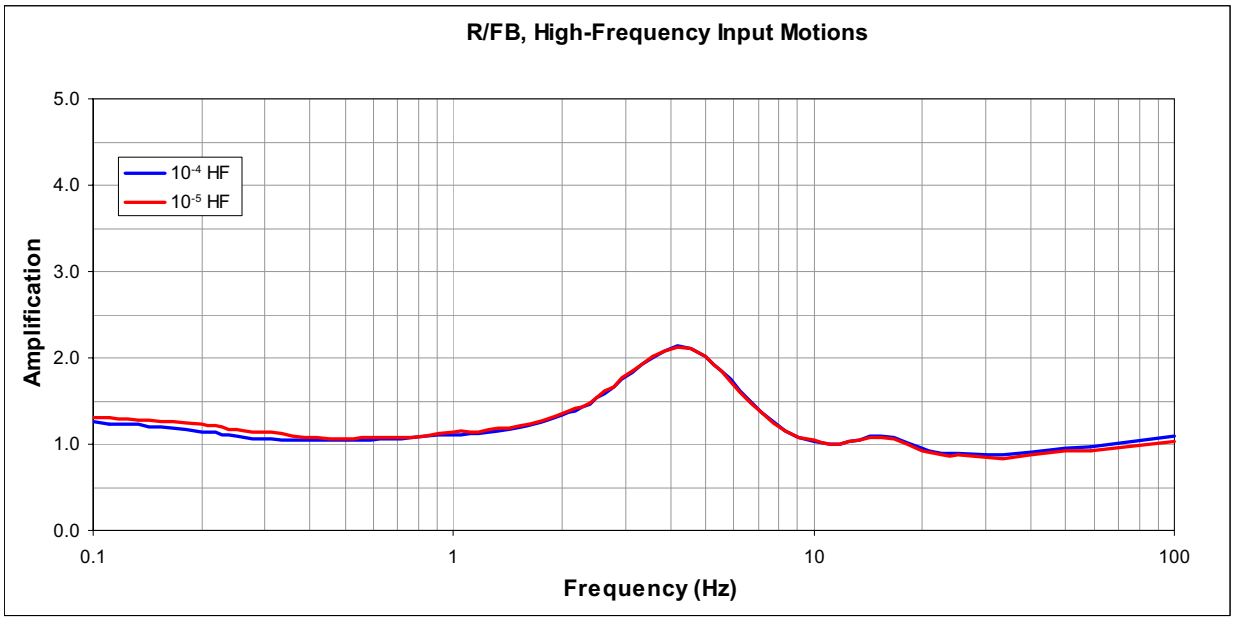


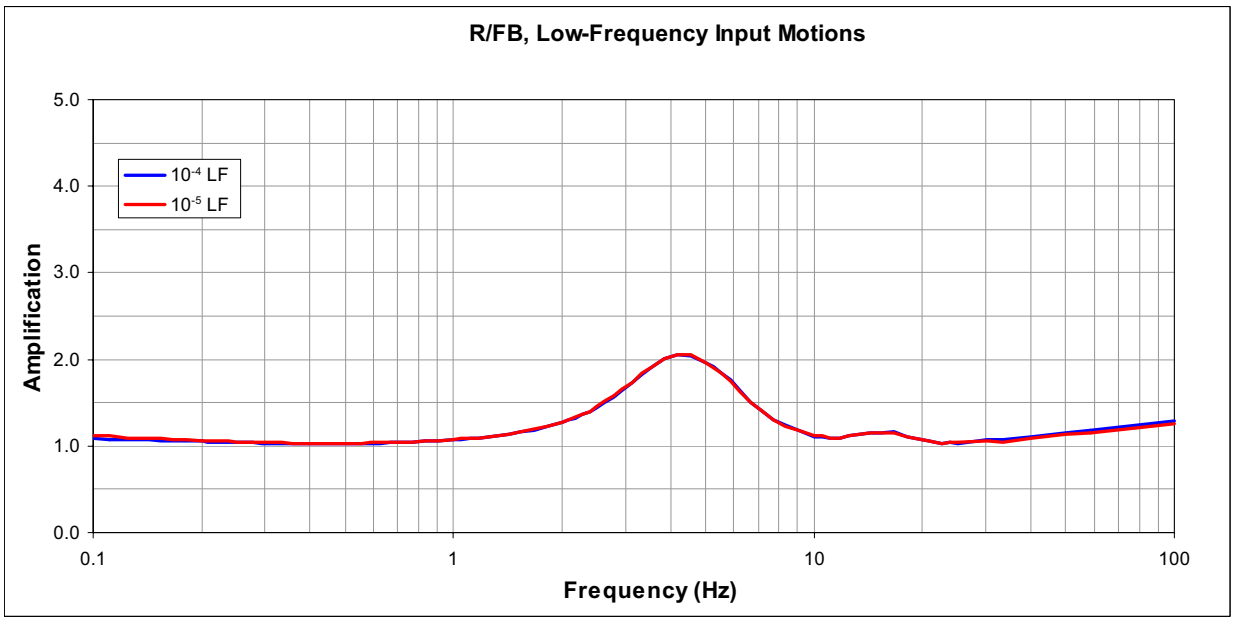

## Figure 2.5.2-274 CB FIRS Amplification Functions for the Fermi 3 Site

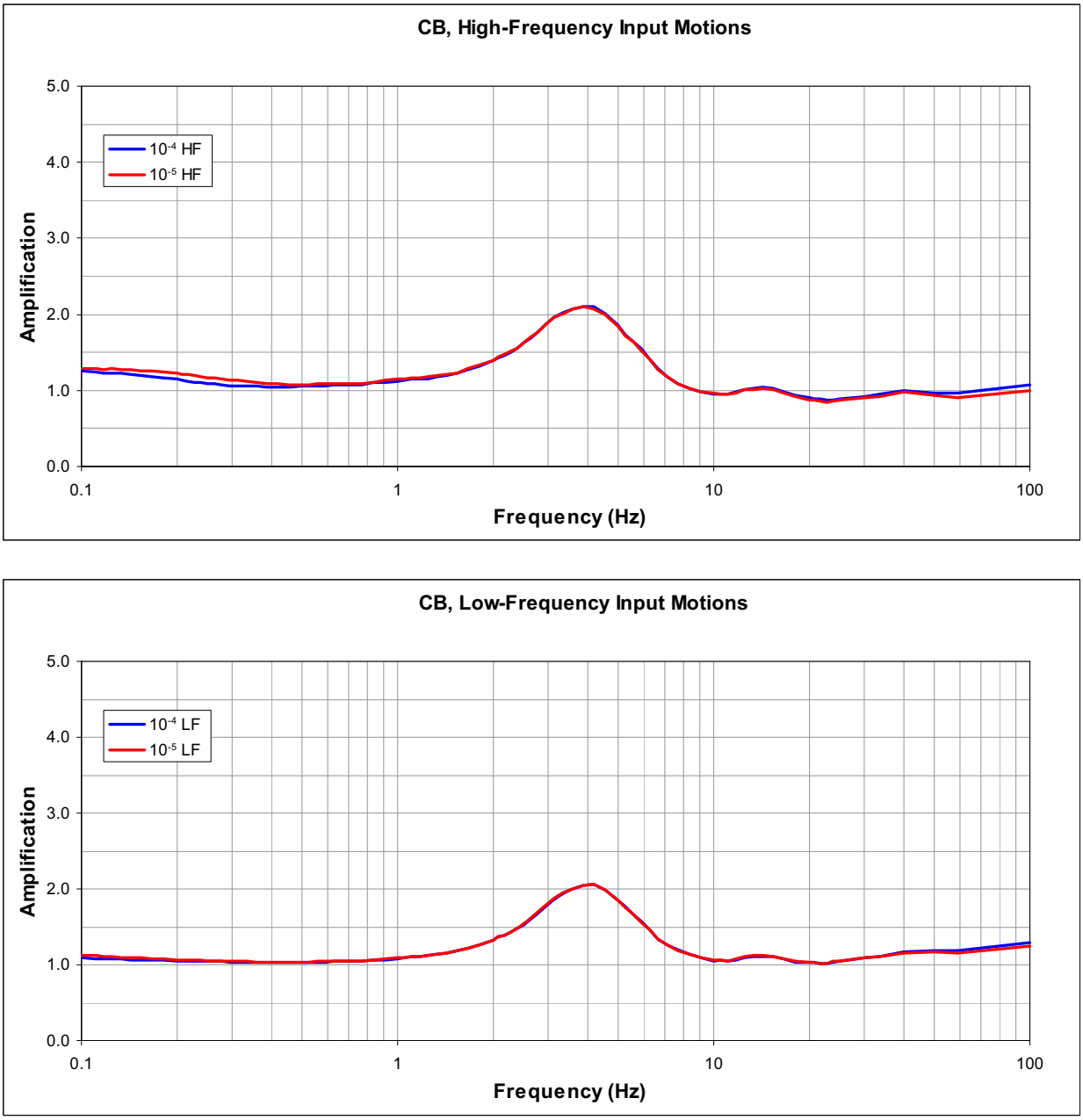

## Figure 2.5.2-275 FWSC FIRS Amplification Functions for the Fermi 3 Site

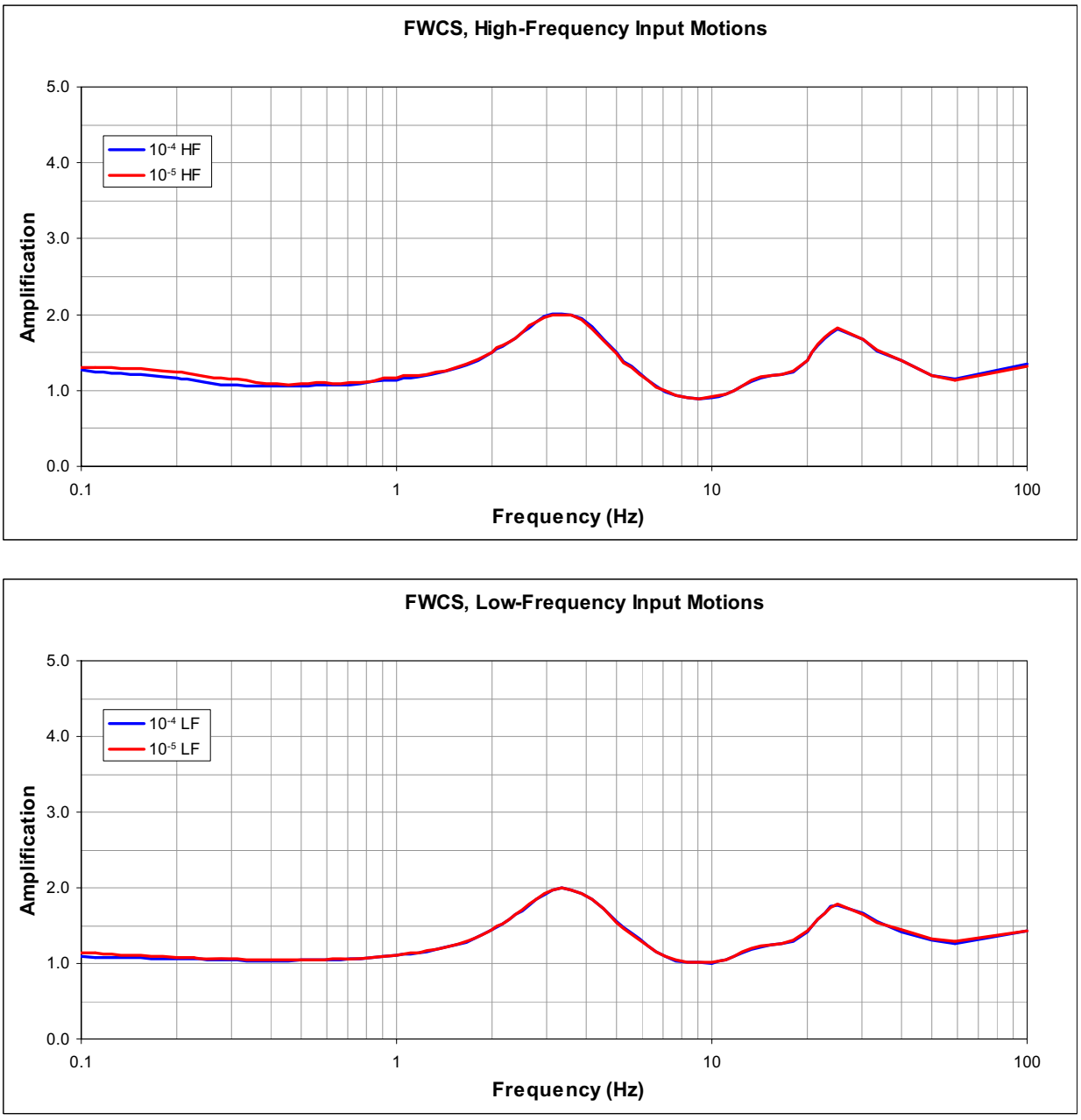

**Figure 2.5.2-276 Development of $10^{-4}$ Surface UHRS for the GMRS Profile**

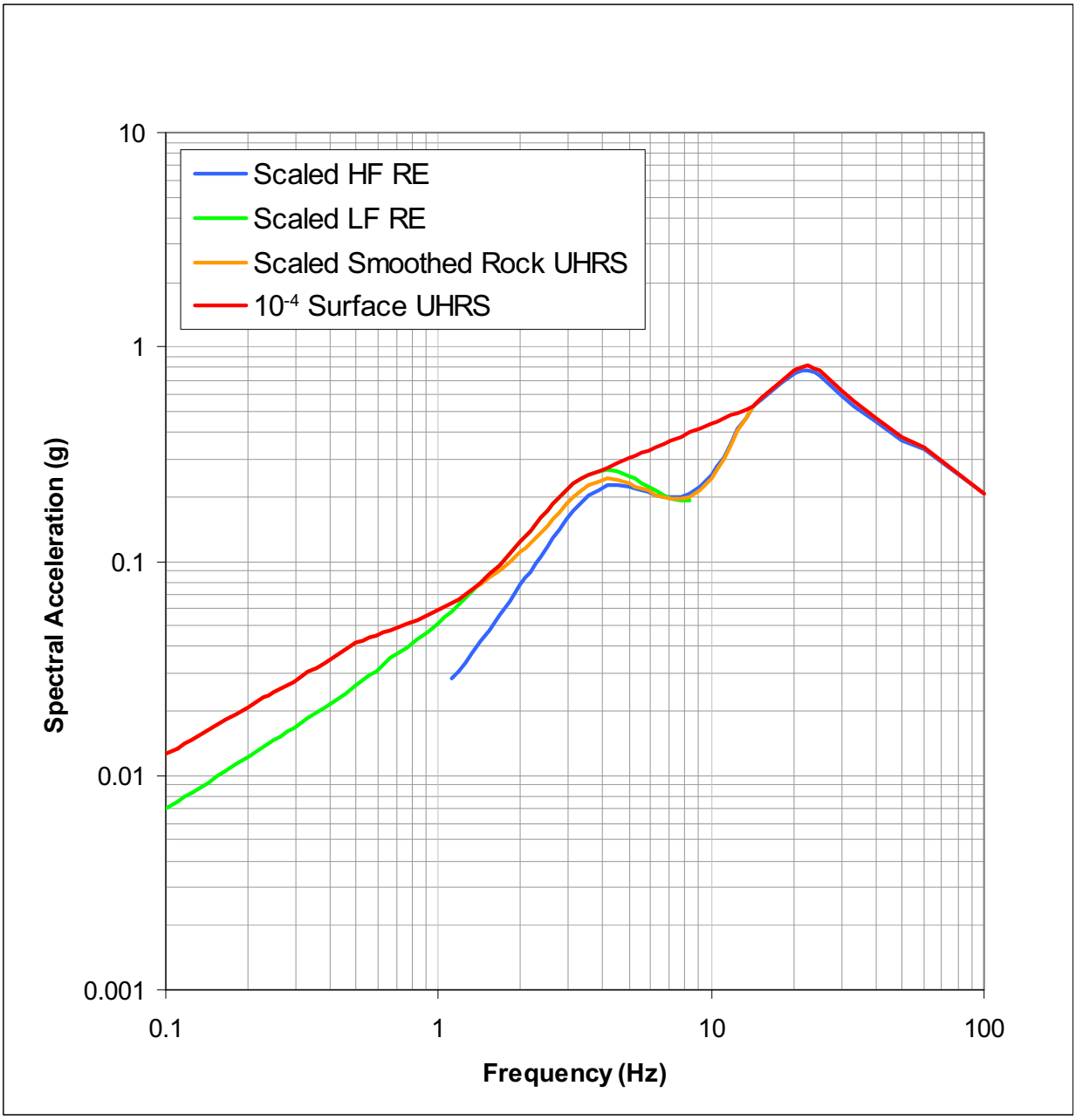

**Figure 2.5.2-277 Development of $10^{-4}$ Surface UHRS for the R/FB FIRS Profile**

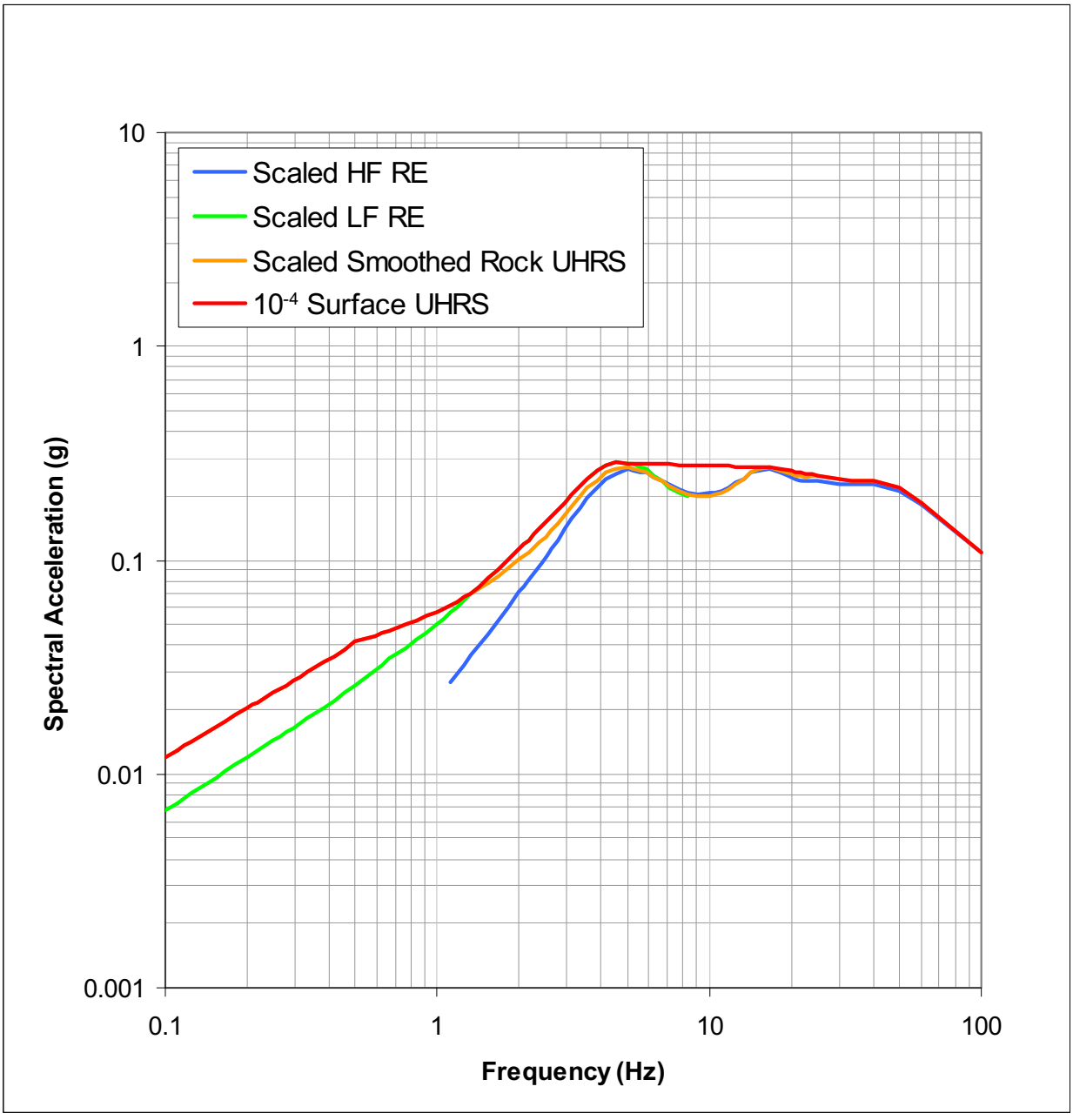

**Figure 2.5.2-278 Surface Hazard Curves for the GMRS Profile Computed with and without CAV for 0.5-Hz Spectral Acceleration**

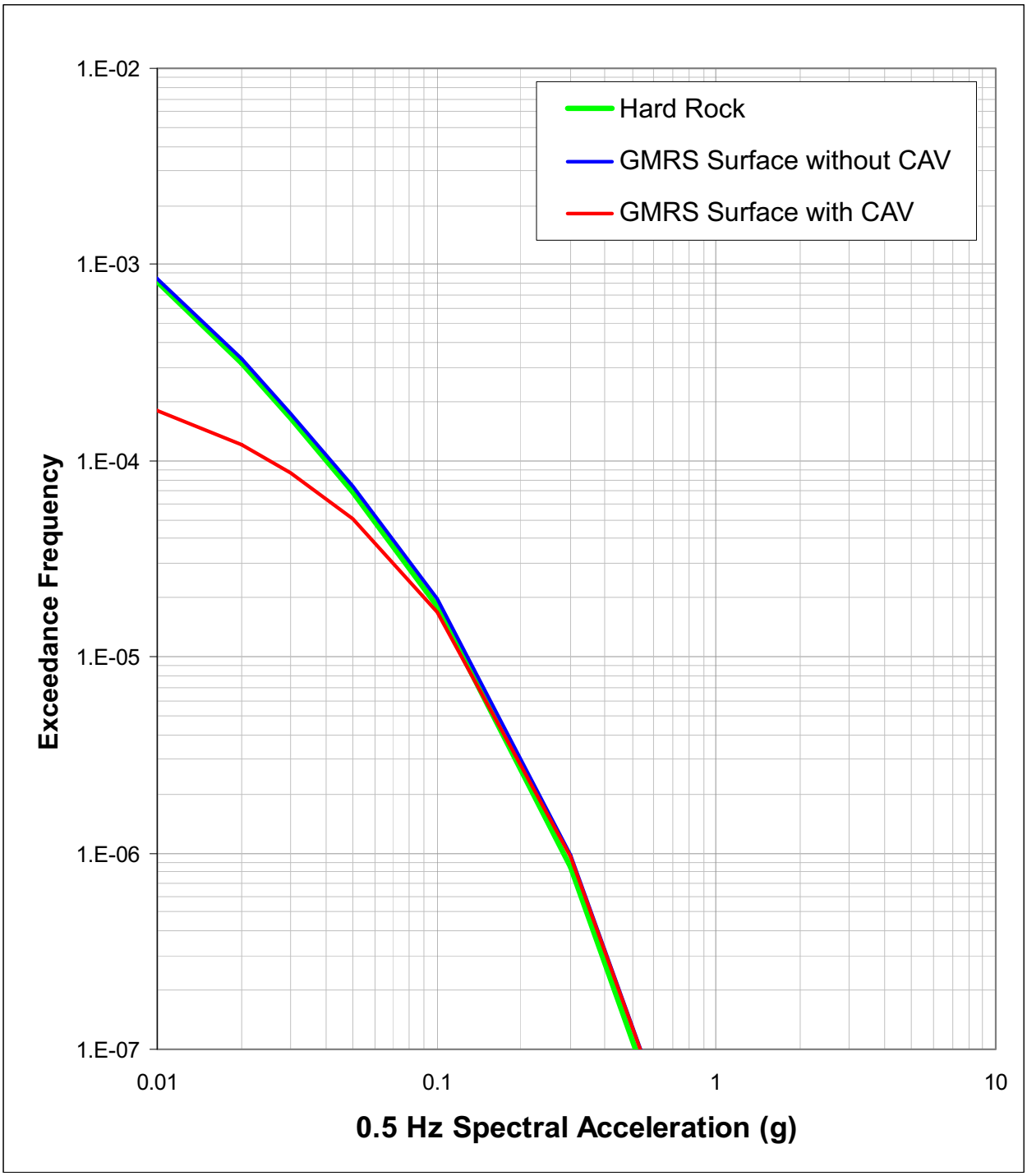

**Figure 2.5.2-279 Surface Hazard Curves for the GMRS Profile Computed with and without CAV for 1-Hz Spectral Acceleration**

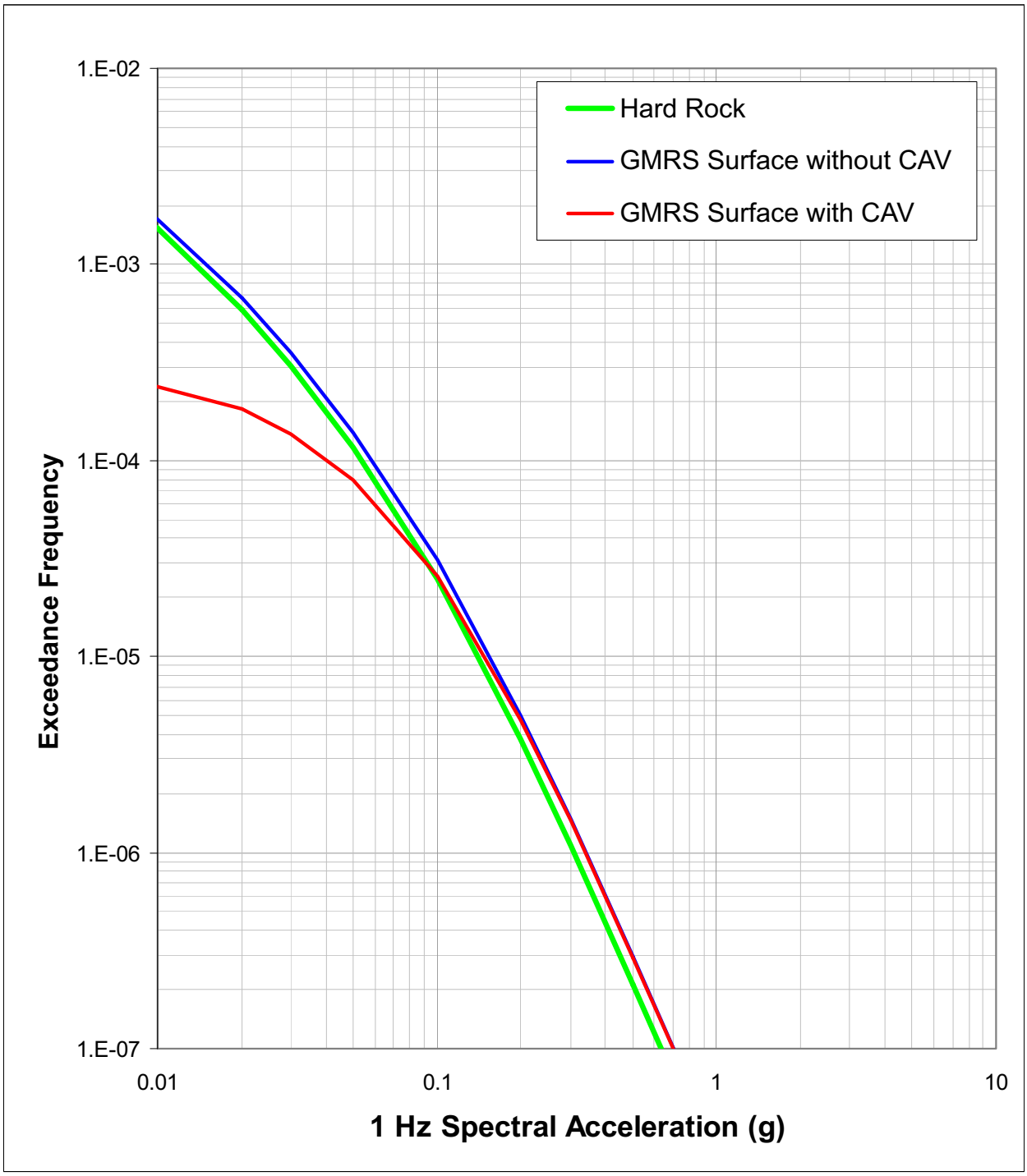

**Figure 2.5.2-280 Surface Hazard Curves for the GMRS Profile Computed with and without CAV for 2.5-Hz Spectral Acceleration**

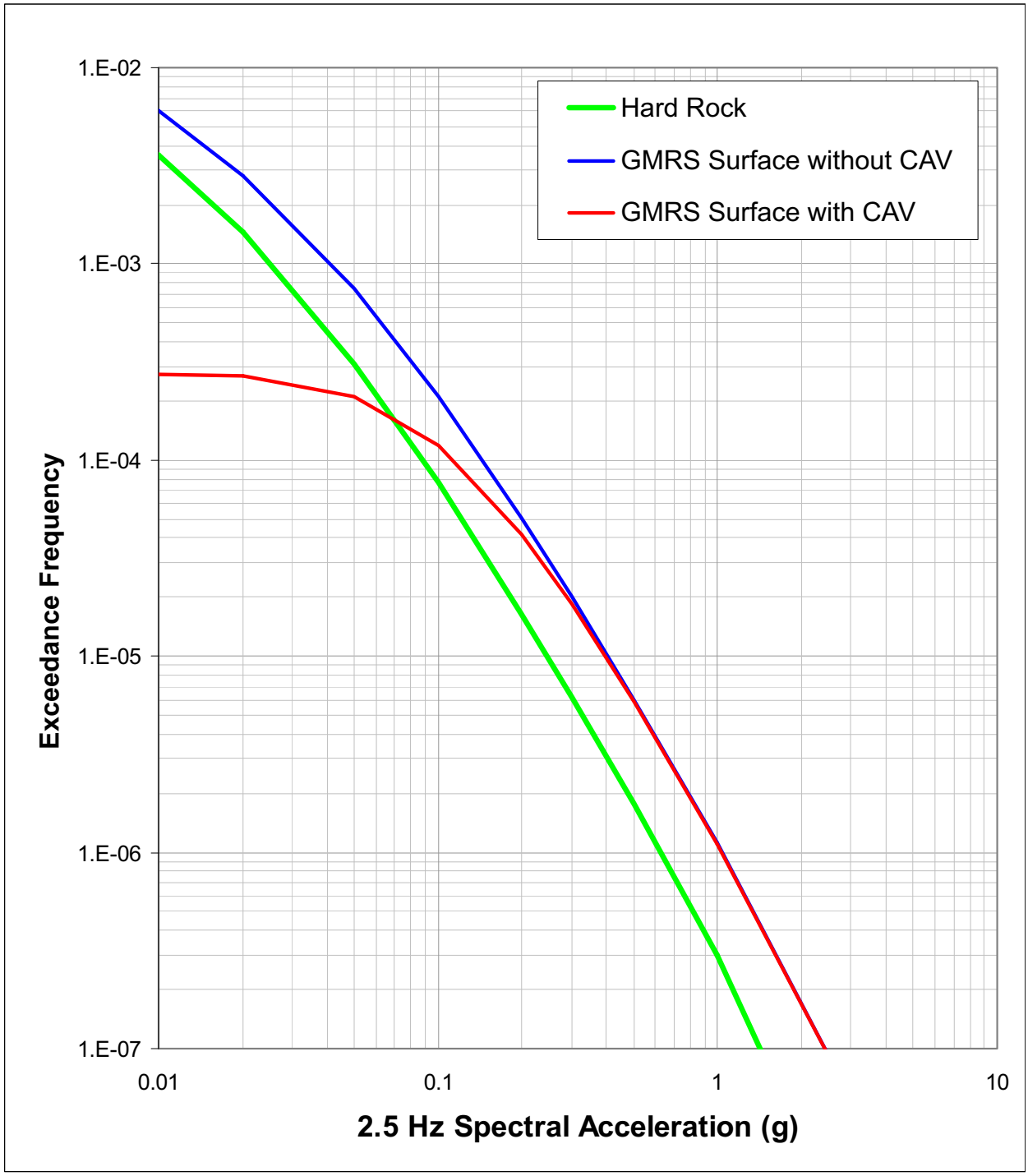

**Figure 2.5.2-281 Surface Hazard Curves for the GMRS Profile Computed with and without CAV for 5-Hz Spectral Acceleration**

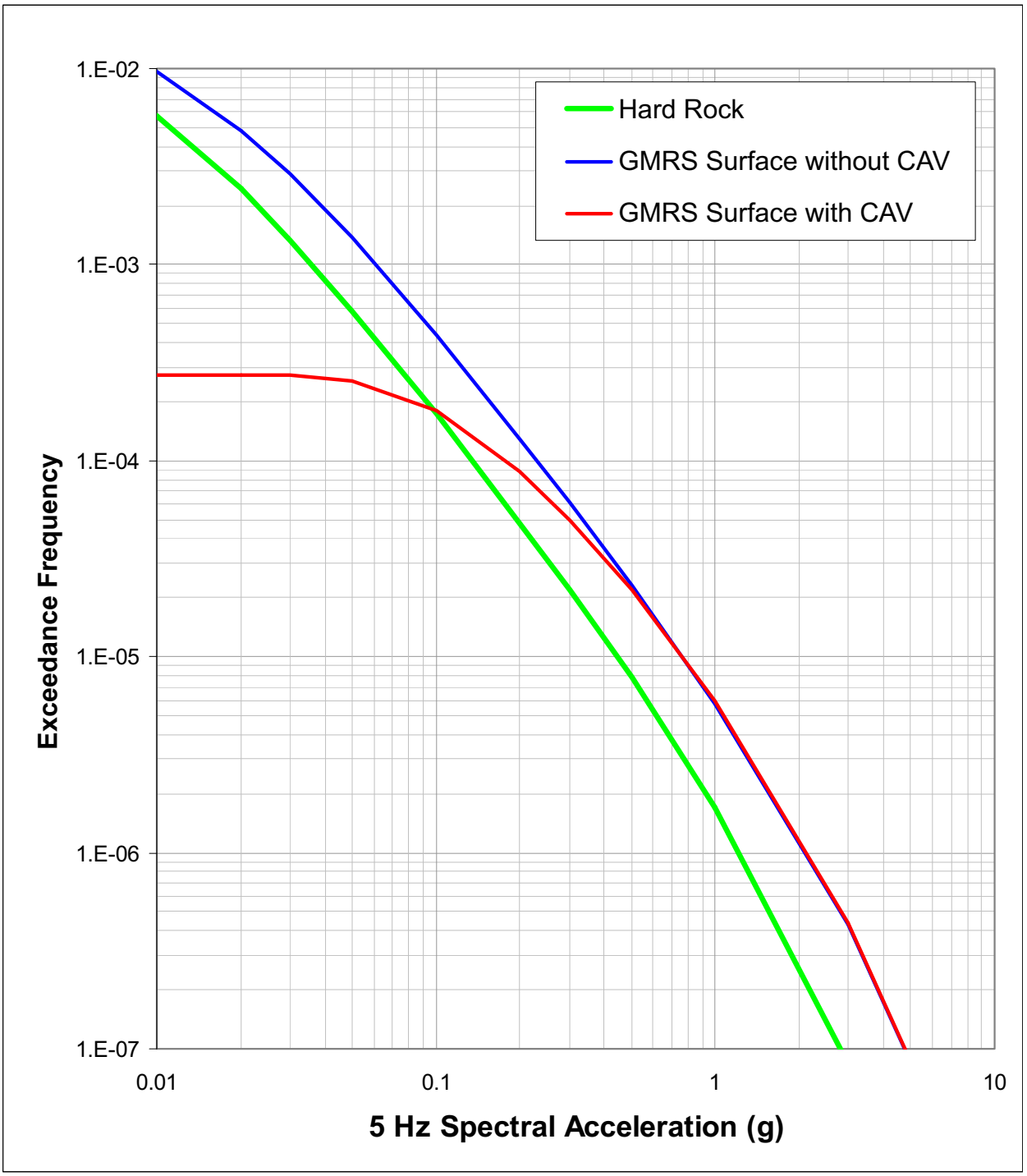

**Figure 2.5.2-282 Surface Hazard Curves for the GMRS Profile Computed with and without CAV for 10-Hz Spectral Acceleration**

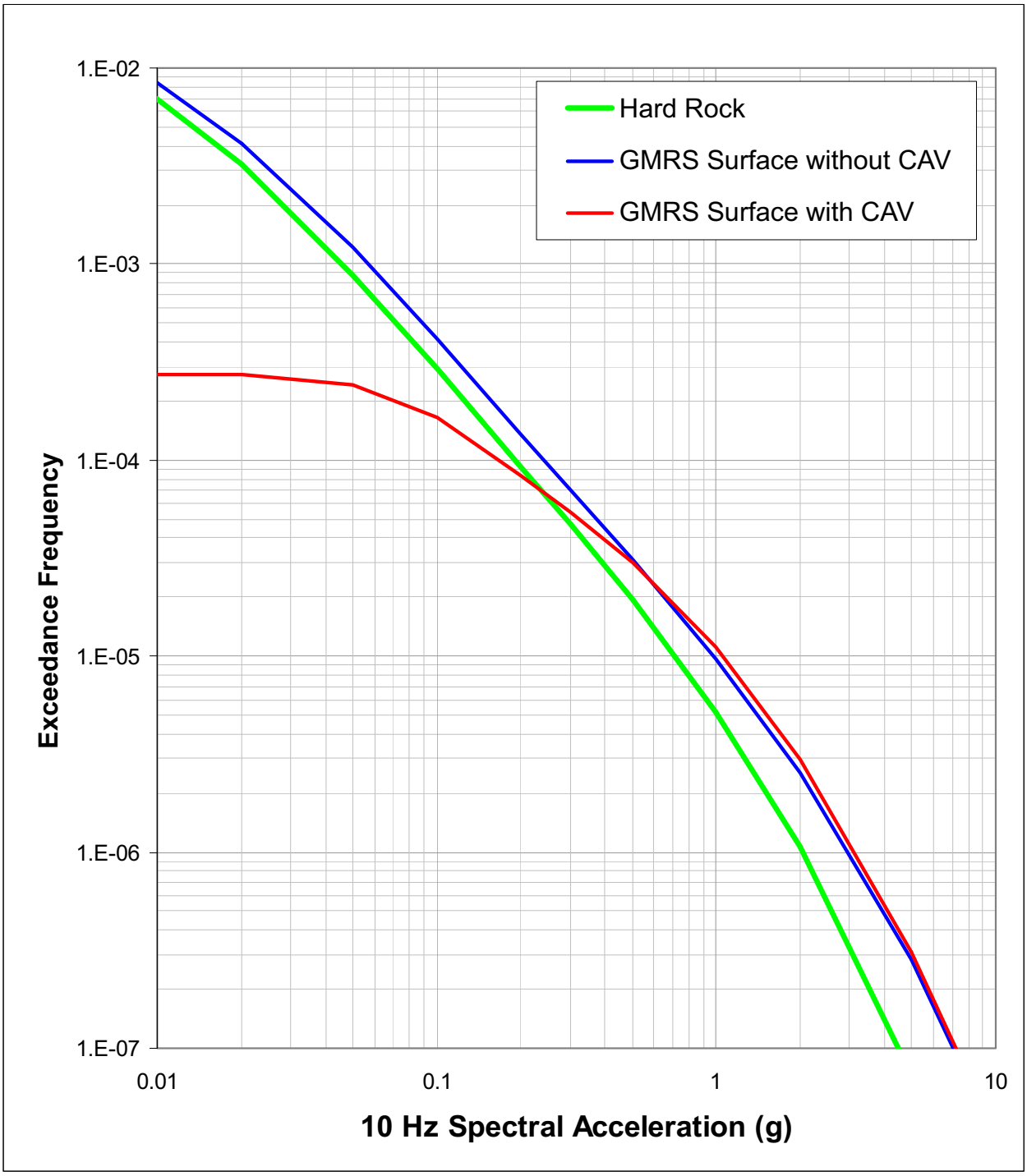

**Figure 2.5.2-283 Surface Hazard Curves for the GMRS Profile Computed with and without CAV for 25-Hz Spectral Acceleration**

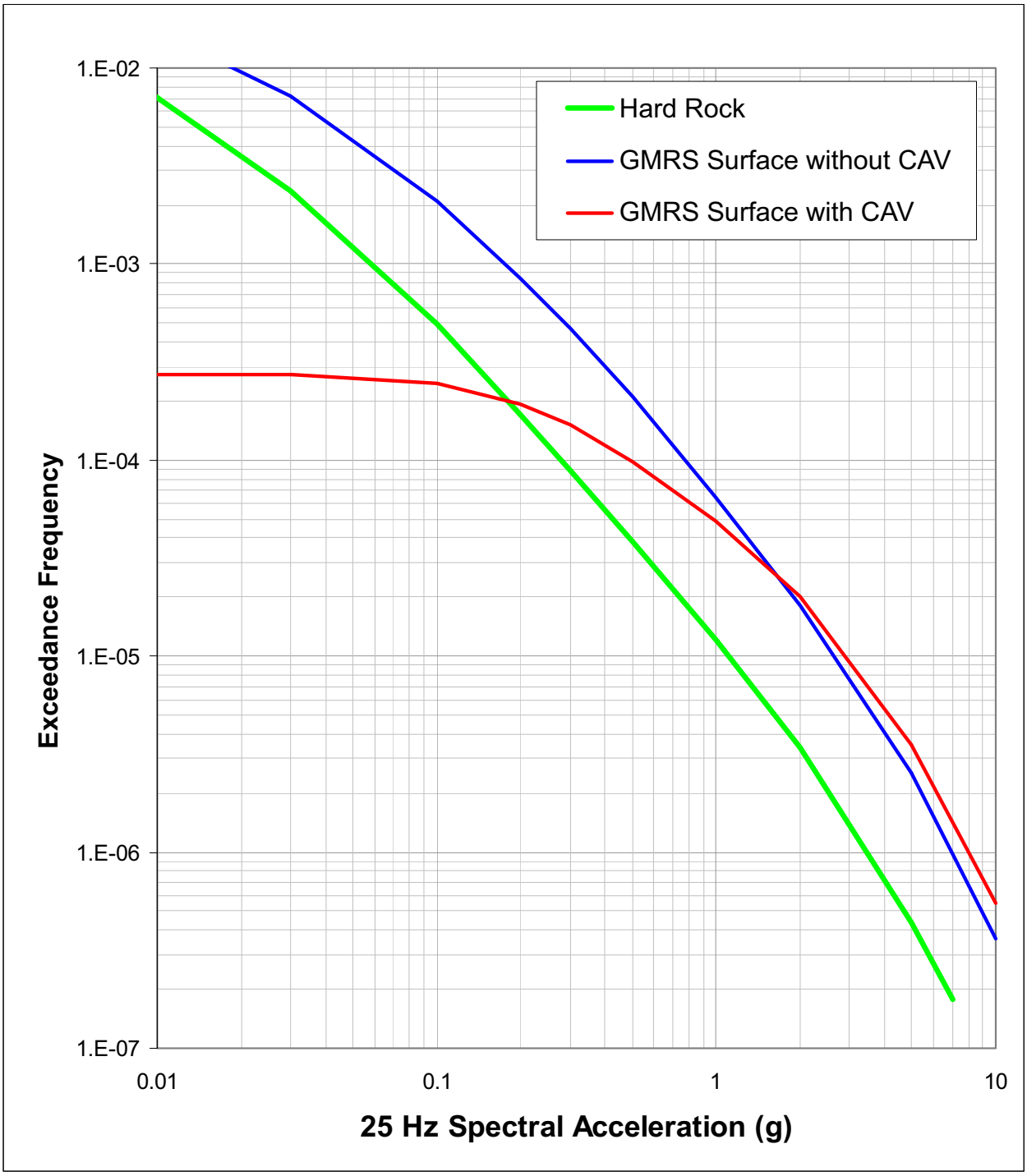

**Figure 2.5.2-284 Surface Hazard Curves for the GMRS Profile Computed with and without CAV for 100-Hz Spectral Acceleration**

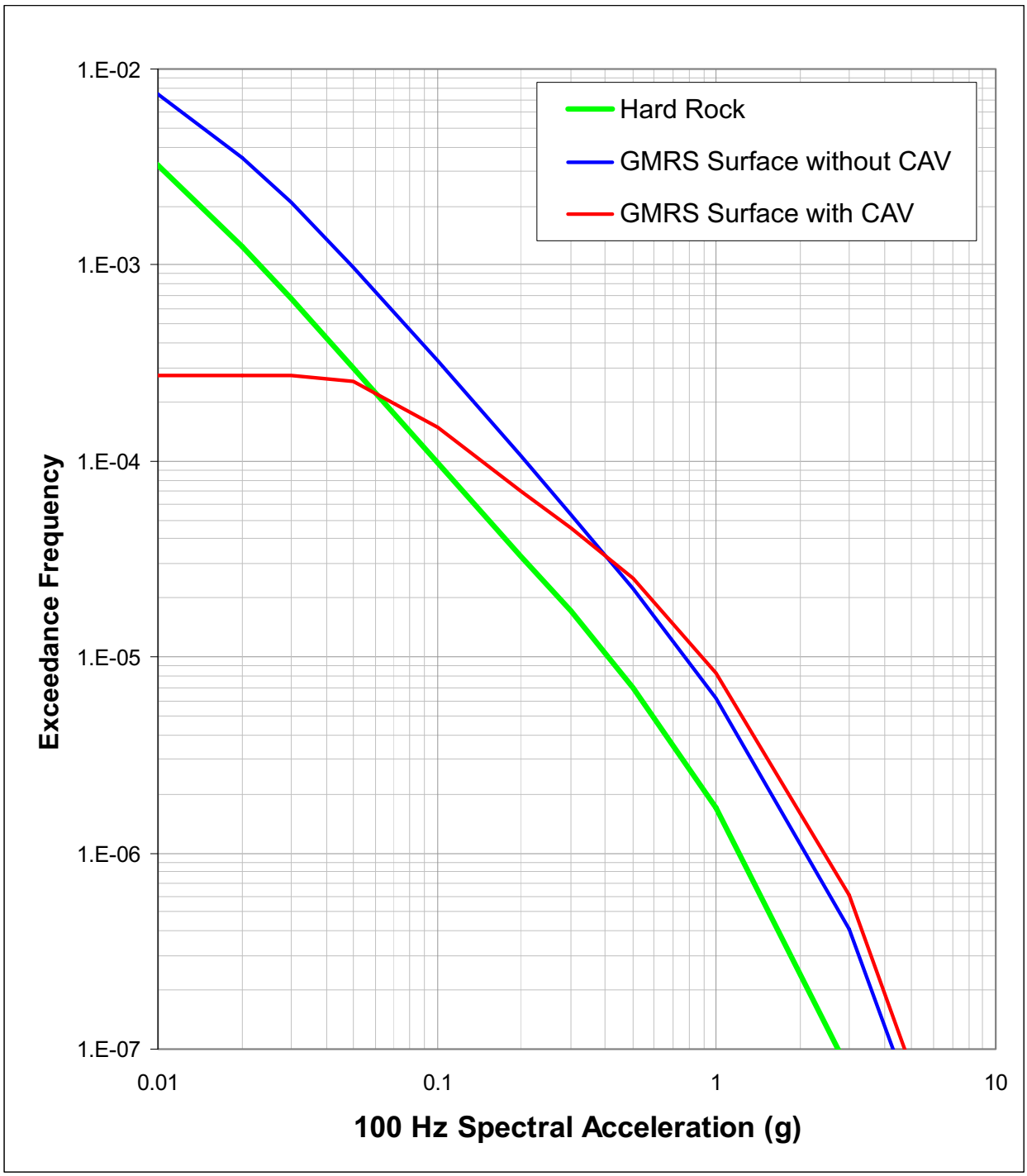

**Figure 2.5.2-285 Surface UHRS for the GMRS Profile Computed with and without CAV**

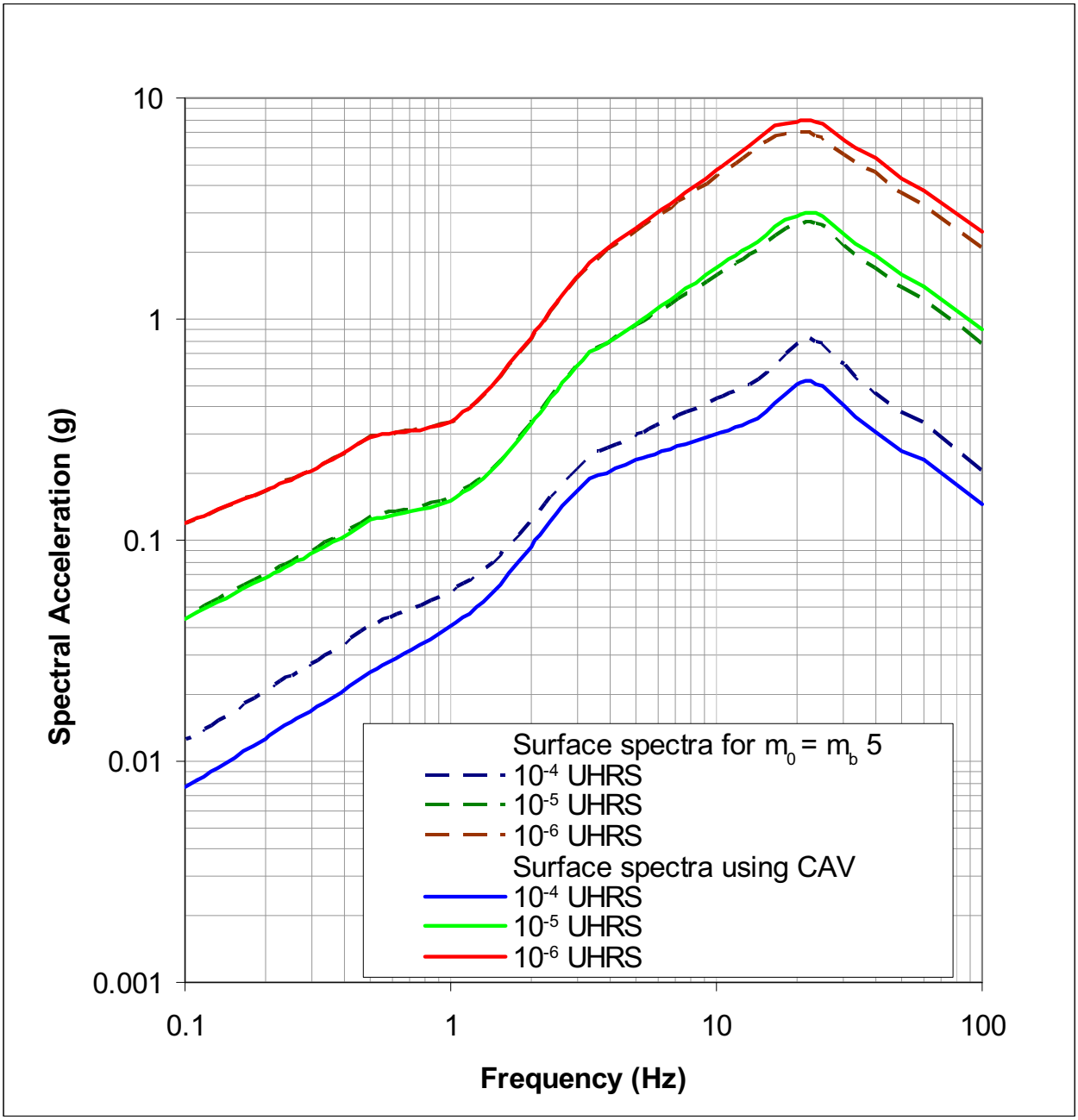

**Figure 2.5.2-286 Horizontal GMRS for the Fermi 3 Site**

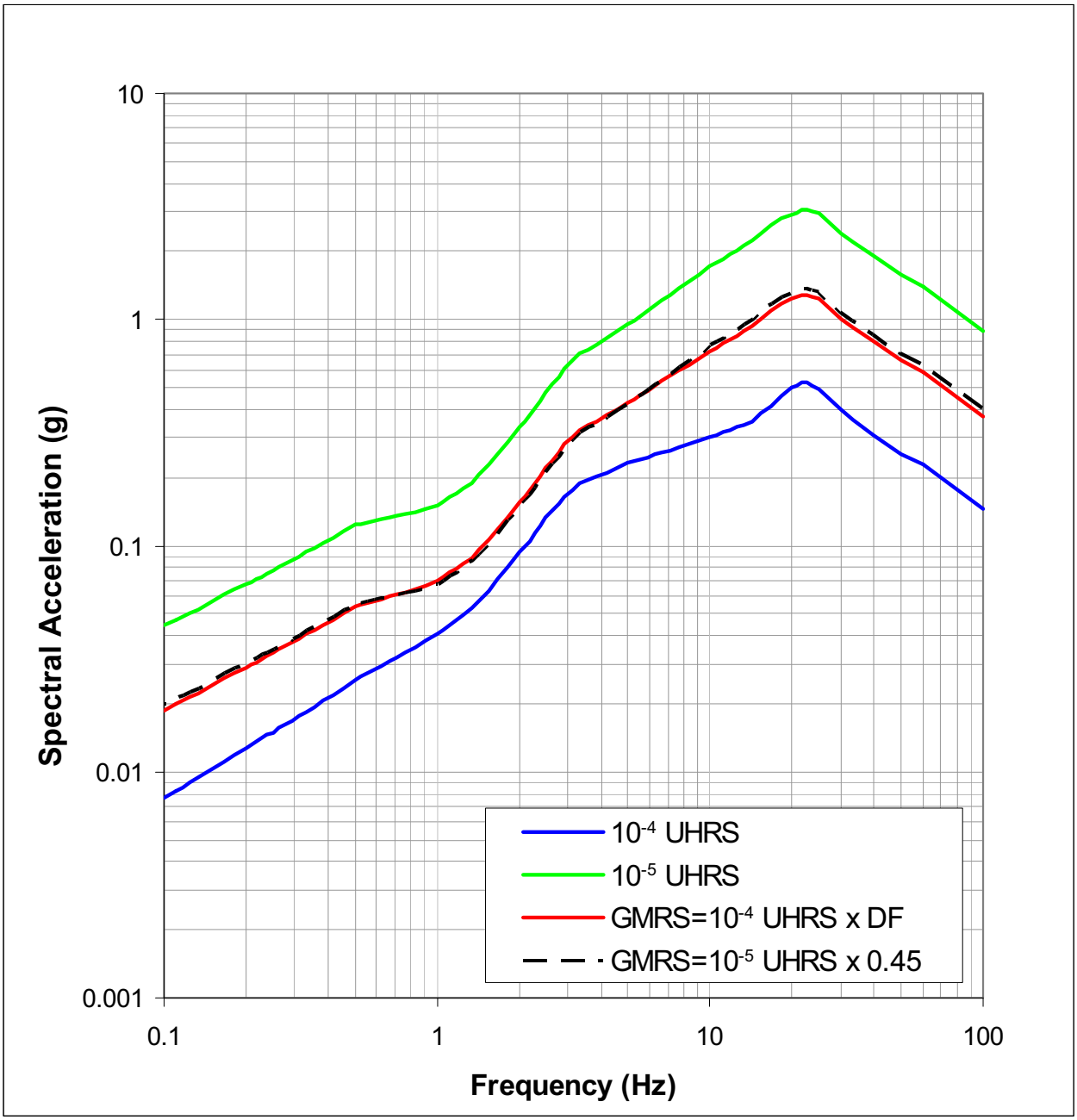

**Figure 2.5.2-287 Vertical to Horizontal Spectral Ratios for Generic CEUS Hard Rock**

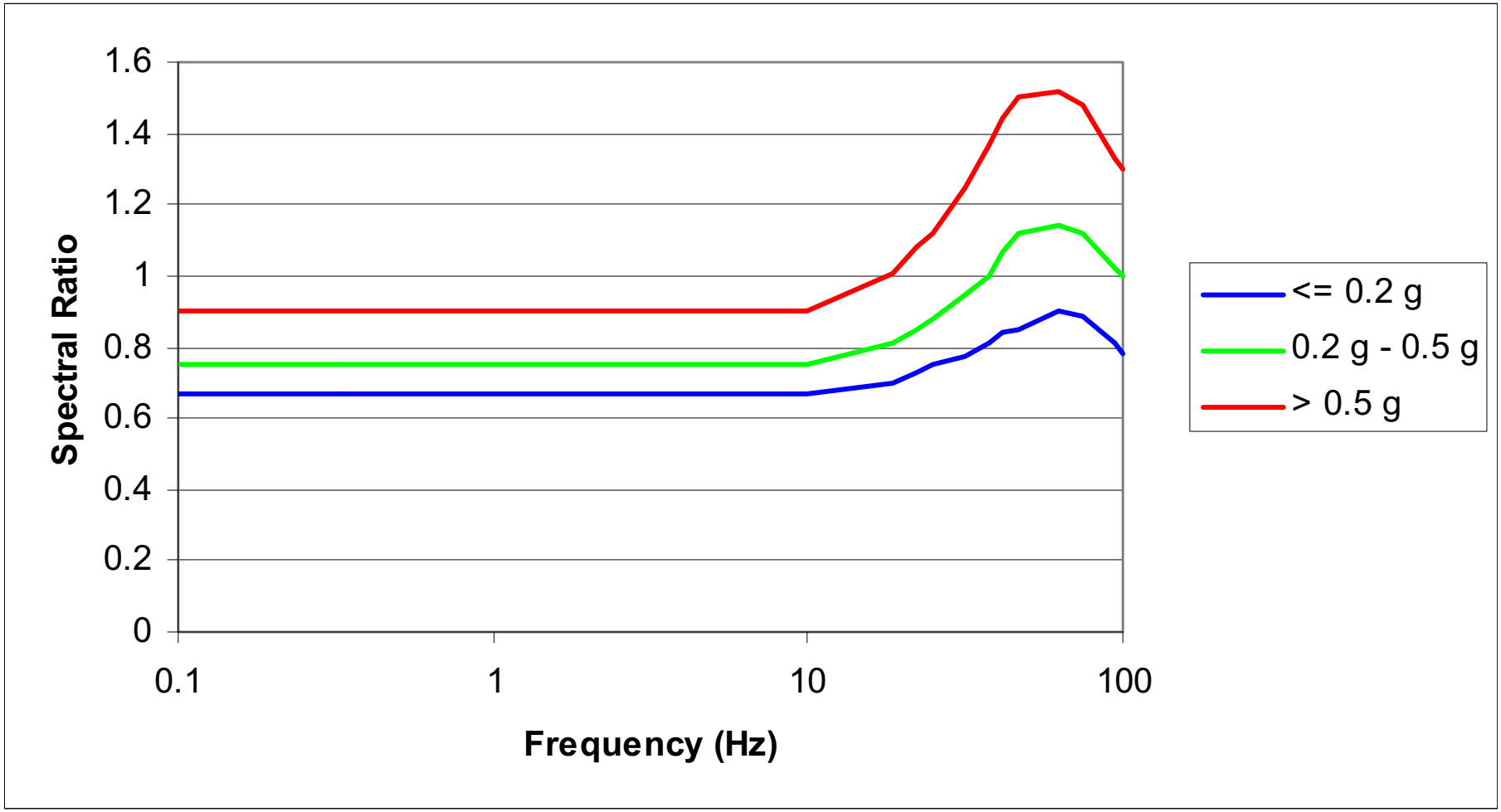

**Figure 2.5.2-288 Fermi 3 GMRS (5% damping)**

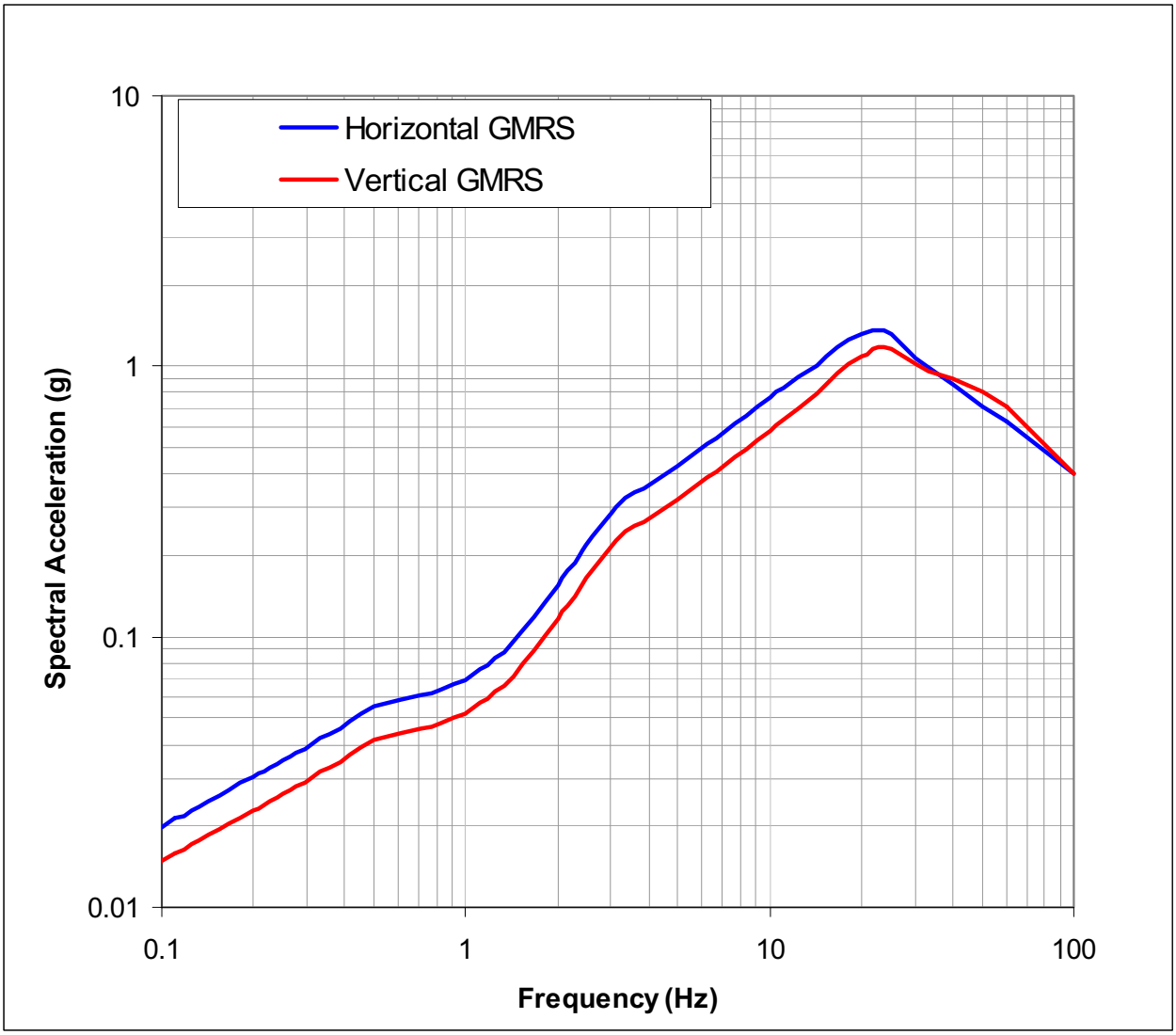

**Figure 2.5.2-289 Fermi 3 R/FB FIRS (5% damping)**

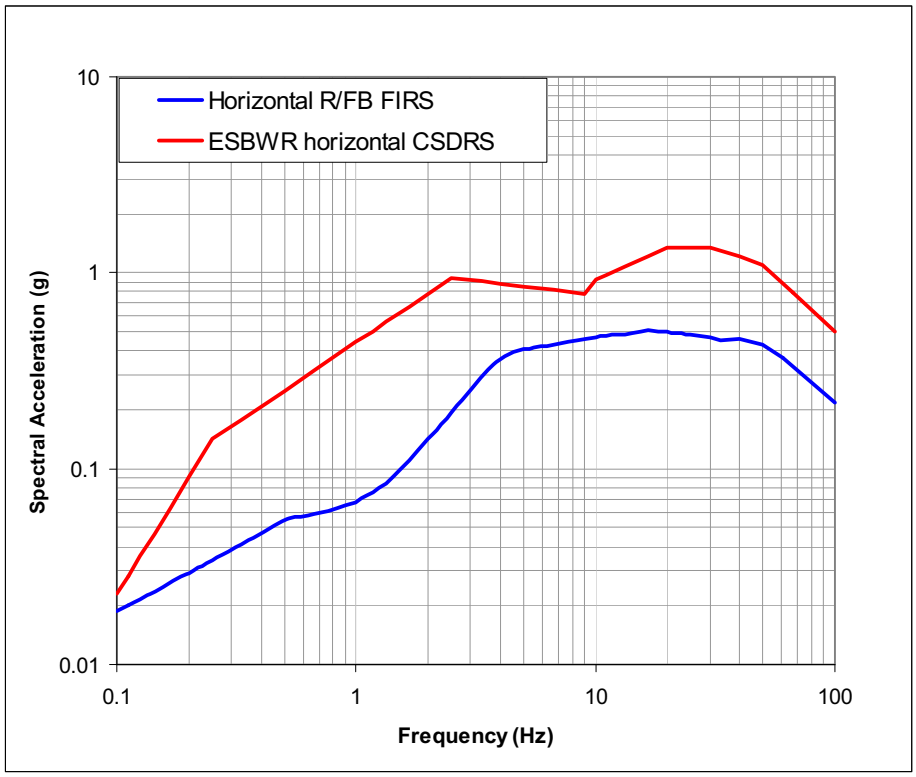


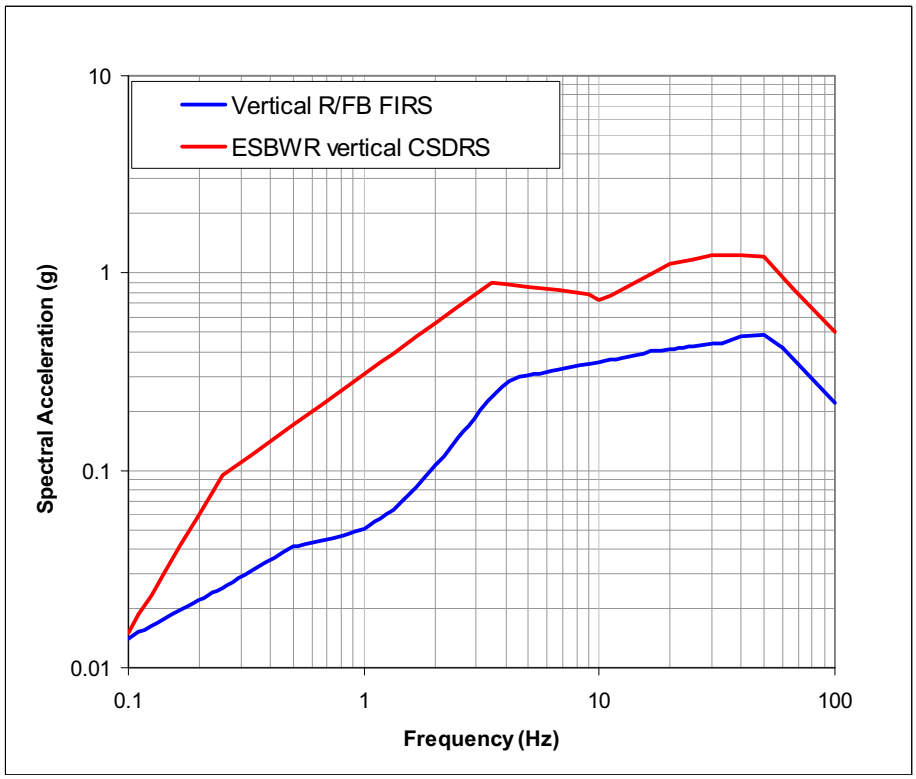

**Figure 2.5.2-290 Fermi 3 CB FIRS (5% damping)**

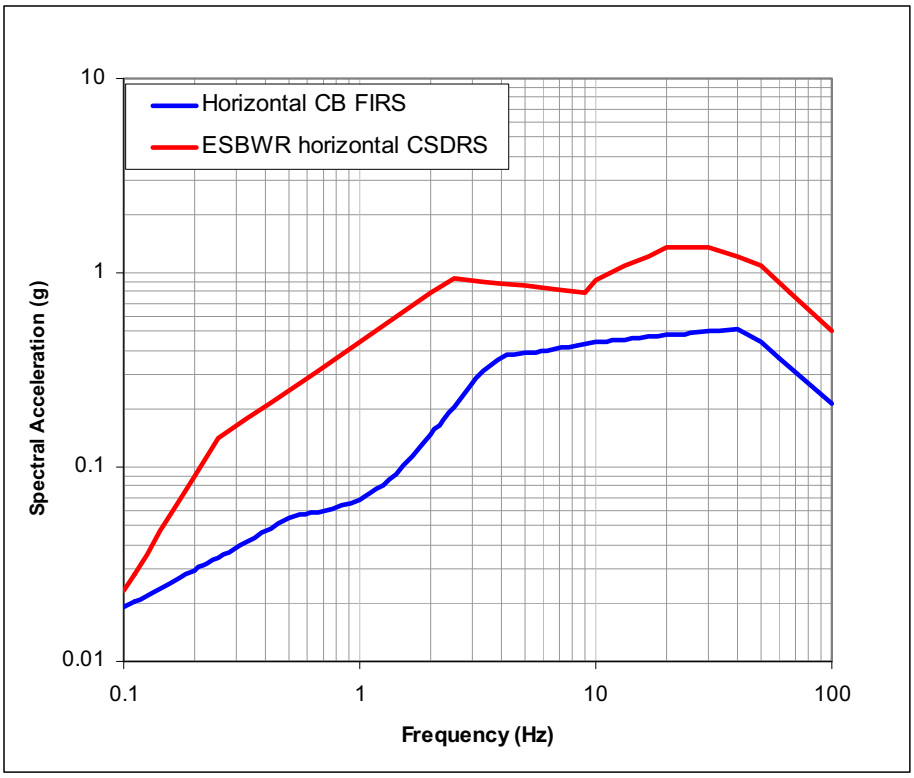


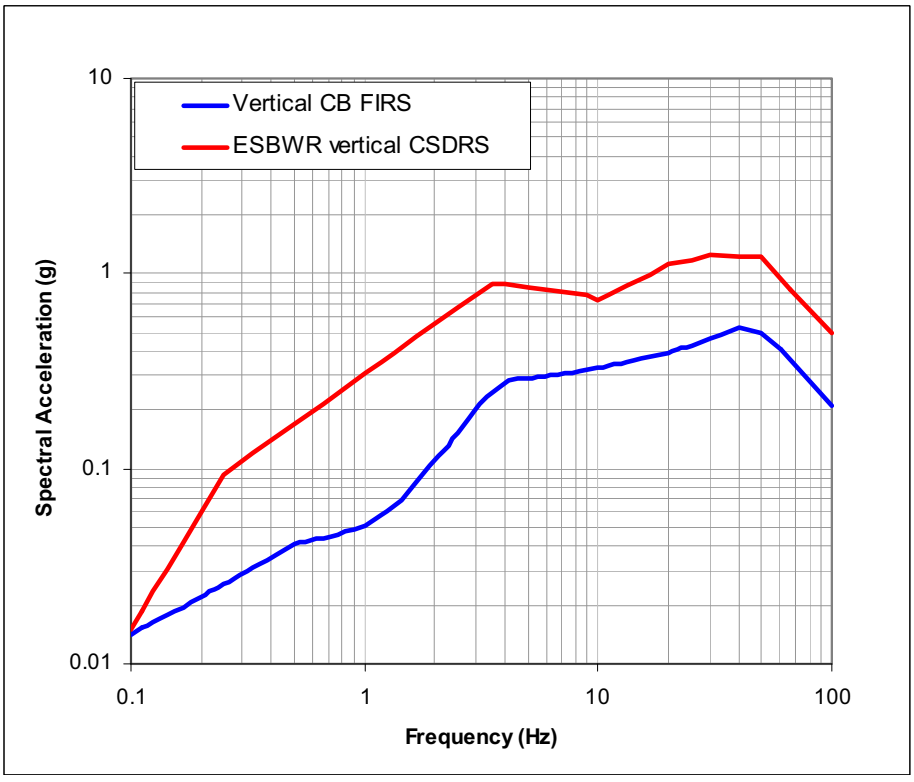

**Figure 2.5.2-291 Fermi 3 FWSC FIRS (5% damping)**